Apollonian emulsions - coalescence in high internal-phase-ratio emulsions

Yii-Wenn Sylvie Kwok

PSL UNIVERSITÉ PARIS

THÈSE DE DOCTORAT
DE L'UNIVERSITÉ PSL

Préparée à l'École Supérieure de Physique et de Chimie Industrielles de la Ville de Paris

Les émulsions Apolloniennes – la coalescence dans des émulsions à haut rapport de phase interne

Soutenue par
Yii-Wenn Sylvie KWOK
Le 13 décembre 2019

Ecole doctorale n° 388
Chimie Physique et Chimie Analytique de Paris-Centre

Spécialité
Physico-chimie

ESPCI PARIS PSL

Composition du jury :

Jean-François, JOANNY Professeur, Collège de France	*Président*
Sylvie, BEAUFILS Professeur, Université de Rennes 1	*Rapporteuse*
Emmanuelle, RIO Maître de conférence, Université Paris-Sud	*Rapporteuse*
Odile, AUBRUN Ingénieur de recherche, L'Oréal Recherche et Innovation	*Examinatrice*
Robert, BOTET Directeur de recherche, Université Paris-Sud	*Examinateur*
Bernard, CABANE Directeur de recherche émérite, ESPCI Paris	*Invité*
Jérôme, BIBETTE Professeur, ESPCI Paris	*Directeur de thèse*

To anyone who feels in over their heads:
Just try. And sleep well knowing that you gave it your best.

To the Giants on whose shoulders I stand:
Thank you for giving us what we know, and for paving the way so we can discover what we don't.

To my paternal grandmother who sat outside her village's school to listen in on lessons a hundred years ago because girls weren't given an education back then:
I hope I have done you proud.

Acknowledgements

First and foremost, I have to thank **Jérôme Bibette**, who welcomed me to his laboratory and always treated me with a lot of trust and good humour. This work also could not have been done without my supervisor, **Bernard Cabane**, who came out of emeritum and took me on as a protégée. I am honoured you both thought I was worth it, and I hope I haven't let you down. You taught me to work mindfully, to understand what each experiment was telling us instead of trying to produce what I was expecting (*"si l'expérience dit blanc, je dis blanc; si l'expérience dit noir, je dis noir"*), and to investigate how and why it differed from theory. Your methodical approach towards the unknown taught me to face challenges with courage and fearlessness; like the poster on my wall says, "Durch Mut und Unerschrockenheit erreicht man mit kleinen Mitteln grosse Zwecke" (Through courage and fearlessness, one achieves great purposes with small means). These are some of the most precious skills anyone could impart to me, so I thank you truly from the bottom of my soul for guiding and training me with such patience. I am equally grateful to **Robert Botet**, whose *maaaad* mathematical skills, brilliant intuitions, thoroughness and tremendous patience transformed our wildest ideas into sensible conjectures. You always listened to what I had to say whenever we discussed and made me feel validated by seeing in me what I couldn't see in myself. I couldn't have been in better hands.

I would also like to express gratitude to the following organisations for selecting our proposals and allocating us beam time to carry out the experiments that were integral to this dissertation. The infrastructure and personnel support I received during those arduous hours when I barely had time to sleep were truly excellent: **European Synchrotron Radiation Facility** (ID02 beamline); **Institut Laue-Langevin** (D11 beamline); **SOLEIL** (SWING beamline); **European Soft Matter Infrastructure** (**Lund University**, department of Physical Chemistry). I also have to thank the following organisations for their various forms of financial support: my employers, **DSO National Laboratories**, for awarding me a PhD scholarship; my school and lab **ESPCI LCMD**; and collaborators, **Saint-Gobain Recherche**.

Tusen tack, **Håkan Wennerström** (Lund University), for taking time to discuss our work with us in Lund and in Paris. Your simple encouragement to me to continue down this path in the early days of the work was very reassuring, especially at moments when I faltered. Similarly, I would like to thank **Ishi Talmon**, **Irina Davidovitch and Lucy Liberman** (Technion, Israel Institute of Technology) for taking an interest in Apollonian emulsions and doing their microscopy voodoo to produce absolutely breathtaking images of these structures. Until you managed to take such high-resolution pictures, there was always a small nagging voice in the back of my mind wondering if it was air bubbles that I had been studying instead. Many thanks also to **Anke Lindner** (PMMH, ESPCI) and **Frédéric Pignon** (LRP, Université Grenoble Alpes) for revisiting the basics of rheology with me. I had to teach other PhD students how to use a rheometer and they were floored by how much I knew, which I learnt from you.

Je tiens à remercier également: **Isabelle Borsenberger** and **Hélène Dodier** for helping me make administrative troubles go away; **Florence Condamine** for going above and beyond to manage the mess in the labs; my friends **Eren Ayata, Édouard Duliège, Jean-Baptiste Dupin**, **Klaus Eyer, Jairo Garnica, Rory Giles, Hojjat Madadi, Magda Rybczyńska, Andy Prokop** who showed me a lot of kindness; and in particular, **Abdul Shglabow**, who always went out of his way to help me, especially taking care of my cats when I had to travel for experiments. It gave me two fewer things to worry about during those intensely stressful times; and all colleagues from LCMD, past and present, who respected my boundaries and working style.

Anybody who has been through this process knows that it's no cake walk. It has at times taken a toll on my mental health, but I have been truly blessed to have so many generous friends who opened their homes to me and became my surrogate families: **Celie Fox-Cabane**, thank you for always looking out for me, teaching me to cope with my own feelings, to discover and to embrace myself. You and Bernard have done so much for me in the last few years, and I can only hope that my being in your lives has given you something back; la mia famiglia, **Laura, Riccardo e Marco Chetoni e Marina Bartalini**, who always have a room for me in their homes whenever I want. The affection you show me and the pride you feel about my smallest achievements are palpable, and I am very touched; similarly, my brother and sister, **Krzysztof Langer and Magda Widłak-Langer**, who let me escape to their little Swedish house, and taught me by example to lead a compassionate, mindful life; my Swiss-German family, **Luke and Gabriela Dunwell**, who always welcome me with so much warmth to their beautiful home; my friends out in Fontainebleau, **Dushan, Alison and Zoë Hanisko**, who support my musical endeavours with lots of enthusiasm, and give me somewhere to go breathe whenever I feel overwhelmed in Paris; **Dahlia and Ian Cochran**, living Down Under, thank you for being so giving, so supportive and so proud of me all these years.

I am thankful to my inexplicable fan club, a ragtag collection of friends living all over the world, who believe so much in me *all the time*, and care enough to let me know I'm on your minds. I don't know what good I've done to deserve having you in my life. (In alphabetical order so nobody gets jealous): **Philippe Bodin**, your ridiculously difficult *Motet* that I had to sing gave me something to focus on besides the very difficult time I was going through. Succeeding at it gave me back the strength to face other challenges. Thank you for being a listening ear and a great friend all around; the very talented **Maria Bundgård,** who is genuinely fascinated by my work with mayonnaise, so full of positivity and always put a smile on my face; the **Baba Yetu Chamber Gang**, it means a lot to me to know that I'm missed when you all get together. In particular **Fran Ho, Jonjon Macpherson, Keane Ong, JJ Pereira**, **Jamie Thom**, who check in on me and cheer me on. Most of all, **Sharanyaa de Laure**, you're a pure force for good and you bring so much light into my life. Thanks for enduring all my texts; Scanning Electron Microscope **Qëndrim Gashi,** thanks the spirited discussions and encouragements over Leibniz packings; **Reinaldo García, Mabel Gomez** and **Salomé Gutiérrez** who simply understand my soul, love me the way I am, and made me an honorary Latina; **Klára Lukášová** who genuinely cares about my well-being; **Thomas Manhart**, who has a lot of love for me and just understands; **Zainal Mantaha and Jennifer Cheng,** who have been quietly looking out for me with great kindness, and whom I can tell are proud of me even if Zainal insists I'm a nerd; **Alessandra Meoni,** la mia gemella who makef me lavgh and brightenf my fhitty day; **Yana Pesheva**, a loving princess who is always sweet and supportive towards me. I wish we could have spent more time together; **Shannon Rennie** who is always there for me, all the way in Canada, when I need someone to talk to. Thank you for your patience and always trying to save me from myself with your wise advice; **Ingrid Vallée**, my oldest friend here in Paris, who has seen me through the good, the bad and the ugly. And to anyone else who has ever treated me with kindness, please know that you also have my gratitude.

Last but not least, I thank my own **Kwok** family for understanding why I need to do this so far from home. I am sorry I haven't been around, and I'm sorry you haven't had a chance to see the person I've become. I hope you will be proud of me. To my "other" **Lim** family, thank you for always believing in my dreams. And finally, to my long-suffering flatmates, **Célestine and Giovanni**, who are illiterate and therefore will never read this, I love you too my darlings, but please stop making caca on my bed because I'm not home enough. I work hard to give you the idyllic life you deserve.

"Two roads diverged in a wood, and I—
I took the one less traveled by,
And that has made all the difference."

- Robert Frost (1916)

Apollonian Emulsions

Coalescence in High Internal-Phase-Ratio Emulsions

Table of contents

1. Introduction

In *Science: Abridged Beyond the Point of Usefulness (2017)*, cartoonist Zach Weiner satirically summarized the history of Physics as:

> "Aristotle said a bunch of stuff that was wrong. Galileo and Newton fixed things up. Then Einstein broke everything again. Now, we've basically got it all worked out, except for small stuff, big stuff, hot stuff, cold stuff, fast stuff, heavy stuff, dark stuff, turbulence and the concept of time".[1]

In this dissertation, I will be presenting our attempt at trying to figure out how a mixture of "small stuff" and "big stuff" behaves. I use the collective pronoun "we" throughout this work because it was not just my effort alone. We took a particular interest in a peculiar structure known as an Apollonian packing, where all available space is filled with increasingly smaller non-overlapping spheres by putting them in voids formed by larger existing spheres. This elegant mathematical concept has fascinated scholars for the last 2200 years – from its namesake, Apollonius of Perga (2nd century BC) to Mandelbrot (20th century AD), passing through the hands (and minds) of some of the most celebrated personalities in the scientific pantheon in between. It was a widely held belief that such a structure would only exist in theory, never to be made or encountered in real life, because an "infinitely infinite number of spheres" (Soddy, 1937) with an infinitely-wide range of sizes would be necessary to construct it. And so, it was with a great amount of serendipity that we stumbled upon a very simple way to create an Apollonian packing with minimal effort… just because I was laughably terrible at making mayonnaise (Figure 1). As Newton put it, "truth is ever to be found in simplicity".

Figure 1: a scene from the oil painting "Netherlandish Proverbs" by Dutch and Flemish Renaissance maestro, Pieter Bruegel the Elder (1559),[2] uncannily foretelling my reaction 460 years later when I made a mayonnaise that flowed and had to explain to my supervisor why it was not a failure. Note: the scene actually depicts the proverb "He who has spilt his porridge cannot scrape it all up again" or "There is no use crying over spilled milk".

Most of us are familiar with the condiment, mayonnaise. Some people even inexplicably adore it, so much so that supermarkets have shelves full of it. But talk to any serious chef and one can sense the romanticism attached to the savoir-faire of making this plain, old, boring, whitish yellowish stuff from scratch, *ideally by hand*, with oil, egg yolks and lemon juice. (I admit at this point my personal animosity towards mayonnaise because my kindergarten teacher used to ruin perfectly good fruit salads with it). The key to making mayonnaise is adding oil slowly under constant whisking, until all

oil has been perfectly incorporated. The criterion for a successful mayonnaise is its thick, non-flowing texture. Until now, that is, for we will be demonstrating in this work that a flowing mayonnaise is far more interesting than the banal non-flowing sort: a flowing mayonnaise is an example of the mythical Apollonian packing.

"*Pfft! A flowing mayonnaise isn't anything new. They already sell them in squeeze bottles in the supermarket,"* scowled the cynical reader dismissively. True, but take a look at the list of ingredients and we will likely find "Xanthan gum", a shear-thinning viscosifying agent whose role is to thicken and keep the product from separating under gravity while at rest, and facilitating flow should one squeeze the bottle. In other words, the supermarket stuff flows because Big Food companies added something to help it do that. It is just not the same.

"So did you really study mayonnaise for 4 years?" Not exactly. What I have been referring to as mayonnaise is but a common example of a high internal-phase-ratio emulsion (HIPE) (if I had opened with this ten-syllable double-hyphenated mouthful, I would probably have not been able to pique your interest and lure you in). An emulsion is a mixture of two immiscible liquids, often oil and water, that is stabilized with surfactants. If we consider an oil-in-water emulsion, we have oil droplets (internal phase) whose surfaces are protected by surfactant molecules, and these droplets are dispersed in an outer continuous phase made of water. Given enough time, an emulsion will fail (or break), because the domains of the two liquids naturally want to separate from one another under the effect of intermolecular forces such as Van der Waals attractions. The process by which this happens is through coalescence – oil droplets will collide with one another every now and then and fuse into a larger one, and with repeated coalescence, the emulsion ends in macroscopic phase separation. Ostwald ripening is another way by which an emulsion can fail – this is when the two liquid phases are partially soluble in each other. Smaller droplets of oil can then dissolve in water and migrate through it to feed and grow larger droplets of oil. We will not be considering Ostwald ripening here, because we have chosen a heavy mineral oil that is very insoluble in water.

A HIPE is a special type of emulsion where we keep the oil-in-water topology, but the total amount of oil exceeds the total amount of water. Mayonnaise recipes always stress the importance of adding oil slowly, because we have to induce the aqueous phase (the egg yolk) to accommodate more oil than it would "like" to hold. In the final product, there are so many oil droplets forced into the little amount of outer aqueous phase that they are squeezed up against one another and deformed into polyhedrons. The surfactant films protecting each oil droplet then become flat thin films separating the polyhedrons (in a mayonnaise, egg proteins are the surfactants, and their separating power is heightened because lemon juice donates OH^- ions to the proteins). The result of this oil droplet deformation and the presence of flat films is a resistance against flow. Naturally, the lifespan of a HIPE depends on how robust these protective surfactant films are, which is why people studying such structures have always used large quantities of surfactants to prevent coalescence. We have provided a brief summary of work done on these surfactant-rich, solid-like HIPEs in section "2.1 High Internal-Phase-Ratio Emulsions (HIPEs)".

Coalescence is generally considered a nuisance when it comes to emulsions. It is then somewhat unthinkable that we should allow it to happen in a crowded, precariously out-of-equilibrium structure like a HIPE, by not putting enough protective surfactants. Surely the HIPE will rapidly break and invert into a water-in-oil flowing mixture, the layman's criterion for judging that a mayonnaise

has failed? This is where we demonstrate that, on the contrary, by allowing *some* coalescence to happen in a HIPE, the oil droplets will spontaneously evolve and arrange themselves into an Apollonian packing. As stated in the opening paragraph of this introduction, minimal effort. In section "3. Materials and methods for HIPEs", we share our "mayonnaise" recipe (try this at home but do not eat it) and introduce characterization techniques that we used throughout the course of our work.

In section "4.1 Macroscopic behaviour of a HIPE vs. its composition", we present the major observable differences between conventional surfactant-rich HIPEs and our surfactant-poor variant. We subsequently provide conclusive experimental evidence in section "4.2 Evolution of liquid HIPEs" that these surfactant-poor HIPEs indeed possess the elusive Apollonian packing. Based on our experimental results, we believe that the structure develops through a mechanism that we have named coalescence-fragmentation. This mechanism is considerably different from typical coalescence in that it entails the creation of many small droplets. The next section "4.3 Discussions on Apollonian HIPEs" is dedicated to discussing coalescence-fragmentation, first through numerical simulations, then by examining its compatibility with thermodynamic considerations particular to HIPEs. Finally, in section "5. Suggestions for applications of Apollonian HIPEs", we propose several ways in which the space-filling structure of Apollonian packings can be used in materials fabrication and pharmaceutical sciences for the prolonged release of therapeutic molecules.

And so it is through 4 years of studying "mayonnaise" that I hope to have made a modest contribution towards figuring out how some of the "small stuff" and "big stuff" get together. Newton wrote, "To explain all nature is too difficult a task for any one [wo]man or even for any one age. 'Tis much better to do a little with certainty, and leave the rest for others that come after". Indeed, that we should – through blind luck, no less – materialize an Apollonian packing structure on which he and so many other brilliant minds philosophized over the course of the last two millennia, "if [we] have seen further it is by standing on ye shoulders of Giants."

2. Literature review

2.1 High Internal-Phase-Ratio Emulsions (HIPEs)

2.1.1 The earliest HIPEs

An emulsion consists of an ensemble of droplets, filled with a liquid and dispersed in another non-miscible liquid. The former is known as the internal phase while the latter is called the continuous phase. The rheological properties of the emulsion are largely determined by the volume fraction of the internal phase, ϕ, in the system. At low values of ϕ, emulsions generally behave and flow like the prevailing continuous phase. As ϕ increases, internal-phase domains get in the way of one another, and the emulsion may acquire a resistance to flow and become increasingly solid-like. Remarkably, this flow behaviour was reported by Pickering as early as 1907, in oil-in-water emulsions stabilised with soap:

> "An ordinary emulsion, although containing 70 to 80 per cent of mobile paraffin oil, is as viscid as thick cream, and its viscidity increases with the proportion of oil present… With very high percentages of oil, the emulsion becomes practically solid, resembling a blancmange. Emulsions containing as much as 99 per cent of… oil have been made, the remaining… being a 1 per cent solution of soap."[3]

Although casually qualified as "ordinary" in his article, these emulsions that Pickering described were far from it. He had succeeded in formulating high internal-phase-ratio emulsions (HIPEs) without inverting the emulsion topology. **Modern convention now defines HIPE as an emulsion in which ϕ exceeds 0.74**, the densest close-packing factor in a monodisperse system of spheres (Ostwald, 1910)[4]. Keeping in mind that the first emulsifier was produced only two decades later[5], Pickering's success with HIPEs up to ϕ = 0.99 was all the more impressive. He further noted that "such strong emulsions, however, cannot be obtained directly; they must be made by taking a weaker emulsion, and gradually increasing the [oil] in it, churning it after each addition." While he made no explicit allusion to it, we now know that this prescribed protocol of slowly adding internal phase under constant mixing is in fact the age-old method (or at least it was formalized in 1820 in a French recipe book "Le Cuisinier Royal") for making mayonnaise[6], an oil-in-water HIPE stabilised by proteins and lecithin in egg yolks. The 21-page paper then went on to explore the nature of oil and of emulsifiers on the formulation's stability and properties. Experimentation at the time was limited to visual inspection, or at best observation under an optical microscope, and thus explanations were deductive and qualitative. Nonetheless, Pickering noted several more very interesting observations which we shall come back to later:

- His emulsions were semi-solid and liquefied quickly when exposed to dry air but not to moist air.
- The emulsions contained a transparent jelly, also void of observable structure, but very stable and instantly turned opaque upon contact with water, giving a milky emulsion.

On a side note, Pickering described in this same paper emulsions that would later be named after him: internal-phase droplets stabilised by solid particles at their interfaces.

Between the 1930s and 1950s, surfactant science had considerably progressed and more emulsifiers were being produced. For instance, in the food science industry, synthetic emulsifiers such as mono- and diglycerides began to find their foothold in the production of margarine[7]. Elsewhere, the role of surfactants in interfacial physics was driven by military applications during the Second World War and its immediate aftermath, notably and unfortunately in the field of chemical warfare agents and their effects on lung alveoli[8]. This leap forward meant that emulsifiers were more readily available, allowing for the formulation of more metastable emulsions.

2.1.2 The internal structure of a HIPE

2.1.2.1 How is space filled?

There are two routes that can lead to high internal-phase ratios. The first uses a broad distribution of droplet sizes to fill space, whereas the second takes advantage of the deformability of liquid droplets to achieve the same goal. It would appear that empirical literature published before the 60s, including the earlier-cited paper by Pickering, *assumed* the first approach: that droplets remained spherical and therefore necessarily had to resort to polydispersity to fill space. Adopting this premise is understandable due to technological limitations at the time; it might be that deforming spherical droplets was unfathomable simply because it had not been observed before. Indeed, electron microscopy images of polyhedral emulsion droplets (Figure 2) were only published in 1965 by Groves and Scarlett in *Nature* and they cited just two earlier – albeit somewhat obscure – works that observed the same: a German book titled "Emulsionen" by Manegold (1952) and an English PhD thesis by Phipps (1963).

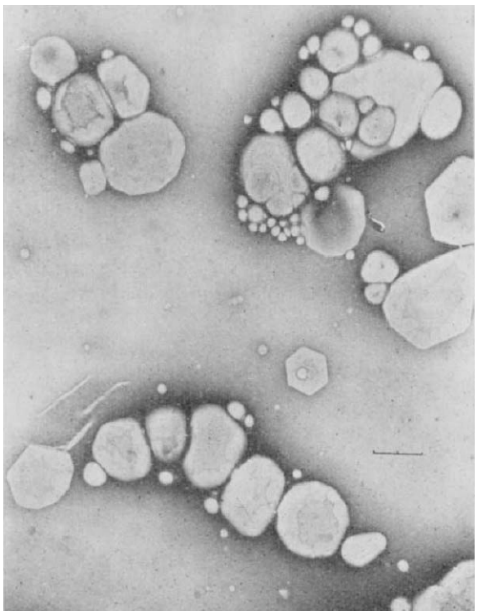

Figure 2: electron microscopy image of polyhedral emulsion droplets (Groves and Scarlett, 1965).[9]

We note here that Groves and Scarlett were working with emulsions at $\phi = 0.225$ and showed that local clustering of spherical droplets could lead to deformation that gave polyhedral emulsion droplets. They further wrote that Manegold "described the formation of honeycomb or 'polyhedral drop foams' in unstable close-packed emulsions with disperse phase ratios in excess of 0.74"[9]. This would be the first-known instance of a HIPE that exploited the second approach of droplet deformation to fill space.

2.1.2.2 HIPE droplet geometry

By 1966, thanks to advances in surfactant chemistry, and armed with the idea that deforming spherical droplets into polyhedral ones was possible, Lissant would revisit HIPEs and undertake the task of extensively describing droplet geometry in his formulations[10]. He focused primarily on the second approach of liquid droplet deformability, beginning with a strictly monodisperse population (in practice, we may qualify a population as "monodisperse" by convention if the largest droplet is no more than ten times bigger than the smallest one). From a purely geometrical standpoint, Lissant argued that droplets remained spherical and may rearrange themselves up to $\phi = 0.74$, the close-packing limit. Beyond 0.74, the spherical droplets undergo deformation and adopt two types of packing possible: rhomboidal dodecahedral (RDH) packing between $\phi = 0.74$ and 0.94 (Figure 3), and tetrakaidecahedral (TKDH) packing for $\phi > 0.94$ (Figure 4) because it requires less angular distortion, giving greater geometrical stability. In both cases, the distorted droplets are effectively gridlocked: they are all in direct contact while the continuous phase exists as flat thin films in-between, meeting at Plateau borders[11,12] (Figure 5).

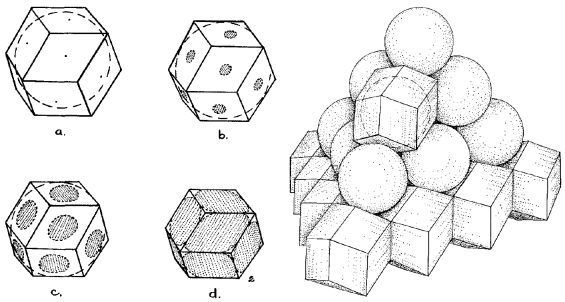

Figure 3: deforming a sphere into a rhomboidal dodecahedron (a to d) and its subsequent packing.[10]

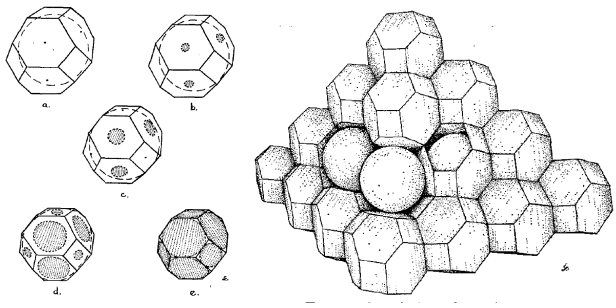

Figure 4: deforming a sphere into a tetrakaidecahedron (a to e) and its subsequent packing.[10]

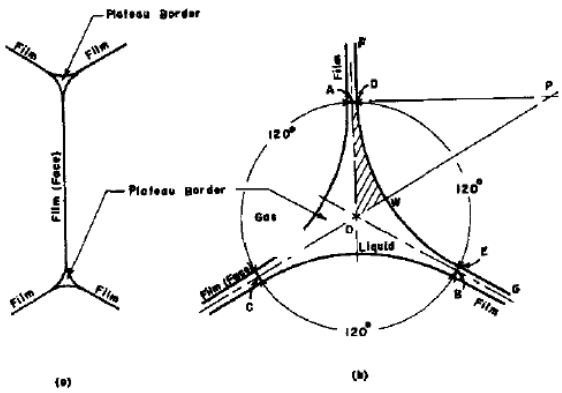

Figure 5: drawing of a Plateau border[12]**: (a) three flat films meet at 120°; (b) zoom-in of the Plateau border.**

2.1.3 Linking the macroscopic properties of a HIPE with its microscopic structure

2.1.3.1. Flow behaviour

In the same paper, Lissant described the preparation of oil-in-water HIPE using the mayonnaise method. The continuous phase was a 14% (v/v) aqueous solution of non-ionic surfactant and the internal phase was paraffinic mineral oil (kerosene). He found that the yield stress of his HIPEs increased as ϕ approaches ever closer to unity[10]. In fact, Lissant subsequently extended his geometrical musings to emulsions of lower internal-phase ratios, stating that monodisperse emulsions were expected to begin exhibiting non-Newtonian flow at ϕ = 0.52 due to droplets having to deform when moving past one another, and it was empirically found to be the case[13]. Qualitatively, we may understand the origin of a HIPE's gel-like behaviour and resistance to flow as such: displacing a gridlocked droplet requires deforming it further through stretching, and this action is opposed by the tension in the surfactant thin films separating the droplets. Lissant's comprehensive description on internal-phase droplet geometry paved the way for establishing and quantifying the relationship between macroscopic flow behaviours of HIPEs and their microscopic structures through rheological studies conducted by Princen et al. in the 1980s.

Not only did Princen theoretically formulate equation of states for film structures in HIPEs[11,14–17], extensive experimental work spanning nearly the entire decade allowed him and his team to verify these equations and/or draw empirical relationships linking hydrodynamic and thermodynamic parameters with HIPE characteristics, such as ϕ, droplet size, interfacial tension and contact angle.[12,17] Princen began by re-examining the mathematics behind packing structures and supported Lissant's assertion of RDH packing for ϕ up to 0.96[15]. However, in addition to using the mayonnaise method[17,19] for their experiments, they also innovatively made use of creaming and sedimentation – either by gravity or by centrifuging[14,15] – to further concentrate their HIPEs and attain even higher ϕ by draining continuous phase from the Plateau borders where they are primarily found.[20,21] Creaming was bound to occur in the emulsions due to density differences between the two liquid phases. If the interfaces were well stabilised by surfactant molecules, then the dispersed-phase droplets could be physically concentrated in the cream without undergoing coalescence events. Using this method, it would be possible to attain even ϕ = 0.99[18,22–24]. Physically, this translates into the thinning of Plateau borders which eventually lead to their collapse at ϕ > 0.964 and a measurable contact angle between the surfactant films. Taking into account these additional geometrical constraints, Princen et al. concluded that the regular pentagonal dodecahedron (RPD) (Figure 6) packing was more likely than TKDH at such high values of ϕ. Incidentally, this RPD geometry was also the model put forward by Manegold in *Emulsionen* (1952).[15] We note here that packing with long-range order has been found to be incompatible with five-fold symmetry.

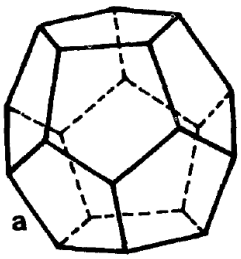

Figure 6: a regular pentagonal dodecahedron, an alternative geometry for spherical droplet deformation when ϕ exceeds 0.964.[15]

The group subsequently investigated the rheological properties of HIPEs as a function of HIPE droplet geometry.[17,18,20,25] By thinning and draining the Plateau borders where most of the continuous phase was found, their contributions to mechanical properties of HIPEs could be discounted, and a clearer link between the macroscopic measurable properties could be drawn with those of the surfactant thin films separating internal-phase droplets. Key results from the group's exploits are summarized below (non-exhaustively):

- Yield stress and storage modulus G' increase with internal volume fraction ϕ, interfacial tension and decrease with droplet size.[17,20,25]
- Yield stress of the HIPE increases with surfactant film thickness.[20]

2.1.3.2. HIPE stability

Coalescence

Several interesting observations were also made during their rheological experiments on the stability of HIPEs. Plastic containers and instruments were reported to incite oil droplet coalescence at walls.[20,25] Mechanical strain exerted on the HIPE was also observed to break the emulsion: when subjected to shear or flow, the thin films became depleted of surfactant molecules. Diffusion of surfactant from within the films or from Plateau borders being too slow to repair these flaws[26], interfacial tension rose and led to emulsion instability.[20] However, this view of rising interfacial tension resulting in instability rising has since been questioned.

Dilution

Pickering had previously observed that his gel-like oil-in-water HIPE readily dissolved in water to give a milky emulsion. Princen would observe the same. He introduced the notion of "compression" applied to HIPE: if the concentrated emulsion was allowed to be at equilibrium with bulk continuous phase, then it would be considered "uncompressed". Therefore by his reckoning, the mayonnaise method would give "compressed" emulsions because there was no excess bulk continuous phase. He advised that a practical way to differentiate the two types would be to add some excess continuous phase to a HIPE – if it is absorbed by the HIPE then said HIPE is compressed.[15] Clearly then, the ease of dilution that Pickering had observed with his jelly samples indicated that he had compressed HIPEs. Princen explained this affinity towards dilution in terms of osmotic pressure in the HIPE; allowing more continuous phase to enter the HIPE's interdroplet regions would relieve this osmotic pressure[14,20] and counter the Laplace pressure that distorted the droplets[24], allowing them to relax and return to their original spherical shape. Princen and Kiss also observed that a HIPE was stable when diluted by the constituent continuous phase, showing no signs of coalescence nor ripening over a period of 4 weeks. Interfacial tension was also found to remain constant.[17,20] This was to be expected since the diluting medium contained the same surfactant concentration as the continuous phase and so the surfactant's chemical potential should remain constant.

2.1.4 The physical chemistry of HIPEs

Clearly, there was a link between the rheological and thermodynamic properties of HIPEs and their microscopic structure. Mason et al. would continue work in this direction with monodisperse HIPEs in the 1990s. Theoretical reasoning had, until then, been resolved largely in a two-dimensional plane. Thanks to numerical simulations, Mason et al. could now develop three-dimensional models that took into account droplet positions and repulsions, and formulate equations of state based on these models. Compared with empirical measurements, their models for osmotic pressure and rheological

properties (storage modulus, yield stress) as a function of ϕ appeared to describe reality fairly well.[24,27,28] They used polymer dialysis to impose a very high osmotic pressure on a HIPE by drawing out as much continuous phase as possible, a clever experimental technique invented by Parsegian et al. (1986)[29], thereby further concentrating it more than even centrifugation creaming could (Figure 7).

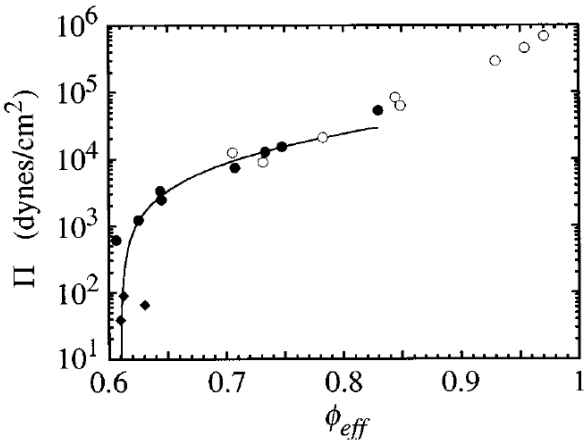

Figure 7: osmotic pressure in a concentrated emulsion obtained with different compression techniques – gravitational creaming (diamonds); centrifugal creaming (solid circles); polymer dialysis (blank circles).[24]

Mason et al. would also go on to perform neutron scattering on monodisperse concentrated nanoemulsions to gain insight on the in-situ organisation of droplets as a function of ϕ.[30,31] Although the emulsions were prepared only up until ϕ = 0.72 and therefore not strictly HIPE, evidence suggesting droplet deformation as ϕ approached the close-packing limit was found. This set of experiments was – to quote the authors – "strategic", as conventional light scattering methods would require dilution of the HIPEs in order to avoid multiple scattering, whereas here the concentrated emulsions could be studied as is. This would inspire us to use X-ray and neutron scattering to study our HIPEs. We note here that another way to avoid multiple scattering would be to match the refractive index of the emulsion to the solvent[32].

2.1.5 Practical uses of a HIPE

2.1.5.1 Controlling the droplet-size distribution

Fundamental research on HIPE geometry and properties appeared to wane towards the end of 1990s and attention shifted to the conditions surrounding the emulsification process.

Mason and Bibette would discover that a polydisperse concentrated emulsion crudely prepared by the mayonnaise method could be made highly monodisperse through shear rupturing[33–36] (Figure 8). The continuous phase had to be viscoelastic enough to delay the onset of capillary instability, allowing the internal liquid stream to be stretched for a longer period before breaking up into droplets of more or less equal sizes. The viscoelastic property of the continuous phase was conferred by solubilizing large amounts of non-ionic surfactant, up to 40%. It was also determined that a high internal volume fraction significantly raised the effective viscosity of the HIPE[35]. Therefore, shear rupturing behaviour depended on the effective viscosity in the medium, rather than just the rheology of the continuous phase (Figure 9). These results overturned earlier rheological studies conducted by Schwartz and Princen who maintained that the dispersed phase's viscosity had negligible effect on the overall behaviour[21].

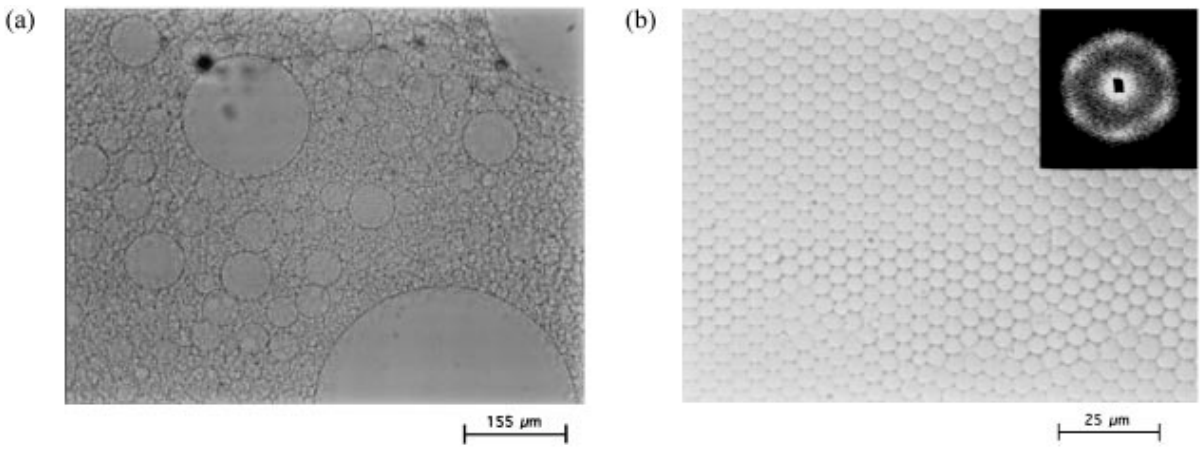

Figure 8: (a) the polydispersity of a concentrated emulsion prepared by the mayonnaise method is greatly refined into a monodisperse population (b) through shear rupturing. The periodicity (or space invariance) of the resulting HIPE is demonstrated by the small-angle light scattering spectra displaying six bright Bragg spots as shown in the inset.[33]

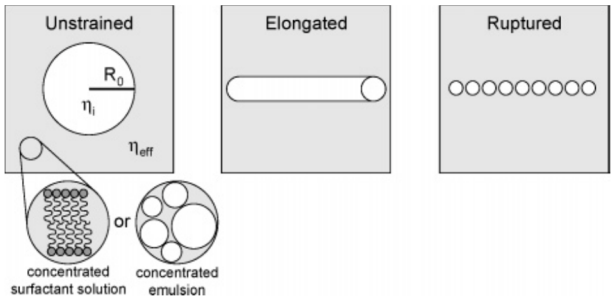

Figure 9: shear rupturing of a single droplet in a viscoelastic continuous phase. The viscoelastic character is obtained either by solubilizing large amounts of surfactant, or by considering the effective viscosity of other droplets, especially in a HIPE.[37]

As previously mentioned, modern HIPE research was focused on the monodisperse variant and obtaining emulsions of controlled sizes was especially enticing especially for industrial applications. This penchant was fulfilled by the invention of the Couette Injection Mixer[38] (Figure 10) which enabled a high-throughput means of production.

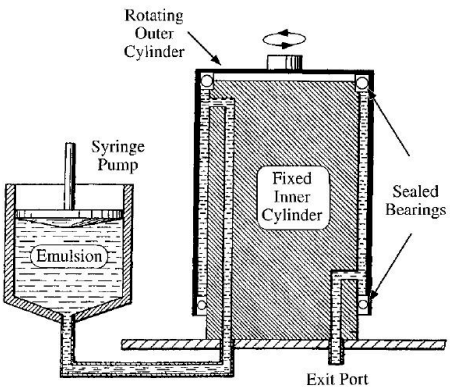

Schematic diagram of an injection couette shear mixer. The premixed emulsion, contained initially in the syringe, is pumped into the thin gap between the outer rotating and inner fixed cylinders. Sealed bearings prevent the sheared emulsion from escaping out the ends and force it to leave through the exit port.

Figure 10: the Couette injection mixer for producing highly monodisperse emulsions, based on the shear rupturing principle as described by Mason and Bibette.[35]

2.1.5.2 Emulsifying viscous oils

Repeated observations in the domain of colloidal sciences holds that efficient emulsification cannot take place if the viscosity of the internal phase exceeds 3.5 times that of the external phase due to poor mixing (Grace, 1982).[39] To overcome this problem, we may exploit the increased effective viscosity by working at higher internal-phase ratios. In the 2000s, making HIPEs was shown to be a practical way of emulsifying viscous silicone oils[36,40], with the most extreme example sitting pretty at 300 Pa.s[37]. All the HIPEs thus made were of the monodisperse variant. Tcholakova et al. (2011) also found that the oil's viscosity did not have much influence on the droplet-size distribution in HIPEs beyond $\phi > 0.8$[40].

2.1.6. Making a HIPE: choosing a surfactant

We have already noted that HIPEs could be fabricated either by the mayonnaise method[3,10,17,19,33,35] or by creaming under gravity or centrifugation[15,22–24,27,30,34] an already concentrated emulsion, or even a combination of both[41]. Regardless of protocols, it was frequently emphasized in literature that the choice of surfactant was crucial.

The surfactants commonly used were either non-ionic[10] (alcohol ethoxylates[19], sorbitan esters[41], fatty acid glycerides[41], polyoxyethylene alkyl/phenyl ether[33,35–37,40,41], polyoxyethylene fatty alcohol[41], polyvinyl alcohol[40]), solubilised at around 7-30% in the continuous phase, or anionic (sodium dodecyl sulfate[15,17,22,24,27,30,34], fatty acid salt or soap[3,15], ammonium alkyl ether sulfate[19], sodium lauryl ether sulfate[37]) typically solubilised at 0.2-2% in the continuous phase. The nature of surfactant necessary depends on the HIPE topology desired – direct (oil-in-water) or inverse (water-in-oil). Lissant stressed the importance of beginning with the right internal phase[10], and to ensure that this liquid stayed the internal phase even as more is gradually added, the Bancroft rule needs to be followed: the continuous phase of the HIPE will be the one favoured by the surfactant[26]. Kabalnov and Wennerström (1996) would later interpret and explain Bancroft's rule through physical processes.

2.1.6.1 Non-ionic surfactants

Temperature is an additional consideration when working with non-ionic polyoxyethylene surfactants for there is a Phase Inversion Temperature (PIT), intrinsic to each surfactant, at which the surfactant attains its spontaneous curvature, $H_0 = 1/R_0$, where R_0 is the radius of a micelle. PIT increases as the hydrophilic chain length increases.[42] At temperatures below the PIT, the curvature of the surfactant, H is positive and $H \gg H_0$. Then, should a pore spontaneously nucleate between two oil droplets, the surfactant monolayer situated at the pore acquires a high curvature energy and linear tension (Kabalnov and Wennerström, 1996)[26]. The nucleated pore is consequently energetically unstable and closes up (Figure 11), ensuring that the emulsions obtained are oil-in-water.

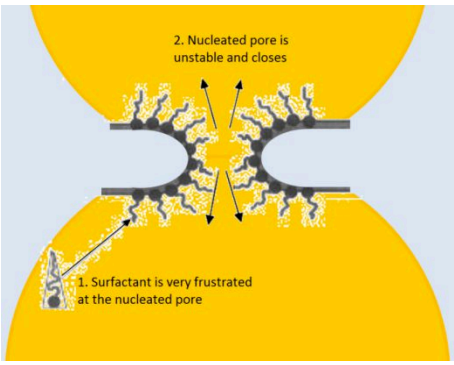

Figure 11: depiction of surfactant monolayer frustration should a pore open between two oil droplets. The curvature of the surfactant at the pore is very high and therefore the pore is energetically unstable and closes back up. Figure adapted from Kabalnov and Wennerström (1996)[26].

The amount of surfactant to use depends then on the nature of the surfactant. Non-ionic surfactants form a protective monolayer around dispersed-phase droplets, preventing sterically any coalescence events when two droplets meet.[26,43,44] If we consider that a non-ionic surfactant molecule occupies about 50Å^2 in area[45], to fully saturate every dispersed-phase droplet surface at just $\phi = 0.74$, we would require a minimum surfactant concentration of 1-10% in the continuous phase (for dispersed droplets 1µm and 100nm in size respectively, supposing they are monodisperse: the smaller the dispersed droplets the more surface area there is to cover).

2.1.6.2 Ionic surfactants

On the other hand, ionic surfactants do not have to saturate a droplet's surface in order to protect it. Electrostatic repulsion[22,34,46] from the adsorbed ionic surfactant molecules prevent droplets from coming into close contact with each other, and the repulsion acts over a distance known as the Debye length, typically around 10nm[47]. The Debye length is inversely proportional to the square-root of ionic strength of the medium. Given that the ionic strength depends on the concentration of all charged species present, the Debye length is shorter if the concentration of charges is higher. Hence, we want to put as little ionic surfactant as possible in the system, but not too little: in the event where droplets do collide with each other, either due to Brownian motion or mechanical agitation, surfactant molecules can be knocked off and we want to have just enough surfactant in the system so that these molecules can quickly diffuse to readsorb onto the droplet surface. Surfaces of freshly created droplets may also be protected by a Marangoni effect as described by Taisne, Walstra and Cabane (1996)[48]. The CMCs of common anionic surfactants are usually in the range of 0.1-1% (w/w)[49,50], with that of SDS at 0.23%[22].

2.1.7 Current applications

2.1.7.1 Safety fuel

Since HIPEs pack an exceedingly high amount of one phase into another immiscible phase, they have found their use in applications that require maximum active ingredient efficiency per unit volume of formulation. A notable example is a gel-like safety fuel, where jet engine fuel was the dispersed phase and formamide – a hydrophilic organic liquid – the continuous, stabilised with a mixture of non-ionic surfactants. This was first published in 1968 by Nixon and Beerbower.[51] The HIPE was observed under microscope to have polyhedral deformed droplets.

2.1.7.2 Oil recovery

HIPEs have also been used as fracturing fluids in oil recovery, as described in the presently-active patents.[52–54] Fracturing fluid are typically highly viscous, either oil-based or water-based thickened with cross-linking polymers. The fluid is pumped underground into rock formations, delivering large suspended solid particles into cracks that would then keep the fractures open. However, subterranean heat causes the fluids to lose their viscosity, thereby reducing their rock-fracturing efficiency. Polymer thickeners may also be left behind in the cracks. The first HIPEs proposed for this application were oil-in-water, and exploited a HIPE's high viscosity as a result of the gridlocking of deformed oil droplets up to $\phi = 0.8$.[52] The fracturing fluid was then removed by breaking the emulsion; either by adding a demulsifier or by stabilising the HIPE fracturing fluid with cationic surfactant that would adsorb onto the rock wall underground. Non-ionic surfactants (1-6% in the continuous phase) were later proposed as an alternative: by choosing surfactants with PITs close to the ambient temperature in the rock formation, the HIPE would invert when thermally equilibrated with its surroundings, and turn into a fluid easy to remove.[53] A later innovation would propose using

an inverse HIPE in order to reduce costs associated with the large amount of oil necessary to formulate a direct HIPE. Using an inverse HIPE was also purportedly more eco-friendly as it did not leave behind polymer residues in the rock formation.[54]

2.1.7.3 Emulsion templating

More recent applications of HIPEs are in polymer synthesis, specifically in a process known as emulsion templating.[55] If the polymerisable species is present only in the continuous phase, then after polymerisation and removal of the internal phase, only the interconnected network of continuous films and Plateau borders would be left (Figure 12). The result is a highly porous material known as a polyHIPE.[51] It was also found that the amount of surfactant stabilising the interfaces played a role in the final structure of the polyHIPE. Similarly, high density, low-porosity materials such as latex can also be obtained if the polymerisable species is found instead in the dispersed phase (Figure 13).[56] Finally, if both phases are polymerised, a composite material would be the final product.[57] The advantage of this process is that nanosized porosities can be achieved, so long as the HIPE droplet sizes are well-controlled.

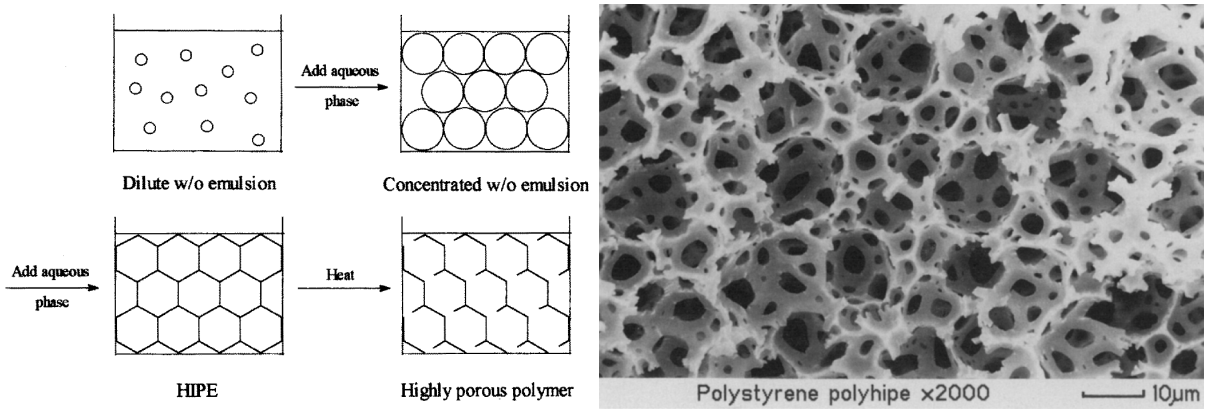

Figure 12: (left) figure showing the polymerisation process a polyHIPE; (right) a Scanning Electron Microscope photo of a poly(styrene/divinylbenzene) polyHIPE.[51]

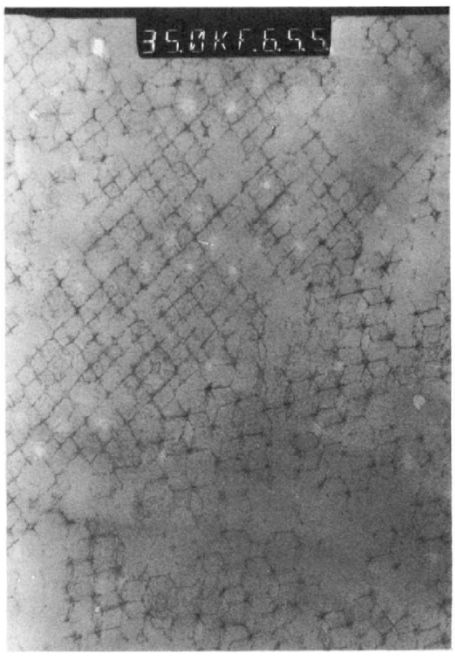

Figure 13: transmission electron microscope image of a dense latex film displaying a foam structure after water (the solvent) was removed.[56]

2.1.8 Future explorations

Filling space with scale invariance

Although Princen would regularly evoke "polydispersity" as a reason for real systems' deviation from predicted theoretical values, we should note that his definition meant "not strictly monodisperse" and the emulsions that he studied could have been considered practically monodisperse. Indeed, contrary to pre-Lissant pioneers in the field who rather believed that they had very polydisperse droplet populations on hand, neither Lissant nor Princen thought it practically feasible to fill space in this manner:

> "It can be argued that polydisperse systems can arrange so that the droplets need not be distorted. In order for this to occur at internal phase ratios above 90%, the emulsion would have to be extremely polydisperse. Experimental determinations of particle size distributions do not show this extreme polydispersity. Experimental evidence seems to show that, on aging, the [HIPEs] tend toward monodispersity… Remembering also that the smaller droplets, having a shorter radius of curvature… will probably have more difficulty in maintaining a coherent film on the more curved surfaces… It seems clear then that **although, theoretically, highly polydispersed configurations can be used to achieve [HIPEs], they would require significantly higher inputs of energy to produce**" – Lissant, 1970.[13]

> "When the emulsion is strongly heterodisperse (preferably multimodal with each size group being monodisperse and of a particular size relative to the next mode), the interstices between the spherical droplets can be filled successively by smaller ones. This would, in principle, allow ϕ to closely approach unity. In practice, **this peculiar kind of heterodispersity will rarely, if ever, be encountered**" – Princen, 1979.[14]

Perhaps it is this dogma, and the neater idea of working with a monodisperse population of droplets that would lead modern research in HIPEs to focus primarily on the Lissant-approach of filling space with tessellating deformed droplets. Little attention has been devoted in colloidal literature to *truly* polydisperse HIPEs possessing the "peculiar" type of polydispersity required to fill all available space. This type of packing is what is mathematically known as an Apollonian packing of spheres[58–60] (Figure 14). Indeed, polydispersity in HIPEs would fall by the wayside in soft matter research, a phenomenon that researchers sought to eliminate in favour of monodispersity that seemed to possess a Holy Grail status in the community.

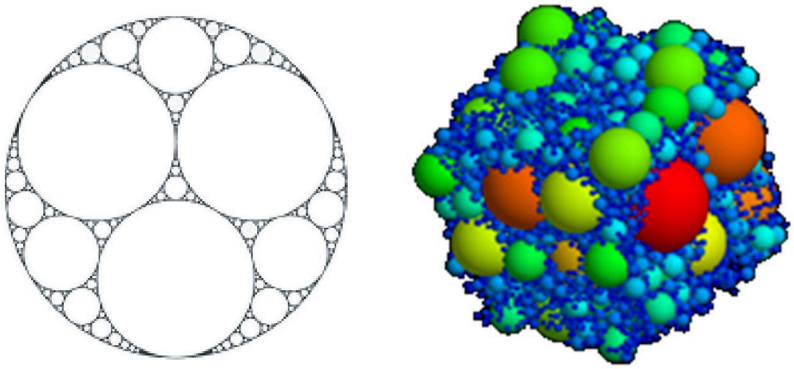

Figure 14: (left) a two-dimensional view of an Apollonian gasket[61]; (right) a three-dimensional numerically simulated Apollonian packing[62].

Yet, in spite of prevailing sentiments towards polydispersity, and most of all, in spite of Princen's claim that this sort of space-filling size distribution will rarely be encountered, we have found a very reproducible way to make precisely such extremely polydisperse oil-in-water HIPE. By greatly reducing the quantity of surfactant in the continuous phase, and thanks to centuries-old mayonnaise recipe, we have repeatedly found that our HIPEs self-assembled into an Apollonian packing of droplets. The study of these emulsions and their properties is the focal point of this present dissertation.

2.2 Apollonian packing of spheres

2.2.1 A timeless problem

Apollonius of Perga was an ancient Greek geometer who lived around 200BC.[63] He was reportedly the first to describe and solve the problem of filling a Euclidian plane with co-tangent circles. This mathematical solution was published in a book named *Tangencies*, now lost to us in the sands of time. It was Pappus of Alexandria, who lived half a millennia later, who would review Apollonius' work in Book IV of his *Collection*[64], thereby preserving the memory of its existence and the premise of the geometrical problem.

Apollonius' problem has occupied some of the most brilliant mathematicians through history. While Viète (1646) attempted to reconstruct the lost solution through clues in literature[65], others proposed original solutions and refined one another's work: van Roomen (1596), Newton (1687), Euler (1790), Carnot (1801), Cauchy (1806), Gauss (1873), Petersen (1879).[66] The problem, as we know it today announced by Mandlebrot[58], is that of a sequential construction where a circle of the largest possible diameter is placed without overlapping in the interstice between three pre-existing ones in mutual contact (a premise introduced by Descartes in 1643[67]); iterating the process an infinite number of times eventually leads to a structure with zero porosity, known as "Leibniz packing" (1706)[68]. The two-dimensional construction was extended to spheres in the three-dimensional space by de Fermat (1679) and Soddy (1937)[69], and it was Mandelbrot (1977) who established the scale-invariant nature of such packings[58], summarily called "Apollonian packings". Herrmann et al. (2012) would then show that this is the densest packing of spheres attainable.[70] This paragraph of (shameless) name-dropping serves a purpose in this dissertation: to demonstrate the timelessness and still-current relevance of Apollonius' problem as an intellectual exercise.

2.2.2 Present-day research

The complete Apollonian process requires an extremely polydisperse population of spheres with a definite power-law distribution of diameters[58,71]. The scale-invariance of such a construction manifests as the fractal nature of the collective interfaces of constituent spheres. Thus, the size-distribution by numbers of such a population, $n(a)$, follows the equation:

$$n(a) \propto a^{-(d_f+1)}$$

where a is the diameter, and d_f a number known as "fractal dimension".

Considering the power-law distribution of sizes involved, it is unfeasible to synthesize Apollonian packings; a very large number of particles of very different sizes would all have to be lodged at the right places. Modern research in the domain has therefore remained theoretical and heavily oriented towards calculating the value of the fractal dimension, supported by numerical simulations. The d_f in

a three-dimensional Apollonian packing of spheres has variously been estimated at 2.45-2.52[59,60,72–74]. Mild discrepancies in values are due to the difference in algorithms used to generate the Apollonian packing. A brief discussion on these differences may be found in our manuscript[62].

At this point, we disclose having encountered work that attempted to fill space with three to four size-classes of droplets (Das and Ghosh, 1990)[75]. While the published micrographs of their systems may *look* somewhat Apollonian (Figure 15, left), they managed to attain no more than $\phi = 0.89$. Moreover, a tetradisperse population is far from a power-law size-distribution required of true Apollonian packing. The authors also reported distortion in their droplets, which no longer remained spherical (from left to right in Figure 15) as emulsification progressed, gradually refining into a monodisperse population.

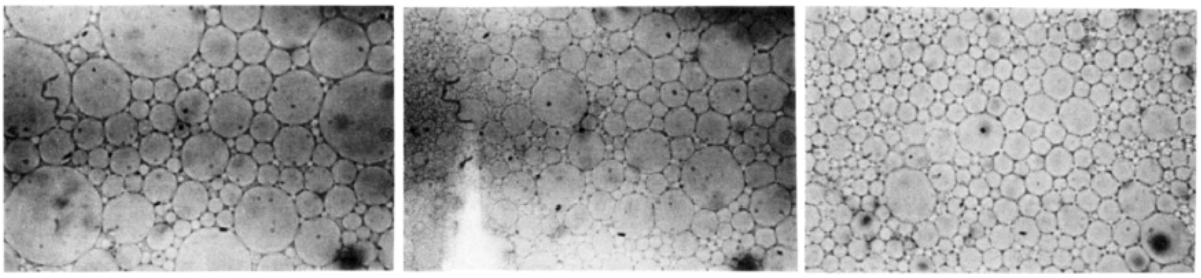

Figure 15: micrographs of polydisperse concentrated emulsions at $\phi \approx 0.88$, comprising 3-4 size classes of droplets (left). As emulsification progressed, the droplets became increasingly distorted and polydispersity was reduced.[75]

2.2.3 Fractals

Naturally, Apollonian systems are not regular occurrences in the real world. This is not to be confused with fractal structures commonly found growing in aggregating colloidal particles, similarly describable by power laws (Figure 16). It is essential to note here that these power laws do not describe the *size* distribution of the aggregating particles, but rather their *spatial* distribution[58]. The volume fractions of these colloidal fractals are far below unity, and their usual fractal dimensions are in the range of 1.8-2.2[76–80]: neither space-filling, nor Apollonian-like.

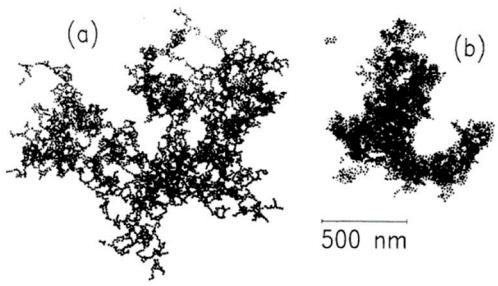

Transmission electron micrographs of clusters aggregated by use of (a) diffusion-limited kinetics and (b) reaction-limited kinetics.

Figure 16: fractal structures formed by aggregating colloidal particles, as observed by Weitz et al. (1985).[77]

Our literature review in the domain of colloids has not revealed power-law size distributions to be common, nor found any mentions of Apollonian packing. In this dissertation, we claim to be the first to observe and report the existence of the mythical Apollonian packing in our extremely polydisperse oil-in-water HIPEs. Droplet size-distribution measurements of our samples by Light Scattering show

that they obey a power law, with measured fractal dimensions of 2.47-2.5. We also measured structure factors of our HIPEs by Small-Angle X-ray Scattering (SAXS), and found them to converge with the theoretical structure factor calculated from a numerically constructed disordered Apollonian packing of spheres.

It would seem, then, that some 2000 years after Apollonius' musings, we have had the good fortune of observing the physical manifestation of a timeless mathematical curiosity.

3. Materials and methods for HIPEs

3.1 Preparing HIPEs

The HIPEs studied throughout the course of this dissertation had a direct (i.e. oil-in-water) topology. We fixed the internal-phase ratio at around $\phi = 0.95$. Each emulsion was made with the non-ionic surfactant, hexaethylene glycol monododecyl ether (C12E6, molecular weight 450.65g/mol), water and mineral oil. The surfactant was purchased as a 25%(w/w) aqueous solution from Anatrace (USA) at >99.9% purity and stored under argon, refrigerated at around 6°C until use. It was then diluted in Millipore Milli-Q water to the required concentration to constitute the HIPE's continuous phase.

C12E6 belongs to the family of polyoxyethylene alkyl ethers, collectively known as CiEj which abbreviates their general chemical formulae $C_iH_{2i+1}(OCH_2CH_2)_jOH$. We selected this particular molecule for its hydrophilic nature (Figure 17) in order to discourage the formation of pores or channels that would connect oily domains leading to a water-in-oil emulsion topology. It also presented a very simple phase diagram in water in the typical range of concentrations used in emulsion formulation at ambient temperatures (Figure 18, coloured portion). Complex mesophases like hexagonal, cubic and lamellar structures significantly change the viscosity of the aqueous continuous phase, influencing the emulsification mechanism[35]. In our region of operation, for concentrations above its Critical Micelle Concentration (CMC), 8.7 x 10^{-5} M at 25°C[81,82] or 0.004%wt, only the micellar phase L_1 would be encountered.

Figure 17: chemical structure of non-ionic surfactant, hexaethylene glycol monododecyl ether (C12E6).[83] The size of the polar polyoxyethylene "head" (E6) in comparison to the hydrophobic hydrocarbon "tail" (C12) gives the molecule an overall hydrophilic nature.

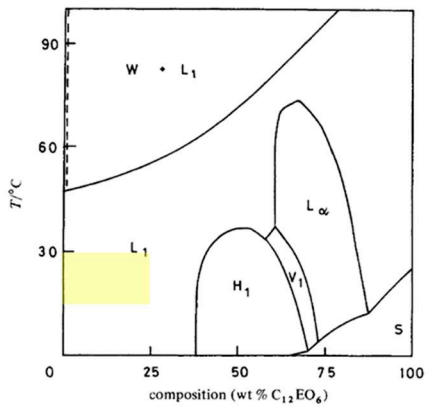

Figure 18: phase diagram of C12E6 in water.[84] Only the micellar structure (L_1) will be encountered at surfactant concentrations under 25% and at ambient temperatures (coloured portion). Other mesophases (H_1: hexagonal, V_1: cubic, L_α: lamellar) occur at higher temperatures and surfactant concentrations. S denotes a solid phase, while W represents water containing some surfactant monomers. The cloud point is around 48°C.

The mineral oil was paraffinic in nature with the following characteristics: density of 905 kg/m^3 at 15°C, refractive index of 1.498 at 20°C, and a kinematic viscosity of 2300 mm^2/s. It was found to be Newtonian over the range of shear rates tested – 1s^{-1} to 700s^{-1} – with a dynamic viscosity value of 1.26 Pa.s at 25°C.

As described earlier, HIPEs may be prepared directly by the mayonnaise method, or by creaming an already concentrated emulsion. Here, the mayonnaise method was favoured for its simplicity: all that was required were the tools necessary for emulsification. And lots of patience.

3.1.1 Tools required

- An overhead mixer with a four-bladed stainless steel propeller stirrer (IKA R1342, stirrer diameter 50mm)
- A tall borosilicate glass beaker (diameter 60mm)

3.1.2 Protocol

The following protocol pertains to the preparation of 20g of extremely polydisperse HIPE at $\phi = 0.95$, with an aqueous continuous phase containing 0.6%(w/w) surfactant. Increasing the amount of solubilized surfactant results reduces the polydispersity and changes physical properties of the HIPE (refer to section "4.1 Macroscopic behaviour of a HIPE vs. its composition").

1. Prepare the continuous phase.
   Weigh 6mg of pure surfactant in the beaker. Top up with water to 1g. Note the mass of the continuous phase at this point.

2. Turn on the overhead stirrer to mix the continuous phase for a few seconds.
   Setting the stirring speed at 500rpm in this *specific* geometry gives emulsion droplets whose diameters are mostly centered on 2µm. Stirring speed may be varied from 80 to 1000 rpm depending on the final emulsion droplet-size desired. A higher speed gives smaller droplets.

3. Add 19g of mineral oil <u>dropwise</u> under constant shearing from the overhead stirrer.
   To avoid emulsion inversion, the addition has to be ***slow***. Introduce a new drop with a Pasteur pipette only after the previous one appears to have been homogeneously dispersed. The entire process typically takes 30-40 minutes.

4. Weigh the final mixture. Subtract the mass of the continuous phase to deduce the exact quantity of oil added.

3.1.3 Reproducibility of the protocol

We note that mineral oil used here was fairly viscous. Its chemical composition is also not precisely defined, as mineral oils are generally a mixture of alkanes of different carbon-chain lengths, with possible inclusion of some fatty acid groups. As such, we tested oils of different viscosities and chemical natures to verify the reproducibility of the HIPE preparation method, while keeping the surfactant C12E6 constant.

3.1.3.1 Chemical properties of oil

Incompatibility with alkanes

Three aliphatic alkanes, dodecane ($C_{12}H_{26}$), hexadecane ($C_{16}H_{34}$) and squalane ($C_{30}H_{62}$) were tested with our protocol. Regardless of the amount of C12E6 solubilized in the continuous phase, whether 0.6% or 15%, all three resulting emulsions had phase-inverted. Water droplets sank to the bottom of the beaker as soon as shearing stopped. Dodecane was the quickest to invert whereas squalane demonstrated some resistance, but inverted nonetheless.

In their study on emulsification mechanisms in concentrated emulsions, Tcholakova et al. (2011) successfully prepared monodisperse HIPEs from hexadecane, in the presence of a continuous phase containing non-ionic surfactant C13E8 solubilized at 10%.[40] They noted that "selecting a proper surfactant for emulsification at high ϕ is a nontrivial task, and we tested a large set of surfactants to find the emulsifiers described". Their observations, as well as ours, would appear to suggest that C12E6 is not an appropriate surfactant for aliphatic alkanes. This is because when the oil to be emulsified is more compatible with the surfactant's hydrocarbon chains, the solvation of the surfactant by some oil molecules increases, resulting in a decrease in the spontaneous curvature of the surfactant monolayers. Coalescence then becomes easier and quicker[26], thereby favouring the inverse water-in-oil topology when emulsifying. Indeed, it was shown in literature that HIPEs could be made using a myriad of surfactants, as long as the appropriate one was chosen in accordance with the empirical Bancroft rule (refer to section "2.1.6. Making a HIPE: choosing a surfactant").

Compatibility with silicone oil

Although there was little indication to suggest that our mineral oil contained fatty acid groups, we wondered nonetheless if these contaminants could have helped the emulsification process by playing the role of a co-surfactant. Consequently, we tested a non-polar silicone oil (Figure 19) with a comparable viscosity of 1Pa.s at 25°C.

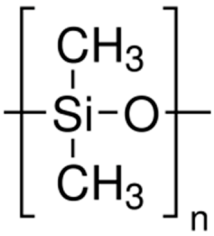

Figure 19: chemical structure of silicone oil.[85] The longer the chain, the more viscous the product.

The silicone oil emulsified wonderfully with the surfactant, at both 25%C12E6 and 0.6%C12E6 in the aqueous continuous phase. The behaviours of these resulting HIPEs were consistent with their mineral oil counterparts, such as rheological properties and most crucially, droplet-size distributions (Figure 20). We note here that the sample with little surfactant presented an Apollonian exponent of -2.47 (refer to section "4.2.1 Evolution towards an Apollonian exponent").

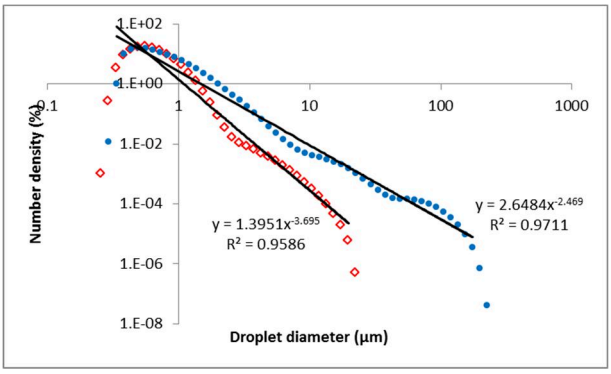

Figure 20: droplet-size distributions measured by Light Scattering of two HIPEs made from silicone oil (viscosity 1Pa.s at 25°C) at 500rpm. Open diamonds: 94.6%oil in 25%C12E6(aq); solid dots: 94.2%oil in 0.6%C12E6(aq).

3.1.3.2 Physical properties of oil

Viscosity

In section "2.1.5.2 Emulsifying viscous oils", it was demonstrated that HIPEs were an efficient tool to emulsify viscous oils into an external aqueous phase. However, the HIPEs investigated were of the monodisperse variant, with lots of surfactants solubilized in the continuous phase. Our objective in this present work is to study extremely polydisperse HIPEs and our protocol calls for very little surfactant – only 0.6% solubilized in the continuous phase. As such, we put six silicone oils (purchased from Sigma-Aldrich) with viscosities ranging from 5 mPa.s to 10 Pa.s to the test.

We found that at the lower range of viscosities, 5 mPa.s and 10 mPa.s, no HIPE was possible and the aqueous phase separated during emulsification. As long as the silicone oil's viscosity was 50 mPa.s and above, we could make extremely polydisperse HIPEs whose size distributions obeyed a power law over two decades of droplet sizes, with a measured exponent of -2.5 ± 0.1 (Figure 21).

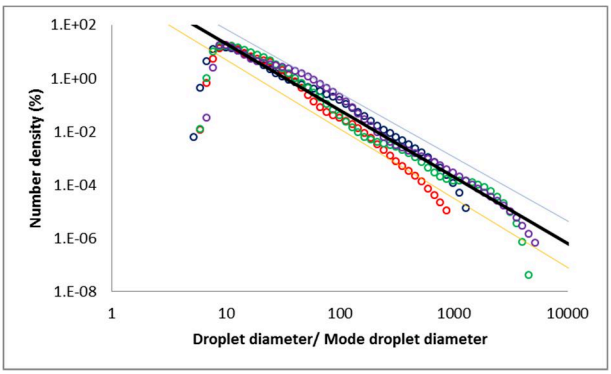

Figure 21: droplet-size distribution of polydisperse HIPEs made from viscous silicone oils at ϕ = 0.95 with 0.6%C12E6 in the continuous phase. The horizontal axis has been rescaled to arbitrarily center each size distribution at 10. Blue circle: 50mPa.s; red: 350mPa.s; green: 1Pa.s; purple: 10Pa.s. The power-law exponent of -2.5 is indicated by the bold line, ± 0.1 by faint lines.

3.2 Characterizing HIPEs

3.2.1 Rheology

An emulsion is a soft matter material that behaves viscoelastically when subjected to external mechanical stresses. In other words, its response – known as the dynamic modulus, G^* – may be deconstructed into an "elastic solid" component and a "viscous liquid" component. G', is the storage modulus that measures the former's capacity of conserving energy; G'' is the loss modulus that measures the latter's capacity to dissipate energy transmitted to the emulsion. G^* then is a complex number that follows the relation:

$$G^* = G' + iG''$$

with δ denoting the phase shift in an Argand diagram or "représentation de Fresnel" (Figure 22).

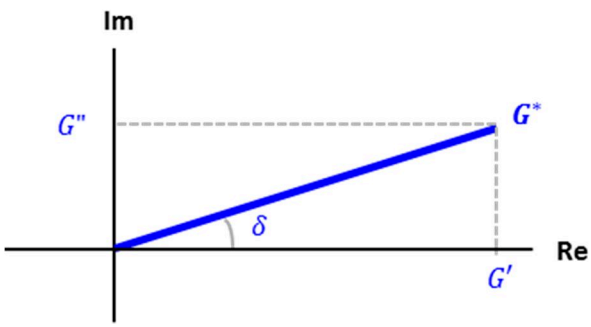

Figure 22: visual representation of the complex viscoelastic modulus G^*, with storage modulus G' as the real part, and loss modulus G'' as the imaginary part.

A material's viscosity characterizes how resistant the material is towards flowing, when it is subjected to shear. A fluid is considered Newtonian if its viscosity is constant regardless of the shear applied. If it becomes easier for a fluid to flow (i.e. viscosity decreases) as we apply more shear stress, then the fluid is shear-thinning. On the contrary, if viscosity increases in spite of the higher shear stress applied to the fluid, it is known a shear-thickening fluid.

A flow curve charts the measured viscosity of a fluid as a function of applied shear rate. When the curve is expressed as a double-logarithmic plot, the difference between these three types of fluids' rheological responses to applied shear immediately becomes visually apparent (Figure 23).

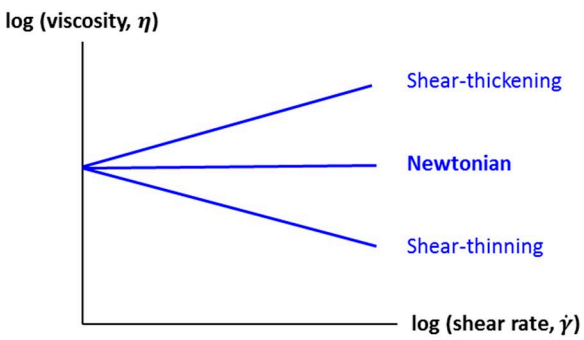

Figure 23: a fluid's flow curve (viscosity vs. shear rate) expressed in a double-logarithmic plot reveals its Newtonian behaviour if the slope is 0. If the slope is positive, the fluid exhibits shear-thickening behaviour; if it is negative, the fluid is shear-thinning.

If a material presents a resistance to flow unless the applied stress exceeds a certain value, σ_y, it is said to possess a yield stress. This value can be determined from plotting the applied shear stress, σ, as a function of the shear rate, $\dot{\gamma}$ – the dynamic yield stress, σ_y, is determined from the plateau value of σ, i.e. when it becomes constant regardless of the shear rate (Figure 24) (Persello et al., 1994)[86].

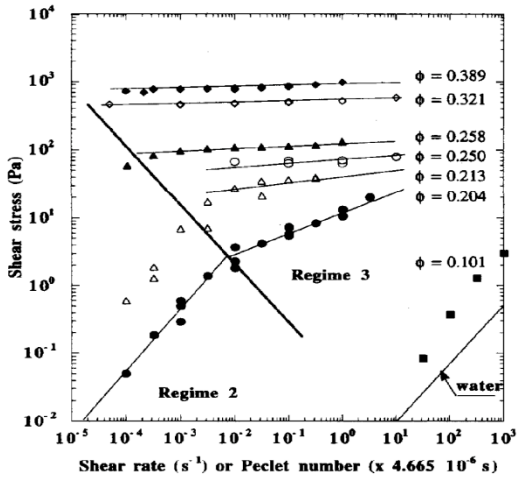

Figure 24: in this figure, regime 2 denotes Newtonian behaviour where shear stress is proportional to the shear rate. Regime 3 denotes yield behaviour, where shear stress becomes independent of the shear rate.[86]

To quantify the mechanical behaviour of our HIPEs containing different amounts of surfactant, we used a rotational rheometer (Anton Paar Physica MCR 501) to make G' and G'' measurements as the samples were subjected to shear. We also constructed the flow curve for each sample.

3.2.1.1 Selecting a shearing geometry

Shape

A stainless steel cone and plate geometry was selected for the rheological measurements. Parallel plates were found unsuitable, giving erratic measurements, due to wall slip created by oil droplets squeezed out of the HIPEs when shear was applied.

For flowing liquid-like HIPEs, a cone with a larger diameter (Anton Paar CP60-0.5, cone diameter 59.979mm, cone angle 0.491°, gap 58µm) was used to increase the sensitivity of the measurements. A smaller cone (Anton Paar CP25-2, cone diameter 24.974mm, cone angle 2.011°, gap 105µm) was adequate for non-flowing solid-like samples.

Surface roughness

Seeing as the HIPEs adhered well to stainless steel without wall slip, a smooth surface for the cone and plate geometry was well adapted. Rough surfaces on the geometry are not recommended because it is difficult to ensure that solid-like HIPEs are evenly spread between the serrations (Figure 25).

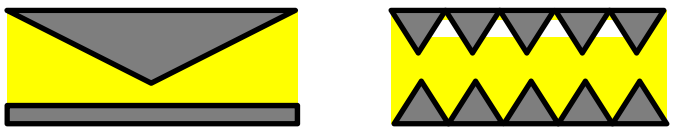

Figure 25: schema depicting the spreading of a HIPE sample in a smooth cone-plane geometry (left) and a roughened geometry (right). It is more difficult to ensure that all the gaps between the teeth in a serrated geometry are evenly filled, especially with a solid-like sample.

3.2.1.2 Protocol

The rheometer was thermostated at 15°C to avoid evaporating the little amount of continuous phase present in the HIPEs.

It is also important not to define the measurement duration for each point, so as to allow the sample to attain steady-state behaviour before the rheometer proceeds to the next measurement point.

1. Oscillatory pre-shear at low imposed strain γ and low imposed frequency f
   The pre-shear step allows the sample to recover from any stresses that may have been applied to it, such as the act of spreading it on the rheometer. A low strain of$\gamma = 0.1\%$ and a low frequency of $f = 1Hz$ are imposed to find the amount of time necessary for the sample to demonstrate a linear behaviour where G' and G'' are constant. This corresponds to the relaxation time of the sample.

2. Strain sweep at low imposed frequency
   The oscillatory frequency is set to $f = 1Hz$, and a strain sweep between $\gamma = 0.01 - 100\%$ is performed. A first sweep is done at increasing strain. The sample is then allowed to rest for the duration necessary (as found in step 1), before a second sweep is done at decreasing strain. The two curves should superimpose on each other if the sample's internal structure has not been altered by the rheological measurement.

   Strain sweeps allow us to determine the linear viscoelastic (LVE) region. For flowing samples, it is the region where the G'' curve becomes constant (because these samples behave like viscous liquids). For non-flowing samples, the G' curve should be examined. We may then identify a particular value of strain, γ_0, in the LVE region for any subsequent measurements where strain is imposed, such as a frequency sweep.

3. Flow curve at imposed shear rate $\dot{\gamma}$
   The shear rate is imposed, varying from $\dot{\gamma} = 0.01 - 10s^{-1}$. The sample's viscosity η, and the corresponding shear stress, σ, are then measured. Two measurement points are made per decade of shear rate.

   A plot of η as a function of $\dot{\gamma}$ is made in double-logarithmic scales for each sample to determine the slope of the flow curve. At high shear rates, wall slip may occur. This may be identified by a sudden change in slope of the flow curve where $\log \eta$ drops off dramatically.

   A plot of σ as a function of $\dot{\gamma}$ is also made in double-logarithmic scales to identify yield behaviour. Where σ becomes constant regardless of the shear rate, the value of the plateau gives the dynamic yield stress, σ_y.

3.2.2 Measuring droplet-size distribution by Light Scattering

Light Scattering is a common technique used to measure the size distribution of particles or droplets in dispersions. A monochromatic, coherent light source is shone through the sample, whereupon the photons deviate in their directions when they encounter particles in the sample. The bigger the particles encountered, the smaller the scattering angle. The measuring instrument is usually equipped with an array of sensors at different scattering angles with respect to the light source, and these detect the incident intensities of the scattered light. The Mie scattering theory is applied to generate a theoretical scattering model, which is compared to the actual measured scattering. The instrument's algorithm then adjusts the size distribution of model to find the best fit, and finally reports the size distribution of the sample[87].

Our light scattering instrument (Malvern Mastersizer 3000, paired with Malvern Hydro SV small volume wet dispersion unit) was equipped with red and blue lasers of wavelengths 632.8nm and 470nm respectively. It was used to measure our polydisperse emulsions in which droplet sizes were between several hundred nanometers to a few millimeters.

For samples containing much smaller droplets where the particles are approximately the size of, or slightly larger than the wavelength of the incident photon, the latter may also lose a small amount of energy when it is deviated. This is the case of quasi-elastic light scattering or Dynamic Light Scattering. Due to Brownian motion in the sample (either of the particles themselves, or of solvent molecules that may bump into the particles), detected intensities vary temporally. The instrument analyzes these temporal fluctuations to deduce D, the diffusion coefficient of the particles. From there, assuming spherical particles, the Stokes-Einstein equation gives the radius, R, of the particles:

$$D = k_B T / 6\pi\eta R$$

where k_B is the Boltzmann constant, T the temperature and η the viscosity of the sample.

Our Dynamic Light Scattering instrument (Malvern Zetasizer Nano ZS) was equipped with a green laser of 532nm, adapted for measuring in the range several nanometers to several microns. This instrument was used to measure the droplet size in our microemulsions.

3.2.2.1 Protocol

1. Define the parameters of the measurement
    - Density and refractive index of the solvent: water; sample: mineral oil (HIPE droplets)
    - Droplet shape: spherical

2. Measure the scattering background of water.

3. Dilute the HIPE sample in water approximately 800x and measure the scattering.
   Sufficiently diluting the HIPEs will prevent the droplets from frequently encountering one another and coalescing during the measurements.
   If the sample is insufficiently diluted, we may encounter multiple scattering where a photon is deviated multiple times, resulting in a larger detecting scattering angle. The instrument then falsely reports a smaller particle size.
   If the sample is too diluted, the signal-to-noise ratio may be too low to obtain reproducible results.

4. Assess the quality of the data fit.
   If the fit is poor and presents large residuals with the measured scattering, the given size distribution is inaccurate and the measurement should be repeated.

3.2.2.2 Interpreting the results

Number density or volume density?

Light Scattering results may be reported as a volume-weighted or number-weighted size distribution. For a strictly monodisperse sample, these two results are identical.

For practical purposes, if we wish to find out how many droplets are present in each size class in a polydisperse sample, the number-weighted distribution – or number density – is generally more pertinent.

If we wish to study the *evolution* of a polydisperse population of droplets, then the volume-weighted distribution – or volume density – will allow us to infer the proportion of material that is found in the larger droplets.

Revealing a power-law behaviour

In this work, we were mainly interested in the **number density, $\boldsymbol{n(a)}$,** of our samples as the Light Scattering measurements may be considered snapshots of the droplet arrangements in our HIPEs at a given moment. To reveal any power-law behaviour, the number-weighted distributions were represented on a double-logarithmic scale. A regression line was then traced to deduce the exponent. Since our Light Scattering instrument uses a geometrical progression to bin the measured droplet diameters, a, into 100 sampling size classes (i.e. 10.7nm, 12.1nm, 13.8nm, 15.6nm etc. to 3.5mm; common ratio 1.136), **the slope of $\boldsymbol{log\ n(a)}$ vs. $\boldsymbol{\log a}$ gives the fractal dimension directly** (refer to Supplementary Information section "11.1 Deducing d_f from the double-log plot of Light Scattering measurements").

3.2.3 Small-Angle X-ray Scattering (SAXS)

The principle of Small-Angle X-ray Scattering is similar to that of Light Scattering, where an incident ray of coherent, monochromatic photons is diffracted by a material, and we measure the deviation to garner information on the material's structure. Using X-rays of wavelength on the order of 1Å – around four thousand times shorter than that of visible light – we can study structures on a much smaller sub-nanometric scale. Whereas a direct observation technique such as microscopy measures physical distances in the real space, diffraction techniques like SAXS measure in the reciprocal space of a material.

A vector in this reciprocal space is known as a scattering vector. We denote its magnitude by q, given as:

$$q = \frac{4\pi \sin(\theta/2)}{\lambda}$$

where θ is the scattering angle (the angle by which the incident ray has been deviated), and λ is the wavelength of the photons[88]. The unit of q is in $Å^{-1}$. Then, the quantity measured in SAXS is $I(q)$, the amplitude of the intensity of X-rays that have been diffracted. Taking into account the experimental configurations of the system (thickness of sampling cells, size of beamstop etc.), $I(q)$ is usually given as an "absolute intensity" in cm^{-1}.

SAXS may be performed at a synchrotron or in a laboratory. On a synchrotron beamline, the X-ray source's flux (or brilliance) is incredibly high (up to 5 x 10^{13} photons per second), which allows for excellent signal-to-noise ratios and very short spectra acquisition times (generally 0.01 to 5 seconds). However, working with such high-energy sources entails having to adjust the sample exposure constantly, to avoid radiation damage or detector saturation. Access to these facilities are also difficult and in high-demand. At the laboratory scale, the source's flux is significantly lower (up to 6 x 10^{6} photons per second) and therefore safer for the sample: the downside is then a longer spectra acquisition time (usually 1h, sometimes up to 6h to improve the signal-to-noise ratio).

Our experiments were primarily performed on the ID02 beamline at the European Synchrotron Radiation Facility (ESRF)[89] in Grenoble, France, and on the SWING beamline at the SOLEIL Synchrotron[90] in Saclay, France. We also complemented these experiments with laboratory-scale SAXS (SAXSLAB Ganesha) at Lund University, Sweden.

Based on the experimental set-up at each facility, we used them to study different features in our samples (Table 1). For instance, thanks to the larger sample-detector distances available at synchrotrons, a wider scattering range was achievable and measures could be made at extremely low q values to gather information on larger structures in the sample.

Table 1: summary of experimental set-up at each SAXS facility

	ID02 (ESRF)	SWING (SOLEIL)	GANESHA (Lund University)
Detector distances	0.8 – 31m	1 – 6m	0.5 – 1.5m
Scattering q-range	1.8 x 10^{-4} – 0.76 $Å^{-1}$	1.5 x 10^{-3} – 1.08 $Å^{-1}$	3 x 10^{-3} – 0.67 $Å^{-1}$
Corresponding length-scales	Å to µm	Å to ≈500nm	Å to ≈200nm

The experiments were performed at 21-22°C at all three facilities.

3.2.3.1 Protocol

1. Choose an appropriate sampling cell
    - On a synchrotron beamline

    Due to the highly dense nature of our extremely polydisperse "liquid" HIPEs that did not present any periodicity, and due to the low scattering contrast between the sample and our background references (mineral oil for concentrated samples, constituent aqueous phase for diluted samples), perfect background subtraction was very crucial to our work. Consequently, we used the same flow-through glass capillary (diameter 1.5 – 2mm, wall thickness 0.05mm) throughout each set of experiment, and measured at the same spot. The capillary was mounted on a moving stage and its position with respect to the X-ray beam could be remotely controlled.

    For less polydisperse "solid" HIPEs that had some longer-range order, since the subtraction was less crucial, we could use brand new individual glass capillaries (Hilgenberg 4017520, diameter 2mm, wall thickness 0.01mm) that we pre-filled with a syringe, and then sealed with wax and inserted onto a capillary holder before the X-ray beam.

    - For laboratory-scale SAXS

    We used glass capillaries that were sealed on each end with stainless-steel screw caps. We noted which glass capillary was used for a sample and the position at which the spectra was measured. The corresponding background for the sample was then performed in the same capillary (after thorough cleaning) at the same spot.
2. Ensure the capillary's cleanliness by measuring the spectra of water between samples
    - On a synchrotron beamline

    This step was essential, especially when using the same flow-through capillary for the entire experiment lasting 48 – 56 hours where up to two thousand spectra were measured. The flow-through capillary was cleaned by flushing a series of solvents in decreasing order of polarity between each sample: hexane, isopropanol, acetone then ethanol. The capillary was dried using a stream of compressed air, and the spectra of pure water was measured. We then compared the spectra to previous ones to ensure that they were identical. Otherwise, the capillary was cleaned again.

3. Inject the sample into the capillary with a disposable syringe.
    - On a synchrotron beamline

      The flow-through capillary is connected on one end to an injection port, and to waste collection on the other. Around 300µL of sample required.

    - For laboratory-scale SAXS

      Only 100µL of sample is required to fill the capillary here. The instrument functions under ultra-high vacuum so the capillary must be properly sealed. It was particularly tricky to fill the capillary with aqueuous surfactant solutions because their very low interfacial tension wetted the O-rings that were supposed to seal the capillary. This led to some leakage and subsequent evaporation of the sample under ultra-high vacuum. The trick was to keep the O-rings dry during filling, and to tighten the stainless steep caps on each end of the capillary gradually and alternately.

4. Perform a capillary scan
   This is a quick transmission scan with different purposes at each facility.

   - On a synchrotron beamline

   As previously mentioned, the X-ray beam is very brilliant. A capillary scan allows us to find the optimal sample exposure time to have a sufficient photon count arriving at the detector without saturating the detector.

   - For laboratory-scale SAXS

   A capillary scan here allows us to determine if it has been correctly filled: the level of transmission is lower where there is sample, and higher where there are air bubbles (or no sample if a leak and evaporation has occurred under ultra-high vacuum).

5. Spectra acquisition
   - Concentrated spectra, $I(q)$

   This is the spectra of a HIPE in its undiluted, concentrated state. It allows us to get information on the correlations between droplets in-situ.

   - Diluted spectra, $P(q)$

   Theoretically, $P(q)$ is defined as the form factor of a lone emulsion droplet bereft of neighbouring correlations. Experimentally, a good approximation for $P(q)$ is the scattering spectra of the same emulsion so diluted that the droplets are sufficiently spaced out to be considered independent from one another. We found that diluting a HIPE 40x in an excess of its constituent continuous phase, to ϕ = 0.024, was quite enough.

3.2.3.2 Data treatment

Background subtraction

For concentrated spectra of the HIPEs, the background to subtract is $\phi \cdot I_{oil}(q)$ where $I_{oil}(q)$ is the spectra of the mineral oil. For the diluted spectra, the corresponding background is that of the diluting medium, i.e. an aqueous micellar solution at the same concentration as the HIPE's continuous phase. Subtraction was first done for spectra acquired at each detector distance, then merged by scaling at higher q-values. These operations were performed using SAXSUtilities[91].

Calculating the experimental structure factor, $S_{exp}(q)$

The structure factor $S(q)$ describes the correlation between droplets in regions of the same electronic density. In other words, $S(q)$ characterizes the probability of finding an oil domain of a given size at a given distance from another oil domain of known size. We can then deduce the in-situ spatial disposition of our emulsion droplets in the undiluted HIPE.

Given that $I(q) \propto P(q) \cdot S(q)$, multiplied by n, the number of particles per unit volume, a HIPE's experimental structure factor, $S_{exp}(q)$, is calculated as the ratio between the concentrated and diluted spectra. This operation was performed on Microsoft Excel. The distinctive features of a $S(q)$ are the position, height and shape of its first peak, the presence of any oscillations and a tail that rapidly approaches $S(q) = 1$. As such, we were only interested in examining $S(q)$ in the scattering range up to q = 2 x 10^{-3} $Å^{-1}$.

Spectra fitting

The analytical expressions for the scattering intensities are known for many models, such as spherical structures, lamellar structures, crystal lattices etc. By generating these theoretical scatterings, and adjusting their parameters to fit experimental data, we can deduce information about the structures that may exist in our samples. The models that we most frequently used in this work were

- Power law: to deduce the experimental exponent from our SAXS spectra;
- Bilayer lamellar: to model the surfactant film between deformed droplets in solid HIPEs;
- Onion: to model the surfactant flat film between deformed droplets in hybrid HIPEs;
- Core-shell spheres: to model swollen micelles found in liquid HIPEs.

Such fits were performed with the software SasView[92].

3.2.4 Numerical simulations

In this dissertation, numerical simulation was an important tool for generating reference models on which virtual experiments and theoretical calculations could be carried out. The results obtained served as a basis for comparison to our experimental ones, and helped validate or disprove our conjectures along the way. The following simulations and algorithms described were performed and developed by Robert Botet at the Laboratoire de Physique des Solides, University of Paris-Sud.

3.2.4.1 Osculatory Random Apollonian Packing

We began by representing empty space using a unit cubic box with periodic boundary conditions in all three directions. The initial system was a *disordered* dispersion, created by placing a few random hard spheres in random positions inside the box. The algorithm then initiated the random Apollonian filling process by an osculatory packing of spheres[93] (Figure 26). The constraint imposed was to find, by Monte-Carlo, the largest sphere possible, to be placed in a void without overlapping existing particles, until the pre-set volume fraction was attained (with ϕ approaching unity).

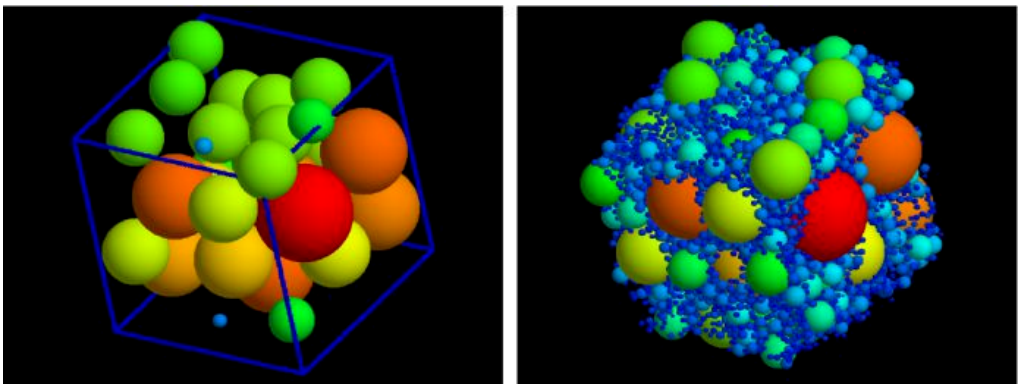

Figure 26: initial disordered dispersion of 32 random hard spheres (left); the same system after running the random Apollonian filling process until the pre-set volume fraction is achieved (right). Here, ϕ = 0.85, and the final system is composed of 6410 hard spheres with diameter ranging from 0.03 to 1. Colours correspond to different sphere diameters, red being the largest and blue being the smallest.

Our RAP algorithm was based on the method described by Varrato and Foffi (2011)[74], to which we further applied a global optimization approach: after the initial stage of randomly placing spheres of random sizes, we examined a great number of points in all existing voids, and determined for each point the largest corresponding sphere size that could be centered upon it without overlaps with

existing neighbours. From this constituted set of candidate spheres, we then only lodged the largest one found in its resident void. We believe that our ORAP algorithm that examines the global structure at each filling step is an accurate representation of what happens in colloids, where we assume that a polydisperse population of droplets resulting from emulsification can rearrange themselves in the available space. This maximisation of radii is more consistent with the definition of an Apollonian construction according to Mandelbrot[58]:

- "Apollonian circles are the **largest** circles inscribed in these [circular] triangles."
- "Repeating the same procedure, we draw the **largest** inscribed circle in each triangle. Infinite further repetition is called Apollonian packing."
- "Apollonian packing recalls a construction I call Leibniz packing of a circle… 'Imagine a circle; inscribe within it three other circles congruent to each other and **of maximum radius**; proceed similarly within each of these circles and within each interval between them, and imagine the process continues to infinity…"

We consistently found d_f = 2.47 with our algorithm, which is in good agreement with d_f values given in literature using similar methods: 2.474[59,74] and 2.48 – 2.52[72].

3.2.4.2 Calculating the Apollonian structure factor, $S_{cal}(q)$

We proceeded to calculate the structure factor $S_{cal}(q)$ for the constructed Apollonian system, dividing the theoretical scattering intensity for the compacted system by that of the corresponding infinitely diluted system[94].

Understandably, as the pre-set ϕ gets ever closer to unity, the computational power and time required for such numerical simulations increases significantly. For the curious, more than 3 weeks was necessary to simulate an Apollonian system at ϕ = 0.93, and over two days to calculate the corresponding structure factor. We were thus unable to obtain $S_{cal}(q)$ at ϕ = 0.95, the same volume fraction as our experimental HIPE systems. However, we could calculate and compare $S_{cal}(q)$ for ϕ = 0.84 – 0.92 within a reasonable amount of computing time. We found that they were nearly identical when the scattering vector, q, was rescaled by $(\phi/N)^{1/3}$ which physically represents the "average" radius in each system (Figure 27). This rescaling operation was legitimate thanks to the scale-invariant property of Apollonian systems. We could therefore assume the similarity between $S_{cal}(q)$ at ϕ = 0.95 and ϕ = 0.92, and use the latter as a valid comparison to our experimental $S_{exp}(q)$ at ϕ = 0.95.

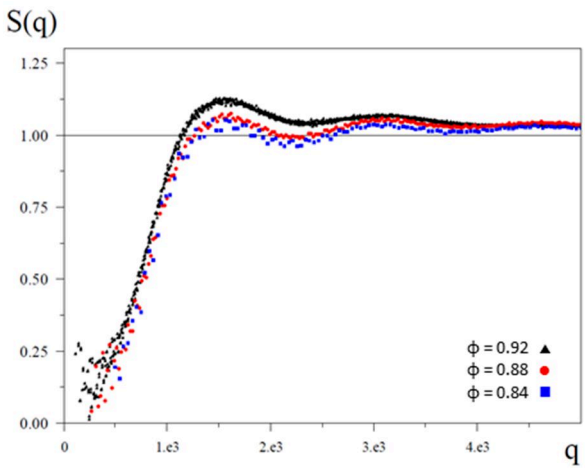

Figure 27: comparison of $S_{cal}(q)$ obtained through numerical simulation for Apollonian systems at ϕ = 0.84, 0.88 and 0.92. The horizontal axis representing scattering vector, q, has been rescaled by $(\phi/N)^{1/3}$.

3.2.4.3 Smoluchowski coalescence algorithm

Coalescence in a monodisperse population

Marian Smoluchowski's theory of coagulation (1916) is a frequently referenced model for coalescence studies in colloidal sciences[95]. His differential equation is applied to describe hierarchical agglomeration (i.e. droplets of the same size react at each stage, and each coalescence event is irreversible), and gives $n(t)$, droplet concentration (number of droplets per unit volume) as a function of time[96] :

$$-\frac{dn(t)}{dt} \cong \frac{8}{3}\frac{k_B T}{\eta} n(t)^2$$

$$\frac{1}{n(t)} = \frac{1}{n_0} + \frac{8}{3}\frac{k_B T}{\eta} t$$

In this expression, n_0 is the initial droplet concentration, k_B Boltzmann's constant and T the temperature of the medium of viscosity η.

Since the total volume, V_T, in the system is conserved:

$$V_T = n_0 \cdot 4\pi/3 \cdot {R_0}^3 = n(t) \cdot 4\pi/3 \cdot R(t)^3$$

where R_0 is the initial droplet radius, and $R(t)$ the droplet radius at time t.

An expression for the evolution of droplet sizes with time is then obtained:

$$R(t)^3 = {R_0}^3 + kt$$

with $k = \frac{2k_B mT}{\pi\eta\rho}$, a scalar constant that depends on the droplets' total mass, m, and density, ρ.

Therefore, for a monodisperse population of droplets with a well-defined initial radius, Smoluchowski's coalescence equation is a fairly straightforward model. What then, for a population that is already polydisperse to begin with?

Coalescence in a polydisperse population

We developed an algorithm that simulates coalescence experiments of a polydisperse population of droplets, of known initial size distribution and volume fraction, according to Smoluchowski's coalescence equations. The objective was then to compare these simulated results to actual experimental results of extremely polydisperse emulsions, to find out up to what extent Smoluchowski's model might still be valid even at high ϕ.

The algorithm assumed Brownian motion in the virtual droplets and allowed them to randomly coalesce with one another, following Smoluchowski's equation including the standard Brownian kernel, over a pre-defined duration. It then calculated the droplet-size distribution at ten different time points of the simulated experiment ($t_{j=0}, t_{j=1}, \dots, t_{j=9}$). For each sample population, we performed ten such experiments. The results were averaged to give at the end of each set of simulations:

- $n_{sim}(a, t_{j=0,1...9})$, the droplet-size distribution at each of the ten time points
- N_f, the number of remaining droplets
- the existence of any unmanageably large droplets, indicated by $ex \neq 0$.

Protocol

1. Define the initial system, N_i, ϕ and $n_{i,sim}(a)$

   To begin the simulation, we defined N_i, the initial number of droplets in the system. We found that $N_i = 600{,}000$ was quite sufficient. A smaller number sometimes led to the virtual system giving macroscopic phase separation (indicated by the existence of unmanageably large droplets) by the end of the simulation; a larger number led to excessively long computing time. It typically took 3 hours to run a simulation of ten numerical experiments, although one simulation at high ϕ took 20 hours to complete (on account of our very modest desktop computer which was last updated five years ago. Legend has it that newer computers take just a third of that computing time).

   Since we were comparing these simulations to actual experimental systems, ϕ was that of the experimental samples. We also measured the initial experimental droplet-size distribution by Light Scattering, $n_{i,exp}(a)$, and set it as the initial size distribution of the simulated system, $n_{i,sim}(a)$. The algorithm then generated a system of 600,000 virtual droplets which obeyed these parameters.

2. Define the numerical experiment duration

   This step demanded trial and error. It could be between 1 x 10^4 to 2 x 10^6 seconds. The numerical experiment had to last long enough such that we could find an output size distribution, $n_{sim}(a, t_j)$, that replicated the experimental size distribution, $n_{f,exp}(a, t_{f,exp})$, of a real emulsion that had evolved for a certain amount of time. If the simulation was too long, then the system may present macroscopic phase separation by the end of the simulation, indicated by $ex \neq 0$.

   Depending on samples, $t_{f,exp}$ was between 5min to 2 hours, and 24 hours for one of our polydisperse HIPE at ϕ = 0.95 which did not present a significant change sooner. We note here that $t_{f,exp}$ was chosen such that $n_{f,exp}(a)$ was not *too* significantly evolved from $n_{i,exp}(a)$, i.e. the smallest droplets had grown no more than 20% in diameter.

3. Comparison between simulated results and experimental results

   We determined the time point in the simulation, $t_{f,sim}$ that gave a $n_{sim}(a, t_j = t_{f,sim})$ which replicated $n_{f,exp}(a, t_{f,exp})$. We then plotted $t_{f,sim}/t_{f,exp}$ as a function of ϕ to determine if there was any trend.

4. Results and Discussion

At the beginning, our objective was to find a way to fabricate monodisperse micrometric droplets. By chance, we came across a review[51] which indicated that high internal-phase-ratio emulsions were a viable route for this purpose. Unaware then that large amounts of surfactant were prescribed to make such monodisperse, Lissant-type HIPEs, we proceeded to calculate the minimum amount of surfactant necessary – 0.6%(w/w) in the continuous phase – to make a test HIPE at $\phi = 0.8$, with diameters of 6µm, by assuming that each surfactant molecule occupied $0.5nm^2$ at the oil droplet interface[45]. The desire to use the bare minimum of surfactant was a direct response to our shock at the prices of surfactants. Little did we know that frugality was the key to the door that would open out into the lost world of Apollonian emulsions.

4.1 Macroscopic behaviour of a HIPE vs. its composition

4.1.1 Increasing gel-like character with increasing surfactant concentration

Having succeeded in making the test HIPE without phase inversion, I naively declared success and proudly brandished the sample before our supervisor, Bernard Cabane who, with almost 50 years of experience in colloidal science research, promptly asked, "Why is it flowing?" The following exchange is my recollection of the discussion that followed:

- "I don't know… Should it not flow?"
- "It shouldn't flow if the internal volume fraction is beyond 50%."
- "Oh. But I'm quite sure it didn't invert though."

This sent me back to search for the first known publication on HIPEs, Lissant's 1966 paper, to check and replicate his protocol:

> "The emulsification equipment used was a household mixer [Kitchen Aid, Model 3C]… with the mixer set at No.2… The external phase consisted of a mixture of 6 volumes of distilled water and 1 volume of emulsifier [a proprietary, non-ionic material, D-28000, supplied by Petrolite Corporation of St. Louis, Missouri, and not otherwise identified]."[10]

I deduced from technical specifications and some blurry scans of said mixer's owner's manual (published in 1954) that the No.2 setting probably corresponded to 81rpm. And while there was no luck identifying the surfactant since the supplier ceased to exist in the mid-1990s, I gathered that Lissant had used a continuous aqueous phase with surfactants solubilized at 14%.

Remaking HIPEs with the non-ionic surfactant we had at hand, C12E6, we varied surfactant concentrations in the continuous phase from 0.6%(w/w) to 25%(w/w). The most striking observation was that the more surfactant in the composition, the more the HIPEs behaved as they were described in literature: a gel-like non-flowing substance. At the other end of the spectrum, at low C12E6 concentration, we once again found a flowing emulsion. Somewhere between the two types of behaviour, at intermediate surfactant concentrations, we observed a hybrid consistency where the HIPE flowed poorly, looking like a poorly homogenized yogurt with chunks of gel embedded in a liquid emulsion.

Figure 28 shows samples exhibiting these three behaviours, as a function of increasing surfactant concentration. All three photographed HIPE samples were made at $\phi = 0.95$, at 500rpm.

Figure 28: (left) flowing HIPE with 0.6%C12E6 in the continuous phase; (middle) hybrid behaviour, semi-gelified with 5%C12E6 in the continuous phase; (right) gelified, non-flowing HIPE with 25%C12E6 in the continuous phase.

4.1.2 Rheology

To properly characterize the flow behaviour of the different types of HIPEs, we performed rheological measurements by systematically varying the surfactant concentration. Oscillatory shear at low frequency and low strain was performed on the samples.

A sample's G' and G'' values respectively quantify its "elastic solid" and "viscous liquid" behaviour in response to applied stresses. The values reported hereafter were measured in each sample's linear viscoelastic region (Figure 29).

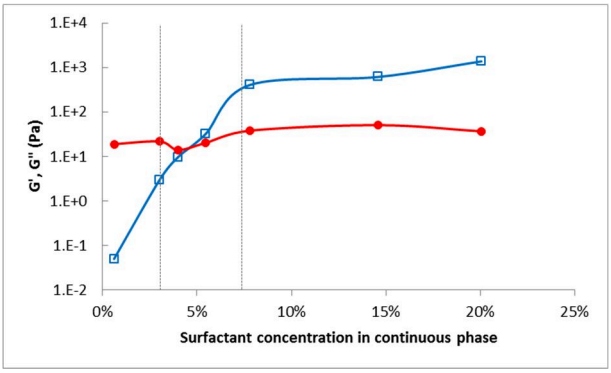

Figure 29: steady-state rheological measurements in the linear viscoelastic region of HIPEs as a function of surfactant concentration in the aqueous phase. Open squares are the G' points which measure the "elastic solid" response of a HIPE, while solid circles are the G'' points measuring the "viscous liquid" response. The faint dotted lines illustrate three distinguishable regimes: viscous liquid behaviour at low surfactant concentrations < 3%C12E6, an elastic solid behaviour at high surfactant concentrations ≥ 8%C12E6, and a transition regime for intermediate amounts of surfactant.

G' registered a 4.5-decade increase in value, from $G' = 0.05Pa$ for a HIPE with 0.6%C12E6 in the continuous phase to $G' = 1370Pa$ for a HIPE with 20%C12E6. The increase appeared to be a continuous function. G'' was observed to be more or less constant regardless of the HIPE's surfactant concentration, at around $G'' = 28.6Pa$. This was principally due to the fact that all the HIPEs contained the same amount of oil (ϕ = 0.95), and that the viscous-liquid component of the behaviour was largely conferred by the mineral oil droplets.

In the Argand diagram (or Fresnel representation) for dynamic modulus $G^* = G' + iG''$, if there is more than a decade of difference in value between G' and G'', we may consider the sample's predominant behaviour follows the larger modulus. Therefore, by comparing these two quantities

and the difference between their orders of magnitude, we were able to identify three distinguishable regimes:

- $G' < 10G''$: liquid, flowing HIPE for < 3%C12E6 in the continuous phase
- $G' > 10G''$: solid, non-flowing HIPE for ≥ 8%C12E6
- $G' \approx G''$: transition regime, hybrid HIPE for intermediate surfactant concentrations.

Our identification of the solid-liquid transition in our HIPEs is coherent with the Winter-Chambon criterion (1986) which originally states that at a polymer's gel point, $G' = G''$, when the material is placed under oscillatory shear at constant frequency[97]. This criterion has been demonstrated to be valid for a wide variety of materials that exhibit gelling behaviour, whether they are chemically cross-linked or physically percolating[98].

The flow curves constructed for all the HIPE samples also appeared to corroborate the distinction of these three regimes (Figure 30 and Figure 31). Surfactant-rich samples with ≥ 7.8%C12E6 in the continuous phase possessed a dynamic yield stress, σ_y, as evidenced by the presence of a plateau where shear stress, σ, became more or less constant from about $\dot{\gamma} \geq 0.3s^{-1}$. σ_y was between 100 – 450Pa as surfactant concentration increased. No such plateau was observable for the other types of HIPEs, which was consistent with their flowing character (Figure 30).

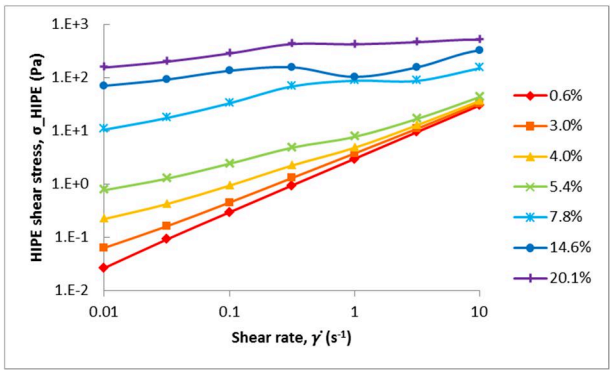

Figure 30: solid HIPEs presented a shear stress plateau where σ became constant as a function of shear rate. This value gave access to the dynamic yield stress, σ_y, of the sample. Hybrid and liquid HIPEs did not present such a plateau.

The surfactant-rich samples also presented a negative slope for their flow curves where shear viscosity was expressed as a function of shear rate in a double-logarithmic plot (Figure 31). The negative slope was indicative of shear-thinning behaviour, a finding consistent with that of HIPEs reported in literature, similarly stabilized with great amounts of surfactant.[25,35,37,99–101] This behaviour is a result of the flow of liquid surfactant films separating the droplets and is independent of the viscosity of the internal phase[37].

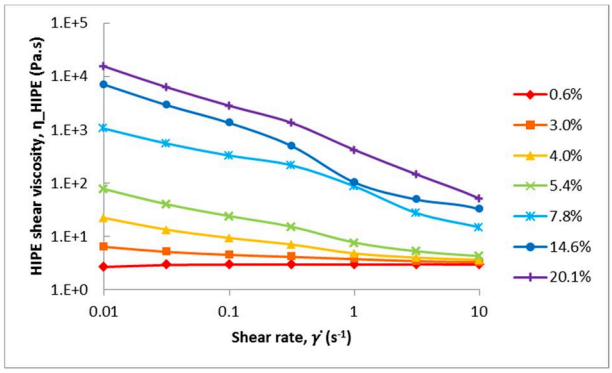

Figure 31: flow curves of HIPEs with different amounts of surfactant in the continuous phase. Low-surfactant HIPEs containing less than 3%C12E6 display Newtonian flow behaviour, evidenced by the flat slope of the flow curve. As surfactant concentration increases, shear-thinning flow behaviour is observed.

Samples with intermediate surfactant concentrations of 4.0% and 5.4% displayed similar shear-thinning behaviour at low shear rates, but their flow curve slopes appeared to taper off to resemble that of low-surfactant HIPEs when shear rates were increased to beyond $\dot{\gamma} > 3.2s^{-1}$. The flat slope for samples containing 0.6% and 3%C12E6 imply that these **HIPEs at ϕ = 0.95 stabilized by very little surfactants behave like Newtonian liquids[35]. This is a finding that has not been reported in literature** at such high volume fraction. Newtonian flow-behaviour has been reported only for emulsions of volume fractions ϕ < 0.60[100,102], beyond which shear-thinning behaviour was found. In the case of polydisperse hard-sphere suspensions, the volume fraction limit for Newtonian behaviour was even lower, at ϕ < 0.45[103]. It appears then, that our HIPEs at low surfactant concentrations may be assimilated to ideal hard-sphere suspensions where every droplet is assumed to follow the same trajectory when subjected to shear[104].

We shall henceforth refer to HIPEs with low surfactant concentrations as "liquid HIPEs" and those at high surfactant concentrations "solid HIPEs" or "Lissant-type HIPEs" on account of their non-flowing property. Samples displaying intermediate characteristics will be called "hybrid HIPEs". We attempt to address the difference in rheological properties of the three types by examining their internal structure.

4.1.3 Different droplet geometries corresponding to each regime

We examined each type of HIPE at ϕ = 0.95 by optical microscopy and found that they presented vastly different droplet geometries depending on the amount of surfactants solubilized in the continuous phase of the sample.

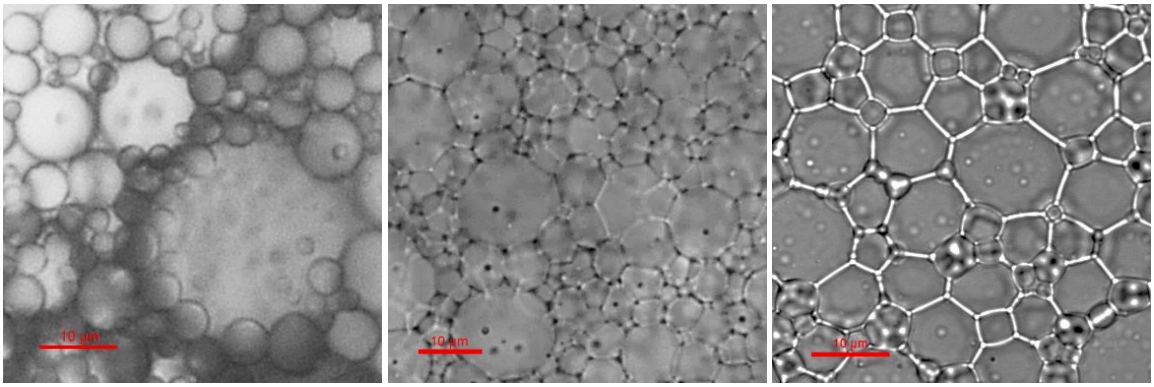

Figure 32: bright-field micrographs of a liquid HIPE containing 0.6%C12E6 in the continuous phase (left), hybrid HIPE containing 5%C12E6 (middle), and solid HIPE containing 20%C12E6 (right).

The droplets in a solid HIPE (with 20%C12E6 in the aqueous phase) were greatly distorted into tessellating polyhedral cells separated by flat, thin films (Figure 32, right). This observation was highly consistent with the multitude of literature on Lissant-type HIPEs which similarly required large quantities of surfactants to stabilise. By lowering the surfactant concentration to 5% (Figure 32, middle), a hybrid geometry was observed, where smaller, faceted droplets could be seen lodged between larger spherical ones with relaxed interfaces. Further reducing the surfactant concentration in the continuous phase to just 0.6%, we found that the droplets in a liquid HIPE transited towards an assembly of undeformed spheres with no visible flat films separating them (Figure 32, left).

The difference in droplet-size distributions between the samples was also immediately apparent when observing under lower magnification (not pictured). The droplets became increasingly polydisperse as the amount of surfactant in the HIPEs was reduced: in the surfactant-rich solid HIPE, the polyhedral droplets were 2 – 20µm across; in the hybrid HIPE, the droplets were between 2 – 30µm; in the surfactant-poor liquid HIPE, the spherical droplets were estimated to have diameters between 1 – 100µm. This strong heterogeneity in sizes exacerbated the difficulty in capturing an image of all the spheres at the same focal depth. We note that sizes under 1µm are also not resolved under an optical microscopy. Thus, we used Light Scattering to properly measure the size distributions in our HIPEs.

Nonetheless, it was surprising that oil droplets in the low-surfactant HIPE retained their spherical shapes with no visible deformation, even at ϕ = 0.95. This type of droplet disposition had been theoretically proposed in literature, but widely believed to be unrealistic (refer to section "2.1.8 Future explorations: Filling space with scale invariance"). We came across a work[75] that briefly observed undeformed spherical droplets in an emulsion at ϕ = 0.88, but only at the beginning of emulsification, and the droplets became increasingly distorted as emulsification progressed (Figure 15). **We therefore believe to be the first to observe, at an internal-phase ratio as high as 0.95, a spherical geometry that is preserved even long after emulsification has stopped.**

4.1.4 Size distribution of each type of HIPE

Herrmann et al. (2012) demonstrated by numerical simulation that in order to pack spheres of an arbitrary size distribution up to a volume fraction approaching unity, the distribution has to be a power law.[70] Using Light Scattering, we measured $n(a)$, the distribution of diameters, a, in our HIPEs to find out if this was really the case. The results were then presented as a double-logarithmic plot to reveal any power-law behaviour (Figure 33).

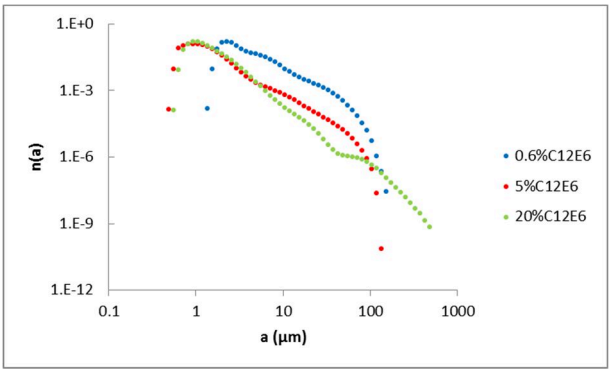

Figure 33: double-logarithmic plot of the diameter distributions measured by Light Scattering of a liquid HIPE (blue), a hybrid HIPE (red) and a solid HIPE (green) containing 0.6%, 5% and 20%C12E6 in the continuous phase. All three samples' distributions obeyed a power law.

We found that the diameter distributions were indeed of the form $n(a) \sim a^{-\gamma}$ over at least two decades of diameters. The power-law exponent, γ, was estimated from the slope of the double-logarithmic plot (Table 2). As mentioned in section "3.2.2.2 Revealing a power-law behaviour" and proven in Supplementary Information section "11.1 Deducing d_f from the double-log plot of Light Scattering measurements", the exponent of our Light Scattering measurements corresponds to the fractal dimension of our samples.

Table 2: the diameter distributions of droplets in each type of HIPE were found to follow a power law over at least two decades of diameters. a_{min} and a_{max} are the minimum and maximum diameters measured for each sample, and γ is the estimated power-law exponent, also the fractal dimension d_f.

HIPE type	a_{min} (µm)	a_{max} (µm)	$\gamma = d_f$
Liquid, 0.6%C12E6	1.36	154	2.01
Hybrid, 5%C12E6	0.82	225	2.28
Solid, 20%C12E6	0.56	484	2.97

4.1.4.1 How to judge polydispersity in power-law distributions

At first glance, one may jump to the conclusion that the Light Scattering measurements contradict micrographs shown in the previous section, because the sizes in a solid HIPE span over a much wider range of values and is therefore more polydisperse than those in a liquid HIPE. However, it is important to note that at the tail end of the size distribution (Figure 33), diameters larger than 20µm were present at proportions between 7 x 10^{-10} and 2 x 10^{-5}. This means that if there were 1.44 billion droplets in the solid HIPE sample measured, it would only take *one* abnormally obese droplet 484µm in diameter to artificially widen the range measured. If we examined cumulative frequencies, however, then there is no contradiction with our visual observations: at 99th percentile, in a liquid HIPE, droplets were 15.4µm or smaller; in a hybrid, 6.3µm or smaller; and in a solid HIPE, 3.8µm or smaller. Thus, we <u>must not</u> only look at the width of the size distribution to judge the polydispersity of a sample. A more accurate determination for power-law distributions is to look at the exponent or fractal dimension.

For a power-law distribution, polydispersity, f, is a decreasing function of fractal dimension (Figure 34). Its expression is given by:

$$f = \left[d_f(d_f - 2)\right]^{-1/2}$$

for any non-integer $d_f > 2$ (refer to Supplementary Information section "11.2 Polydispersity as a function of fractal dimension" for the mathematical proof).

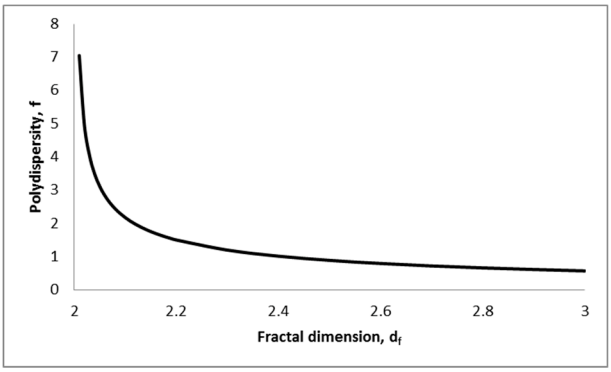

Figure 34: polydispersity, f, as a function of fractal dimension, d_f for a power-law size distribution.

Hence, by this definition of polydispersity in power-law distributions, since d_f was found to increase with surfactant concentration in HIPEs (Table 2), our Light Scattering measurements were coherent with observations under microscope: a surfactant-poor liquid HIPE is indeed the most polydisperse amongst HIPEs, and a surfactant-rich solid HIPE the least polydisperse. This implies that a large

amount of surfactant leads to a less polydisperse population, in agreement with a commonly reported experimental observation that surfactants provide excellent protection from coalescence, a motor for polydispersity in emulsions.

4.1.4.2 Coalescence and fragmentation in HIPEs

Coalescence provokes polydispersity

We calculated the total surface area, A_{oil}, and total volume, V_{oil}, in each of the emulsions. Assuming that each C12E6 surfactant molecule occupies 52 – 55Å^2 in a monolayer at the oil droplet interface[43,45], we then calculated, A_{C12E6}, the total hypothetical surface area that all the surfactant molecules could have occupied, in order to determine the maximum interface coverage by surfactants. The expression for each quantity is given as follows:

$$A_{oil} = \sum_{a_{min}}^{a_{max}} n(a_i) \cdot 4\pi(a_i/2)^2$$

$$V_{oil} = \sum_{a_{min}}^{a_{max}} n(a_i) \cdot (4/3)\pi(a_i/2)^3$$

$$m_{C12E6} = \frac{(V_{oil} \cdot \rho_{oil})}{\varphi}(1-\varphi) \cdot \left(\frac{\%C12E6}{100}\right)$$

where $\rho_{oil} = 905 kg/m^3$, $\varphi = 0.95$, and $\%C12E6$ is the concentration (w/w) of surfactant in the continuous phase of the HIPE;

$$A_{surf} = \frac{m_{C12E6}}{M_{C12E6}} N_A \cdot 55\text{Å}^2$$

with $M_{C12E6} = 450.65 g/mol$ the molecular weight of C12E6, and $N_A = 6.02 \times 10^{23}$ Avogadro's constant.

Table 3: calculation of maximum interface coverage by C12E6 surfactant molecules in each type of HIPE

HIPE	%C12E6	A_{oil} (10^{-12} m^2)	V_{oil} (10^{-18} m^3)	m_{C12E6} (10^{-14} g)	A_{surf} (10^{-12} m^2)	Maximum interface coverage by C12E6 (= A_{surf}/A_{oil})
Liquid	0.6	87.5	273	7.79	57.2	65.4%
Hybrid	5	25.5	72.0	17.1	126	494%
Solid	20	7.65	6.85	6.53	48.0	600%

We found that in liquid HIPEs, only 65.4% of the droplet interfaces were covered by surfactant molecules, whereas in hybrid and solid HIPEs, the coverage was far superior to 100%, i.e. the interfaces were saturated and there was excess C12E6 (Table 3). **This implies that coalescence can occur in liquid HIPEs due to incomplete protection, whereas it is severely inhibited in hybrid and solid HIPEs**: were a pore to randomly open between two adjacent HIPE droplets, there would be an abundance of surfactants floating around to rush in and plug and repair the pore in hybrid and solid HIPEs, but not in liquid HIPEs. Considering this finding with the polydispersity of droplet-size distributions measured in the previous section, we may discern the correlation between coalescence in the system leading to higher polydispersity.

Fragmentation causes power-law size distributions in all HIPEs

If having lots of surfactant in the system inhibits coalescence, why would hybrid and solid HIPEs still possess a power-law distribution of sizes, instead of being monodisperse? This may be explained by *how* our HIPEs are made: by fragmentation under high-energy shear from the propeller mixer.

Studies on fragmentation mechanism in granular materials regularly find either log-normal or power-law distributions. The former is obtained when grains fragment independently of one another at the same frequency, whereas the latter is obtained through on-going (sometimes explosive) fragmentation, where the breakage of a particle depends on forces transmitted to it by its immediate neighbours (Herrmann et al.)[105,106]. The exponent is then between 2.0 and 2.8, the value being dependent on the number of immediate neighbours (Steacy and Sammis, 1991)[107]. Clearly, in a HIPE, oil droplets are so densely packed that they are in contact with one another and independent fragmentation under shear becomes highly improbable in such a structure. The independent fragmentation theory could also explain why log-normal and normal distributions (described and characterized by their means and variances) are so commonly reported in polydisperse emulsions at low volume fractions – because colloidal droplets are sufficiently spaced apart – while power-law size distributions remain a rarity.

It has also been documented in existing literature that prolonged stirring of HIPEs (Lissant-type, with lots of surfactant) refines the size distribution[51,75], resulting in monodisperse emulsions. This is where our protocol differs, because we stopped stirring as soon as the last drop of oil had been added, hence why we were able to repeatedly observe power-law distributions in our solid and hybrid HIPEs.

As such, we propose that all HIPEs go through a stage during emulsification where the prevailing size distribution is a power law due to the fragmentation of densely packed droplets within close confines. As emulsification progresses, each smaller droplet created through fragmentation is preserved in hybrid and solid HIPEs thanks to the abundance of surfactants. With prolonged stirring, the sizes become increasingly homogeneous, stabilizing at the smallest size created through fragmentation.

A novel approach: simultaneous fragmentation and coalescence in liquid HIPEs

In the case of liquid HIPEs, the lack of surfactant means that smaller droplets created through emulsification are not preserved, and may undergo coalescence with one another *during* fragmentation. **The novelty in our approach is to allow both coalescence and fragmentation to take place simultaneously, especially in a HIPE at $\phi = 0.95$.** As demonstrated in our literature review and in published works cited throughout this dissertation, coalescence in HIPEs has always been suppressed by virtue of formulating with large amounts of surfactant. In work done on dilute colloids, the usual approach is to favour one process over another, and to consider fragmentation as independent and with opposing consequences to coalescence:

> "Breakage tends to decrease droplet size and increase the number of drops, while coalescence has the reverse effect… The problem can be simplified… by first analyzing only the breakage process, since coalescence is often reduced to a negligible level… in dilute dispersed phase systems or when surface-active agents are present" – Amundson et al. (1966) in "Analysis of breakage in dispersed phase systems."[108]

We therefore believe that it is this novel approach that allowed us to obtain an Apollonian packing in our liquid HIPEs, which will be discussed further.

4.1.5 Link between a HIPE's microstructure and its rheological behaviour

A strong correlation between the macroscopic flow behaviour of the HIPEs and their microscopic structures in terms of droplet geometry seems to exist.

4.1.5.1 Rheological properties of solid and hybrid HIPEs

Although we call our surfactant-rich, Lissant-type HIPEs "solids" in this work, they are really viscoelastic soft matter materials and begin to flow beyond their "yield stress". This class of HIPEs has been extensively studied and their flow behaviour has been explained in terms of the flow of liquid surfactant films separating the polyhedral droplets.[19,25,35,37,99–101] In addition, the fairly high G' values of solid HIPEs, characterizing their elastic responses to applied stress, are attributed to the storage of energy in the already-deformed droplet interfaces by further distorting them.[28,101]

While our rheological results and microscopic observations appeared to be in qualitative agreement with existing literature on solid HIPEs, we noticed that these investigations focused largely on the variation of rheological properties as a function of volume fraction and droplet size of rather monodisperse populations. For instance, Mason et al. (1995) found empirically that above a critical volume fraction, $\varphi_c \approx 0.64$ when droplets begin to undergo deformation and jamming,

$$G'(\varphi_{eff}) \sim (\sigma/a)\varphi_{eff}(\varphi_{eff} - \varphi_c)$$

with σ the interfacial tension, a the radius the monodisperse droplets, and φ_{eff} the effective volume fraction of the emulsion, which considers the thickness of surfactant films as part of the droplets.[27] The definition of φ_{eff} is given by:

$$\varphi_{eff} \approx \varphi(1 + 3h/2a)$$

where φ is the real volume fraction and h is the thickness of the films that depends on φ.[15] Most importantly, the underlying assumption for this approximation is that the droplets are spherical[24,27] (which they are not).

In our work, we kept volume fraction constant at 0.95. σ/a, being the energy density of undeformed droplets[27], was also more or less constant in the solid HIPEs. Yet, in Figure 29, we could discern a half a decade's increase in G' between the samples with 7.8% and 20.1% surfactant in the continuous phase. There was also a two-decade increase in G' between hybrid and solid HIPEs. It would appear then that our work may contribute to filling the gap in literature where φ is kept constant while h is varied.

We subsequently used Small-Angle X-Ray Scattering to study the surfactant film structures in our HIPEs to measure h, which so far has deluded the previous works cited and has been variously estimated to be anywhere between 5nm[27], 17.5nm[24,27], 20nm[19], or summarily assumed to not exceed 100nm[25,101].

4.1.5.2 Measure of surfactant film thickness by SAXS

To study the surfactant film structures in-situ, we measured the concentrated spectra of undiluted solid HIPEs by SAXS. Since the internal-phase volume fraction of our HIPEs was incredibly high (ϕ ≈ 0.95), it was easier to analyze their spectra as interferences between the films that separated oil droplets, thanks to the Babinet principle of reciprocity (1837)[109]. The theorem states that "complementary objects produce the same diffraction effects" and Guinier and Fournet (1955) demonstrated mathematically that the principle holds true for small-angle scattering by "an ensemble of particles".[110] This is why the background that we subtracted from the samples' concentrated spectra was ϕ· $I_{oil}(q)$.

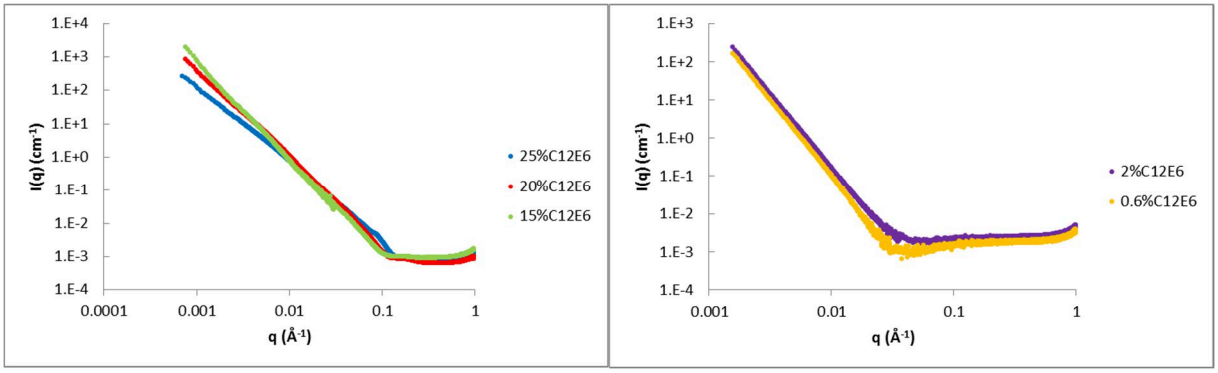

Figure 35: concentrated spectra after background subtraction of HIPEs containing 25%C12E6 (blue), 20%C12E6 (red), 15%C12E6 (green), 2%C12E6 (purple), 0.6%C12E6 (yellow) in the continuous phase. Note: for the HIPE with 25%C12E6, a corrective factor of 0.9 was applied to background subtraction at q values > 0.01Å^{-1}. This was to account for slight variations in glass capillary thickness (2 ± 0.1mm) in which the background (oil) and the sample were measured. If no corrective factor was applied, $I(q)$ for this sample became negative at high q which was physically unrealistic. The spectra on the left were measured at ESRF and those on the right at SOLEIL, hence the difference in q-range.

Figure 35 shows I(q), the scattered intensity after background subtraction, of three solid HIPEs containing 25%C12E6, 20%C12E6 and 15%C12E6 in the continuous phase, one borderline hybrid HIPE made with 2%C12E6 and one liquid HIPE made with 0.6%C12E6. A notable result was that $I(q)$ appeared to follow a power law over two decades of q values (for spectra measured at ESRF) while spanning over five decades in magnitude. It is uncommon to find concentrated systems in which pair-correlations are self-similar functions over such a wide range and we attempted to interpret the spectra.

For starters, we assumed that contributions from Plateau borders may be neligible, as our HIPEs had such low continuous-phase content that they resembled dry foams rather than wet foams[11]. We further assumed that thanks to the thinness of the surfactant films, the distribution of distances between pairs of points in these films may be assimilated to the distribution of chord segments. At physical scales much larger than the average film thickness h, i.e. $qh \ll 1$, the system appears as a set of thin self-similar (fractal) films. These films may be characterized by their fractal dimension, d_s, and the scattered intensity varies as[111]:

$$I(q) \sim q^{d_s - 6}$$

On the contrary, at physical scales much smaller than the average film thickness, $qh \gg 1$, the scattering necessarily has to follow Porod's law:

$$I(q) \sim q^{-4}$$

We used SASview to fit a power-law model to the spectra in Figure 35 for q = 0.001 – 0.05Å^{-1}. The power-law exponent found are presented in Table 4.

Table 4: power-law modelling of concentrated spectra of HIPEs.

C12E6 concentration in HIPE's aqueous phase	Power-law exponent	d_s
25%	-2.2997	3.70
20%	-2.548	3.45
15%	-3.003	3.00
2%	-3.9176	2.08
0.6%	-3.9886	N/A; Porod's law

For the hybrid and surfactant-rich solid HIPEs, their exponents allowed us to calculate a value for d_s by adding 6. The fractal dimensions found of solid HIPEs with a power-law distribution between 3-4 indicate that they are surface fractals[111], whereas the the liquid HIPE was found to obey Porod's law, indicating that the droplet interfaces were entirely smooth[112] and that there were no flat surfaces. This result corroborates our observations that oil droplets are not deformed in liquid HIPEs. The trend in increasing fractal dimension as a function of surfactant concentration also confirmed results found by Light Scattering (refer to section "4.1.4 Size distribution of each type of HIPE").

We may imagine that $I(q)$ is a sum of the scattering by the set of fractal films, and by whatever is in each of these films. As such, we subtracted the power-law model from $I(q)$, and analyzed the remainder accordingly. A "hump" feature consistently showed up between q = 0.002 – 0.02Å^{-1} for the solid and hybrid HIPEs (Figure 36). The hump was conspicuously absent for the liquid HIPE, coherent with the sample obeying Porod's law and presenting no flat films.

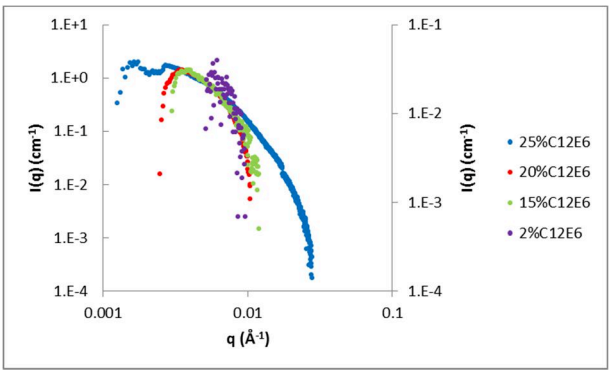

Figure 36: upon subtracting the power-law model, a hump feature appeared at q = 0.002 – 0.02Å^{-1} in the scattering of all three solid HIPEs (blue, red, green) and the hybrid HIPE (purple). Note: the hybrid HIPE's $I(q)$ has been plotted on a secondary vertical axis on the right, for the purpose of visualization.

Every material has its own scattering length density (SLD), which characterizes its X-ray diffusivity and is a function of its electronic density. We calculated the SLD of the components in our system for an X-ray source of 1Å-wavelength (Table 5). As the exact chemical composition of the mineral oil was unknown, we assumed that it was chemically similar to a heavy alkane like squalane.

We postulated that a multi-layer lamellar model would most likely describe the structure of the thin films separating adjacent HIPE droplets in surfactant-rich solid samples. Since a hybrid HIPE's droplets is somewhere between round and polyhedral (Figure 32, middle), we used a 5-shell "onion"

model description for it. The lamellar model inherently assumed solvation of the surfactant's hydrocarbon chain in the mineral oil. In the onion model, oil was taken to be both the core of the onion and the solvent, hence five symmetrical shells formed by C12E6's hydrocarbon chain (C12) and polyoxyethylene groups (POE), and water. Locally, by examining the space between two oil droplets, these models can be considered equivalent, as depicted in Figure 37, because we set the radius of the onion core to 0.

The area per molecule for a monolayer of C12E6 saturating a liquid interface is given in literature as 52 – 55Å^2.[43,45] Knowing its molecular mass and its density – 450.65g/mol and 1g/cm^3 – we calculated the volume of a C12E6 molecule to be 750Å^3. The corresponding length of the molecule is then approximately 14Å. Compared to the 38 – 39Å found in literature as its extended molecular length[43,81], the order parameter of the surfactant is roughly 0.36. Since it is known that a C-C bond length is 1.54Å, we estimated the thickness of the C12 layer and the POE layer at 7Å each and set these values in our modelling.

Table 5: calculated values of SLD for oil, surfactant and water. These parameters were subsequently used for spectra modelling.

	Chemical formula	Density (g/cm^3)	SLD (10^{-6} Å^{-2})	Layer thickness (Å)
Mineral oil	Assimilated to $C_{30}H_{62}$	0.905	8.8	0
C12 chain of surfactant	$C_{12}H_{26}$	0.75	7.33	7
POE groups of surfactant	$C_{12}H_{24}O_7$	1.12	10.3	7
Water	H_2O	1	9.44	To be determined

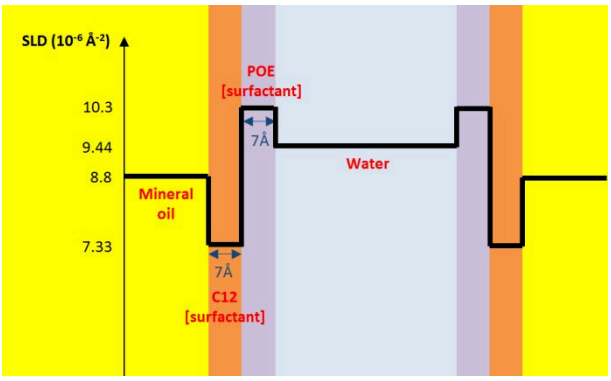

Figure 37: the SLD profile used to model the surfactant films separating two oil droplets

We found that the respective models fitted relatively well experimental data points between q = 0.003 – 0.01Å^{-1} (Figure 38). In the case of the solid HIPE containing 25%C12E6 in its continuous phase (Figure 38a), although the experimental points did not show any discernible oscillations due to noise from spectra subtraction, oscillations from the bilayer model coincided with abrupt amplitude variations in the experimental data at the same q values. The values of the water layer thickness found from the model fitting are summarized in Table 6. We deduced the total surfactant film thickness separating two adjacent HIPE droplets by adding 28Å corresponding to the combined thicknesses of the C12 and POE layers.

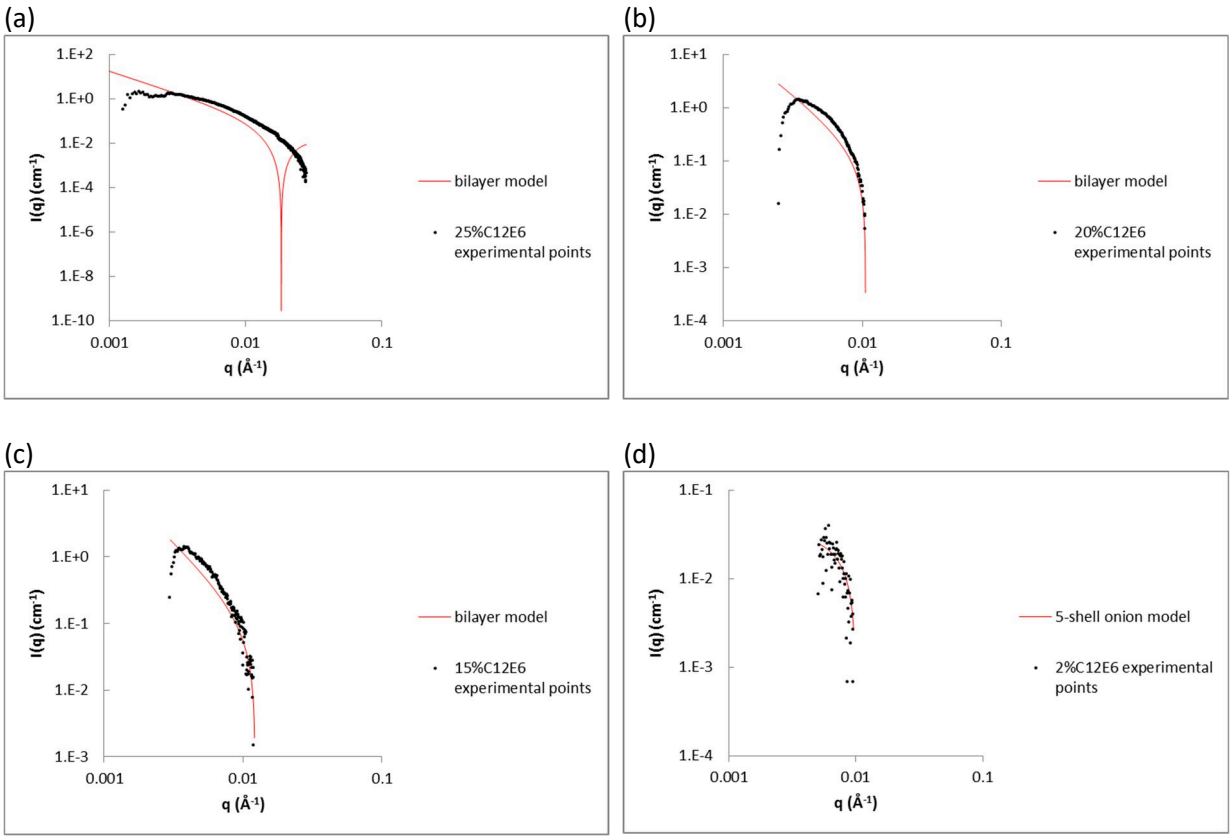

Figure 38: fitting experimental points (black circles) with a bilayer lamellar model (red solid line) for (a) – (c); and by a 5-shell onion model (red solid line) for (d) to deduce the thickness of surfactant films separating oil droplets. Each layer's SLD value is found in Table 5. The hydrocarbon chain was assumed to be solvated in the bilayer model, while oil was taken to be the onion's core (with its radius set at zero) as well as the solvent. The thickness of each C12 layer and POE layer was set at 7Å.

Table 6: thickness of the water layer given by modelling for each HIPE sample. The surfactant film thickness was deduced by adding 28Å.

%C12E6 in HIPE's continuous phase	Water layer thickness from modelling (Å)	Surfactant film thickness (= water layer + 2 x C12 layer + 2 x POE layer) (Å)
25	172	200
20	130	158
15	104	132
2	81.005	109

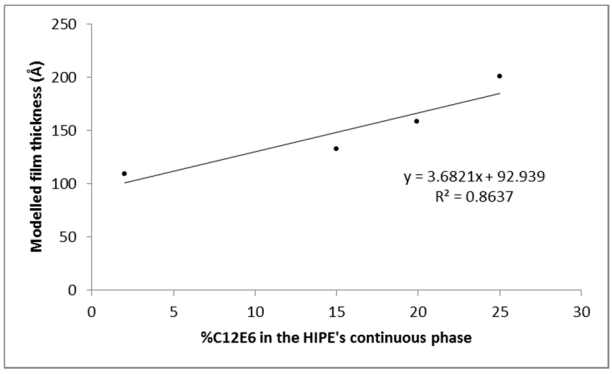

Figure 39: surfactant film thickness separating adjacent HIPE droplets were deduced from modelling, and found to be 200Å, 158Å and 132Å in solid HIPEs containing 25%, 20% and 15%C12E6 in the continuous phase respectively. For the hybrid HIPE containing 2%C12E6, the film thickness was 109Å.

Our modelling found surfactant film thickness in solid HIPEs to be 13.2 – 20nm. These values are quite similar to values estimated in literature at 17.5 – 20nm[19,24,27]. For the borderline-hybrid HIPE containing 2%C12E6, it was approximately 10.9nm. There appeared to be a proportional relationship between film thickness and surfactant concentration in the HIPE's continuous phase, as demonstrated by the regression line traced in Figure 39. Our results here appear to qualitatively validate the empirical relations between G' and film thickness, h, and this could very well explain the increasing trend of G' that we observed as we increased surfactant concentration in our HIPEs (Figure 29). We believe that when a HIPE is subjected to external mechanical stresses, a thicker film allows for more deformation of the droplet interfaces without rupturing the film, and thus more elastic energy can be stored.

Nevertheless, we wish to be prudent and caution against drawing any firm conclusion at this point: it would have been ideal if we could have performed a series of SAXS experiments on the same instrument, over the same q-range while systematically varying HIPE surfactant concentration and ensuring perfect background subtraction. Then, the measurement and modelling of film thickness of HIPEs could have been done with more certainty and the results gleaned been more conclusive.

4.1.5.3 The Farris effect

To begin, we compare the order of magnitude of our samples' shear viscosities (Figure 31) at rest or very low shear rates ($\dot{\gamma} = 0.01 - 0.03s^{-1}$). Liquid HIPEs' shear viscosities are only 3 – 6 Pa.s, and this rises to 20 – 60 Pa.s for hybrid HIPEs, and then jumps to 800 – 10000 Pa.s for solid HIPEs. Clearly, the presence of thin, flat films in solid HIPEs separating the polyhedral droplets has a pronounced effect on a sample's resistance to flow. But if we were to restrict our comparison to liquid and hybrid HIPEs which possess closer droplet geometries, we may notice that the variation in shear viscosity appears to demonstrate the Farris effect (1968).

Farris proposed the theory and verified it against published experimental data that at the same volume fraction, the viscosity of a suspension of spheres decreases as the spheres' size distribution becomes more polydisperse[113]. The underlying assumptions made were that the spheres of each size class behaved independently of one another and had no interactions. Although Farris only demonstrated his calculations up to $\phi = 0.75$ with a tridisperse population, it would seem that the effect is also present in our HIPEs at $\phi = 0.95$ as we confirmed by Light Scattering measurements and from SAXS fractal dimensions that a liquid HIPE is indeed more polydisperse and less viscous than a hybrid one.

4.1.5.4 Newtonian flow behaviour in liquid HIPE

In our liquid HIPEs, the oil droplets appear to be free of mutual deformation in spite of their close proximity to one another in such a dense packing. We interpret the retention of their spherical shapes as a physical manifestation of the absence of strong interactions between them. Consequently, they may be approximated as a collection of hard spheres, even if the hard-sphere approximation for colloidal droplets is conventionally only valid at low volume fractions. Furthermore, SAXS measurements indicate that there are no flat continuous-phase thin films separating the emulsion droplets, unlike in hybrid and solid HIPEs. Then that the droplets are free to roll over one another without creating torsion friction, much like what happens in space-filling bearings[114]: in such bearings, a sphere in the cluster can rotate freely in space and its neighbours react correspondingly without slippage and without getting in the way of one another (no torsion friction).

This idea of droplets not getting in the way of one another is also explained in Farris' work. It has been shown that in bimodal and multi-modal suspensions, smaller particles could be considered to constitute a homogeneous viscous fluid to larger particles moving in said fluid, if the ratio of their sizes was less than 10%. Otherwise, the larger particles experienced a zig-zag motion.[113,115] Since the oil droplet sizes in our liquid HIPEs effectively follow a continuous power law, **we hypothesize that each smaller size-class may serve as a homogeneous lubricating fluid to the larger ones**, acting like a "third-body fluid"[116] (a concept introduced by Godet and widely applied in tribology). Thus, when the liquid HIPE is subjected to shear, all the droplets can roll over one another and undergo laminar trajectories, resulting in the sample's overall Newtonian behaviour[104].

We believe that our ability to make liquid HIPEs with persisting spherical droplet geometry enabled us to be the first to observe Newtonian behaviour in such a highly dense emulsion. Moreover, it would seem that nobody was particularly interested in such a geometry – others studying rheological properties of concentrated emulsions had simply worked polyhedral droplets in solid HIPEs.

4.2 Evolution of liquid HIPEs

4.2.1 Evolution towards an Apollonian exponent

From Light Scattering measurements, we found that droplet sizes in our liquid HIPEs were power-law distributed and the exponent gave directly the fractal dimension, d_f. We also established that coalescence could occur due to the incomplete coverage of interfaces. Naturally, the next step was to find out how liquid HIPEs evolved through coalescence.

We made many liquid HIPEs at ϕ = 0.95 with 0.6%C12E6 in the continuous phase under different shearing conditions (250rpm, 500rpm and 1000rpm). We then allowed them to age at room temperature over a month and their size distributions were periodically measured by Light Scattering (Figure 40).

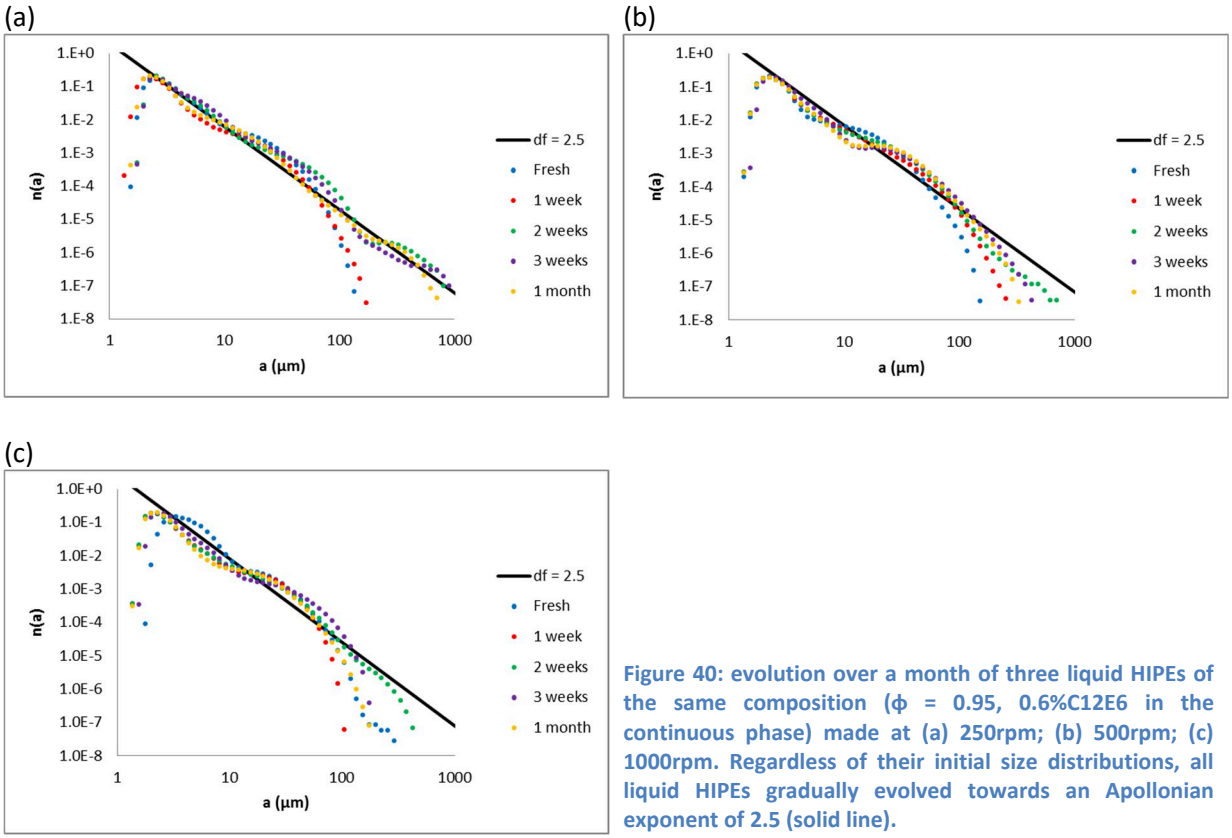

Figure 40: evolution over a month of three liquid HIPEs of the same composition (ϕ = 0.95, 0.6%C12E6 in the continuous phase) made at (a) 250rpm; (b) 500rpm; (c) 1000rpm. Regardless of their initial size distributions, all liquid HIPEs gradually evolved towards an Apollonian exponent of 2.5 (solid line).

At the outset of emulsification when the samples were fresh, d_f could take on any value between 2 and 2.5, with diameters measured between 1.36 – 290µm. This was entirely dependent on the emulsification conditions that were specific to each sample. Yet, regardless of the initial state of the liquid HIPEs, we found the same evolution repeatedly across samples: after about a week, in spite of the creation of droplets as large as 916µm by coalescence, d_f consistently tended towards and remained at 2.5. This value coincides with that for a Random Apollonian Packing of spheres, for which the most commonly cited value is 2.47[59,73], and has been variously calculated by numerical simulations to be between 2.45 – 2.52.[60,72,74] We calculated, just as we did in section "4.1.4.2 Coalescence and fragmentation in HIPEs", the total droplet surface area in the liquid HIPEs, and the interface coverage by surfactant molecules.

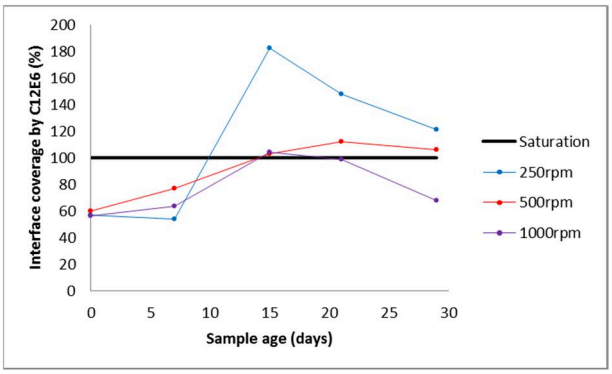

Figure 41: variation over a month of oil droplet interface coverage by surfactant molecules in the same liquid HIPE samples as in Figure 40, made at 250rpm (blue), 500rpm (red) and 1000rpm (purple). The black solid line on the graph on indicates 100% interface coverage: this means that values > 100% correspond to an excess amount of surfactant in the system with respect to the droplet surface area to occupy.

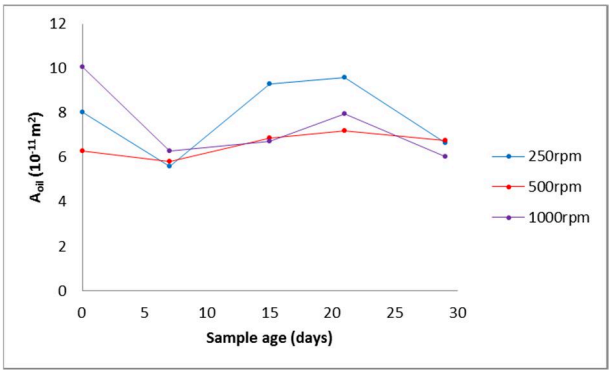

Figure 42: variation over a month of the total oil droplet surface area in the same liquid HIPE samples as in Figure 40.

We found that immediately after emulsification, only 60% of the interface in all the liquid HIPEs were protected by surfactants (Figure 41). Coalescence could therefore occur. As it proceeded, larger droplets began to be created and the total surface area diminished (Figure 42). Then, at some point between 10 – 15 days after the HIPEs were made, all the droplets' interfaces became saturated with surfactant molecules (crossing the solid black line in Figure 41). From then on, we may assume that there would be excess surfactant molecules in the continuous phase. At around the same time, total droplet surface area began to increase, signalling the appearance of small droplets, an opposite effect to coalescence.

Our interpretation is here is that somehow, the system created small droplets to consume the excess surfactants, because surface area steadily increased until day 21 (Figure 42). We may then imagine that eventually so many small droplets (and so much surface area) were created that the system began to run out of excess surfactant. Thus, coalescence could occur again, as indicated by the lowering surface area after the three-week time point. This discussion will be further explored in section "4.3.1 Creation of smaller droplets in a HIPE".

In the case of the 1000rpm liquid HIPE (Figure 41, purple), surfactant coverage of interface appeared to even fall below saturation after day 21. We do not see any real reason why surfactant molecules sitting pretty at a droplet interface would be extracted to feed other smaller droplets, so this drop below interface saturation should be interpreted with a pinch of salt.

We would like to caution at this point that Light Scattering measurements could not measure the presence of these small droplets due to the limits of detection by laser diffraction – our instrument was equipped with two lasers of wavelengths 470nm and 632.8nm, which means that particles smaller than half-wavelength, i.e. 235nm, may not be properly resolved.

4.2.2 Persistence of the Apollonian exponent

We kept at room temperature a liquid HIPE containing 0.6%C12E6 in the continuous phase and measured its size distribution over 8 months (Figure 43). Even after such a long time, the Apollonian fractal dimension of 2.5 was still clearly present. The droplet diameters were initially between 0.93 – 62.8µm and had expanded to 1.54 – 916µm with ageing. We were unfortunately unable to make further measurements by Light Scattering due to instrument maintenance, but the sample was kept up to a year and still remained visually emulsified. This particular sample was analyzed by SAXS when it was 327 days old (11 months) and its result is presented in section "4.2 Evolution of liquid HIPEs - 4.2.5.1 Two populations of swollen micelles".

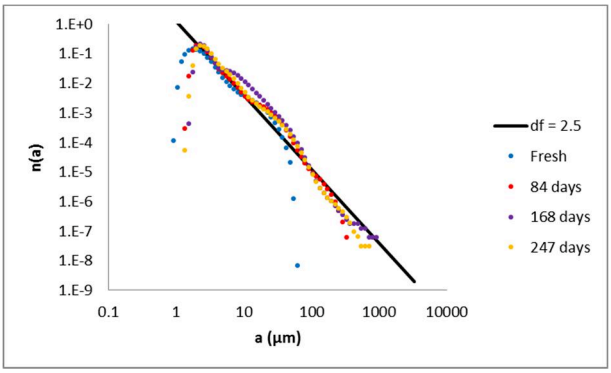

Figure 43: Light Scattering measurement over 8 months of a liquid HIPE. The Apollonian exponent was clearly still present in spite of coalescence over time, shifting the droplet diameters from 0.93 – 62.8µm to 1.54 – 916µm.

4.2.3 Proof of Apollonian droplet packing through SAXS

Although our liquid HIPEs possessed the right exponent indicating that they had the necessary size distribution for a Random Apollonian Packing (RAP), this was not sufficient proof. To determine if we indeed had this peculiar droplet packing which has never been observed in real systems, we measured $S_{exp}(q)$, the structure factor, of our samples by SAXS at ESRF. $S(q)$ reflects the relative in-situ positions of neighbouring droplets and is therefore a much better indicator of packing than d_f measured by Light Scattering where the HIPEs were diluted. In any case, fractal dimension is not a unique identifier. We allowed our liquid HIPE samples from section "4.2.1 Evolution towards an Apollonian exponent" to age for a month before the SAXS experiments, so that d_f could attain 2.48 – 2.50.

$S_{exp}(q)$ was obtained from dividing the concentrated spectra by the diluted spectra, i.e. $I(q)/P(q)$ (refer to section "3.2.3.2 Calculating the experimental structure factor, $S_{exp}(q)$" for more details). At the same time, we performed a numerical simulation of RAP and calculated its $S_{cal}(q)$ to serve as a basis for comparison (Figure 44).

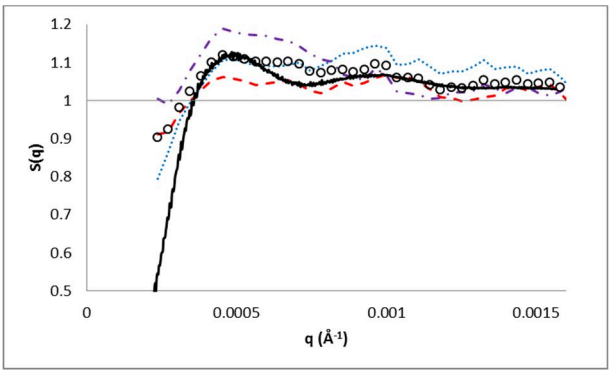

Figure 44: comparison between $S_{exp}(q)$ for liquid HIPE samples at ϕ = 0.95, aged 1 month, made at 250rpm (blue dots), 500rpm (red dash), and 1000rpm (purple dot-dash). The open circles are average values of these three samples. The solid black line is $S_{cal}(q)$ for a numerically simulated RAP at ϕ = 0.92. We demonstrated in section "3.2.4.2 Calculating the Apollonian structure factor, $S_{cal}(q)$" that $S_{cal}(q)$ was nearly identical for ϕ = 0.84 – 0.92 and should still be a valid comparison for ϕ = 0.95.

We found great agreement between $S_{exp}(q)$ and $S_{cal}(q)$ which presented the same features of a broad primary peak at $S_{max}(q)$ = 1.1 – 1.2, and a tapering tail that rapidly approached 1. The flattened nature of the peak and lack of oscillations signified that there was an absence of periodicity neither in our liquid HIPE samples nor in the simulated RAP. Such an allure for $S(q)$ is rarely found in colloids, because as soon as there is any long-range ordering, even in moderately polydisperse systems, $S(q)$ shows tell-tale oscillations with sharp peaks[117] and $S_{max}(q)$ > 2.85.[118] Only in the case of extreme polydispersity is $S_{max}(q)$ depressed and close to 1 (Van Beurten and Vrij, 1981).[119]

We took the precaution of combing through literature for other size distributions that could potentially give similar S(q) to our HIPEs (Figure 45, Figure 46 and Figure 47). While these structure factors do resemble our $S_{exp}(q)$, their reported size distributions and polydispersities were markedly different from that of our HIPEs. Most importantly, the volume fractions involved were significantly inferior to ϕ = 0.95. As such, we could conclude that **our liquid HIPEs were indeed a Random Apollonian Packing**.

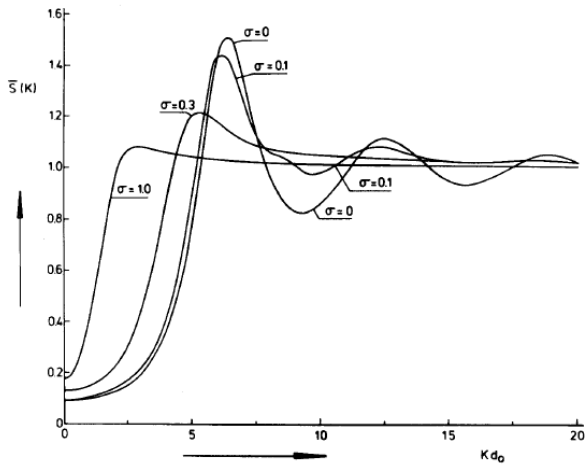

Figure 45: $S(q)$ for Schulz distributions of hard spheres with σ = 0.3-1.0 at ϕ = 0.3.[119]

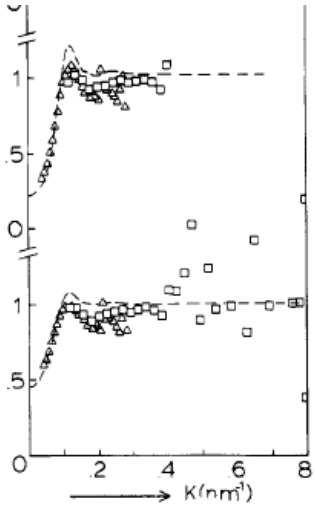

Figure 46 : $S(q)$ for log-normal distributions of hard spheres with σ = 0.12 at ϕ < 0.5.[120]

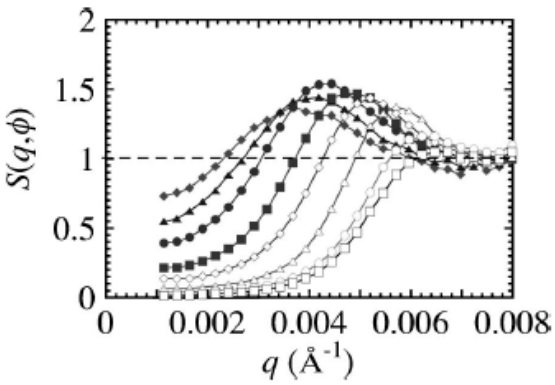

Figure 47 : the flattest $S(q)$ belongs to a unimodal distribution with σ = 0.25 at ϕ = 0.53.[31]

4.2.4 Confirming Light Scattering observations by SAXS

4.2.4.1 Evolving towards RAP after 1 week

Since Light Scattering measurements indicated that the Apollonian fractal dimension was typically attained after 1 week (Figure 40), we measured $S_{exp}(q)$ for liquid HIPEs of different ages (freshly made, 1 week old, 1 month old) made at 500rpm, and compared it to $S_{cal}(q)$ (Figure 48).

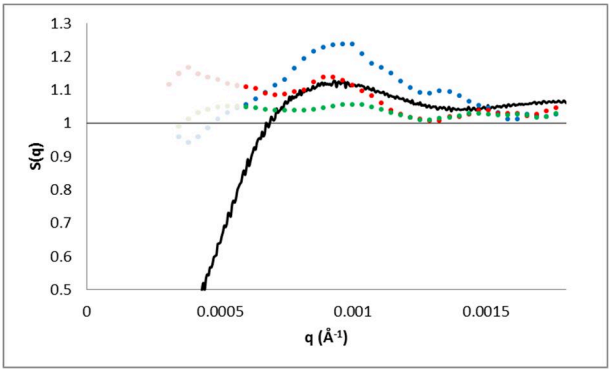

Figure 48: comparison between $S_{cal}(q)$ for a simulated RAP (solid black line) and $S_{exp}(q)$ for liquid HIPE sample made at 500rpm at different ages: fresh sample (blue), 1 week old (red), 1 month old (green). The first ten or so points are in the beam stop and have been greyed out.

The first ten or so measurement points in the lowest q-region are usually in the SAXS instrument's beam stop and so these are not considered. Once again, we found the same $S_{exp}(q)$ shape and there was excellent correspondence between the experimental data and the calculated $S(q)$ for a simulated RAP. $S_{max}(q)$ was between 1.05 and 1.24, with the fresh sample showing the highest peak, and the oldest sample showing the lowest. Since polydispersity depresses the peak[119], it stands to reason that the HIPE that has been allowed to evolve through coalescence for a longer period would possess the flattest peak. Thus, our observations by Light Scattering were validated through $S(q)$ comparison – liquid HIPE allowed to evolve for a week or more had a droplet packing that were closer to a RAP.

4.2.4.2 Increasing surface area with time

We also used SAXS to confirm the increase in surface area that was given by Light Scattering measurements. By examining the diluted spectra, $P(q)$, for the liquid HIPEs at different ages (same samples as in section "4.2.4.1 Evolving towards RAP after 1 week"), we found a substantial segment over 2 decades of q values that could be described by a power law (Figure 49) due to the scale invariance of the samples.

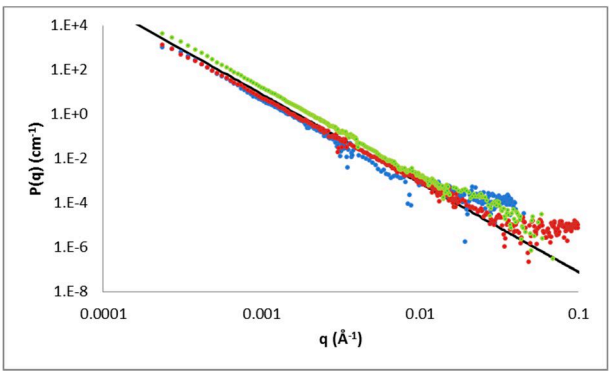

Figure 49: diluted spectra of liquid HIPEs made at 500rpm at different ages: fresh sample (blue), 1 week old (red), 1 month old (green). The solid black line has a power-law exponent of -4, corresponding to Porod's law.

We used SASview to do the power-law fitting from q = 5 x 10^{-4} – 6 x 10^{-2} $Å^{-1}$, ignoring the first points at low q values that were in the beam stop. The exponents were very close to -4 which corresponds to Porod's law. In this regime, a particle's scattering $I(q)$ is given by the following expression[121]:

$$I(q) \approx 2\pi(\Delta\rho)^2 A \cdot q^{-4}$$

where $\Delta\rho$ is the difference in SLD between the object and its surrounding solvent, and A is the total interface area. This approximation was independently derived by Porod (1951)[122] and by Debye et al. (1957)[123], and has been experimentally validated. Thus, by examining the scaling factor of our power-law fitting, we could determine the evolution of A with time (Table 7 and Figure 50).

Table 7: power-law fitting using SASview of $P(q)$ at different liquid HIPE ages

Age of liquid HIPE	Power-law exponent	Scaling factor ≈ $2\pi(\Delta\rho)^2 A$
Fresh	4.2609	1.29e-8
1 week	3.9935	5.76e-8
1 month	4.0558	1.24e-7

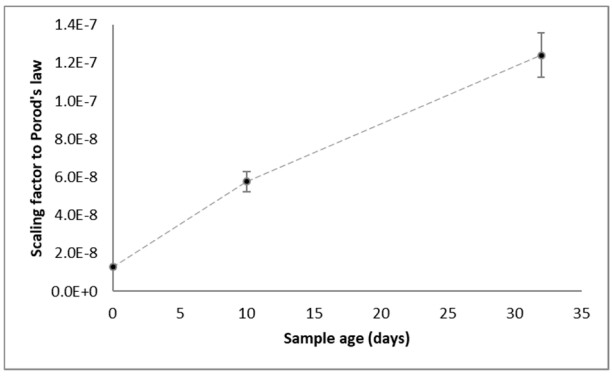

Figure 50: plot of the scaling factor to Porod's law, which is directly proportional to the total interface area, as a function of sample age. The increasing trend appeared to validate observations by Light Scattering.

The scaling factor increased with time, signalling an increase of total surface area in the liquid HIPEs as the samples aged. This trend appeared to validate the *net* increase in surface area observed from Light Scattering measurements, reported in Figure 42. The corroboration between SAXS and Light Scattering lends weight to the inference that more and more small droplets were appearing in liquid HIPEs as they evolved through coalescence.

4.2.5 Existence of swollen micelles observed by SAXS

What could be these small droplets that were too small to be resolved by laser diffraction-based Light Scattering? Did they really exist, and if so, why were they being created? To answer these questions, we used SAXS to study the higher q-region in our liquid HIPEs at different ages. The region of interest was q > 0.01Å^{-1}, corresponding to physical distances smaller than 100nm. Having established that oil droplets in the liquid HIPEs were self-organised as a Random Apollonian Packing, we henceforth refer to the samples as Apollonian HIPEs.

From the spectra measured at ESRF, we noticed that $P(q)$ consistently presented a power law and a shoulder appearing around q = 0.03Å^{-1}. This was particularly evident in the Apollonian HIPE that was a month old (Figure 51).

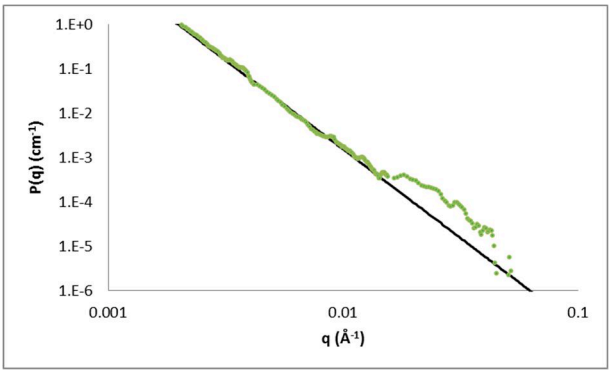

Figure 51: a zoom-in of Figure 49 in the scattering region where q > 0.01Å^{-1}. The scattering could be decomposed into a power law (given by the solid black line), and a shoulder feature appearing at q = 0.03Å^{-1}. This decomposition was valid for other Apollonian HIPEs of different ages, but only the 1-month old sample has been plotted here for clearer visuals.

We were certain that the shoulder was not due to excess continuous phase – the diluting medium for measuring $P(q)$ – because the signal of the pure micellar solution of C12E6 at 0.6%(w/w) had already been subtracted as background. Since we also demonstrated that there were no flat films in liquid HIPEs (see section "4.1.5.2 Measure of surfactant film thickness by SAXS"), and since the shoulder only appeared in the diluted spectra where HIPE droplets were sufficiently spaced out, this excess signal with respect to the power law had to come from objects that were located in the regions of between HIPE droplets.

Setting the solvent SLD to be that of water, we began by testing a hard-sphere model and found that spheres approximately 20nm in diameter could describe the shoulder, provided that the sphere's SLD was 8.8952 (found by fitting). This value closely replicated the SLD of mineral oil that we had estimated in Table 5, at 8.8. Based on these indications, we proceeded to fit the shoulder with a core-multi-shell model, because any oil droplets would have to be stabilized by a layer of surfactant.

The parameters and SLD profile used for the core-multi-shell model (Figure 52) were in accordance to the calculations applied in Table 5.

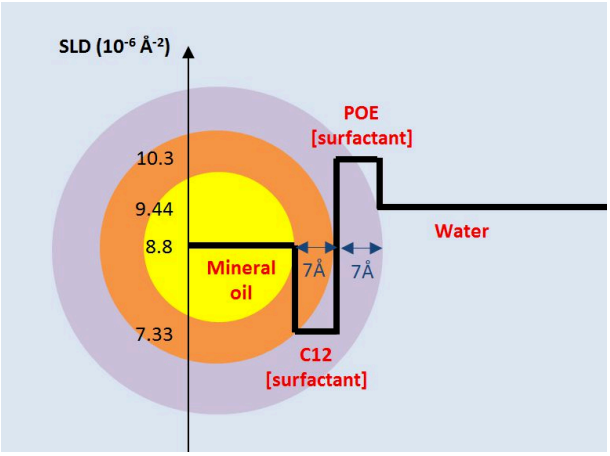

Figure 52: the SLD profile of the core-multi-shell structure used to model the objects between HIPE droplets.

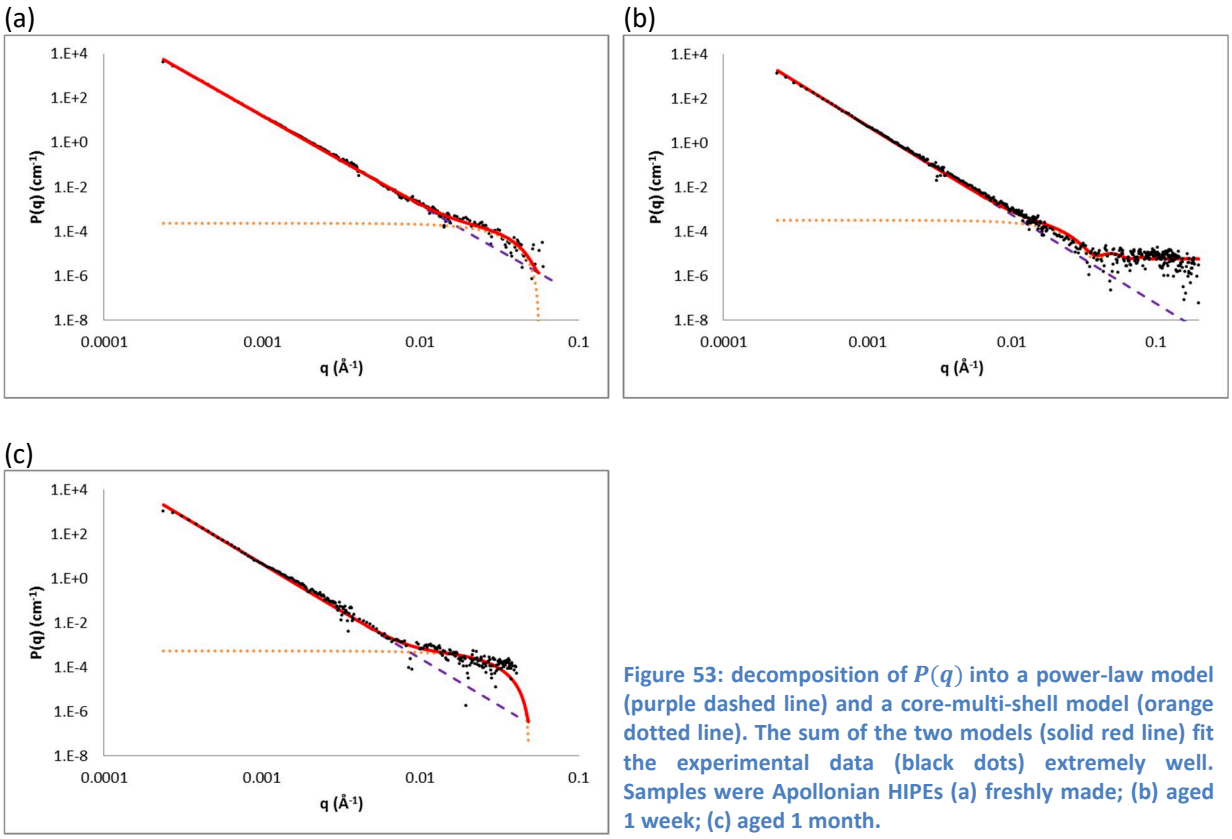

Figure 53: decomposition of $P(q)$ into a power-law model (purple dashed line) and a core-multi-shell model (orange dotted line). The sum of the two models (solid red line) fit the experimental data (black dots) extremely well. Samples were Apollonian HIPEs (a) freshly made; (b) aged 1 week; (c) aged 1 month.

Table 8: fitting $P(q)$ of Apollonian HIPEs at different ages with a power-law and a core-multi-shell model. The objects giving the excess signal with respect to the power law were found to be between 17 – 24nm in diameter.

Age of Apollonian HIPE	Power-law exponent	Core radius (Å)	C12 shell thickness (Å)	POE shell thickness (Å)	Diameter of objects (nm)	Volume fraction of objects
Fresh	4.2609	82.4	7	7	19.3	4.1 x 10^{-6}
1 week	3.9935	105.9			24.0	1.2 x 10^{-6}
1 month	4.0558	70.6			16.9	2.8 x 10^{-6}

The experimental $P(q)$ were very well fitted by the sum of a power law and the core-multi-shell model (solid red lines in Figure 53). The exponents of the power law were the same as in Table 7 and the diameters of the objects causing the shoulder were found to be 19.3nm, 24.0nm and 16.9nm for a fresh, 1-week old and 1-month old Apollonian HIPE respectively (Table 8). They were present at volume fractions of 1 – 4 x 10^{-6} in these samples that had been diluted 40x. This meant that in the undiluted Apollonian HIPEs, they were only present at ϕ = 4.8 x 10^{-5} – 1.6 x 10^{-4}, explaining why any signal caused by them were masked and undetected in the concentrated spectra.

C12E6 micelles in pure water have been previously reported to exist as spherical shapes at temperatures below 25°C[124], and their neutron or X-ray scattering could be modelled by core-shell structures with overall diameters between 5.8 – 6.7nm[125,126]. Dynamic Light Scattering similarly measured a hydrodynamic diameter of 7.4nm[81]. In comparison to the diameters we found (Table 8), we inferred that the objects causing the excess signal were C12E6 micelles swollen with some mineral oil.

4.2.5.1 Two populations of swollen micelles

We repeated this experiment on the SWING beamline at SOLEIL, and similarly observed a population of swollen micelles 17.5 – 26.3nm in diameter that gave a signal at $q \approx 0.005 - 0.03$Å^{-1} (Figure 54, orange dotted lines). We named this population α, because we also observed a second population β of smaller swollen micelles, 6nm in diameter, scattering at $q \approx 0.03 - 0.2$Å^{-1} (blue dotted lines in Figure 54b and Figure 54c), particularly conspicuous in the 11-month old Apollonian HIPE. Re-examining the SAXS data from ESRF, the one-week old Apollonian HIPE (Figure 53b) appeared to have this second β hump, but its intensity was too close to the background for any meaningful interpretation.

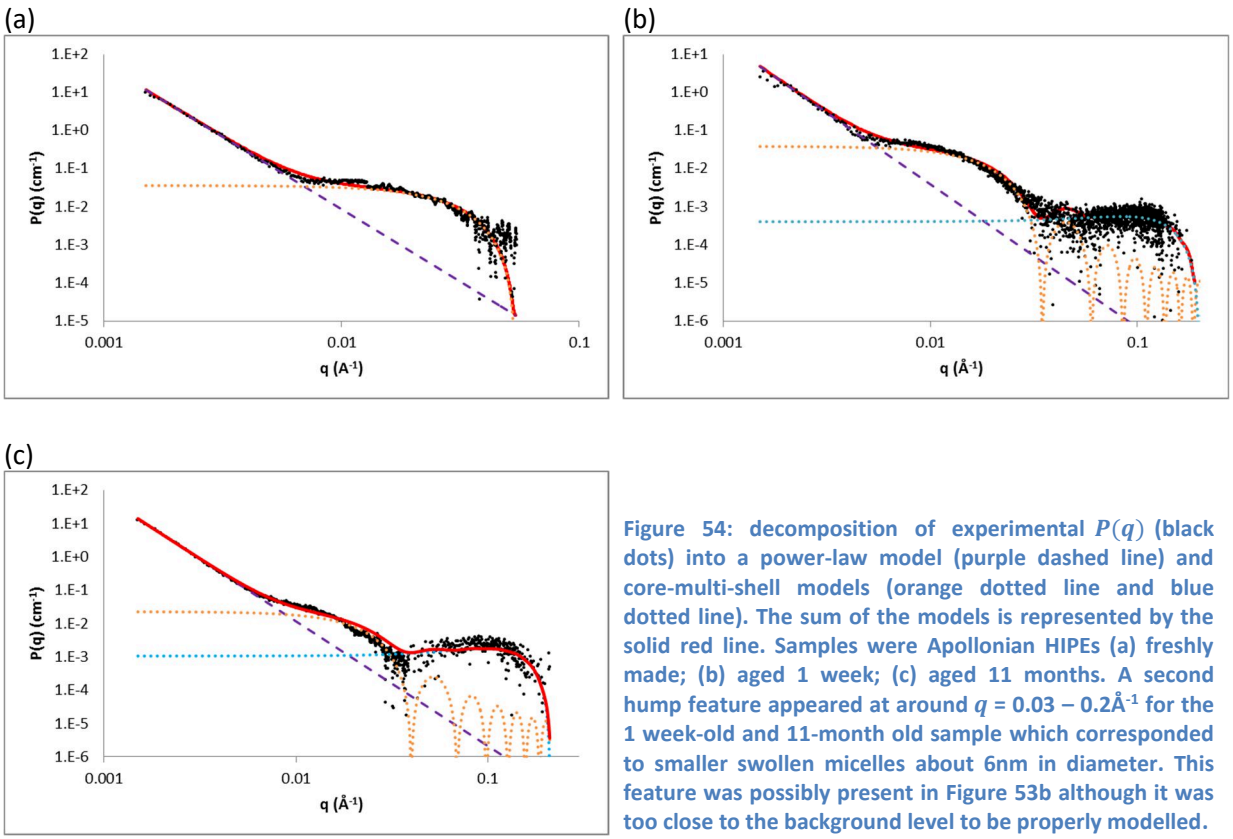

Figure 54: decomposition of experimental $P(q)$ (black dots) into a power-law model (purple dashed line) and core-multi-shell models (orange dotted line and blue dotted line). The sum of the models is represented by the solid red line. Samples were Apollonian HIPEs (a) freshly made; (b) aged 1 week; (c) aged 11 months. A second hump feature appeared at around q = 0.03 – 0.2Å^{-1} for the 1 week-old and 11-month old sample which corresponded to smaller swollen micelles about 6nm in diameter. This feature was possibly present in Figure 53b although it was too close to the background level to be properly modelled.

Table 9: fitting $P(q)$ of Apollonian HIPEs at different ages with a power-law and core-multi-shell models. The swollen micelles giving the excess signal with respect to the power law were between 18 – 26nm in diameter (population α). A second population (β) of swollen micelles 5.7 – 6nm in diameter was also found in the aged Apollonian emulsions.

Age of Apollonian HIPE	Power-law exponent	Core radius (Å)		C12 shell thickness (Å)	POE shell thickness (Å)	Diameter of swollen micelles (nm)		Volume fraction of swollen micelles (10^{-4})	
		α	β			α	β	α	β
Fresh	3.7956	73.4	Absent	7	7	17.5	-	3.9	-
1 week	3.7486	117.7	15.8			26.3	6.0	1.1	1.4
11 months	3.7372	101.3	14.5			23.1	5.7	0.95	22

By analyzing the volume fractions of α and β swollen micelles, the data suggests that **β swollen micelles are a by-product of emulsion ageing** (Table 9): in the 1-week old HIPE, α and β swollen micelles were present at the same proportion, but in the 11-month old HIPE, β's volume fraction had increased to more than 20 times that of population α, which was still roughly the same. The existence of two populations implied that the droplets, big and small, were still not at equilibrium even after 11 months of evolution.

Could these swollen micelles have been created through the act of diluting Apollonian HIPE with excess surfactant solution when $P(q)$ was measured? If this had been the case, the volume fractions found for each population, α and β, would have been the same across all the samples in Table 8 and Table 9, since every aspect of the experimental protocol was the same (operator, dilution factor, amount of time elapsed between dilution and spectra measurement which was no more than 30 minutes).

We also verified the identity of these β swollen micelles by comparing them to those made directly by the Phase Inversion Temperature (PIT) method.

4.2.5.2 Making swollen micelles by the PIT method

Roger et al. (2010) described in their paper a method of making microemulsions (swollen micelles at thermodynamic equilibrium) between 10 – 100nm. By heating an oil-surfactant-water mixture beyond its clearing boundary (the temperature where the turbidity was the lowest), and then quickly quenching it in ice, the microemulsions droplets were preserved. This is called the PIT method.[127] The surfactant they used was C16E8, which had a similar phase diagram in water as C12E6, but transposed towards higher temperatures. The oil used was hexadecane, with an oil: surfactant mass ratio of 2:1.

Inspired by this method, we attempted to make such a microemulsion with our mineral oil and C12E6. We began with the same continuous phase as our Apollonian HIPEs, that is a micellar solution of C12E6 at 0.6%(w/w), and calculated the maximum amount of oil that could be solubilized if they were entirely contained in swollen micelles 20nm in diameter.

$$A_{swollen\ micelle} = 4\pi R^2 = 1.26\ \times 10^{-15}\ m^2$$

Keeping in mind that a C12E6 molecule occupies 52 – 55Å^2, a swollen micelle's surface would be saturated at most by 2284 surfactant molecules.

In 1g of continuous phase, there was 6mg of C12E6, corresponding to 8 x 10^{18} C12E6 molecules, therefore a maximum of 3.5 x 10^{15} swollen micelles could be created.

$$\sum V_{swollen\ micelle} = 3.5 \times 10^{15} \times {}^{4}/_{3}\,\pi R^3 = 1.4 \times 10^{-8}\ m^3$$

$$m_{oil} = \rho_{oil} \sum V_{swollen\ micelle} = 13mg$$

13mg of oil could thus be dissolved in 1g of 0.6% surfactant solution and the mass ratio of oil to surfactant is approximately 2: 1.

As our mineral oil was likely a mixture of alkanes, no decisive clearing boundary was observable although turbidity appeared to be at its lowest at between 48 – 56°C. Thus, we heated our mixture under constant stirring at approximately 100rpm to 54°C and quickly quenched it in ice for 90 seconds. We then measured the resulting size distribution by Dynamic Light Scattering (Malvern Zetasizer Nano ZS) and consistently found a population centered upon 3µm in diameter. By passing the mixture slowly through a filter with 0.2µm pores (to prevent re-emulsification by shearing), we were able to recover and detect a population of droplets that were 7 – 10nm in diameter. We tested this method many times and found it reproducible.

It was therefore necessary to determine if these 7 – 10nm droplets were just empty C12E6 micelles, or if they were indeed oil-swollen. We verified this by SAXS, finding that the PIT and filtering method gave micelles that scattered differently from a pure surfactant solution at the same concentration. Their unadulterated spectra are shown in Figure 55 and these were measured without dilution.

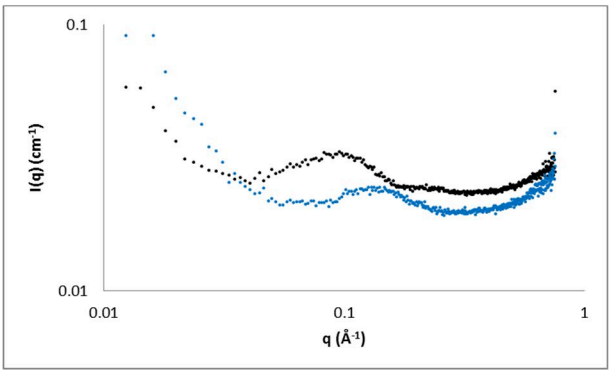

Figure 55: SAXS spectra of swollen micelles made using the PIT and filtering method (black), and a pure C12E6 solution at 0.6%(w/w) (blue). No subtraction has been applied in this figure.

For convenience, we shall hence refer to swollen micelles made by PIT and filtering as "microemulsion", and micelles from a pure surfactant solution as "empty micelles". We noted that the **hump of the microemulsion occurred at q = 0.03 – 0.18Å^{-1}, the same placement as β swollen micelles**, while the empty micelles' hump began at slightly higher q values, from 0.07 – 0.22Å^{-1}. We subsequently took water to be the background and subtracted it from Figure 55. The resulting spectrum for the microemulsion (Figure 56, left) was fitted with the same core-multi-shell model and SLD profile depicted in Figure 52. The microemulsion droplet's oil core radius was found to be 14.5Å. Taking into account the C12 and POE shells, **the microemulsion's overall diameter was then 5.7nm, the same size as β swollen micelles** calculated in Table 9.

On the other hand, empty micelles could be fitted with a simple C12 core-POE shell model (Figure 56, right). The core's radius would be 18Å, the extended length of the surfactant's hydrocarbon chain. Setting the volume fraction was 0.006 because the micellar solution's concentration was 0.6%, we fitted the thickness of the POE shell, found to be 7.7Å. Thus, the overall diameter of empty micelles was 5.1nm. This value was smaller than the 5.7nm reported by Penfold et al. (1997) possibly because they were working at 5%C12E6 and also assumed polydispersity and a Schulz distribution in their neutron scattering modelling[125]; Wijaya et al. (2016) reported 6.7nm but were working at higher temperatures (25°C and 50°C)[126], as opposed to our working temperature of 21 – 22°C.

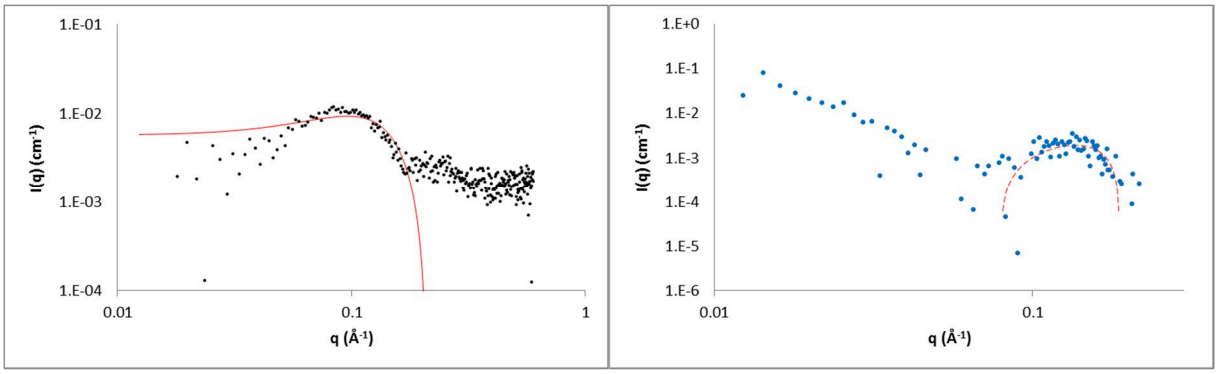

Figure 56: fitting the SAXS spectrum of a microemulsion (black dots, left) and pure surfactant micelles (blue dots, right) respectively with a core-multi-shell model (red solid line, left) and a simple core-shell model (red dashed line, right). The fitting gave 5.7nm as the microemulsion's overall diameter, and 5.1nm for the empty micelles.

4.3 Discussions on Apollonian HIPEs

We established in the previous sections that liquid HIPEs are able to undergo coalescence due to the low surfactant availability. We also established that their droplets are undeformed at rest and that their sizes follow a power-law size distribution, probably a consequence of high-energy fragmentation at very high volume fractions. These liquid HIPEs continuously evolve and their droplet-packing structure attains a Random Apollonian Packing after about a week. At the same time, this evolution is accompanied by the creation swollen micelles, as well as smaller emulsion droplets that cause an increase in total surface area. Once the emulsion becomes an Apollonian HIPE, it demonstrates exceptional metastability, staying in that configuration for almost a year, in spite of continued evolution. The following discussions aim to qualitatively address major questions that result from our experimental observations. We also include further experimental results where available to support our proposed arguments.

In this section, we show that the mechanism of coalescence in a structure as crowded as a liquid HIPE at $\phi = 0.95$ is very different from the typical view of coalescence in diluted emulsions. In diluted emulsions, coalescence creates only larger droplets with lower surface area, resulting in the expulsion of excess surfactants. These surfactants can freely diffuse away in the large amount of continuous phase. However, in a liquid HIPE, the evicted surfactants do not have this luxury. We believe that the consequence of this limitation leads to a radically different mechanism of evolution, where smaller emulsion droplets are created in addition to larger ones. We have named this mechanism "coalescence-fragmentation". The result of coalescence-fragmentation is then an Apollonian structure.

In section "4.3.1.1 How are smaller droplets created during coalescence?", we will explore the geometrical coalescence-fragmentation mechanism by which these smaller drops are created, and in section "4.3.1.2 Why are smaller droplets created during coalescence in a liquid HIPE?", we show that the creation of these smaller droplets (and more surface area) is compatible with thermodynamic considerations, even though conventional ideas of coalescence dictate that surface area should decrease to reduce surface energy. Section "4.3.2 How is an Apollonian HIPE so metastable?" is dedicated to the discussion of the unexpected metastability of Apollonian HIPEs, in spite of coalescence happening within such a crowded, yet surfactant-poor system. In section "4.3.2.1 Measure of coalescence rate", we measure and compare their coalescence rates to other polydisperse emulsions of lower volume fractions, and we demonstrate that the metastability of Apollonian emulsions does not come from a slower rate of coalescence, but is rather the consequence of their peculiar evolution mechanism (section "4.3.2.2 The consequence of coalescence-fragmentation". Finally, in section "4.3.2.3 Thermodynamic considerations", we apply thermodynamics arguments and interpret the longevity of the Apollonian structure in HIPEs as a local free energy minimum.

4.3.1 Creation of smaller droplets in a HIPE

4.3.1.1 How are smaller droplets created during coalescence?

We consider the coalescence of two random droplets, of radii a_1 and a_2. Volume is necessarily conserved because of the law of conservation of mass. Then, the following outcomes are possible:

- Two droplets giving one big daughter droplet: typical coalescence.

The radius of the daughter droplet, a, would be $({a_1}^3 + {a_2}^3)^{1/3}$. This is the classic view of coalescence. If we began with more than a pair of parent droplets, and at each step of the process, $a_1 \approx a_2$, then the coalescence is hierarchical and follows the model proposed by Smoluchowski (see section "3.2.4.3 Smoluchowski coalescence algorithm"). However, the distribution of sizes obtained at the end would not be a power law because we would quickly end up with 1 giant macroscopic droplet.

- Two droplets giving two droplets.

This process corresponds to the spatial rearrangement of the two parent droplets.

- Two droplets giving multiple daughter droplets: coalescence-fragmentation.

We verified by numerical simulation (done by Robert Botet) that this situation indeed resulted in power-law size distributions. Therefore, to obtain such an extremely polydisperse population, **a coalescence event between two droplets has to happen in tandem with fragmentation** (since the resulting number of droplets is larger than the initial number). However, we found that the exponent of the distribution depended on the number of daughters created. Under the strictest conditions where we assumed that each coalescence event created 3 non-overlapping daughter droplets, the resulting power-law exponent ($= d_f + 1$) was consistently inferior to 2, much lower than 3.47 expected of an Apollonian packing. Figure 57 shows the result of one such simulation, where we began with two identical droplets and ended up with 10^8 droplets through successive coalescence.

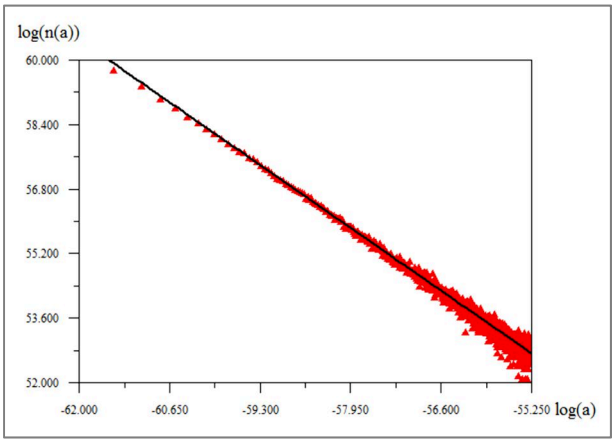

Figure 57: numerical simulation result for the coalescence between two droplets giving 3 non-overlapping daughter droplets. A power-law size distribution could indeed be obtained, but its exponent was far too low. Here shown, the power-law exponent was about 1.2.

By relaxing the condition of number of daughters produced, the exponent could be raised to give the right power-law size distribution. However, these simulations do not yet take into account the spatial organization of all the resulting droplets. As we observed in section "4.1.4 Size distribution of each type of HIPE", Figure 33 and Table 2, the right power-law exponent can be obtained if we allowed droplet deformation (such as in hybrid HIPEs). Thus, it was insufficient to find the conditions of obtaining the right size distribution. We had to also consider the conditions that allow the droplets to remain spherical and undistorted.

In a liquid HIPE, spherical droplets only have one point of contact with one another. As such, we resorted to a more generalized simulation where two coalescing parent droplets may create any number of non-overlapping daughters respecting conservation of volume and tangency constraints. We christened this process the "Rabbit" algorithm (on account of their proliferation prowess). In practical terms, this means that spherical daughter droplets are created such that they occupy the maximum available space in the principal void left behind by the coalesced parents, as well as any neighbouring voids, without causing overlaps with spectator droplets constituting the walls of the voids. The maximal filling of voids is justified by the liquid nature of the HIPEs we were trying to simulate, and filling of neighbouring voids is justified by capillary flow. The simulation occurred as follows (Figure 58):

1. 60 spheres of equal size were randomly seeded in a unit volume. Overlap was authorized at this point to identify which pairs will undergo "coalescence". (Figure 58a)

2. An overlapping pair was chosen, and we calculated the sum of their volume, v_{12}, as well as their center of mass x_{12}. The offending pair of spheres was then removed, leaving behind a principal void roughly centered on x_{12}.

3. We considered voids surrounding x_{12}, including the principal void, such that their total volume came to $2v_{12}$. This condition prevented the system from examining a void too far away from the offending pair of spheres.

4. The voids from step 3 were filled in descending order of volume. One daughter sphere respecting tangency constraints was created to occupy each void. The filling process stopped when the total volume of daughter spheres created attained v_{12} (Figure 58b).

5. Steps 2 – 4 were repeated (Figure 58c–e) until no overlapping spheres remained (Figure 58f).

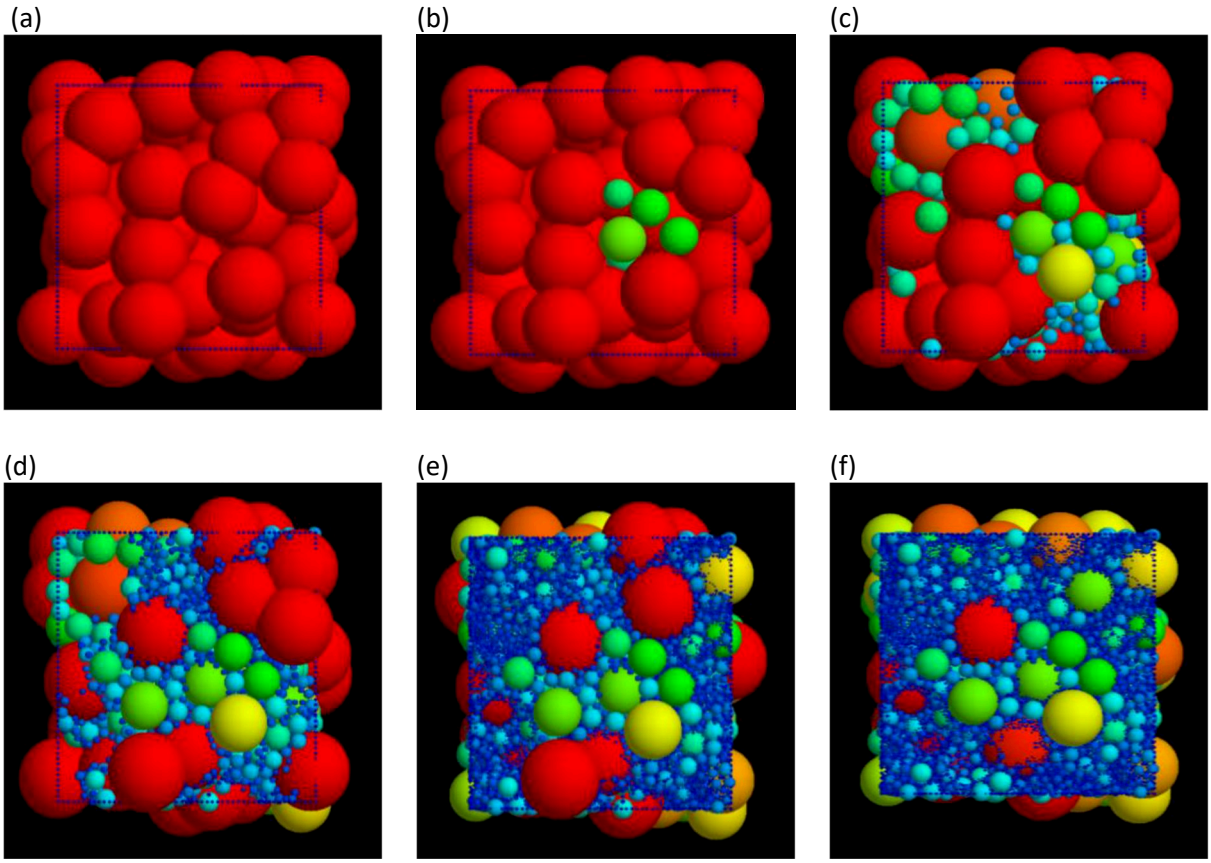

Figure 58: numerical simulation using the Rabbit algorithm. (a) Overlapping pairs of spheres were first created, then replaced with daughter spheres that occupied the principal void left behind, as well as neighbouring voids. The first iteration is shown in (b). Every fourth subsequent iteration is shown in (c) to (e). (f) is the final state of the system, at the end of the Rabbit algorithm when there were no overlapping spheres left. The spheres were colour-coded to show their different sizes, with dark blue being the smallest and red being the largest.

The first iteration produced 13 daughter droplets (Figure 58b), and subsequent iteration step produced between 22 and 8210 daughters each. It required 32 iterations of the Rabbit algorithm to completely eliminate all overlaps (Figure 58f). We noticed that in one of the final iterations, there was a "coalescence" event where only two non-overlapping daughter droplets were created (Figure 59). We verified that this effectively corresponded to a spatial rearrangement of the parents, where one slightly increased in volume at the expense of the other to better fit the voids in accordance to tangency constraints.

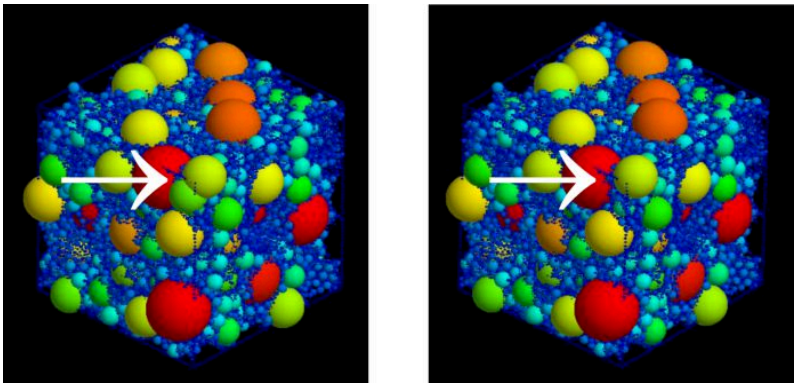

Figure 59: (left) two overlapping droplets identified by the white arrow. The result of this particular iteration by the Rabbit algorithm gave two non-overlapping daughter droplets (right), i.e. a local spatial rearrangement of the parents to better fit the voids.

A sharp reader would notice that the maximisation of sphere radii in voids is consistent with the definition of a local Apollonian construction (Mandelbrot, 1983)[58]. Thus, it would appear that the **Rabbit algorithm creates Apollonian structures locally, and the union of these structures is a global Apollonian packing**. We verified this by plotting the size distribution resulting from the Rabbit simulation and found that it was indeed a power law with an exponent close to that of an Apollonian packing (Figure 60). The calculated $S(q)$ for the Rabbit simulation at ϕ = 0.85 also produced the same $S_{cal}(q)$ for a simulated RAP at ϕ = 0.92 (Figure 61). Both structure factors had an almost inexistent S_{max} peak, which means that there was no positional order in the system. In other words, the probability of having a large or small neighbouring droplet is independent of the size of the droplet that was being considered.

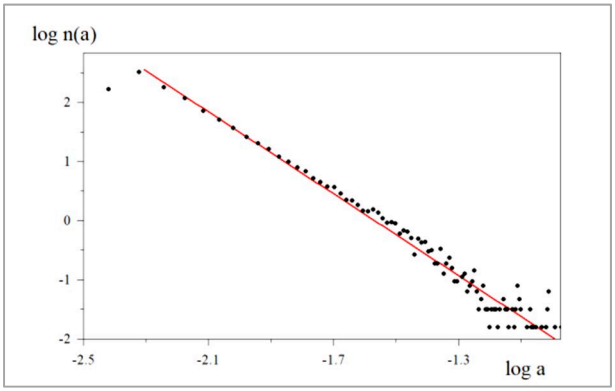

Figure 60: size distribution from a numerical simulation following the Rabbit algorithm, expressed in double-logarithmic plot (black dots). The red line represents a power law with an exponent of -3.47, corresponding to the Apollonian d_f = 2.47.

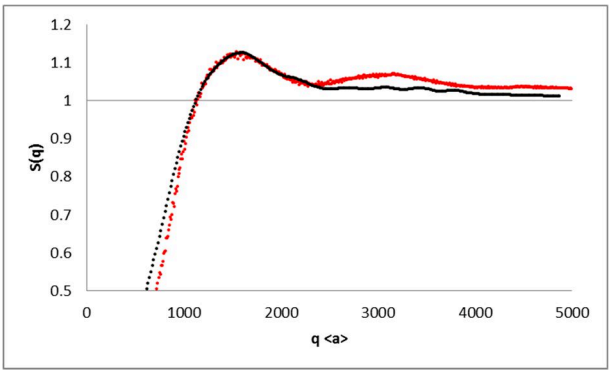

Figure 61: $S_{cal}(q)$ for a numerical simulation following the Rabbit algorithm at ϕ = 0.85 (black) sharing the same features as $S_{cal}(q)$ for a simulated RAP at ϕ = 0.92 (red).

Since the Rabbit algorithm appears to be another way to generate a Random Apollonian Packing, we compared its calculated $S(q)$ to our experimental $S(q)$ for Apollonian HIPEs and found great agreement between them (Figure 62). We also examined the variation of specific surface area by the Rabbit algorithm, and found that it increased with time (Figure 63), corroborating our experimental observations by Light Scattering and by SAXS and consequently, our inference that lots of small droplets were created as Apollonian HIPEs evolve.

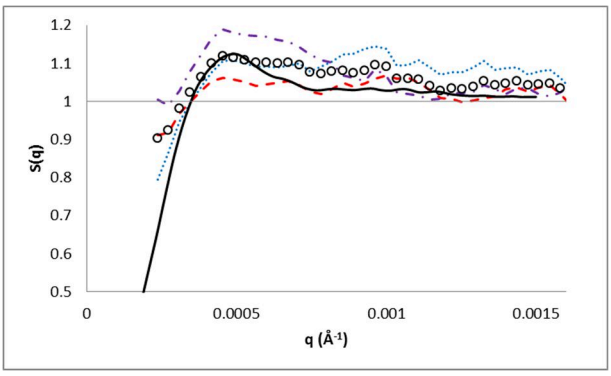

Figure 62: comparison between $S_{cal}(q)$ from the Rabbit algorithm at ϕ = 0.85 (black solid line) and $S_{exp}(q)$ for Apollonian HIPEs at ϕ = 0.95 aged for 1 month, made at 250rpm (blue dots), 500rpm (red dashes) and 1000rpm (purple dot-dashes). The open circles represent the average values over the three samples.

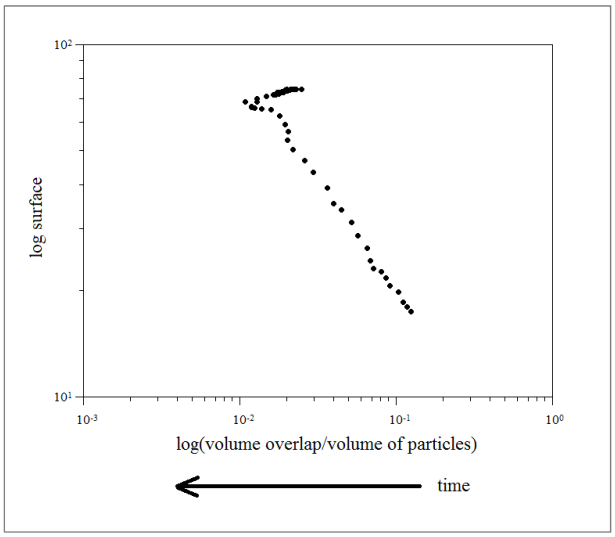

Figure 63: variation of surface area as a function of the proportion of overlapping particles left in the system. As the Rabbit simulation progresses, the amount of overlaps decreases, so time progresses from right to left. There is therefore a net increase in surface area with time.

As such, we infer that **liquid HIPEs likely evolve according to a mechanism of coalescence-fragmentation similar to that described by the Rabbit algorithm, which entails the creation of many small droplets at every coalescence event** between two droplets in order to optimally fill available surrounding voids. The sum of these local Apollonian constructions then results in a global Apollonian packing and hence an Apollonian emulsion.

4.3.1.2 Why are smaller droplets created during coalescence in a liquid HIPE?

In the Rabbit algorithm, there are no energetic considerations. It is a purely geometrical mechanism by which overlaps are removed and by which smaller spheres are created. We then proceeded to examine if the creation of these smaller droplets can occur, and the reason for it.

Evicted surfactants cannot be evacuated by the continuous phase

To answer this question, we have to examine what happens in the aftermath of a successful coalescence event. Let the subscripts 0 and 1 denote before and after coalescence respectively. We consider two parent droplets of radius a_0 = 1µm and we assume that their interfaces are saturated by surfactant molecules.

$$V_0 = V_1 = (8/3)\pi {a_0}^3$$

$$A_0 = 8\pi {a_0}^2$$

In a typical emulsion, if only one daughter was produced, then the daughter droplet's radius would be $2^{1/3}a_0$. Its area would then decrease to:

$$A_1 = 2^{8/3}\pi {a_0}^2$$

which results in a net loss of interface:

$$\Delta A = A_1 - A_0 \approx -5.2\ \mu m^2$$

Assuming that a surfactant molecule occupies 55Å^2 at the droplet interface, coalescence would result in the eviction of N surfactants:

$$N = \Delta A/(55\text{Å}^2) = 9.43 \times 10^6 \text{ molecules}$$

Normally, in a typical emulsion where ϕ is low and there is a lot of continuous phase, these molecules can disappear into the reservoir of continuous phase without causing a significant rise in concentration. However, in a liquid HIPE where ϕ = 0.95, assuming a homogeneous repartition of continuous phase around each oil droplet, the volume of continuous phase associated to two coalescing parent droplets, V_{aq}, is:

$$V_{aq} = \frac{V_0}{\varphi} \times (1 - \varphi) \approx 0.053V_0 = 0.44\ \mu m^3 = 4.4 \times 10^{-16} L$$

If the N evicted surfactant were to be solubilized in this little amount of continuous phase, then the concentration of surfactant would increase by 0.036mol/L.

The initial surfactant concentration was 0.6%(w/w) in the continuous phase, corresponding to C_0 = 0.013mol/L. The new concentration is therefore C_1 = 0.049mol/L. Assuming an ideal solution, we can then calculate the variation in chemical potential $\Delta\mu$ of the surfactant:

$$\Delta\mu = \mu_1 - \mu_0 = RT \ln \frac{C_1}{C_0}$$

where R = 8.31 J/(mol.K) is the ideal gas constant, and T = 21-22°C in our experimental systems:

$$\Delta\mu \approx 3300\ J/mol$$

The solubilization of evicted surfactant molecules would result in a massive increase in chemical potential in the continuous phase in the vicinity of the coalescing oil droplets. We qualify this increase in chemical potential as significant, because if we applied the same calculations to emulsions of lower volume fractions, for example ϕ < 0.6, $\Delta\mu$ is no more than $480\ J/mol$. In fact, $\Delta\mu$ increases exponentially as function of ϕ in the domain of HIPEs where ϕ > 0.64 (Figure 64). **Therefore, in a HIPE at ϕ = 0.95, contrary to typical emulsions, evicted surfactants from coalescence events cannot be accommodated by the continuous phase.**

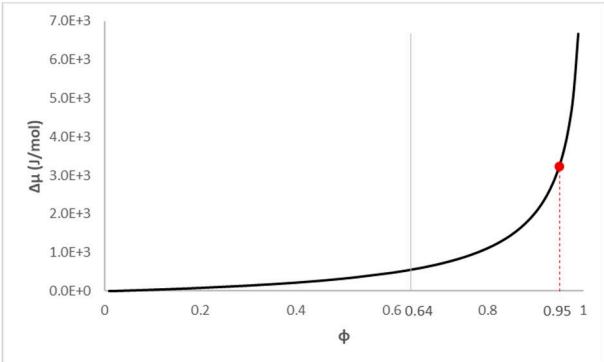

Figure 64: variation of chemical potential, $\Delta\mu$, as a function of emulsion volume fraction, ϕ, if all evicted surfactant molecules following a coalescence event were solubilized in the surrounding continuous phase. The chemical potential increases exponentially if the emulsion is a HIPE (ϕ > 0.64). The red dot corresponds to our Apollonian HIPE at ϕ = 0.95.

Evicted surfactant molecules are confined locally

So far we have assumed that the evicted surfactant molecules are confined to a very small volume of continuous phase next the coalescing oil droplets. This kinetic view is correct at very short time-frames immediately following coalescence. Would it be possible for evicted surfactant molecules to form empty micelles that could diffuse away scot-free?

Putting aside the previous chemical potential considerations and assuming that evicted surfactants can form empty micelles, whose diameter we have found to be 5.1nm through SAXS (Figure 56), we calculated their diffusion coefficient, D, by the Stokes-Einstein equation:

$$D = k_B T / 6\pi\eta a$$

where k_B is Boltzmann's constant, T the temperature (21-22°C in our experimental systems), η the viscosity of the continuous phase, assumed to be that of water, and a the radius of an empty micelle. We found that D = 8.5 x 10^{-11} m^2/s.

Guinier and Fournet (1955) demonstrated that in X-ray scattering, beyond a particular $q_0 = 2\pi/x_0$ where x_0 corresponds to the average dimension of the irradiated sample, the scattered intensity becomes negligible.[128] From our $P(q)$ measurements by SAXS (Figure 53 and Figure 54), the power-law generally ends at around q = 0.005$Å^{-1}$, which corresponds to a physical distance of $x = 126nm$. We may approximate this to a characteristic length in our HIPEs.

Since the characteristic diffusion length is given as:

$$x = 2\sqrt{Dt}$$

an empty micelle would only have 50µs to get away before it ventures into the vicinity of other oil droplets and their associated continuous phase. Our kinetic consideration is therefore valid – surfactants cannot form empty micelles and freely circulate in a structure as crowded as an Apollonian HIPE without provoking a substantial increase in chemical potential.

Where else can they go? Our hypothesis, in conjunction with our experimental observations, is that **these evicted surfactant molecules are mopped up through the creation of smaller droplets**, either on the interfaces of other daughter droplets in the vicinity (as demonstrated by the Rabbit algorithm), or swollen micelles (as we found by SAXS). We show subsequently that the creation of these smaller droplets is energetically feasible.

Free energy is reduced by creating small droplets rather than maintaining flat films

We begin by examining G, the Gibbs free energy of the monolayer of surfactants around one small droplet. It is the sum of W, the elastic bending energy of the droplet film, and F, the surface energy:

$$G = W + F$$

We define here the mean droplet curvature, $H = 1/R$. The bending energy of the surfactant monolayer on a droplet is given by Helfrich (1973) as[26]:

$$W = 2\kappa \int (H_0 - H)^2 \, dA$$

with κ the elastic modulus of stretching [J/m^2], for zero saddle-splay modulus.[129]

Safran (1991) demonstrated that W is minimal at spontaneous curvature, $H_0 = 1/R_0$. In the case of spherical microemulsion droplets (which possess spontaneous curvature), because their saddle-splay modulus is zero, their bending free energy W is also zero.[130]

The expression for surface energy is given by:

$$F = \int \sigma \, dA$$

where σ is the interfacial tension and dA an elementary area of interface. This energy is used to counteract the difference in pressure $\Delta\Pi$ on either side of the droplet's interface[131] and therefore,

$$F = \int \sigma \, dA = \int (-\Delta\Pi) \, dV$$

The expression of $\Delta\Pi$ is given by the Young-Laplace equation, where $\Delta\Pi = 2\sigma/R$. By a change in variable,

$$F = -8\pi\sigma \int R \, dR$$

Then, for any value of $R > R_0$,

$$F = 4\pi\sigma\left({R_0}^2 - R^2\right)$$

Technically, a spherical microemulsion droplet still has a minimal surface energy F, because $R_0 \neq 0$. However, if we accept the premise that microemulsions are objects at thermodynamic equilibrium, then $G = 0$, which means that we can define $F(R = R_0) = 0$.

Having laid the groundwork for the expression of G, and having identified β swollen micelles as spherical microemulsion droplets by SAXS, we find that **the creation of β swollen micelles is favourable because it does not cause any increase in Gibbs free energy.**

What about α swollen micelles and small daughter HIPE droplets in the vicinity (from the Rabbit algorithm), all of which are clearly not at spontaneous curvature?

Since $A = 4\pi R^2$, by a variable change,

$$W_{droplet} = 2\kappa \int (H_0 - H)^2 \, dA = 16\pi\kappa(H_0 - H)^2 \int R \, dR$$

$$W_{droplet} = 8\pi\kappa(H_0 - H)^2 R^2 + const.$$

When $R = R_0 = 1/H_0$, $W_{droplet} = 0$. Thus,

$$const. = 0$$

And so, at a given R,

$$W_{droplet} = 8\pi\kappa(R/R_0 - 1)^2$$

The expression of surface energy for a droplet is the same as that for a β swollen micelle:

$$F_{droplet} = 4\pi\sigma\left({R_0}^2 - R^2\right)$$

Therefore, the Gibbs free energy of α swollen micelles and other small daughter droplets is

$$G_{droplet} = 8\pi\kappa(R/R_0 - 1)^2 + 4\pi\sigma\left({R_0}^2 - R^2\right)$$

Supposing these α swollen micelles and small daughter droplets did not exist, coalescing parent droplets would be forced to maintain a flat film between them (overlaps in the Rabbit algorithm). This flat film, in reality a surfactant bilayer separating the two oil droplets, would have an equivalent area $A \cong 8\pi R^2$. Kabalnov and Wennerström (1996) calculated the bending energy of a flat film and found it to be[26]:

$$W_{film} = 2{H_0}^2\kappa A = 16\pi\kappa(R/R_0)^2$$

For surface energy,

$$F_{film} = \sigma A = 8\pi\sigma R^2$$

Thus, the Gibbs free energy of a flat film of surfactant is

$$G_{film} = 16\pi\kappa(R/R_0)^2 + 8\pi\sigma R^2$$

We see that for all values of $R > R_0$,

$$G_{film} > G_{droplet}$$

Therefore, we can conclude that **the creation of α swollen micelles and/or small daughter droplets would favourably decrease the Gibbs free energy in the system,** because flat films store more energy resulting in higher Gibbs free energy.

4.3.1.3 Summary on the coalescence-fragmentation mechanism

When coalescence occurs in an emulsion, the system attempts to lower its free energy by getting rid of any flat films (droplet deformations) and by creating spherical droplets. In a typical dilute emulsion, one daughter droplet is created from two coalescing parents and excess surfactant molecules are evicted due to the loss in interface area. These evicted molecules can be evacuated by the large amount of continuous phase without major consequences.

However, in a HIPE with a very limited amount of continuous phase, the evicted surfactants cannot be accommodated by their immediate surroundings without provoking a substantial increase in chemical potential, nor can they diffuse far in such a crowded structure before encountering the same problem. Consequently, they are locally confined, translating as a temporary surplus of surfactants in the vicinity of a coalescence event. Then, two coalescing droplets can create multiple daughter droplets whose newly created interfaces will accommodate the evicted surfactants in the neighbourhood. This process is coalescence-fragmentation. There are three conditions pertaining to the creation of the daughter droplets:

1. The size and number of daughter droplets are such that overall volume is conserved.
2. The daughter droplets each seek to occupy the biggest possible volume available to them, because they are liquid.
3. The daughter droplets must respect tangency constraints in relation their neighbours because it is costly in free energy to create flat films.

These three conditions of coalescence-fragmentation in a HIPE then guarantee a structure that is constructed locally according to Apollonian principles, and the global system becomes an Apollonian emulsion.

4.3.2 How is an Apollonian HIPE so metastable?

We observed visually that our Apollonian HIPEs remained emulsified for up to a year in spite of the low surfactant concentration in the continuous phase. This defies conventional expectations of the lifespan of an emulsion with so many oil droplets in close contact that are so poorly protected by surfactants.

4.3.2.1 Measure of coalescence rate

We believed at first that this exceptional metastability could be due to slower rates of coalescence in Apollonian HIPEs, as a result of localized confinement of surfactants explained in the previous section. To test this hypothesis, we measured and compared the rate of coalescence in emulsions at different ϕ but made by the same method as an Apollonian HIPE, at the same surfactant concentration of 0.6%C12E6 (w/w) in the continuous phase. However, because such emulsions were very polydisperse with different initial size distributions depending on the emulsification conditions, we could not directly compare their rates of coalescence. It was therefore necessary to compare to a model. We used numerical simulation (developed by Robert Botet) to predict the rate of coalescence of these polydisperse emulsions by the Smoluchowski model, assuming Brownian motion in the droplets. Each simulation took into account the experimentally measured initial size distribution for each emulsion. The specifics of the algorithm can be found in section "3.2.4.3 Smoluchowski coalescence algorithm".

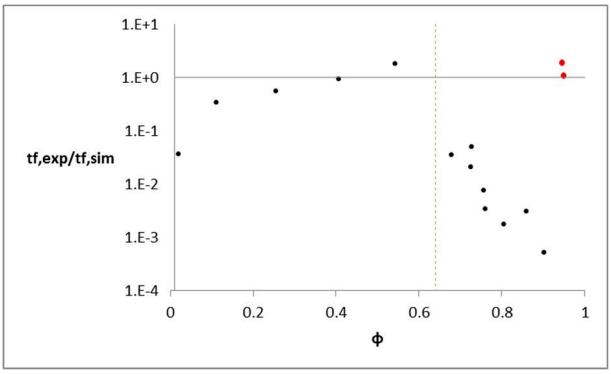

Figure 65: experimentally measured coalescence rates for polydisperse emulsions at different ϕ, compared to the rates predicted by Smoluchowski model with a Brownian kernel. This is expressed as $t_{f,exp}/t_{f,sim}$ on the vertical axis. The red points are Apollonian HIPEs at ϕ = 0.95. A dotted vertical line has been traced at ϕ = 0.64 to represent the random close-packing limit.

Figure 65 summarizes the comparison of experimental coalescence rates to predicted rates, expressed as $t_{f,exp}/t_{f,sim}$ across the samples between ϕ = 0.0208 to ϕ = 0.9491. Since the emulsions were all polydisperse, the random close-packing limit at ϕ = 0.64[27], instead of the densest close-packing limit at ϕ = 0.74 for monodisperse spheres, was used to demarcate whether an emulsion was a HIPE. In other words, any emulsion whose volume fraction was above 0.64 was a HIPE, but because we could not measure their structure factors, we could not determine if they were packed according to an Apollonian construction. The only HIPEs we could be sure were truly Apollonian emulsions were those made at ϕ = 0.95, represented by the red points on Figure 65.

In the most dilute emulsion with ϕ = 0.0208, the experimental rate of coalescence was about thirty times slower than the Smoluchowski model predicted. This was entirely expected – the total surface area of oil droplets measured by Light Scattering was 3.3 x 10^{-12} m^2, whereas there was enough surfactant in the continuous phase to cover 8.4 x 10^{-10} m^2 of interface. Therefore, it is safe to assume that the oil droplets' surfaces were entirely saturated with surfactant, which provided very good protection against coalescence. Furthermore the low volume fraction of the emulsion also ensured that collisions between oil droplets were infrequent. Staying in the domain of "dilute" emulsions up to ϕ = 0.5432, we found that there was still enough surfactant in the system to provide adequate coverage of oil droplet surfaces, yet experimental coalescence rates were found to increase with ϕ. As expected, this increase was due to more frequent collisions between oil droplets.

The increasing trend in experimental coalescence rate buckled as we crossed the threshold of ϕ = 0.64 into HIPE territory. We calculated the amount of interface coverage provided by the surfactants available in the system, and found that up to ϕ = 0.9028, there was still more than enough surfactants to saturate the interfaces. Yet, even though more frequent collisions between oil droplets could be expected as ϕ increased, the Smoluchowski model began to overpredict the rates of coalescence by 30 – 2000 times. Finally, we observed a huge jump in coalescence rate for our two Apollonian HIPEs, at ϕ = 0.9454 and ϕ = 0.9491. We found that now, there was a lack of surfactant in the system (interface coverage was at 28% and 98% respectively) and **the experimental rates of coalescence for Apollonian HIPEs appeared to follow the predictions by the Smoluchowski model, which is a mean-field theory.**

We found that the trend in coalescence rates with respect to the Smoluchowski model could be explained by the effective viscosity, $\eta^*(\varphi)$, of the system. It is intuitive to understand that as ϕ increases, there is less free volume for all the droplets to move around, and so the system appears to be more viscous. Einstein (1906) derived the expression of η^* for a very dilute dispersion of monodisperse spheres in a medium of viscosity η_0 [132,133]:

$$\eta^* = \eta_0(1 + 2.5\varphi)$$

The limit of validity of Einstein's equation is generally ϕ < 0.05.[134] At higher ϕ, the expression becomes a polynomial function of ϕ, because sphere-sphere interactions have to be taken into account. There is little consensus regarding the exact values of higher-order coefficients because they depend on assumptions specific to each interaction model[135]. However, some have found a way around the problem, by using incremental steps of $\Delta\varphi$ to constitute a concentrated suspension from a dilute one. This differential approach then led to the expression:

$$\eta^* = \eta_0(1 - \varphi)^{-2.5}$$

derived by Roscoe (1952), valid for up to ϕ < 1 and even for a polydisperse dispersion.[134]

In the Smoluchowski algorithm underlying our numerical simulations for polydisperse emulsions, effective viscosity was not accounted for. Since the droplets were assumed to be subjected to Brownian motion, we may interpret $t_{f,exp}/t_{f,sim}$ as equivalent to η_0/η^*.

In the regime of "dilute" emulsions where 0.0208 ≤ ϕ ≤ 0.5432, because $\phi \ll 1$, Roscoe's equation converges towards Einstein's by linearization. However, we also needed to take into account the vast difference between the viscosity of the oil phase (1.26 Pa.s) and the continuous phase (1 mPa.s). This means that η^* would primarily depend on the viscosity of the oil droplets, so $\eta^* \gg \eta_0$. This correction applied to Einstein's (or Roscoe's linearized) equation gave:

$$\eta^* - \eta_0 \approx \eta^* = 2.5\eta_0\varphi$$

$$\eta^*/\eta_0 = 2.5\varphi$$

The corrected expression described very well our dilute emulsions (Figure 66, solid purple line). What surprised us was that Apollonian HIPEs appeared to follow Einstein's corrected equation as well, suggesting that in spite of ϕ = 0.95, droplets in Apollonian HIPEs moved around easily as if they were in a homogeneous dilute medium without feeling the effects from other HIPE droplets. This observation is in line with those we had already made of Apollonian emulsions: spherical droplets

(Figure 32), implying that they do not exert forces on one another, and Newtonian flow behaviour (Figure 30 and Figure 31) where we hypothesized that each smaller size-class of droplets served as a homogeneous lubricating fluid to the larger ones. In fact, from our flow curve measurements in Figure 31, we determined the shear (or effective) viscosity for an Apollonian HIPE to be η^*= 3 Pa.s. Applying this value to the corrected expression for Einstein's equation, we would find η_0 = 1.26 Pa.s, which is indeed the viscosity of the oil phase. Hence, it would appear to validate our conjecture that droplets in an Apollonian HIPE behave as if they were in a homogeneous fluid constituted by other droplets. This would also explain why coalescence rates in Apollonian HIPEs appeared to follow predictions by Smoluchowski's mean-field model, because they behaved just as a dilute emulsion would, despite being a scale-invariant structure.

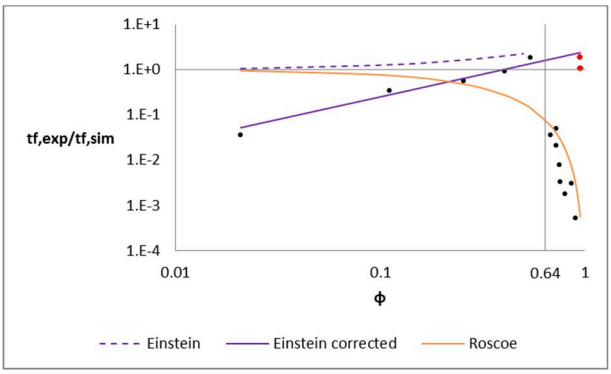

Figure 66: explaining coalescence rates with effective viscosity as a function of ϕ. Apollonian HIPEs were found to behave similarly as dilute emulsions, whereas the effective viscosity of HIPEs that we suspected to be not yet Apollonian had a marked effect in slowing down droplet movements.

As for other HIPEs of 0.6795 ≤ ϕ ≤ 0.9028, Roscoe's equation (Figure 66, orange line) described our experimental points. As such, the seemingly slower experimental coalescence rates with respect to the predicted Smoluchowski rates could be attributed to the increased difficulty for oil droplets to diffuse around due to overcrowding (higher effective viscosity in the system).

We are unsure why a HIPE at ϕ = 0.9028 would behave so differently from Apollonian HIPEs at ϕ = 0.95. It could be that at ϕ = 0.9, the emulsion may not yet be Apollonian, as we calculated and found that there is enough surfactant, even at 0.6% in the continuous phase, to saturate the droplet interfaces. The fact that there is slightly more free volume in a HIPE at ϕ = 0.9 may also play a role. It would be ideal to systematically measure the structure factors, surfactant coverage and $t_{f,exp}/t_{f,sim}$ for HIPEs of volume fractions beyond 0.9 to determine the role of free volume with regards to effective viscosity (and thus coalescence rates).

4.3.2.2 The consequence of coalescence-fragmentation

Having found that coalescence rates were not slower for Apollonian HIPEs and in fact even obeyed Smoluchowski's model very well, **we believe that the exceptional metastability in Apollonian HIPEs could instead be due to simultaneous coalescence and fragmentation (the Rabbit algorithm)**. Consider an intermediate range of size classes in an Apollonian HIPE. Typical coalescence alone would cause a shift towards larger droplet sizes, depleting the lower end of this range. However, in an Apollonian HIPE, the local confinement of surfactants after a coalescence event allows for the creation of many small daughter droplets (fragmentation). Thus, we would effectively be replenishing the system with smaller sizes. The flux of droplets entering this size range would

therefore partially compensate for the flux of droplets leaving, accounting for how the Apollonian HIPE remains emulsified for such a long time.

We know that the flux compensation is not exact, because the size distribution in Apollonian HIPEs does eventually shift towards larger values with time (Figure 43), with a small population of swollen micelles created (detected by SAXS). **What causes the Apollonian HIPE to finally "break" is gravitational separation**, which we observed in samples after more than a year. This occurs when oil droplets created through coalescence get so big that their density difference with the rest of the emulsion causes them to cream, separating out into a macroscopic oil phase. Understandably, the emulsion that remains under the cream falls under ϕ = 0.95, eventually losing its Apollonian structure. Perhaps in the absence of gravity, an Apollonian emulsion may stay indefinitely Apollonian. We make this claim as we believe indicate that an Apollonian structure is a local minimum in free energy, with full-scale macroscopic phase separation as the global minimum.

4.3.2.3 Thermodynamic considerations

We consider the expression for variation of Gibbs free energy, now applied to the entire emulsion:

$$\Delta G = \Delta U - T\Delta S$$

where ΔU represents the variation of internal energy in the system at constant volume and pressure, T is the temperature of the system also assumed to be constant, and ΔS is the variation of entropy of the system.

ΔS in an Apollonian structure

In 1877, Boltzmann published his equation that linked entropy in a system to the number of microstates accessible to the system[136,137]. The expression, as we use it today, takes on the form:

$$S = k_B \ln \Omega$$

where k_B is Boltzmann's constant, and Ω the number of microstates. Since Ω is the number of possible permutations every element in the system is capable of, it becomes clear that entropy depends on the total number of objects, as well as the degree of configurational freedom for each object.

The droplets in an Apollonian emulsion, being spherical, have more degrees of freedom than other faceted shapes – they possess rotational and translational freedom, as evidenced by Newtonian flow of Apollonian HIPEs, whereas polyhedral droplets in Lissant-type HIPEs are gridlocked, presenting an overall yield stress. Therefore, even for the same number of droplets, an Apollonian emulsion maximizes entropy with respect to solid or hybrid types. Moreover, as our Rabbit algorithm shows (Figure 58), every coalescence event between two droplets in fact causes an increase in the total number of droplets in the system. If we now considered the evolution of an Apollonian emulsion, and simplistically approximate Ω as the number of droplets in the system, then ΔS is an increasing function with time between two states of evolution in an Apollonian emulsion.

ΔU in an Apollonian structure

The main contributors to internal energy in a HIPE are the elastic energy that is stored in the droplet interfaces and the total surface energy of the droplets:

$$\Delta U = \Delta E_{elastic} + \Delta E_{surface}$$

Elastic energy

Compared to hybrid or solid HIPEs with faceted shapes storing lots of elastic energy in the flat surfactant films (much higher G' values), Apollonian HIPEs and their undeformed spherical droplets have the lowest elastic energy. A simple experimental evidence is how readily hybrid and solid HIPEs are diluted, also observed and explained by Princen – the high osmotic pressure in the interdroplet regions in (solid) HIPEs can be relieved by spontaneously allowing in more continuous phase[14,20]; then the Laplace pressure is neutralized and deformed droplets can recover their spherical shapes.[24] Princen's explanation is supported by our calculations of bending energies in a flat film vs. in a droplet of equal surface area in section "4.3.1.2 – Free energy is reduced by creating small droplets rather than maintaining flat films".

Our calculations further demonstrate that once a droplet is spherical, it is thermodynamically unfavourable to return to a deformed state by creating flat films. In Apollonian HIPEs, as soon as any overlapping (or deformation) between droplets occurs, evolution takes place through coalescence and fragmentation in tandem. Non-overlapping spherical droplets respecting tangency constraints are created, which translates into keeping elastic energy at its lowest, and $\Delta E_{elastic} < 0$.

Surface energy

Princen and Levinson (1987) calculated the surface area of the ideal foam cell – known as Kelvin's minimal tetrakaidecahedron – and found that the polyhedral droplet in a Lissant-type HIPE has a surface area 9.7% larger than an isovolumetric sphere[11]. Using geometrical arguments, for the same number of emulsion droplets, an Apollonian emulsion would then have lower surface energy than a solid or hybrid HIPE.

Now, examining the evolution of Apollonian emulsions, our experimental evidence indicates an overall increase in surface area with time (Figure 42 and Figure 50) as a result of many smaller droplets created by coalescence-fragmentation. Therefore ΔU is an increasing function with time as:

$$\Delta U = \Delta E_{elastic} + \Delta E_{surface} = \sigma \Delta A$$

Consequently, the evolution of an Apollonian emulsion allows the system to approach an increasingly ideal Apollonian packing but the increase in entropy is offset by an increase in surface energy as well:

$$\Delta G = \sigma \Delta A - T \Delta S$$

We believe that as a result of this push-and-pull between ΔA and ΔS, ΔG may oscillate back and forth in an Apollonian structure, representing a local minimum. This could explain why Apollonian emulsions have such prolonged metastability. We therefore propose the overall evolutionary pathway for a liquid HIPE at ϕ = 0.95 in Figure 67.

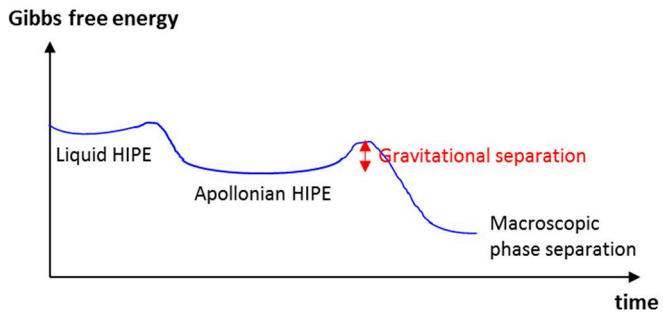

Figure 67: proposed evolutionary pathway for a liquid HIPE towards macroscopic phase separation.

5. Suggestions for applications of Apollonian HIPEs

5.1 Solid material with space-filling structure and ultra-low porosity

Inspired by emulsion templating that is an existing application of Lissant-type HIPEs, the most immediate application from our investigations on Apollonian HIPEs would be to fabricate a solid material with ultra-low porosity, by finding a way to solidify each emulsion droplet. Until now, the manufacture of such materials has been technologically limited, in view of the vast number of particles of different sizes that would have to be made and subsequently lodged at the right places to create a space-filling structure. From a materials science standpoint, it is highly advantageous to eliminate pores. The presence of pores (i.e. the absence of matter) greatly reduces the overall mechanical properties of a material, such as its Young's modulus, hardness, tensile strength etc., sometimes by several orders of magnitude.[138] This is because pores are a feature along which faults can propagate. Pores also impact the thermal and electrical conductivity of a material. It is then evident that ultra-high performance materials, such as composites and ceramics, can be created by eliminating porosity.

We attempted to fabricate such a material, by making a liquid HIPE using our usual protocol. Instead of mineral oil, we now used a polymer-solvent mixture as the internal phase, and an external aqueous phase containing very little surfactant to encourage coalescence. The idea, then, was to solidify the internal phase droplets as the HIPE evolved, so as to preserve the Apollonian structure. The polymer-solvent mixture was polycaprolactone and dichloromethane. Electrospinning and electrospraying of such mixtures is a known way to obtain fibers and spherical particles of solidified polymer as the volatile solvent evaporated.[139] This portion of the work was done in collaboration with Abdulwahed Shglabow of ESPCI Pars, who has extensive experience making microspheres of polycaprolactone in liquid phase through emulsification and solvent evaporation. We modified his protocol by severely reducing the concentration of SDS in the external phase to 0.02%(w/w), and by greatly increasing the internal phase's volume fraction to $\phi = 0.92$ with slow drop-wise addition.

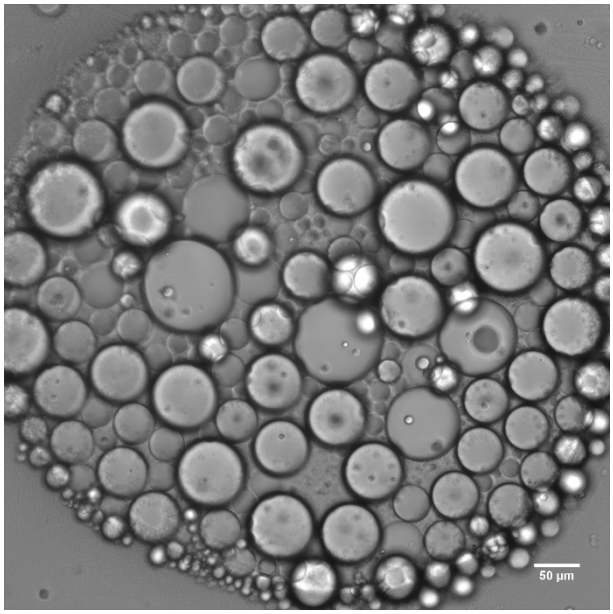

Figure 68: Apollonian structure observed immediately after emulsification of polycaprolactone and dichloromethane as the internal phase, and a 0.02% solution of SDS as the external phase.

Immediately after emulsification, we observed the still-wet product under microscope and found that the droplets indeed presented an Apollonian packing (Figure 68). The Apollonian emulsions studied so far in this present dissertation were stabilized with the non-ionic surfactant, C12E6, so the Apollonian packing obtained here using polycaprolactone, dichloromethane and ionic surfactant, SDS, demonstrates that this structure is not composition-dependent, but is rather a consequence of coalescence in a liquid HIPE.

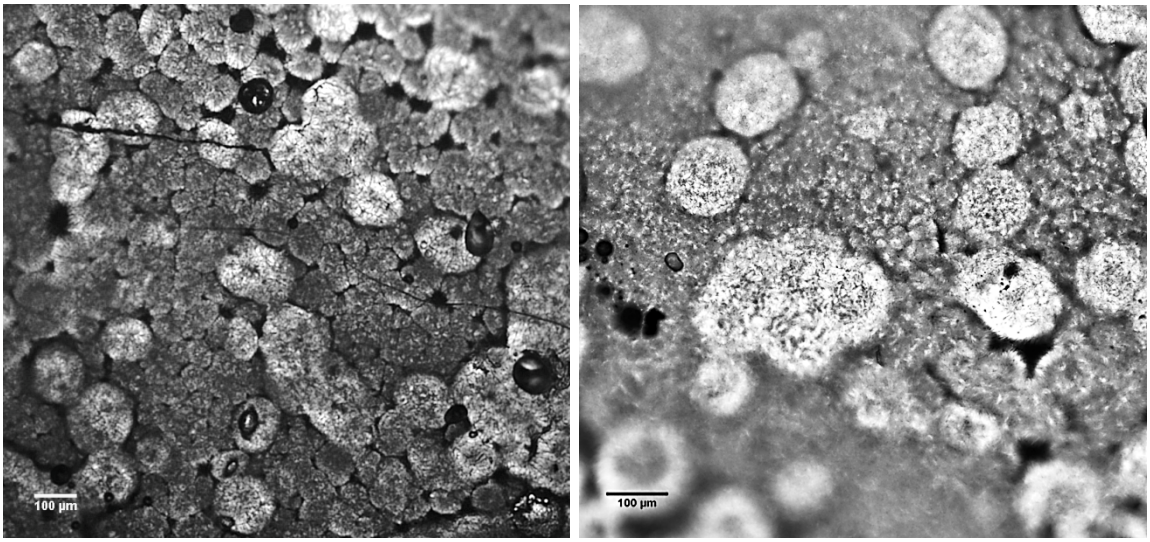

Figure 69: observation of the completely dried and solidified HIPE two months later. The material obtained was constituted of almost-spherical particles, and presented little porosity (left). We observed the areas between larger particles at higher magnification to confirm that

We fabricated about 60g of liquid HIPE in this experiment, and allowed the entire volume to evolve and evaporate at room temperature over the course of 1 – 2 weeks. We observed a sample of the completely dried material about two months later (Figure 69, left), and found an internal structure with little porosity, consisting of almost-spherical particles of very different sizes. We tried to resolve the areas between larger particles at higher magnification and could discern spherical particle interfaces as well (Figure 69, right). It was likely that the evaporation of the dichloromethane was not radially uniform from the Apollonian HIPE droplets, hence the somewhat imperfect spherical particles of polycaprolactone in the dried material. Solvent evaporation also formed a crust of solidified polymer over the HIPE at the beginning of the process, so it was necessary to periodically poke holes in the crust so that dichloromethane could evaporate from the HIPE at the bottom of the beaker. This act of poking resulted in cracks propagating across the final solid material, visible in Figure 69 (left).

Nevertheless, the results from this preliminary experiment are highly encouraging and represent the first steps towards optimized fabrication of ultra-low porosity materials. We have demonstrated that it is a feasible idea to exploit the space-filling property of Apollonian emulsions. By solidifying the emulsion droplets, we may obtain a dense, solid material composed entirely of spherical particles.

5.2 Photon or electron trap

Since an Apollonian emulsion's interfaces are fractal, we could imagine using this scale-invariant property to tune the electromagnetic diffusivity of a material. We may now imagine eliminating the internal-phase droplets in the final material while keeping an imprint of the interfaces that would have been formed by the continuous phase. An aerogel-like structure would be obtained, provided that it is not too brittle due to the thinness of the emulsion interfaces. By doping the continuous phase with percolating reduced graphene oxide platelets or carbon nanotubes (anisotropic electronic conductors), the set of interfaces obtained would also be conductive. A photon or electron entering this fractal structure would soon be trapped in the labyrinth, hence the name photon or electron trap. An example of applications of such a material could be an electromagnetic wave-absorbing coating on military hardware for avoiding radar detection.

5.3 Controlled release of drugs

In the domain of pharmaceutical sciences, controlled release of a drug plays an important role: if the delivery kinetic is too fast, there will be an accumulation of toxicity in the body; if it is too slow, the drug will not deliver its therapeutic effects optimally.[140] It has also become commonplace to use emulsions or encapsulation in polymer microspheres to deliver orally-administered drugs presenting low solubility in water in order to increase bioavailability, i.e. a larger fraction of what is consumed can attain the blood stream and be distributed to receptors where the drug will take effect. Clearly, when emulsions and particles are involved, their size distributions then play a role in the controlled release of active agents. Smaller carriers have been found to more efficiently penetrate tissues and release drugs quicker, while polydispersity appears to give a more tapered rate of release over time (Figure 70).[141]

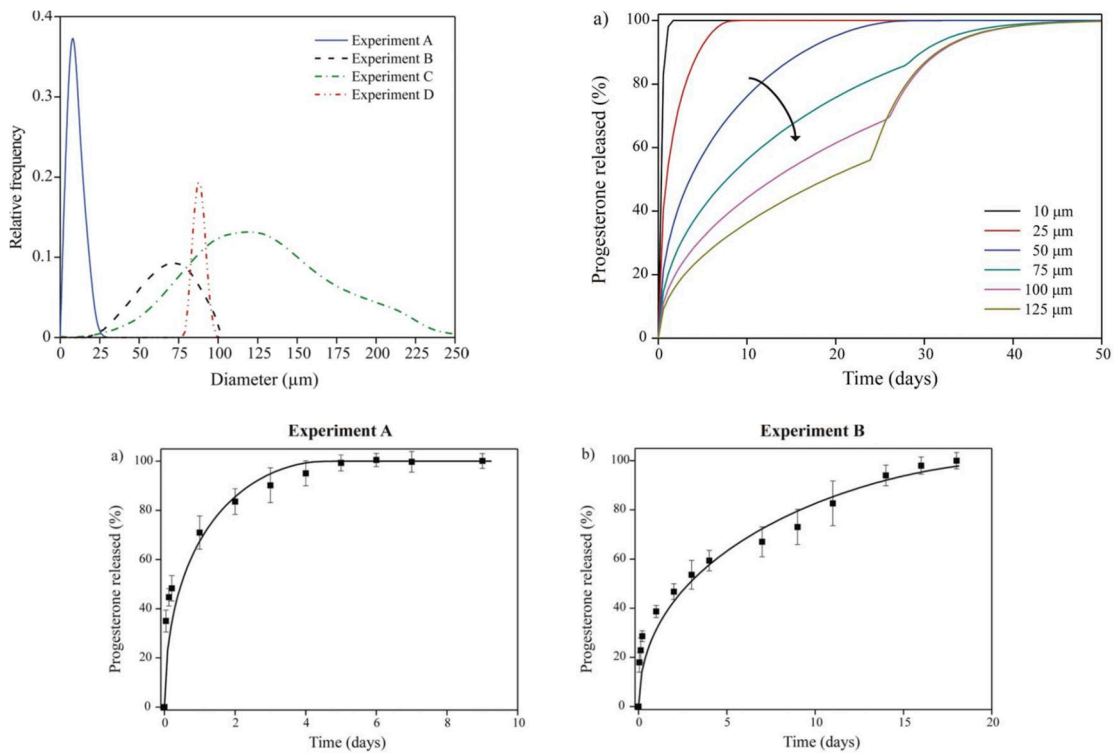

Figure 70: the effects of the size distributions of encapsulating microspheres on the release of active agent, progesterone, were investigated (top left). Smaller polymer microspheres released progesterone quicker (top right), while a polydisperse population of microspheres appeared to release progesterone more gradually with time (bottom right) compared to a monodisperse population (bottom left). Figures taken from Busatto et al. (2018)[141].

Since the size distribution of Apollonian emulsion droplets follow a continuous power law over a range of radii $[a_0, a_1]$, we may envision the staggered release with time by each class of droplet sizes, resulting in an extremely prolonged and overall steady rate of drug release. Such a model of drug release would be particularly advantageous for treatment of chronic conditions requiring repeated doses at regular intervals, for example, Parkinson's, hypertension, contraception, auto-immune diseases. We investigated the feasibility of this idea with some mathematical calculations and modelling, performed by Robert Botet of Université Paris-Sud. The details of the calculations can be found under Supplementary Information section "11.3 Rate of drug release by Apollonian distributions of spheres".

5.3.1 Drug release from a spherical carrier by diffusion

This mode of delivery has been found experimentally to follow Fick's second law of diffusion (D'Aurizio et al., 2011)[142]. If we let m be the proportion of drug molecules already released from the spherical carrier at time t, then the rate of release can be written simply as:

$$\frac{dm}{d\tau} = 6\sum_{n=1}^{\infty} exp(-n^2\pi^2\tau)$$

with $\tau = Dt/R^2$, a reduced unit of time dependent on the sphere's radius R and the drug molecule's coefficient of diffusion D within the spherical carrier.

For a monodisperse population of spheres, the kinetic profile of drug release is shown in Figure 71.

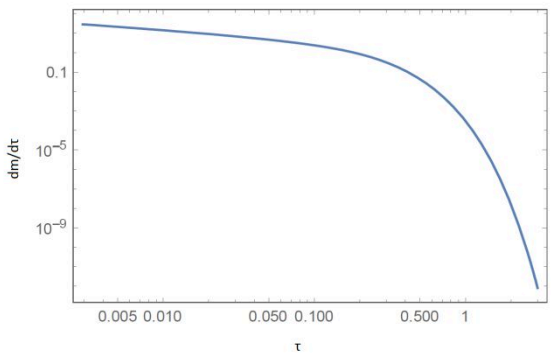

Figure 71: the rate of drug release from a monodisperse population of carrier spheres as a function of time.

For an Apollonian distribution of spherical carriers, to make a fair comparison, we consider the case where the average volume of the spheres is the same as in the monodisperse collection. We find that the rate of drug release is a power-law function of τ:

$$\frac{dm}{d\tau}(\rho, t) \approx \frac{\omega}{\tau^{(d_f-1)/2}}$$

with ω a function that depends on the fractal dimension $d_f = 2.47$ and $\rho = a_1/a_0$ defined as the width of the Apollonian distribution. The derivation of this formula is given in Supplementary Information section "11.3.1 By diffusion from within a spherical carrier".

We then plot the drug release rate, $dm/d\tau$ as a function of reduced time τ, for several values of ρ (Figure 72). We find that the larger the width of the Apollonian distribution, the longer the drug release (τ being proportional to physical time, t). It is also noteworthy that while the monodisperse collection of spherical carriers are almost depleted of drugs, releasing at negligible rates at around $\tau \approx 1$, Apollonian distributions are still going strong, releasing at a rate over a hundred times higher.

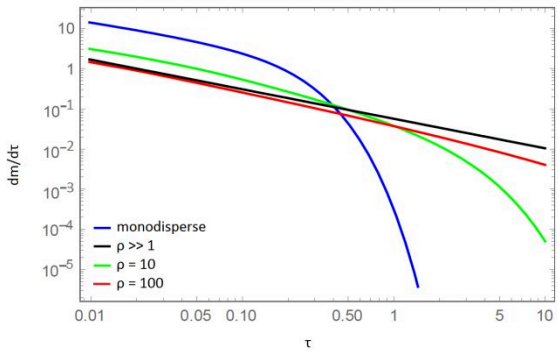

Figure 72: comparing the rate of drug release by diffusion between a monodisperse collection of spherical droplets/particles (blue) and Apollonian distributions of different widths. The plot is double-logarithmic to show that Apollonian distributions are capable of sustained delivery.

5.3.2 Drug release by the dissolution of a solid sphere

Instead of releasing drugs from within a carrier by diffusion, the therapeutic molecule can also be delivered to the body by the gradual dissolution of a solid substrate. The most common examples are orodispersible tablets, subcutaneous implants[143] and biodegradable ocular implants[144]. This mode of delivery may be described by Hopfenberg's zero-order kinetic model for the controlled release of drugs from erodible spheres[140]:

$$m(t) = 1 - \left(1 - \frac{k_0 t}{c_0 R}\right)^3$$

where k_0 is the equilibrium constant, c_0 is the initial concentration of drug molecules in the spherical substrate of radius R. Our calculation of release rate, $dm/d\tau$, from an Apollonian population of spheres is given in Supplementary Information section "11.3.2 By dissolution of a solid spherical substrate".

We then plot the kinetic profiles of drug release from the dissolution of a monodisperse population of spheres and Apollonian populations of spheres at different values of ρ. The release rates for both Apollonian populations are quite similar regardless of their widths (Figure 73).

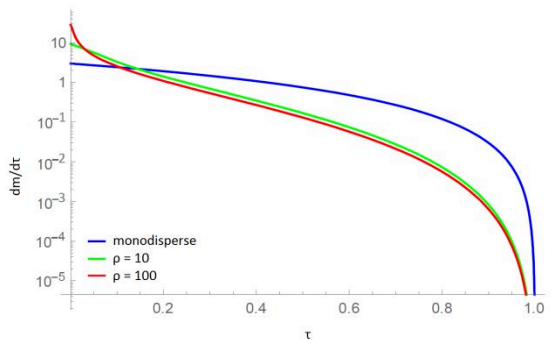

Figure 73: comparing the rate of drug release by dissolution solid spheres between a monodisperse collection (blue) and Apollonian distributions of different widths. Note: $\tau \propto (k_0/Rc_0)\rho^{-(d_f/3)}t$.

To meaningfully interpret Figure 73, we have to realise that the definition of τ here is now:

$$\tau = \alpha\rho^{-(d_f/3)}t$$

where α is a constant coefficient that is proportional to $k_0/(Rc_0)$. This definition is different from the case of diffusion from a spherical carrier.

The factor $\rho^{-(d_f/3)}$ is significant. To demonstrate this point, we solve for the half-time release. This corresponds to the real time t (in units of $1/\alpha$) at which half the number of drug molecules have been released, i.e. $m(t) = 1/2$. We find t = 0.2 for the monodisperse population, and t = 12.3 for the Apollonian population with ρ = 1000. This means that the drug is released on a time scale that is 60 times longer from the dissolution of the Apollonian population of spheres, as compared to the monodisperse population.

Our calculations and modelling therefore demonstrate that Apollonian distributions of spherical carriers or substrates may be capable of extremely prolonged drug release, representing a highly convenient, alternative course of treatment for those suffering from chronic conditions.

6. Conclusion

By severely limiting surfactant availability, we have enabled coalescence in high internal-phase-ratio emulsions (HIPEs), culminating in a new class of HIPEs that have never been described in literature and never thought to physically exist. This new class of emulsions has a structure where all available space is filled with an extremely polydisperse collection of spherical droplets, in accordance with the principles that Apollonius laid down over 2000 years ago. In his honour, we have named these HIPEs, whose internal volume fractions approach unity, "Apollonian emulsions". Their fabrication is incredibly simple yet highly reproducible: all it takes is to add internal phase slowly under constant stirring to a continuous phase containing surfactant, just like making a mayonnaise. The key differences are greatly reducing surfactant concentration, as compared to classic HIPEs that have preoccupied the physical chemistry community thus far, and allowing the emulsion to evolve spontaneously.

The size distribution of spherical droplets in Apollonian emulsions follows a power law with an exponent $-(d_f + 1)$, where the fractal dimension, d_f, was consistently found to be similar to that of a Random Apollonian Packing at 2.47. Thanks to Small-Angle X-ray Scattering measurements and comparisons with numerically simulated Random Apollonian Packing, we were able to conclusively verify the Apollonian structure of our emulsions. We also deduced from microscopic observation and our SAXS data that the spherical droplets have no flat films separating them. This ensures the minimization of elastic energy in the system and consequently, Apollonian emulsions flow spontaneously like a Newtonian liquid, instead of exhibiting shear-thinning flow common to other concentrated emulsions. The Newtonian flow is likely because individual droplets in an Apollonian emulsion behave as if other droplets constituted a homogeneous medium: the effective viscosity of an Apollonian emulsion appears to follow Einstein's equation for dilute dispersions, if we considered the continuous phase to be other oil droplets. There is also no yield stress in Apollonian emulsions, contrary to gel-like HIPEs that have been extensively studied until now.

Our experimental evidence suggests that the mechanism of evolution in a surfactant-poor HIPE towards an Apollonian emulsion, and whilst in the Apollonian structure, is radically different from typical coalescence in dilute emulsions. In the latter, typical coalescence tends to create ever larger and fewer droplets to minimize the total surface area, while excess surfactant expelled in the aftermath of a coalescence event can freely disappear into the reservoir of continuous phase. In our liquid HIPEs, we found unexpectedly that surface area increased with time, implying the creation of many small droplets. We used numerical simulations, which very closely replicated our experimental systems, to demonstrate that every coalescence event between two parent droplets indeed begets many daughter droplets. We have dubbed this mechanism "coalescence-fragmentation" (or the more tongue-in-cheek "Rabbit" algorithm). These progenies are created to accommodate the locally confined evicted surfactant molecules, because these molecules cannot be absorbed by the little available continuous phase in a HIPE without significantly raising the chemical potential. We also determined the three conditions of coalescence-fragmentation: conservation of volume, optimal filling of voids through maximisation of daughter-droplet radii, and avoiding the creation of flat films which are costly in Gibbs free energy. Respecting these three conditions gives Apollonian structures locally, and their union gives a global Apollonian structure in the HIPE. We found from our SAXS results that the daughter droplets created through coalescence-fragmentation can even take on the form of swollen micelles, at spontaneous curvature or not.

Once a HIPE achieves an Apollonian structure, it demonstrates exceptional metastability in defiance of conventional expectations for emulsions of such high volume fraction containing so little surfactant. While conventional coalescence depletes the number of droplets by growing their sizes, coalescence-fragmentation allows Apollonian emulsions to self-feed by creating small droplets, giving the impression that a HIPE remains emulsified for a very long time. We have also found that coalescence rates in Apollonian emulsions can be predicted by the Smoluchowski model of coagulation for polydisperse emulsions. This may seem paradoxical because Apollonian structures are scale-invariant whereas the Smoluchowski model is based on a mean-field theory.

We have interpreted the exceptional metastability of Apollonian emulsion as a local thermodynamic equilibrium, where the rise in surface energy is partially compensated by the entropic term in the expression for Gibbs free energy. Eventually, the system creates droplets so large that they physically separate from the rest of the emulsion due to density differences. Then, the system loses its coveted Apollonian structure, and continues making its way down the Gibbs free energy curve, towards the global free energy minimum that finally results in macroscopic separation between the oil and aqueous phases.

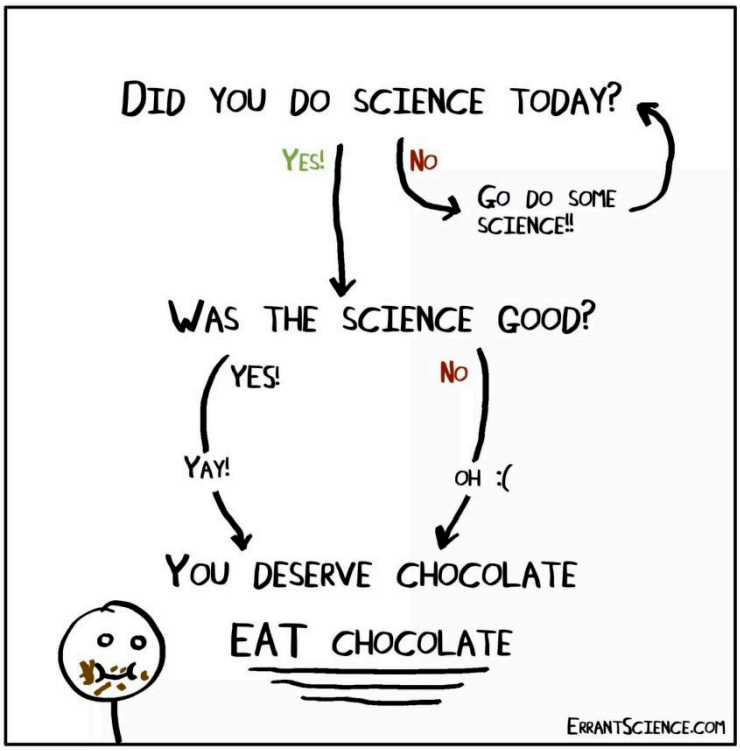

Les émulsions Apolloniennes

La coalescence dans des émulsions à haut rapport de phase interne

Résumé en français

7. Introduction

Dans son bouquin humoristique publié en 2017, le dessinateur américain, Zach Weiner, a donné un résumé des avancements dans le domaine en physique :

> « Aristote prononça des choses qui étaient fausses. Galilée et Newton fixèrent des choses. Puis Einstein cassa tout à nouveau. Maintenant, on a presque tout réglé, sauf pour des petites choses, des grandes choses, des choses chaudes, des choses froides, des choses rapides, des choses lourdes, des matières noires, la turbulence et l'idée du temps. » - in *Science : Abridged Beyond the Point of Usefulness.*[1]

Au cours de ce travail, je présenterai nos réflexions sur un mélange des choses petites et des grandes. J'utilise le pronom pluriel « nous » car il ne s'agit pas de mon effort seul. On s'est intéressé à une structure particulière qui s'appelle un empilement Apollonien, où on remplit tout l'espace avec des cotangentes sphères de plus en plus petites, en les plaçant dans les vides formés par des grosses. Cette idée mathématique bien élégante a bien réunit des savants depuis 2200 ans – à partir de son homonyme, Apollonius de Perge (IIème siècle av. J-C) jusqu'à Mandelbrot (XXème siècle de notre ère), tout en passant entre les mains des grands penseurs scientifiques. On a longtemps cru que ce genre de structure n'existerait pas en réalité, puisqu'il fallait une infinité de sphères de tailles infiniment variées pour la construire. Ainsi, c'était un hasard heureux qu'on a réussi à trouver une façon extrêmement simple pour la réaliser avec un minimum d'effort : parce que j'étais nulle pour faire de la mayonnaise (Figure 1). Comme disait Newton, « la vérité se trouvera toujours dans la simplicité. »

Figure 1: un scène tire du tableau *Les Proverbes flamands,* issu de la main du maître de la Renaissance flamande, Pieter Bruegel l'Ancien (1559)[2], qui a bien prédit ma réaction 460 ans plus tard, lorsque j'ai dû expliquer à mon encadrant pourquoi la mayonnaise coulante que j'avais fabriquée était quand-même une réussite. Note : le vrai proverbe à tirer de la scène est « Rien ne sert de pleurer sur le lait renversé ».

La plupart entre nous connaît bien la mayonnaise et certains entre nous l'adore même. On peut en acheter dans les supermarchés, mais un chef digne de son nom réclamera la supériorité d'une mayonnaise *faite maison* à partir de l'huile, des jaunes d'œuf et du jus de citron. Il y a tout un tas de savoir-faire et du romantisme nostalgique rattachés à la fabrication de la mayonnaise à la main, dont la clé est l'ajout au fur et à mesure de l'huile tout en fouettant vivement le mélange, jusqu'à ce que toute l'huile soit incorporée pour donner une consistance bien onctueuse. Une mayonnaise jugée comme ratée est donc un mélange qui coule… enfin, jusqu'à présent car on démontrera qu'une

mayonnaise coulante est beaucoup plus intéressante – elle est, en effet, un exemple du fameux empilement Apollonien.

« Comment ça? Il n'y a aucune nouveauté de faire une mayonnaise qui coule. On en trouve plein conditionnées dans des bouteilles à presser au supermarché ! » dit un lecteur sceptique. C'est vrai, mais regardons la liste des ingrédients sur la bouteille et on verra certainement la « gomme Xanthane » qui est un épaississeur rhéofluidifiant. Elle sert à stabiliser le produit au repos, en empêchant le crémage sous l'effet de la gravité, et lorsque la bouteille est pressée, elle facilite l'écoulement du produit. Autrement dit, la mayonnaise commercialisée s'écoule parce que l'industrie agroalimentaire a mis un additif à cet effet. Ce n'est pas la même chose.

« Dis, as-tu vraiment étudié la mayonnaise pendant 4 ans ? » Pas exactement. Ce que j'appelle la mayonnaise jusqu'à présent n'est qu'un exemple courant d'une émulsion à haut rapport de phase interne (acronyme HIPE en anglais) (si j'avais commencé à décrire dès la première page cette substance au nom monstrueux imprononçable, j'aurai probablement endormi mes chers lecteurs). Une émulsion est un mélange de deux liquides immiscibles, souvent de l'huile et de l'eau, stabilisés par du tensioactif. Considérons une émulsion d'huile-dans-l'eau : la surface des gouttes d'huile (phase interne) sont protégées par des molécules de tensioactif, et ces gouttes sont dispersées dans une phase continue externe qui contient de l'eau. Si on attendait suffisamment longtemps, une émulsion finira par casser parce que les deux liquides ont envie de se séparer. Le mécanisme par lequel cette séparation se produit est la coalescence : des gouttes d'huile se rencontrent de temps en temps et fusionnent pour donner une plus grosse goutte, et à force de répéter ce mécanisme, l'émulsion se trouvera dans un état de séparation macroscopique. Le mûrissement d'Ostwald est aussi un autre mécanisme de déstabilisation : il a lieu lorsque les deux phases liquides sont partiellement solubles l'une dans l'autre. Ainsi, des petites gouttelettes d'huile peuvent se dissoudre dans la phase aqueuse et migrent pour se rejoindre aux grosses. Dans ce travail, on ne considéra pas le mûrissement d'Ostwald puisque l'on a bien choisi une huile minérale lourde qui est très insoluble dans l'eau.

Une HIPE est un type d'émulsion où on garde la même topologie d'huile dans l'eau, sauf le volume total d'huile dépasse celui de l'eau. Des recettes pour la mayonnaise conseillent toujours d'ajouter l'huile lentement parce qu'on doit faire accepter la phase aqueuse (les jaunes d'œuf) plus d'huile qu'elle aimerait contenir. Dans le produit final, on a réussi à forcer tellement de gouttes d'huile dans un tout petit volume de phase aqueuse externe que ces gouttes sont toutes serrées l'une contre l'autre. Elles finissent par se déformer en polyèdres, séparés par des films minces de tensioactif protecteur (dans la mayonnaise, les protéines d'œuf jouent ce rôle, et le jus de citron sert à charger ces molécules pour les écarter encore plus). Le résultat de cette déformation ainsi que la présence des films minces sont une résistance contre l'écoulement. Bien entendu, la stabilité d'une HIPE dépend alors de la robustesse de ces films protecteurs. C'est donc la raison pour laquelle on a toujours utilisé beaucoup de tensioactif pour empêcher la coalescence lorsqu'on étudiait ce genre de structures. Dans le chapitre « 2.1 High Internal-Phase-Ratio Emulsions (HIPEs) », on a résumé brièvement les travaux qui ont été menés sur ces HIPEs « solides » à fort taux de tensioactif.

La coalescence est souvent un phénomène nuisible dans les émulsions. C'est donc inattendu de produire volontairement ce phénomène dans une structure aussi bondée comme une HIPE en mettant peu de tensioactif. On s'attends à ce que cette structure hors équilibre se casse rapidement pour donner des gouttes d'eau dans une phase huileuse, ce qui donnera un mélange coulant (le critère pour juger une mayonnaise ratée). Toutefois, ce n'est pas du tout le cas. Au contraire, on démontrera que la coalescence dans une HIPE conduira à une évolution spontanée où les gouttes d'huile s'organiseront pour donner un empilement Apollonien, avec un minimum d'effort, comme on avait constaté dans le premier paragraphe de cette introduction. Dans le chapitre « 3. Materials and methods for HIPEs », on vous partagera notre recette et on introduit également des techniques de caractérisation utilisées au cours de ce travail.

Dans le chapitre « 8.1 Le comportement macroscopique d'une HIPE vs. sa composition », on présente des différences majeures de comportement observées pour les HIPEs usuelles riches en tensioactif et nos HIPEs pauvres en tensioactifs. Puis, on fournit des preuves expérimentales dans le chapitre « 8.2 L'évolution des HIPEs liquides » que ces HIPEs pauvre en tensioactif possèdent en effet l'empilement Apollonien. En interprétant ces résultats expérimentaux, on croit que cette structure développe par un mécanisme qu'on a nommé « la coalescence-fragmentation ». Il est considérablement différent de la coalescence typiquement rencontrée dans les émulsions diluées parce que celui-là engendre beaucoup de petites gouttelettes. Le chapitre suivant « 8.3 Discussions sur des HIPEs Apolloniennes » est dédié à la discussion de la coalescence-fragmentation. On essaie de reproduire nos systèmes expérimentaux par des simulations numériques, puis on examine si ce mécanisme est réaliste par des considérations thermodynamiques spécifiques aux HIPEs. Finalement, dans le chapitre « 5. Suggestions for applications of Apollonian HIPEs », on propose quelques applications qui peuvent profiter de la structure Apollonienne, notamment pour la fabrication des matériaux à faible porosité et pour le relargage étendu des médicaments dans le domaine pharmaceutique.

Ainsi, à travers de 4 ans d'étude sur la « mayonnaise », j'espère avoir contribué à la compréhension des « petites choses » et des « grandes choses ». Encore une fois, comme disait Newton, « Expliquer toute la nature est une tâche trop ardue pour [une seule personne] ou une seule époque. Il est plus sage de faire peu en étant sûr de soi et laisser le reste à ceux qui viendront après ». En effet, que l'on puisse – par la chance aveugle – réaliser un empilement Apollonien, une structure qui a préoccupé Newton et d'autres têtes toutes aussi brillantes pendant deux millénaires, « [si on a] vu plus loin que les autres, c'est parce que [l'on s'est] juché sur les épaules de géants. »

8. Résultats et discussions

Notre objectif à l'origine était de trouver un moyen de fabriquer des gouttes micrométriques monodisperses. Par hasard, on est tombé sur une revue[51] où la voie d'émulsification à haut rapport de phase interne était une méthode pour cela. On ignorait du fort taux de tensioactif nécessaire pour fabriquer ces HIPEs monodisperses et on s'est donc mis à calculer la quantité minimale de tensioactif à mettre pour faire une HIPE à $\phi = 0.8$ où les gouttes avaient des diamètres de 6µm. En supposant que chaque tensioactif occupait $0.5nm^2$ à l'interface[45], on a trouvé qu'il fallait une concentration en tensioactif de 0.6% en masse dans la phase continue. Cette opération a été faite par souci d'économiser du tensioactif qu'on trouvait étonnement cher. Il s'est trouvé donc que la frugalité était effectivement la clé à la porte qui s'ouvrait aux univers perdu des émulsions Apolloniennes.

8.1 Le comportement macroscopique d'une HIPE vs. sa composition

8.1.1 La résistance à l'écoulement en présence de plus de tensioactif

Ayant réussi à faire une HIPE sans inversion de phases, j'ai naïvement déclaré ma réussite à mon encadrant, Bernard Cabane, qui avait presque 50 ans d'expériences dans la recherche des colloïdes. Sa première question : « pourquoi ça coule ? »

- « J'en sais rien… est-ce que ça ne devrait pas couler ? »
- « Non ça ne devrait pas couler si la fraction volumique de phase interne dépasse 50%. »
- « Oh. Mais je suis sûre que ça s'est pas inversé. »

Par la suite, on s'est référé à la première publication sur des HIPEs, l'article de Lissant publié en 1966, afin de reproduire son protocole :

> "The emulsification equipment used was a household mixer [Kitchen Aid, Model 3C]… with the mixer set at No.2… The external phase consisted of a mixture of 6 volumes of distilled water and 1 volume of emulsifier [a proprietary, non-ionic material, D-28000, supplied by Petrolite Corporation of St. Louis, Missouri, and not otherwise identified]."[10]

J'ai déduit des fiches techniques et des scans flous du mode d'emploi (publié en 1954) de ce mixeur que la vitesse no. 2 correspondait probablement à 81rpm. Je n'ai pas pu identifier le tensioactif utilisé puisque le fabricant n'existait plus depuis les années 90s, mais c'était clair que Lissant avait utilisé une phase continue aqueuse à 14% de tensioactif solubilisé.

On a lancé une nouvelle tentative avec le tensioactif non-ionique, C12E6, en variant sa concentration dans la phase continue de 0.6% à 25% en masse. C'était bien évident que les HIPEs s'approchaient à leur comportement décrit dans la littérature lorsqu'on augmentait la quantité de tensioactif – on obtenait une substance gélifiée qui ne s'écoulait pas. En revanche, à faible taux de tensioactif, on obtenait des émulsions coulantes. Entre les deux, à une concentration intermédiaire de tensioactif, la consistance de l'émulsion était hybride, comme un yaourt mal homogénéisé où des morceaux de gels étaient suspendus dans une émulsion liquide (Figure 28).

Figure 28 : (gauche) une HIPE coulante à 0.6%C12E6 dans la phase continue; (milieu) un comportement hybride, semi-gélifié à 5%C12E6 dans la phase continue; (droite) une HIPE gélifiée qui ne s'écoule pas, à 25%C12E6 dans la phase continue.

8.1.2 La rhéologie

On a utilisé la rhéologie pour quantifier ces comportements différents observés pour les HIPEs, en variant cette fois-ci systématiquement la concentration en tensioactif. On leur a imposé du cisaillement en rotation à faible fréquence.

Les modules G' et G'' d'un échantillon quantifient respectivement l'aspect « solide élastique » et « liquide visqueux » de son comportement vis-à-vis de la sollicitation mécanique. Les valeurs présentées ci-dessous ont été mesurées dans le régime viscoélastique linéaire de chaque échantillon (Figure 29).

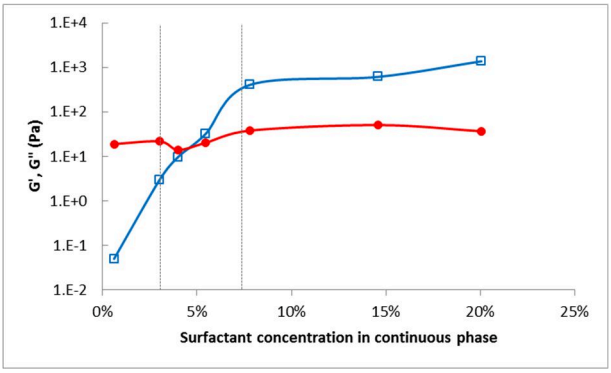

Figure 29 : des mesures réalisées en état stationnaire dans le régime viscoélastique linéaire de chaque HIPE en fonction de sa concentration en tensioactif dans la phase continue. Des carrées sont des mesures de G' et des points rouges sont des mesures de G''. Les lignes pointillées tracées démarquent trois régimes distincts : un comportement majoritairement « liquide visqueux » à faible taux de tensioactif < 3%C12E6, un comportement majoritairement « solide élastique » à forte concentration en tensioactif ≥ 8%C12E6, et un régime intermédiaire entre les deux.

Pour une HIPE à 0,6%C12E6 dans la phase continue, G' = 0,05Pa et celui-ci monte jusqu'à 1370Pa pour une HIPE à 20%C12E6, ce qui représente une augmentation de 4,5 décades en ordre de grandeur. Par contre, G'' est plus ou moins constant à 28,6Pa pour toutes les HIPEs, peu importe la concentration en tensioactif. C'est principalement dû au fait que toutes les HIPEs ont la même quantité d'huile, ϕ = 0,95, et que le comportement « liquide visqueux » vient des gouttes d'huile.

Le module de cisaillement complexe, G^* s'écrit : $G^* = G' + iG''$. Dans la représentation de Fresnel, s'il y a plus d'une décade de différence entre les valeurs de G' and G'', on peut considérer que le module qui l'emporte dirigera le comportement prépondérant de l'échantillon. Ainsi, on peut distinguer trois régimes dans ces HIPEs :

- $G' < 10G''$: régime liquide, écoulement possible, pour <3%C12E6 dans la phase continue ;
- $G' > 10G''$: régime solide, pas d'écoulement, pour ≥ 8%C12E6 ;
- $G' \approx G''$: régime de transition, HIPE à structure hybride pour des concentrations intermédiaires en tensioactif.

Cette identification de la transition solide-liquide dans les HIPEs correspond bien au critère donné par Winter et Chambon (1986)[97]. Ce critère sert à l'origine à identifier le point de gélification pour un polymère, qui se produit lorsque $G' = G''$ sous cisaillement en rotation à fréquence fixe. Son application est ensuite étendue à d'autres matériaux à caractère gélifiant, que ce soit la gélification par la réticulation chimique ou par la percolation physique[98].

Les courbes d'écoulement pour les HIPEs sont aussi en accord avec cette distinction de trois régimes (Figure 30 et Figure 31) Des échantillons riches en tensioactifs où la concentration est supérieure à 7,8%C12E6 dans la phase continue présentent clairement un seuil d'écoulement, σ_y,. Preuve en est, la contrainte de cisaillement appliquée, σ, devient constante et indépendante de la vitesse de déformation à partir de $\dot{\gamma} \geq 0{,}3s^{-1}$. σ_y est entre 100 – 450Pa et il augmente avec la concentration en tensioactif pour les HIPEs solides. On n'observe pas ce plateau pour d'autres HIPEs, ce qui est cohérent avec leur caractère coulant (Figure 30).

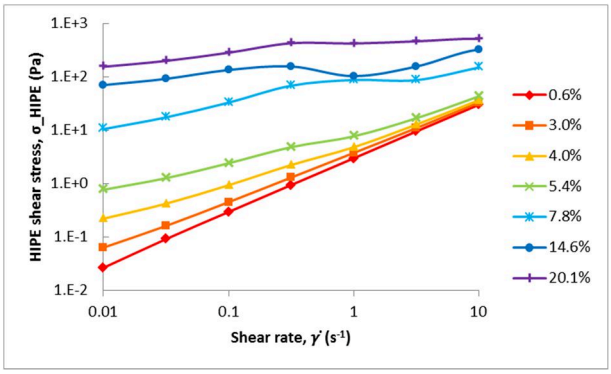

Figure 30 : des HIPEs solides présentent un plateau où la contrainte de cisaillement appliquée, σ, devient constante en fonction de la vitesse de déformation, $\dot{\gamma}$. Cette valeur du plateau renseigne sur le seuil d'écoulement, σ_y. D'autres HIPEs ne présentent pas un tel plateau.

Les HIPEs solides présentent également une pente négative pour leur courbe d'écoulement où la viscosité effective est exprimée en fonction de la vitesse de déformation et représentée en doubles-logarithmes (Figure 31). La pente négative signifie un comportement rhéofluidifiant, ce qui est bien documenté dans la littérature pour des HIPEs étudiées qui sont stabilisées par beaucoup de tensioactif.[25,35,37,99–101] Ce comportement résulte de l'écoulement du tensioactif liquide dans les films minces qui séparent des gouttes d'huile et ne dépend pas de la viscosité de la phase huileuse[37].

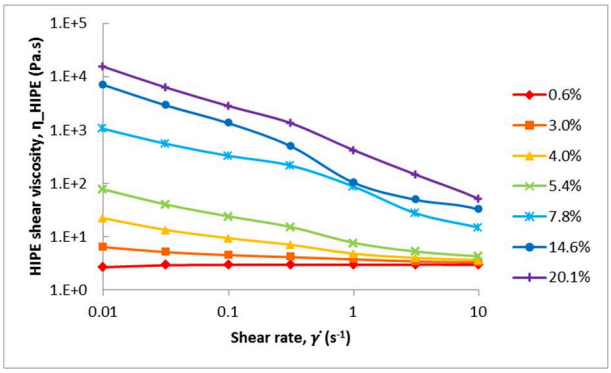

Figure 31 : la courbe d'écoulement pour chaque HIPE à différent taux de tensioactif dans la phase continue. La pente nulle de la courbe pour les HIPEs à < 3%C12E6 indique un comportement Newtonien. Lorsque la concentration en tensioactif augmente, la pente devient négative, ce qui signifie un comportement rhéofluidifiant.

Les échantillons à concentrations intermédiaires, c'est-à-dire 4,0% et 5,4%C12E6, montrent également un caractère rhéofluidifiant. Cependant, leur courbe d'écoulement semble rejoindre celle des HIPEs pauvres en tensioactif lorsque la vitesse de déformation devient plus importante, au-delà de $\dot{\gamma} > 3{,}16s^{-1}$. La pente nulle des celles-ci – à 0,6% et 3%C12E6 dans la phase continue – implique que **ces HIPEs à ϕ = 0,95 stabilisées par peu de tensioactif se comportent comme des fluides Newtoniens[35]. Ceci est une observation inconnue auparavant pour une émulsion à fraction volumique aussi élevée**. Jusqu'à présent, le comportement Newtonien n'est observé que pour des émulsions à ϕ < 0,60[100,102], au-delà de laquelle on retrouve un comportement rhéofluidifiant. Pour des dispersions de sphères dures, cette fraction volumique limite est encore plus faible, à ϕ < 0,45[103]. Il paraît donc que nos HIPEs à faible taux de tensioactif puissent être assimilées aux dispersions idéales de sphères dures où on suppose que chaque goutte suive la même trajectoire lorsqu'elle est mise sous cisaillement[104].

Désormais, en raison de leur propriété d'écoulement, on appellera des HIPEs à faible concentration en tensioactif « des HIPEs liquides » et celles à forte concentration en tensioactif « des HIPEs solides ou type Lissant ». Celles à comportement intermédiaire seront « des HIPEs hybrides ». On essaiera d'expliquer ces différences rhéologiques par un examen de la structure interne des trois types de HIPEs.

8.1.3 Chaque régime correspond à une géométrie particulière des gouttes

On a regardé sous microscope optique chaque type de HIPE à ϕ = 0,95. Selon la quantité de tensioactif solubilisée dans la phase continue de l'échantillon, on retrouve des géométries de gouttes très différentes (Figure 32).

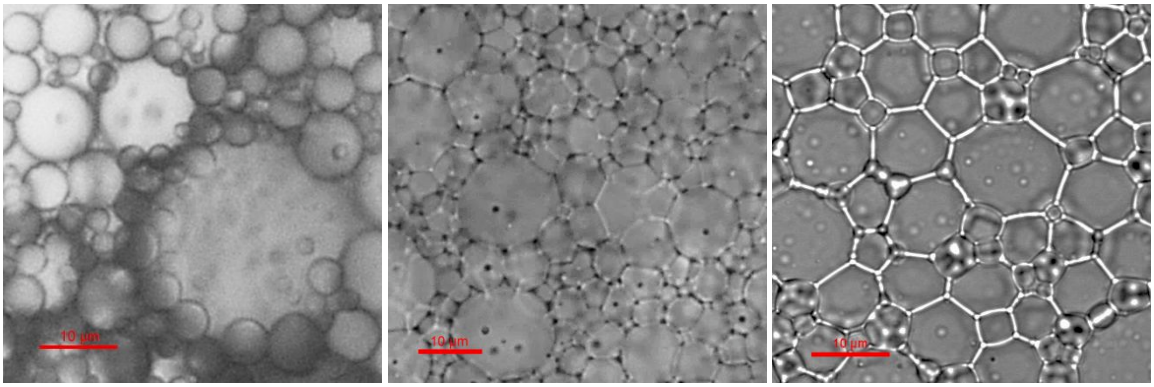

Figure 32 : observation sous microscope d'une HIPE liquide à 0,6%C12E6 dans la phase continue (gauche) ; une HIPE hybride à 5%C12E6 (milieu) ; une HIPE solide à 20%C12E6 (droite).

Les gouttes d'une HIPE solide à 20%C12E6 dans la phase continue sont extrêmement déformées en polyèdres séparés par des films minces (Figure 32, droite). Cette observation reproduit ce qui a été publié sur des HIPEs type « Lissant » qui sont stabilisées par beaucoup de tensioactif. En diminuant la concentration en tensioactif à 5% (Figure 32, milieu), on observe une géométrie mélangée, où on peut identifier des gouttelettes à facettes intercalées entre des gouttes sphériques plus grosses. En réduisant encore la concentration en tensioactif jusqu'à 0,6%, les gouttes d'une HIPE liquide deviennent un ensemble de sphères sans déformation et sans films minces visibles (Figure 32, gauche).

On peut aussi remarquer une forte différence entre la distribution de tailles des gouttes d'un échantillon à l'autre. Elles deviennent de plus en plus polydisperses lorsqu'on réduit la quantité de tensioactif : dans la HIPE solide riche en tensioactif, les gouttes polyédriques sont de 2 – 20µm de diamètre ; dans la HIPE hybride, elles sont entre 2 – 30µm ; dans la HIPE liquide pauvre en tensioactif, les gouttes sphériques sont visiblement entre 1 – 100µm. Cette forte hétérogénéité de tailles rend difficile la capture d'une image nette de toutes les gouttes sphériques au même profondeur du champ focal. On se rappelle également que des tailles < 1µm ne sont pas bien résolues en microscopie optique à lumière blanche non plus. Par conséquent, on a utilisé la diffraction du laser pour mesurer la distribution de tailles des gouttes dans nos HIPEs.

Il est tout de même une observation surprenante de visualiser des gouttes sans déformation apparente dans une HIPE liquide à ϕ = 0,95. Bien que ce genre d'organisation soit théoriquement possible et discutée dans la littérature, on a longtemps cru qu'elle n'était pas réaliste (cf. chapitre « 2.1.8 Future explorations: Filling space with scale invariance »). Lors de notre recherche bibliographique, on a trouvé une publication[75] où les auteurs ont observé brièvement cette organisation seulement au début de l'émulsification à ϕ = 0,88 ; au cours de l'émulsification, des gouttes devenaient de plus en plus tordues (Figure 15). **On croit, à présent, être les premiers à observer une géométrie sphérique préservée même après la fin de l'émulsification, dans une structure à fraction volumique aussi élevée à 0,95.**

8.1.4 La distribution de tailles dans chaque type de HIPE

Hermann et al. (2012) ont démontré par la simulation numérique que l'on peut remplir l'espace à une fraction volumique presque 1 avec sphères en utilisant une distribution de tailles qui suit une loi de puissance.[70] On a donc utilisé la diffraction du laser pour mesurer $n(a)$, la distribution des diamètres a dans nos HIPEs pour vérifier si c'est bien le cas. Ces résultats sont présentés en double logarithmes afin de mettre en évidence des lois de puissance (Figure 33).

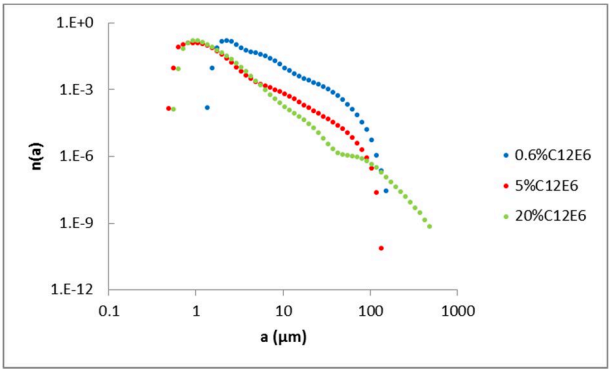

Figure 33 : la distribution des diamètres mesurée par la diffraction du laser d'une HIPE liquide (bleu), une HIPE hybride (rouge) et une HIPE solide (vert) à 0,6%, 5% et 20% de C12E6 solubilisé dans la phase continue. On trouve que les distributions de taille sont effectivement des lois de puissance.

Effectivement, les distributions de tailles sont de la forme : $n(a) \sim a^{-\gamma}$ étendues sur au moins 2 décades de diamètres. On estime ensuite l'exposante γ à partir de la pente de la courbe représentée en double logarithmes (Tableau 2). On a démontré dans le chapitre « 3.2.2.2 Revealing a power-law behaviour » ainsi que dans les Informations Supplémentaires, chapitre «11.1 Deducing d_f from the double-log plot of Light Scattering measurements » que l'exposante donne directement la dimension fractale de l'échantillon.

Tableau 2: la distribution des diamètres des gouttes dans chaque HIPE suit une loi de puissance sur au moins deux décades de valeurs. a_{min} et a_{max} correspondent au plus petit et au plus grand diamètre mesurés pour chaque échantillon et γ, l'exposante de la loi de puissance, donne directement la dimension fractale, d_f.

Type de HIPE	a_{min} (µm)	a_{max} (µm)	$\gamma = d_f$
Liquide, 0,6%C12E6	1,36	154	2,01
Hybride, 5%C12E6	0,82	225	2,28
Solide, 20%C12E6	0,56	484	2,97

8.1.4.1 Comment juger la polydispersité pour une distribution en loi de puissance

On aurait pu croire que les mesures de diffraction du laser soient contradictoires aux interprétations des observations sous microscope dans le chapitre précédent, puisque la gamme des tailles des gouttes dans une HIPE solide semble plus étendue (donc plus polydisperses) que dans une HIPE liquide. Toutefois, il faut noter que les grandes gouttes de diamètre >20µm ne sont présent qu'à une proportion extrêmement faible pour l'HIPE solide, soit $7 \times 10^{-10} - 2 \times 10^{-5}$, ce qui veut dire qu'il suffit d'avoir une seule goutte anormalement large à 484µm dans une population de 1,44 milliard de gouttes pour élargir artificiellement la distribution de tailles. En examinant la fréquence cumulée, cette « contradiction » disparaîtra : au 99ème percentile, des gouttes sont ≤ 15,4µm dans une HIPE liquide ; pour une HIPE hybride, ≤ 6,3µm ; et pour une HIPE solide, ≤ 3,8µm. Ainsi, cela ne suffit pas de regarder la largeur de la gamme des tailles mesurées pour juger la polydispersité d'une population. Il sera d'autant plus juste d'examiner l'exposante (ou la dimension fractale) pour des lois de puissance.

Pour une loi de puissance, la polydispersité est définie par f, qui est une fonction en décroissance de la dimension fractale (Figure 34) :

$$f = \left[d_f(d_f - 2)\right]^{-1/2}$$

pour $d_f > 2$ (cf. chapitre « 11.2 Polydispersity as a function of fractal dimension » pour la preuve mathématique).

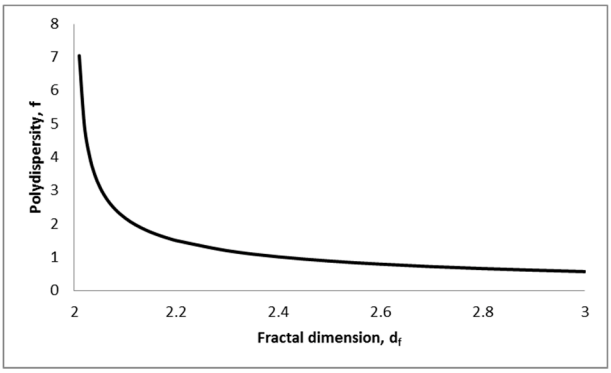

Figure 34 : la polydispersité, f, en fonction de la dimension fractale, d_f, pour une distribution en loi de puissance.

Ainsi, grâce à cette définition de polydispersité pour des distributions en loi de puissance, puisque d_f croît en fonction de la quantité de tensioactif dans les HIPEs (Tableau 2), nos mesures de diffraction du laser sont bien cohérentes avec les observations sous microscope – **une HIPE liquide pauvre en tensioactif est effectivement la plus polydisperse, tandis qu'une HIPE solide riche en tensioactif est la moins polydisperse**. Cela implique qu'un gros excès en tensioactif engendre une population moins polydisperse, ce qui est en accord avec l'observation courante que des tensioactifs fournisse d'excellente protection contre la coalescence des gouttes, un moteur qui conduît à la polydispersité dans des émulsions.

8.1.4.2 La coalescence et la fragmentation dans les HIPEs

La coalescence provoque la polydispersité

On calcul la surface totale, A_{oil}, et le volume total, V_{oil}, pour chacun des émulsions. En supposant que chaque molécule de C12E6 occupe 52 – 55Å^2 dans une monocouche de tensioactif stabilisant à l'interface de la goutte d'huile[43,45], on peut alors calculer A_{C12E6}, la surface hypothétique que toutes les molécules de tensioactif auraient pu occuper, afin de déterminer le taux de couverture réel à l'interface. Chacune de ces quantités s'écrit de la façon suivante :

$$A_{oil} = \sum_{a_{min}}^{a_{max}} n(a_i) \cdot 4\pi(a_i/2)^2$$

$$V_{oil} = \sum_{a_{min}}^{a_{max}} n(a_i) \cdot (4/3)\pi(a_i/2)^3$$

$$m_{C12E6} = \frac{(V_{oil} \cdot \rho_{oil})}{\varphi}(1-\varphi) \cdot \left(\frac{\%C12E6}{100}\right)$$

avec $\rho_{oil} = 905 kg/m^3$, $\varphi = 0{,}95$, et $\%C12E6$ la concentration en masse du tensioactif dans la phase continue de l'HIPE;

$$A_{surf} = \frac{m_{C12E6}}{M_{C12E6}} N_A \cdot 55\text{Å}^2$$

où $M_{C12E6} = 450{,}65 g/mol$ la masse molaire du C12E6, et $N_A = 6{,}02 \times 10^{23}$ le nombre d'Avogadro.

Tableau 3 : calcul du taux maximum de couverture à l'interface par les molécules de C12E6 dans chaque type de HIPE.

HIPE	%C12E6	A_{oil} (10^{-12} m^2)	V_{oil} (10^{-18} m^3)	m_{C12E6} (10^{-14} g)	A_{surf} (10^{-12} m^2)	Taux maximum de couverture à l'interface (= A_{surf}/A_{oil})
Liquide	0,6	87,5	273	7,79	57,2	65,4%
Hybride	5	25,5	72.0	17,1	126	494%
Solide	20	7,65	6,85	6,53	48,0	600%

À partir des valeurs calculées présentées dans le Tableau 3, seulement 65,4% des interfaces sont couvertes par des molécules de tensioactif dans une HIPE liquide, tandis que les taux de couverture pour des HIPEs hybride et solide sont largement supérieur à 100%. Autrement dit, les interfaces dans ces dernières sont bien saturées et il y a même un gros excès en tensioactif. **Ainsi, la coalescence peut avoir lieu dans une HIPE liquide à cause d'une protection incomplète, alors qu'elle est gravement inhibée dans les HIPEs hybrides et solides.** Si un pore s'ouvrait de manière aléatoire entre deux gouttes d'huile côte à côte, on aurait une abondance de tensioactif dans des HIPEs hybrides et solides pour réparer ce défaut ; dans une HIPE liquide, on est en manque de tensioactif. Prenant en compte la mesure de polydispersité dans le chapitre précédent, on perçoit une corrélation entre la coalescence dans le système et une polydispersité plus importante.

La fragmentation engendre une distribution de taille en loi de puissance dans toutes les HIPEs

Cependant, si la présence de beaucoup de tensioactif inhibera la coalescence dans nos HIPEs hybrides et solides, pourquoi ont-elles des distributions de tailles en loi de puissance ? On expliquera la raison pour laquelle nos échantillons ne sont pas monodisperses par leur procédé de fabrication : la fragmentation à haute énergie sous cisaillement par un mixeur à hélice.

Des études menées sur le mécanisme de fragmentation des matériaux granulaires trouvent souvent des distributions de tailles log-normales ou en lois de puissance. On obtient des distributions log-normales lorsque les grains sont fragmentés de manière indépendant l'un et l'autre à la même fréquence, et on obtient des lois de puissance par la fragmentation continue (et parfois explosive) où la rupture d'une particule dépend des forces transmises par ses voisines (Herrmann et al.)[105,106]. L'exposante alors obtenue sera entre 2,0 et 2,8 et dépend du nombre de voisines les plus proches (Steacy et Sammis, 1991)[107]. **C'est donc évident que dans une HIPE où les gouttes d'huiles sont tellement serrées qu'elles sont toutes en contact, la fragmentation indépendante soit très improbable dans une telle structure**. Ce mode de fragmentation indépendante peut expliquer pourquoi on retrouve souvent des distributions log-normales ou normales pour les émulsions polydisperses à faible fraction volumique – les gouttes colloïdales sont suffisamment espacées – et pourquoi des distributions en loi de puissance sont rarement rencontrées.

Il s'avère que l'agitation prolongée des HIPEs (de type « Lissant » stabilisées par beaucoup de tensioactif) raffine la distribution de tailles des gouttes pour donner une population monodisperse[51,75]. Notre protocole de fabrication diffère à ce stade car on a arrêté l'agitation dès que la dernière goutte d'huile soit ajoutée, ce qui explique pourquoi on observe toujours des lois de puissance dans nos HIPEs hybrides et solides.

Ainsi, **on propose que toutes les HIPEs passent par un stade lors de l'émulsification où la distribution de tailles est une loi de puissance, à cause de la fragmentation des gouttes dans un milieu confiné.** Dans des HIPEs hybrides et solides, on peut préserver chaque goutte créée par la fragmentation grâce à l'abondance de tensioactif. Si on prolonge l'agitation, les tailles de gouttes deviennent de plus en plus homogène et stabiliseront à la plus petite taille créée par la fragmentation.

Une nouvelle approche: la coalescence et la fragmentation simultanée dans les HIPEs liquides

Pour les HIPEs liquides, le système est en manque de tensioactif. Cela veut dire que les petites gouttes créées par la fragmentation ne sont pas préservées, et elles peuvent coalescer entre elles pendant l'émulsification. **La nouveauté de notre approche est donc laisser produire la coalescence et la fragmentation en même temps dans une structure aussi bondée comme une HIPE à ϕ = 0,95.** En effet, tous les ouvrages cités dans cette thèse que l'on peut trouver dans la littérature cherchaient toujours à supprimer la coalescence dans les HIPEs. Par ailleurs, l'approche usuelle des études dans le domaine des colloïdes est de favoriser un seul procédé à la fois – la fragmentation *ou* la coalescence – et de les considérer indépendamment avec des conséquences opposantes : la fragmentation mène à un nombre important de gouttes aux tailles plus petites, tandis que la coalescence a un effet opposé[108].

On pense donc que c'est grâce à cette nouvelle approche qu'on a pu obtenir un empilement Apollonien dans nos HIPEs liquides. On a nommé ce mécanisme « la coalescence-fragmentation » qu'on discutera de manière plus détaillées.

8.1.5 Le lien entre la microstructure et la propriété rhéologique d'une HIPE

8.1.5.1 Les propriétés rhéologiques des HIPEs hybrides et solides.

Bien que l'on appelle les HIPEs riches en tensioactif comme des « solides », elles sont en réalité des matières molles viscoélastiques qui s'écoulent au-delà de leur seuil d'écoulement. Ces HIPEs ont été beaucoup étudié dans la littérature, et leur écoulement a été expliqué par l'écoulement du tensioactif liquide dans les films minces qui séparent des gouttes d'huile polyédriques.[19,25,35,37,99–101] Leur module élastique, G', est aussi assez important, ce qui caractérise une réponse élastique aux sollicitations mécaniques : les HIPEs solides stockent de l'énergie dans les interfaces de gouttes déformée en les déformant encore plus.[28,101]

Nos résultats rhéologiques ainsi que nos observations microscopiques semblent être en accord qualitatif avec ce qui est rapporté dans la littérature sur des HIPEs solides. Cependant, on a remarqué que ces études tendent à explorer la variation des propriétés rhéologiques en fonction de ϕ et de la taille des gouttes assez monodisperses. Par exemple, Mason et al. (1995) ont trouvé expérimentalement qu'au-delà d'une fraction volumique seuil, $\varphi_c \approx 0.64$, les gouttes deviennent déformées et coincées :

$$G'(\varphi_{eff}) \sim (\sigma/a)\varphi_{eff}(\varphi_{eff} - \varphi_c)$$

où σ est la tension interfaciale, a le rayon des gouttes monodisperses, φ_{eff} la fraction volumique apparente de l'émulsion, qui considère l'épaisseur des films de phase continue comme étant une partie des gouttes.[27] La définition de φ_{eff} est donnée par la relation :

$$\varphi_{eff} \approx \varphi(1 + 3h/2a)$$

où φ est la fraction volumique réelle et h l'épaisseur des films qui dépend de φ.[15] L'hypothèse sous-entendue est que les gouttes soient sphériques[24,27], malgré le fait qu'elles ne le sont pas.

Dans ce travail, on a gardé une fraction volumique constant à 0,95. σ/a, qui est la densité en énergie des gouttes non déformées[27] est aussi plus ou moins constante dans les HIPEs solides. Pourtant, dans la Figure 29, on peut distinguer une augmentation en G' parmi les HIPEs solides à différentes concentrations en tensioactif. Cette augmentation en G' est encore plus importante en comparant une HIPE hybride et les HIPEs solides. Il se trouve alors que nos conditions expérimentales soient utiles pour combler des lacunes dans la littérature où on ne varie pas φ mais on varie plutôt h.

Par la suite, on a utilisé la diffusion des rayons-X aux petits angles (SAXS) pour étudier la structure des films minces de tensioactif dans nos HIPEs afin de mesurer h. Dans les ouvrages cités, on n'a jamais mesuré h et on a plutôt estimé sa valeur, soit 5nm[27], 17,5nm[24,27], 20nm[19], ou tout simplement inférieure à 100nm[25,101].

8.1.5.2 Mesure de l'épaisseur du film mince de tensioactif par SAXS

Afin d'étudier la structure de ces films *in situ*, on a mesuré par SAXS les spectres concentrés des HIPEs solides en état non dilué. À cause de la fraction volumique interne extrêmement élevée (ϕ = 0,95), c'est plus simple d'appliquer le principe de réciprocité (Babinet, 1837)[109] et d'analyser les spectres comme des interférences encore les films minces qui séparent des gouttes d'huile. Selon le principe de Babinet, des objets compléntaires produisent les mêmes effets diffractifs. Guinier et Fournet (1955) ont démontré mathématiquement que ce principe s'applique également pour la diffusions d'un ensemble de particules aux petits angles.[110] C'est donc la raison pour laquelle on a soustrait ϕ· $I_{oil}(q)$ comme spectre de fond des spectres concentrés des échantillons.

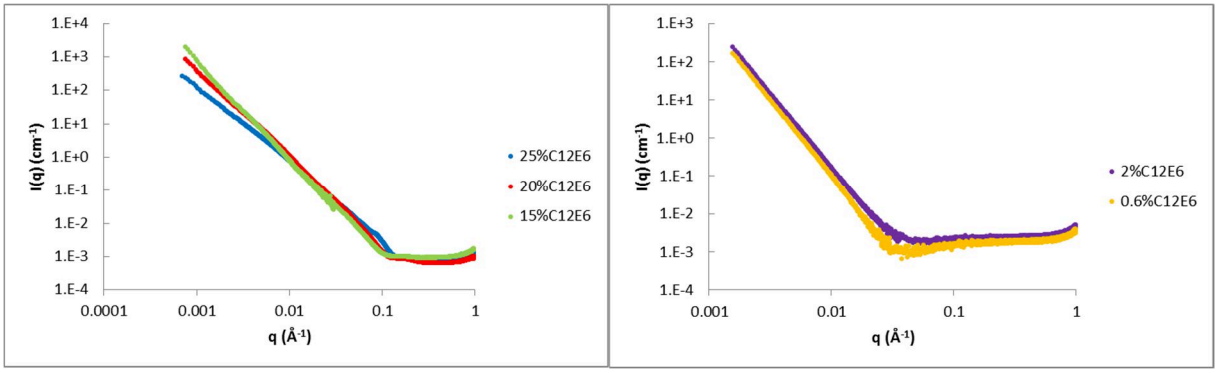

Figure 35 : les spectres concentrés après soustraction du fond. Les échantillons sont des HIPEs qui contiennent 25%C12E6 (bleu), 20%C12E6 (rouge), 15%C12E6 (vert), 2%C12E6 (violet), 0,6%C12E6 (jaune) dans la phase continue. Note : pour l'HIPE à 25%C12E6, on a dû appliquer un facteur correctif de 0,9 à la soustraction aux grandes valeurs de q > 0,01Å^{-1}. Ceci est pour compenser des petites variations d'épaisseur des capillaires portant les échantillons (2 ± 0,1mm). Sans appliquer ce facteur correctif, $I(q)$ pour cet échantillon négative à grandes q, ce qui n'est pas réaliste. Les spectres à gauche ont été mesurés à ESRF, et les spectres à droite à SOLEIL, d'où la différence en gamme de q mesurée.

Dans la Figure 35, on retrouve $I(q)$, l'intensité diffusée par des HIPEs après soustraction du fond. On remarque que $I(q)$ sont des lois de puissance sur deux décades de q (pour les spectres mesurés à ESRF) et cinq décades en intensité. C'est peu courant de trouver des systèmes concentrés dans lequel des corrélations de paires soient des fonctions autosimilaires sur une gamme aussi large.

Pour commencer, on a supposé que des contributions des bordures de Plateau soient négligeables, puisque nos HIPEs ont tellement peu de phase continue qu'elles ressemblent plus aux mousses sèches[11]. On a également supposé que l'épaisseur faible des films minces de tensioactif fait que l'on peut considérer la distribution des distances entre deux points dans ces films comme une distribution de cordes. Aux distances physiques importantes par rapport à l'épaisseur h des films, càd $qh \ll 1$, le système resemble alors à un ensemble de films autosimilaires (donc fractals). Ces films peuvent alors être caractérisés par leur dimension fractale, d_s, et l'intensité diffusée varie comme[111]:

$$I(q) \sim q^{d_s - 6}$$

Par contre, aux distances faibles devant h, $qh \gg 1$, et l'intensité suivra forcément la loi de Porod :

$$I(q) \sim q^{-4}$$

On a utilisé le logiciel SASview pour modéliser la loi de puissance constatée dans les spectres (Figure 35) de q = 0,001 – 0,05Å^{-1}. Les exponsantes trouvées sont présentées dans le Tableau 4.

Tableau 4 : loi de puissance modélisée pour des spectres concentrés des HIPEs

Concentration en C12E6 dans la phase continue de l'HIPE	Exponsante de la loi de puissance	d_s
25%	-2,2997	3,70
20%	-2,548	3,45
15%	-3,003	3,00
2%	-3,9176	2,08
0,6%	-3,9886	N/A; loi de Porod

Les exposantes des HIPEs hybride et solides riches en tensioactif donnent accès à la dimension fractale d_s en ajoutant 6. Ces valeurs trouvées pour les HIPEs solides, soit 3 – 4 indique que ce sont des fractals de surface[111]. Pour l'HIPE liquide, elle suit à la loi de Porod, ce qui veut dire que les interfaces des gouttes sont totalement lisses et qu'il n'y a pas de facettes.[112] Ce résultat confirme nos observations que les gouttes d'huile d'une HIPE liquide ne sont pas déformées. La tendance en croissance de la dimension fratale en fonction de la concentration en tensioactif confirme également les résultats mesurés par la diffraction du laser pour la distribution des tailles (cf. chapitre « 8.1.4 La distribution de tailles dans chaque type de HIPE »).

On peut imaginer que $I(q)$ est la somme de la diffusion par cet ensemble de films fractals, et par la structure interne aux films. On a donc soustrait la loi de puissance de $I(q)$, et on a analysé le reste. On trouve systématiquement une « bosse » entre q = 0,002 – 0,02Å^{-1} pour les HIPEs solides et hybrides (Figure 36). Cette bosse est absente pour l'HIPE liquide, ce qui est cohérent avec une structure qui suit la loi de Porod et qui ne présente pas de facettes.

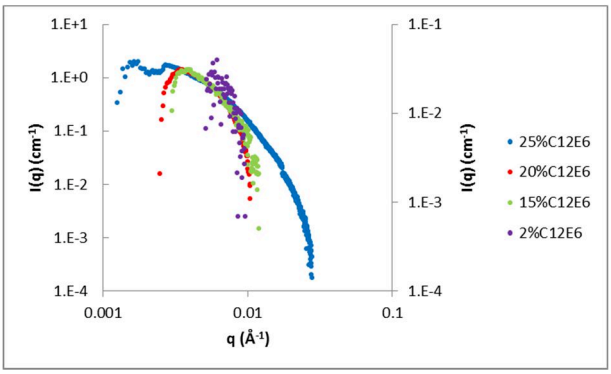

Figure 36 : après soustraction de la loi de puissance, on trouve une bosse entre q = 0,002 – 0,02Å^{-1} pour la diffusion des trois HIPEs solides (bleu, rouge, vert) et l'HIPE hybride (violet). Note : le spectre de l'HIPE hybride a été tracé sur l'axe vertical secondaire à droite, pour le mieux visualiser.

Chaque matériau possède sa propre densité de longueur de diffusion (SLD) des rayons-X en fonction de sa densité électronique. On a calculé la SLD pour chacun des composants dans notre système pour une source de rayons-X à une longueur d'onde de 1Å (Tableau 5). Comme la composition précise de l'huile minérale est inconnue, on a supposé que c'est chimiquement proche d'un alcane lourd comme le squalane.

On a ensuite fait l'hypothèse qu'un modèle lamellaire décrira probablement la structure des films minces qui séparent des gouttes d'HIPE dans les échantillons riches en tensioactif. Pour une HIPE hybride, puisque la géométrie des gouttes est entre sphériques et polyédriques (Figure 32, milieu), on a utilisé un modèle « oignon » à 5 couches pour décrire ces films de tensioactif. Le modèle lamellaire suppose que la chaîne hydrocarbonée C12 du tensioactif est solvatée dans l'huile minérale. Quant au modèle oignon, on a pris l'huile comme le cœur de l'oignon et comme le solvent, d'où 5 couches symétriques formées par la chaîne C12, les groupes polyoxyéthylénés (POE) du tensioactif, et de l'eau. Localement, si on ne considère que la structure entre deux gouttes d'huile, ces deux modèles sont équivalents (Figure 37), puisque l'on a pris le rayon du cœur d'oignon comme 0.

Dans la littérature, on trouve 52 – 55Å^2 pour l'aire par molécule de C12E6 dans une monocouche à l'interface liquide-liquide[43,45]. Connaissant sa masse molaire et sa masse volumique – 450,65g/mol et 1g/cm^3 – on a trouvé que le volume moléculaire de C12E6 soit 750Å^3. Cela donne une longueur moléculaire d'environ 14Å. Si on compare cette valeur au 38 – 39Å donnée dans la littérature comme la longueur moléculaire étendue[43,81], le paramètre d'ordre du tensioactif est environ 0,36. Connaissant que la liaison C-C fait 1,54Å, on a estimé que l'épaisseur de la couche C12 et la couche POE fait 7Å chacune. On a donc utilisé ces valeurs pour notre modélisation de la bosse de la Figure 36.

Tableau 5: valeurs calculées de la densité de longueur de diffusion (SLD) pour l'huile minérale, le tensioactif et l'eau. On a utilisé ensuite ces paramètres pour la modélisation des spectres.

	Formule chimique	Masse volumique (g/cm^3)	SLD (10^{-6} Å^{-2})	Épaisseur de la couche (Å)
Huile minérale	Assimilée à $C_{30}H_{62}$	0,905	8,8	0
Chaîne C12 du tensioactif	$C_{12}H_{26}$	0,75	7,33	7
Groupes POE du tensioactif	$C_{12}H_{24}O_7$	1,12	10,3	7
Eau	H_2O	1	9,44	À déduire

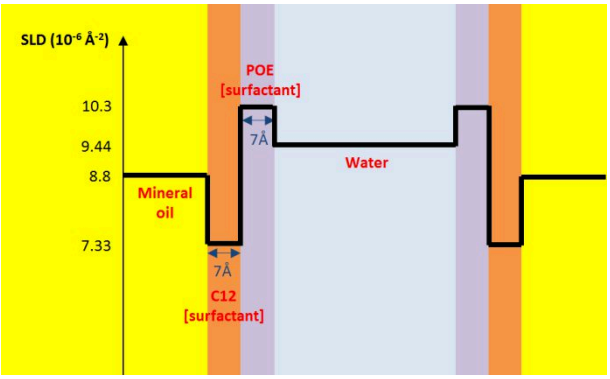

Figure 37 : le profil SLD utilisé pour modéliser la structure des films minces qui séparent deux gouttes d'huile dans une HIPE hybride et solide.

On trouve que ces modèles appliqués décrits bien les données expérimentales entre q = 0,003 – 0,01Å^{-1} (Figure 38). Pour l'HIPE à 25%C12E6 (Figure 38Figure 38a), bien que les points expérimentaux n'aient pas présenté d'oscillations perceptibles à cause du traitement de soustraction, les oscillations du modèle bi-couche reproduisent des variations brusques en intensité que l'on peut observer dans les données expérimentales aux même valeurs de q.

Les valeurs données par la modélisation pour l'épaisseur de la couche d'eau sont résumées dans le Tableau 6. On en déduit l'épaisseur totale du film mince de tensioactif entre deux gouttes d'huile en ajoutant 28Å, ce qui correspond aux couches de C12 et POE.

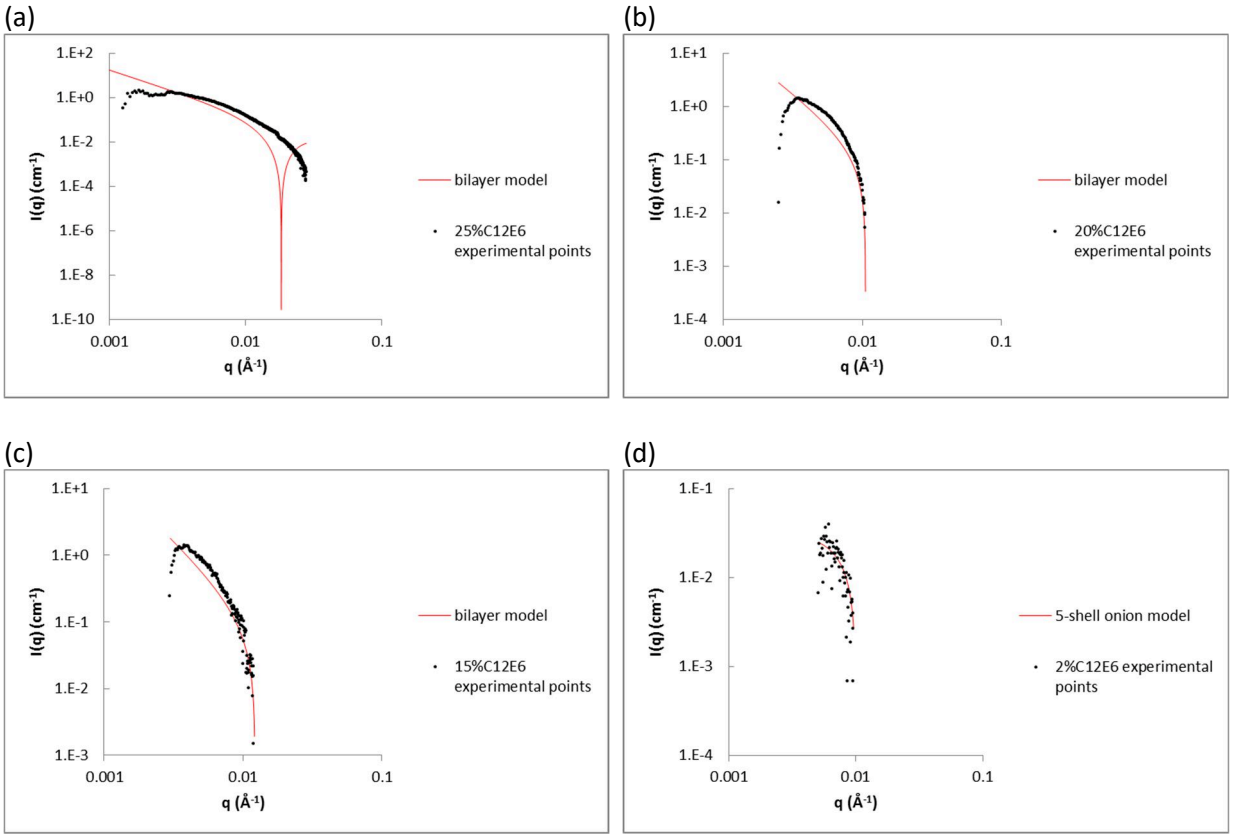

Figure 38 : la modélisation des HIPEs solides par un modèle bicouche lamellaire (a) – (c), et un modèle « oignon » à 5 couches pour une HIPE hybride (d).

Tableau 6: l'épaisseur totale du film mince de tensioactif entre deux gouttes d'huile.

%C12E6 dans la phase continue de l'HIPE	Épaisseur de la couche d'eau donnée par la modélisation (Å)	Épaisseur du film mince (= eau + 2 x C12 + 2 x POE) (Å)
25	172	200
20	130	158
15	104	132
2	81,005	109

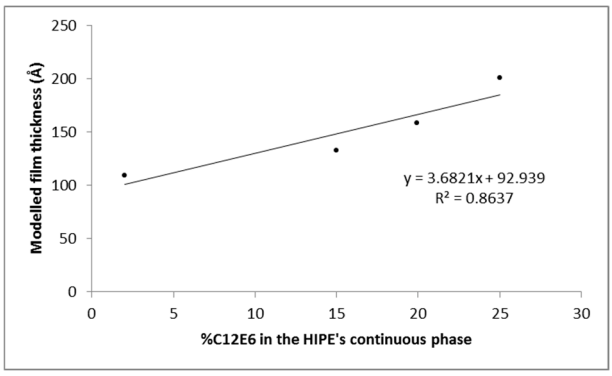

Figure 39 : l'épaisseur du film mince de tensioactif qui sépare deux gouttes côte à côte dans une HIPE, déduite de la modélisation. On trouve 200Å, 158Å et 132Å pour des HIPEs solides à 25%, 20% et 15%C12E6 dans la phase continue. Pour l'HIPE hybride à 2%C12E6, l'épaisseur du film est de 109Å.

Par la modélisation, on trouve que les films minces dans des HIPEs solides font 13,2 – 20nm en épaisseur. Ces valeurs sont très proches aux estimations données dans la littérature comme 17,5 – 20nm[19,24,27]. Pour l'HIPE hybride à 2%C12E6, cette épaisseur est 10,9nm. Il paraît qu'il y ait une relation proportionnelle entre l'épaisseur du film et la quantité de tensioactif dans les HIPEs, comme indiquée par la ligne de régression tracée dans la Figure 39. Nos résultats semble également valider qualitativement les relations empiriques établies entre G' et l'épaisseur du film, h, ce qui peut expliquer la croissance en G' que l'on observe lorsqu'on augmente la concentration en tensioactif dans les HIPEs (Figure 29). On croit qu'un film plus épais, étant plus robuste, permet plus de déformation des interfaces sans rupture. On peut stocker donc plus d'énergie élastique dans ces films.

Toutefois, c'est plus prudent de ne pas tirer des conclusions firmes à ce stade : il aurait été idéal si on a pu faire cette série d'expériences SAXS avec le même instrument sur la même gamme de q, tout en variant de manière systématique la concentration en tensioactif des HIPEs. La soustraction du fond ici des spectres mesurés à ESRF n'était pas parfaite non plus, puisqu'on a utilisé des capillaires individuels cette fois-ci. La mesure et la modélisation de l'épaisseur du film mince aurait pu être faites alors avec plus de certitude. (Par la suite, par souci de soustraction parfaite, toutes les expériences de SAXS ont été faites dans le même capillaire fixé devant le faisceau).

8.1.5.3 L'effet de Farris

On compare les viscosité effectives (Figure 31) au repos ou à faible vitesse de cisaillement ($\dot{\gamma} = 0{,}01 - 0{,}03 s^{-1}$) de nos échantillons. Pour les HIPEs liquides, elles sont 3 – 6 Pa.s et la viscosité effective augmente à 20 – 60 Pa.s pour les hybrides, puis à 800 – 10000 Pa.s pour des HIPEs solides. Clairement, la présence des films minces a un effet prononcé sur la résistance à l'écoulement. Or, si on restreint cette comparaison aux HIPEs liquides et hybrides qui ont des géométries plus comparables, on notera que la variation en viscosité effective démontre l'effet de Farris (1968).

Farris a proposé sa théorie et l'a bien vérifié en comparant aux données expérimentales publiées à la même fraction volumique que la viscosité d'une suspension de sphères diminue lorsque la distribution de tailles devient plus polydipserse[113]. Les hypothèses sous-jacentes sont que des sphères de chaque classe de tailles ont un comportement indépendant des autres et qu'il n'y a pas d'interactions entre elles. Bien que Farris ait démontré ses calculs jusqu'à ϕ = 0,75 pour une population tridisperse, il semble que cet effet existe également dans nos HIPEs à ϕ = 0,95 où une HIPE liquide est effectivement plus polydisperse et moins visqueuse qu'une HIPE hybride (confirmé par nos mesures de diffraction du laser et par les dimensions fractales trouvées par SAXS).

8.1.5.4 Comportement Newtonien d'une HIPE liquide

Dans nos HIPEs liquides, les gouttes ne sont pas mutuellement déformées malgré leur proximité dans une structure aussi bondée. On interprète leur forme sphérique comme une manifestation physique d'une absence de fortes interactions entre elles. Par conséquent, une HIPE liquide peut être assimilée à un ensemble de sphères dures, même si cette approximation de sphères dures pour les colloïdes n'est typiquement valable qu'à faibles fractions volumiques. En outre, nos mesures de SAXS indique qu'il n'y a pas de films minces de phase continue entre des gouttes. Alors, ces gouttes sont libres à rouler l'une sur l'autre sans créer du frottement en torsion, tout comme un roulement à billes[114]: le roulement à billes entraîne la rotation libre des sphères dans le cluster et les voisines réagissent en conséquence, sans glissement aux bords et sans gêner le mouvement des autres (donc sans frottement en torsion).

Farris a également montré dans son travail que dans les suspensions bimodales et multimodales, l'ensemble des petites particules peuvent être considérées comme un fluide homogène visqueux du point de vue d'une particule plus large en mouvement dans ce milieu. La condition est que le rapport des tailles soit < 10%. Sinon, les grosses particules subiront un mouvement en zig-zag.[113,115] Puisque la distribution de tailles des gouttes d'huile dans nos HIPEs liquide est effectivement une loi de puissance continue, **on fait l'hypothèse que chaque classe de tailles plus petites joue le rôle d'un fluide homogène lubrifiant aux gouttes plus grosses.** Il s'agit d'un concept similaire au mouvement du « troisième corps »[116] (une idée introduite par Godet et souvent appliquée en tribologie). Donc, lorsqu'une HIPE liquide est mise sous cisaillement, toutes les gouttes peuvent subir des trajectoires laminaires sans gêne, ce qui donne un comportement global Newtonien[104].

Étant donné qu'on est les premiers à fabriquer des HIPEs liquides à géométrie sphérique qui persiste bien, on croit que c'est la raison pour laquelle on est les premiers à observer un comportement Newtonien dans une émulsion à une fraction volumique aussi élevée. De plus, il semble que personne s'est intéressé à une telle géométrie jusqu'à présent – d'autres chercheurs ont simplement accepté des gouttes polyédriques lorsqu'ils étudiaient les propriétés rhéologiques des émulsions concentrées.

8.2 L'évolution des HIPEs liquides

8.2.1 L'évolution vers une exposante Apollonienne

À partir de nos mesures de diffraction du laser, on a trouvé que la distribution de tailles des gouttes dans nos HIPEs liquides suit une loi de puissance et l'exposante a donné directement la dimension fractale, d_f. On a également établi que la coalescence peut avoir lieu dans ces structures à cause du taux de couverture incomplet. Bien entendu, la prochaine étape est d'étudier l'évolution de ces HIPEs liquides par la coalescence.

On a fabriqué plusieurs HIPEs liquides à ϕ = 0,95 avec 0,6%C12E6 dans la phase continue à différentes vitesses de cisaillement (250rpm, 500rpm and 1000rpm). Ensuite, on les a laissé vieillir à la température ambiante au cours d'un mois et on a mesuré leur distribution de tailles régulièrement par la diffraction du laser (Figure 40).

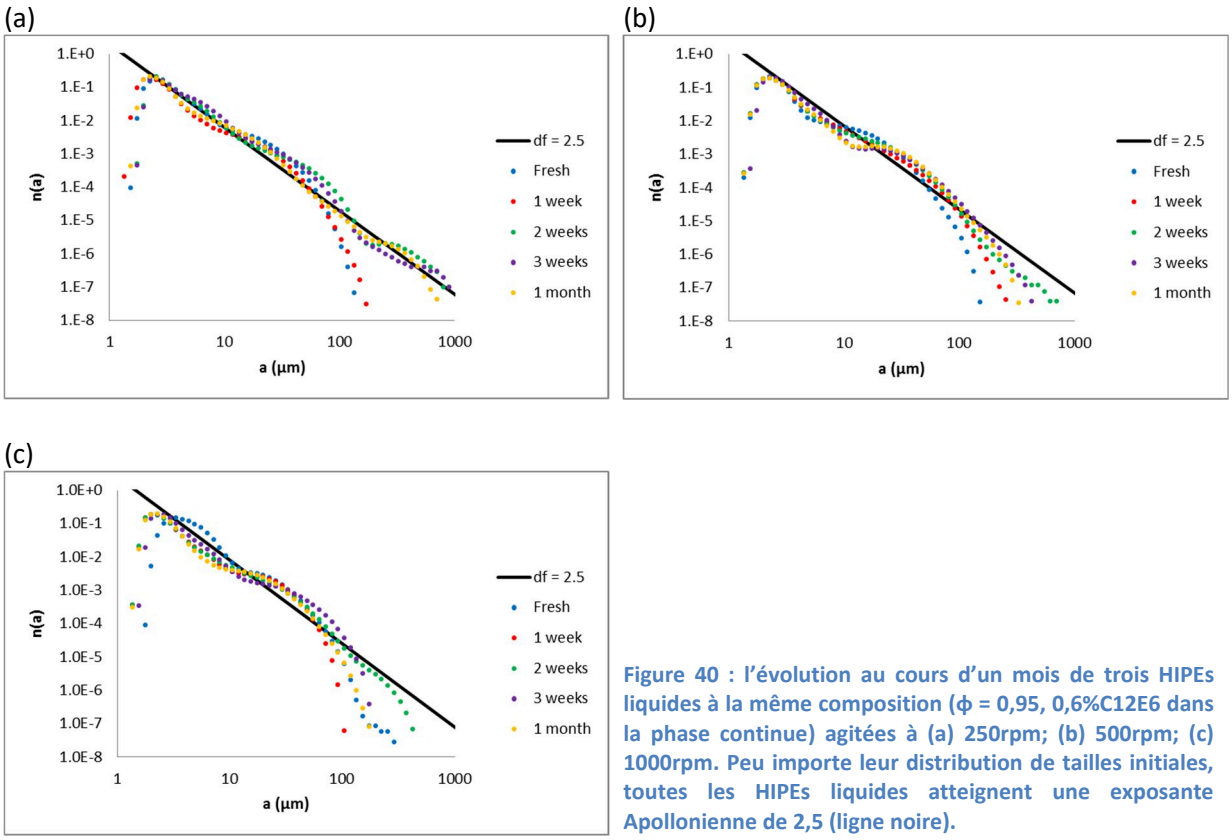

Figure 40 : l'évolution au cours d'un mois de trois HIPEs liquides à la même composition (ϕ = 0,95, 0,6%C12E6 dans la phase continue) agitées à (a) 250rpm; (b) 500rpm; (c) 1000rpm. Peu importe leur distribution de tailles initiales, toutes les HIPEs liquides atteignent une exposante Apollonienne de 2,5 (ligne noire).

Juste après l'émulsification, lorsque les échantillons sont encore frais, la valeur de d_f se trouve entre 2 et 2,5, et les diamètres mesurés sont entre 1,36 – 290µm. Tout cela est entièrement dépendant des conditions d'émulsification spécifiques à chaque échantillon. Cependant, peu importe les distribution de tailles initiales, on constate toujours la même évolution pour toutes les HIPEs liquides : après une semaine d'évolution, la valeur de d_f tends vers et reste à 2,5, malgré l'apparition des grosses gouttes qui peuvent atteindre 916µm par la coalescence. Cette valeur de d_f coïncide avec celle d'un empilement Apollonien des sphères, souvent donnée à 2,45 – 2,52[59,60,72–74]. On a ensuite repris les calculs du taux de couverture des interfaces.

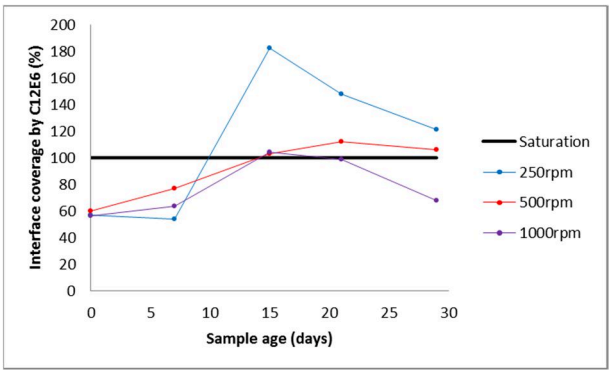

Figure 41 : la variation au cours d'un mois du taux de couverture des interfaces par les molécules de tensioactif dans les mêmes HIPEs liquides que la Figure 40, faites à 250rpm (bleu), 500rpm (rouge) and 1000rpm (violet). La ligne en noir indique 100% de couverture – cela veut dire que des valeurs > 100% correspondent à un excès de tensioactif dans le système par rapport à la quantité d'interface disponible.

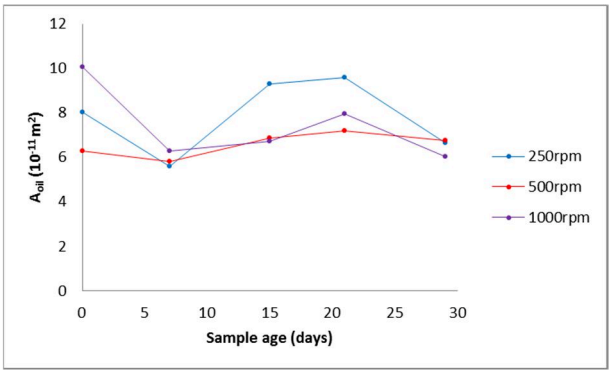

Figure 42 : la variation au cours d'un mois de la surface totale des gouttes d'huile dans les mêmes HIPEs liquides que la Figure 40.

On trouve qu'à l'issu de l'émulsification, seulement 60% des interfaces dans les HIPEs liquides sont couvertes de tensioactif (Figure 41). La coalescence peut alors se produire. Au cours de cette évolution, il y a de plus en plus de grosses gouttes formées et la surface totale diminue (Figure 42). Puis, entre 10 – 15 jours après l'émulsification, toutes les interfaces deviennent saturées de tensioactif (on croise la ligne en noir dans la Figure 41). Désormais, on peut supposer qu'il y ait un excès de tensioactif dans la phase continue. En même temps, on constate une augmentation surprenante de la surface totale dans l'émulsion, ce qui signifie l'apparition des petites gouttelettes, un effet à contre sens de la coalescence.

On interprète que d'une manière quelconque, le système créé des petites gouttelettes pour consommer cet excès de tensioactif initial, puisque la surface totale augmente régulièrement jusqu'au 21ème jour (Figure 42). On peut alors imaginer qu'il y a finalement tellement de petites gouttelettes créées (et donc une telle croissance de surface totale) que cet excès de tensioactif s'épuise. Par la suite, la coalescence peut encore avoir lieu, comme l'indique une baisse de surface totale après 3 semaines. Cette discussion sera reprise dans le chapitre « 8.3.1 La création des petites gouttelettes dans une HIPE ».

Pour l'HIPE liquide faite à 1000rpm (Figure 41, violet), le taux de couverture tombe en dessous de saturation après 3 semaines. À ce stade, on ne voit pas de raison apparente qu'un tensioactif logé confortablement à l'interface d'une goutte soit extrait pour stabiliser d'autres plus petites gouttes. Ainsi, on conseille une interprétation prudente de cette chute en dessous de la saturation.

On précise que la création de ces gouttelettes est inférée de l'augmentation de surface et que la diffraction du laser ne les a pas mesurées. Ceci est lié aux limites de détection de la technique – notre instrument est équipé de deux lasers de λ = 470nm et 632,8nm, ce qui veut dire que des particules plus petites que la demi-longueur d'onde, soit 235nm, sont difficilement résolues.

8.2.2 La persistance de l'exposante Apollonienne

On a gardé à la température ambiante une HIPE liquide à 0,6%C12E6 dans la phase continue et on a mesuré l'évolution de sa distribution de tailles au cours de 8 mois (Figure 43). Même après tout ce temps, la dimension fractale Apollonienne à 2,5 est toujours présente. Les diamètres des gouttes, initialement compris entre 0,93 – 62,8µm s'est élargi à 1,54 – 916µm avec du vieillissement. Malheureusement, on n'a pas pu faire d'autres mesures au-delà de 8 mois à cause de la réparation de l'instrument, mais cet échantillon a été gardé pendant un an et il est resté émulsifié (visuellement). Cet échantillon en particulier a été analysé par SAXS 11 mois après sa fabrication, et les résultats sont présentés dans le chapitre « 8.2 L'évolution des HIPEs liquides - 8.2.5.1 Deux populations de micelles gonflées »

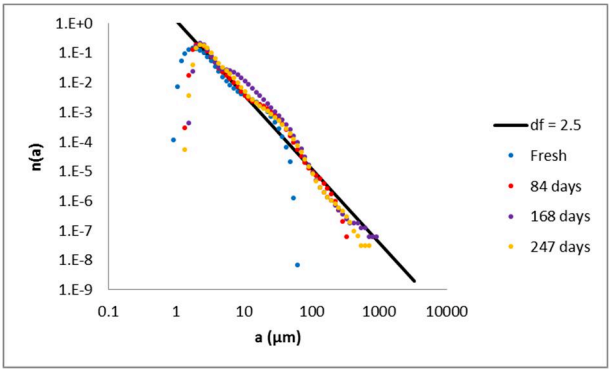

Figure 43 : mesure par la diffraction du laser au cours de 8 mois pour une HIPE liquide. L'exposante Apollonienne est toujours présente malgré la coalescence.

8.2.3 La preuve d'un empilement Apollonien par SAXS

Même si nos HIPEs liquides ont la bonne exposante pour leur distribution de tailles des gouttes, cela n'est pas une condition suffisante pour prouver l'empilement Apollonien des gouttes. On a donc mesuré le facteur de structure expérimental, $S_{exp}(q)$, par SAXS à ESRF, afin de tirer de l'information sur les positions relatives des gouttes voisines dans l'émulsion en état concentré. On a attendu un mois après l'émulsification des échantillons avant d'effectuer ces mesures pour que les échantillons soient suffisamment évolués et qu'ils puissent atteindre une d_f de 2,48 – 2,50.

On obtient $S_{exp}(q)$ en prenant le rapport entre le spectres concentré et le spectre dilué, c.-à-d. $I(q)/P(q)$ (cf. chapitre « 3.2.3.2 Calculating the experimental structure factor, $S_{exp}(q)$ »). En même temps, on a utilisé la simulation numérique pour construire un empilement Apollonien pour lequel on a calculé son facteur de structure théorique, $S_{cal}(q)$, qui sert d'une base de comparaison (Figure 44).

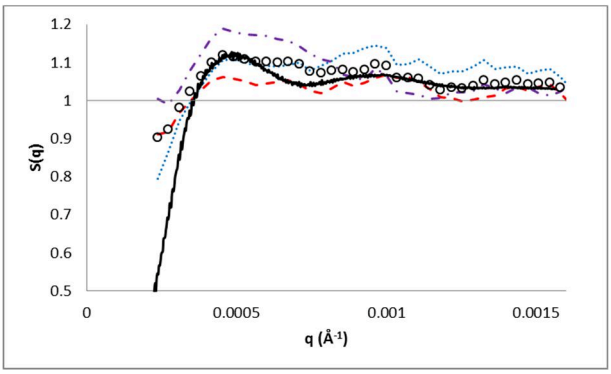

Figure 44 : la comparaison entre les $S_{exp}(q)$ pour des HIPEs liquides à ϕ = 0,95, vieillies pendant 1 mois, faites à 250rpm (points bleus), 500rpm (tirets rouge) et 1000rpm (point-tirets violets). Les cercles sont des valeurs moyennées sur ces trois échantillons. La ligne en noir est le $S_{cal}(q)$ pour une simulation numérique d'un empilement Apollonien à ϕ = 0,92. On a démontré dans le chapitre « 3.2.4.2 Calculating the Apollonian structure factor, $S_{cal}(q)$ » que $S_{cal}(q)$ est identique pour ϕ = 0,84 – 0,92 et donc elle devrait être toujours valable pour comparer à ϕ = 0,95.

L'accord entre $S_{exp}(q)$ et $S_{cal}(q)$ est excellent. Ils présentent tous des mêmes traits : un premier pic large à $S_{max}(q)$ = 1,1 – 1,2 et une queue qui tend vers 1 rapidement. Le pic écrasé et l'absence des oscillations signifient une absence de périodicité pour les HIPEs liquides et l'empilement Apollonien simulé. Ce genre d'allure pour le facteur de structure est rarement rencontré pour des colloïdes : s'il y a le moindre de soupçon de l'ordre à longue portée, même pour les systèmes polydisperses, $S(q)$ montrera des oscillations avec des pics bien définis[117] et $S_{max}(q)$ > 2,85.[118] Il faut un système extrêmement polydisperse pour écraser $S_{max}(q)$ suffisamment pour qu'il soit près de 1 (Van Beurten and Vrij, 1981).[119]

On a cherché dans la littérature pour d'autres types de distributions qui auraient pu fournir la même allure de $S(q)$ (Figure 45, Figure 46 et Figure 47). Bien que ces facteurs de structure ressemblent aux nôtres, la distribution de tailles dans ces systèmes étudiés et leur polydispersité sont très différentes du nôtre. De plus, leur fraction volumique est très inférieure à ϕ = 0,95. **On peut donc conclure sans aucun doute que les gouttes dans nos HIPEs liquides s'organisent comme un empilement Apollonien.**

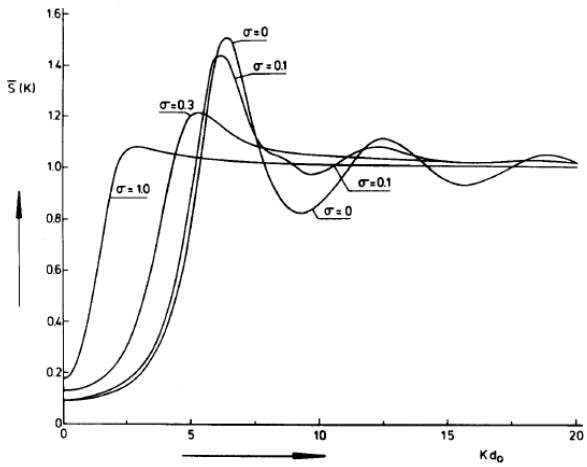

Figure 45 : $S(q)$ d'une distribution de Schulz de sphères dures dont σ = 0.3-1.0 à ϕ = 0.3.[119]

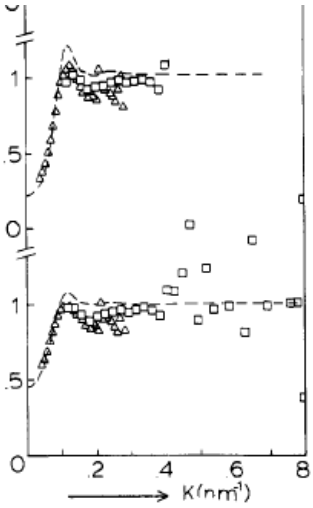

Figure 46 : $S(q)$ d'une distribution log-normale de sphères dures dont σ = 0.12 à ϕ < 0.5.[120]

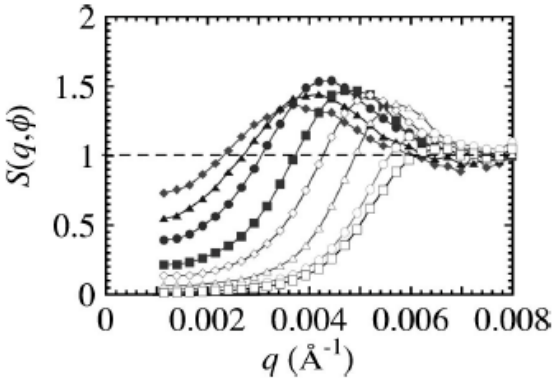

Figure 47 : la $S(q)$ la plus écrasée est celle d'une distribution monomodale dont σ = 0.25 à ϕ = 0.53.[31]

8.2.4 Confirmation par SAXS des observations par la diffusion de la lumière

8.2.4.1 L'évolution vers un empilement Apollonien après une semaine

Puisque les mesures de la diffusion de la lumière indiquent que la dimension fractale Apollonienne soit atteinte typiquement après une semaine d'évolution (Figure 40), on a mesuré $S_{exp}(q)$ des HIPEs liquides à différentes stades d'évolution (fraîche, 1 semaine d'évolution, 1 mois d'évolution) fabriquées à 500rpm. On les a ensuite comparé à $S_{cal}(q)$ (Figure 48).

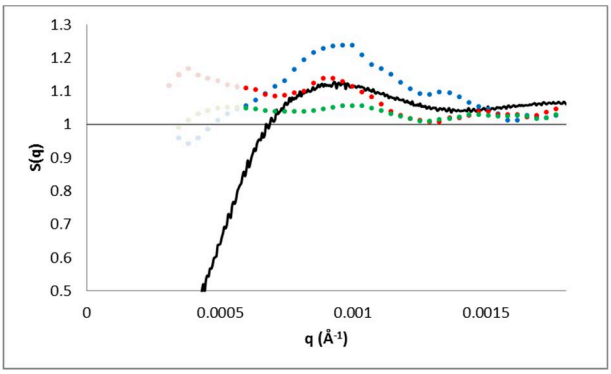

Figure 48 : la comparaison entre $S_{cal}(q)$ d'un empilement Apollonien simulé et $S_{exp}(q)$ des HIPEs liquides faites à 500rpm : échantillon frais (bleu), 1 semaine d'évolution (rouge), 1 mois d'évolution (vert). Les dix premiers points sont dans l'arrêt du faisceau et ils sont donc en gris.

On ne considère pas les dix premiers point de mesures à faible q qui se trouvent habituellement dans l'arrêt du faisceau de l'instrument. Encore une fois, on constate que $S_{exp}(q)$ a la même allure et il y a un excellent accord entre ces résultats expérimentaux et $S_{cal}(q)$ pour l'empilement Apollonien construit par la simulation numérique. $S_{max}(q)$ s'écrase avec l'évolution de l'échantillon, il est à 1,24 pour une HIPE fraîchement préparée, et 1,05 pour un échantillon qui a évolué pendant 1 mois. Comme on a remarqué précédemment, la polydispersité suscite l'écrasement du pic[119] donc c'est bien logique qu'une HIPE qui a évolué plus longtemps par la coalescence aura le pic le plus bas. Ainsi, ces comparaisons de $S(q)$ ont validé notre observation par la diffraction du laser – une HIPE liquide évoluée s'approche à l'empilement Apollonien après une semaine.

8.2.4.2 Augmentation de la surface totale avec le temps

On a également utilisé SAXS pour confirmer cette croissance en surface totale trouvée par des mesures de diffraction du laser. En examinant le spectre dilué, $P(q)$, des HIPEs liquides à différents stades d'évolution (les mêmes échantillons que dans le chapitre précédent « 8.2.4.1 L'évolution vers un empilement Apollonien après une semaine »), on trouve une gamme sur plus de 2 décades en valeurs de q qui suit une loi de puissance (Figure 49) en raison de l'autosimilarité des gouttes des échantillons.

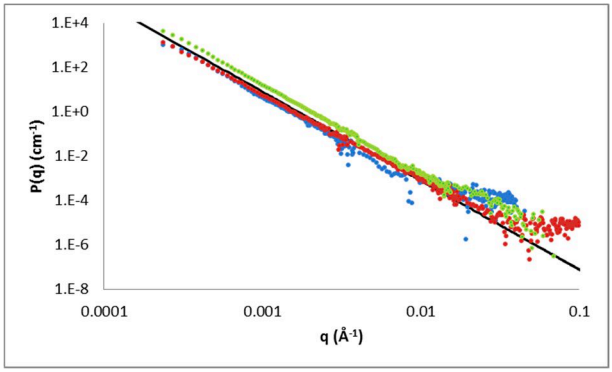

Figure 49 : les spectres dilués des HIPEs faites à 500rpm : fraîchement préparée (bleue), 1 semaine d'évolution (rouge), 1 mois d'évolution (vert). La ligne noire représente la loi de Porod (loi de puissance à l'exposante -4).

On a utilisé SASview pour faire la modélisation de la loi de puissance de q = 5 x 10^{-4} – 6 x 10^{-2} $Å^{-1}$, tout en négligeant les premiers points à faible q qui étaient dans l'arrêt du faisceau. Ces exposantes sont très proches de -4, ce qui correspond à la loi de Porod. Alors, dans ce régime, l'intensité diffusé par une particule est donnée par l'expression[121]:

$$I(q) \approx 2\pi(\Delta\rho)^2 A \cdot q^{-4}$$

avec $\Delta\rho$ la différence entre les SLDs de l'objet et du solvant, et A la surface totale interfaciale. Porod (1951)[122] et Debye et al. (1957)[123] ont indépendamment dérivé cette approximation et elle a été vérifiée expérimentalement. Donc, en regardant le coefficient de la loi de puissance, on peut déduire l'évolution temporelle de A (Tableau 7 et Figure 50).

Tableau 7: la modélisation par SASview de $P(q)$ pour des HIPEs à différentes stades d'évolution.

Âge of l'HIPE liquide	Exposante de la loi de puissance	Coefficient de la loi de puissance ≈ $2\pi(\Delta\rho)^2 A$
Fraîche	4,2609	1,29e-8
1 semaine	3,9935	5,76e-8
1 mois	4,0558	1,24e-7

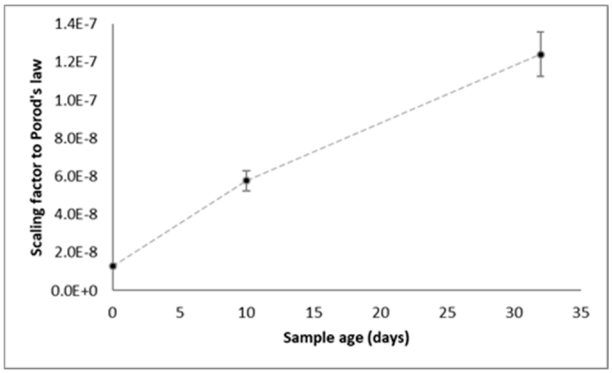

Figure 50 : le coefficient de la loi de Porod tracé en fonction de l'âge des HIPEs liquides. Le coefficient est directement proportionnel à la surface interfaciale dans l'échantillon. Cette tendance en croissance valide nos observations par la diffraction du laser.

On trouve que le coefficient augmente avec le temps d'évolution, ce qui signifie qu'une croissance en surface totale dans les HIPEs liquides au cours du temps. Cette tendance valide bien des observations par diffraction du laser (Figure 42). **L'accord entre les données SAXS et la diffraction du laser nous permet de confirmer que des petites gouttelettes sont créées au sein des HIPEs liquides lorsqu'elles évoluent par la coalescence.**

8.2.5 L'existence des micelles gonflées observée par SAXS

Quelles sont ces gouttelettes trop petites à résoudre par la diffraction du laser? Si elles existent, pourquoi sont-elles créées ? Pour répondre à ces questions, on a utilisé SAXS à nouveau pour étudier la région à haute q des HIPEs liquides à différents âges. La région à laquelle on s'est intéressé est q > 0,01Å^{-1}, ce qui correspond aux distances physiques inférieures à 100nm. Ayant conclu que les gouttes d'huile dans les HIPEs liquides sont organisés comme un empilement Apollonien, on les appelle désormais comme des HIPEs Apolloniennes.

À partir des spectres mesurés à ESRF, on a remarqué que $P(q)$ se présente toujours comme une loi de puissance, avec un épaulement visible à q = 0,03Å^{-1}. Cet épaulement est surtout évident dans l'émulsion Apollonienne vieillie d'un mois (Figure 51).

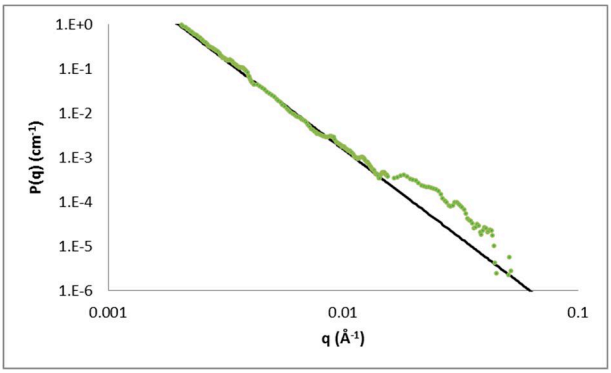

Figure 51 : la Figure 49 agrandie dans la région de diffusion q > 0,01Å^{-1}. Le spectre peut être décomposé en une loi de puissance (ligne noire) et un épaulement à q = 0,03Å^{-1}. Cette décomposition est aussi valable pour d'autres HIPEs Apolloniennes.

On est certain que cet épaulement n'est pas dû à l'excès de phase continue qu'on a utilisée pour diluer l'émulsion pour la mesure de $P(q)$: le signal d'une solution micellaire de C12E6 à 0,6% (w/w) a été déjà soustrait comme le fond. Comme on a également montré qu'il n'y a pas de films minces dans les HIPEs liquides (cf. chapitre « 8.1.5.2 Mesure de l'épaisseur du film mince de tensioactif par SAXS ») et comme l'épaulement n'apparaît que dans les spectres dilués où les gouttes d'HIPE sont suffisamment éloignées les unes des autres, cet excès de signal par rapport à la loi de puissance devrait être dû aux objets localisés dans les régions entre des gouttes d'une HIPE.

En prenant la SLD du solvant comme celle de l'eau, on a commencé par tester le modèle des sphères dures. On trouve que l'épaulement peut être décrit par des sphères de diamètre de 20nm si la SLD des sphères fait 8,8952 (valeur trouvée en ajustant le modèle aux données expérimentales). Cette valeur est très proche de la SLD de l'huile minérale qu'on a estimée dans le Tableau 5, soit 8,8. En partant de ces indications, on a alors modélisé l'épaulement par un modèle « core-shell » à plusieurs coquilles, car une gouttelette d'huile sera stabilisée par une couche de tensioactif.

Les paramètres et le profil SLD utilisés pour la modélisation de l'épaulement se trouve dans le Tableau 5 et dans la Figure 52.

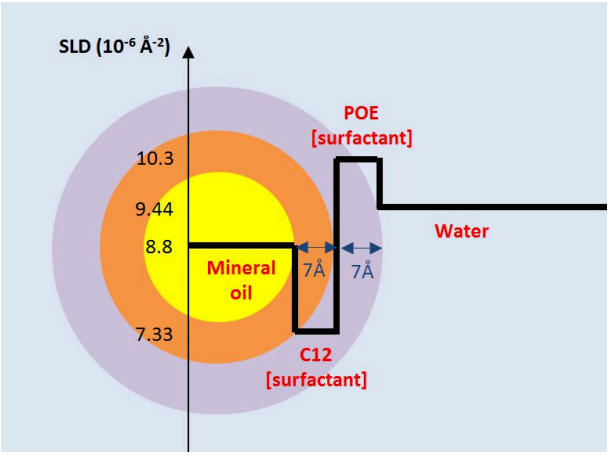

Figure 52 : le profil SLD de la structure « core-shell » à plusieurs coquilles utilisée pour modéliser l'épaulement.

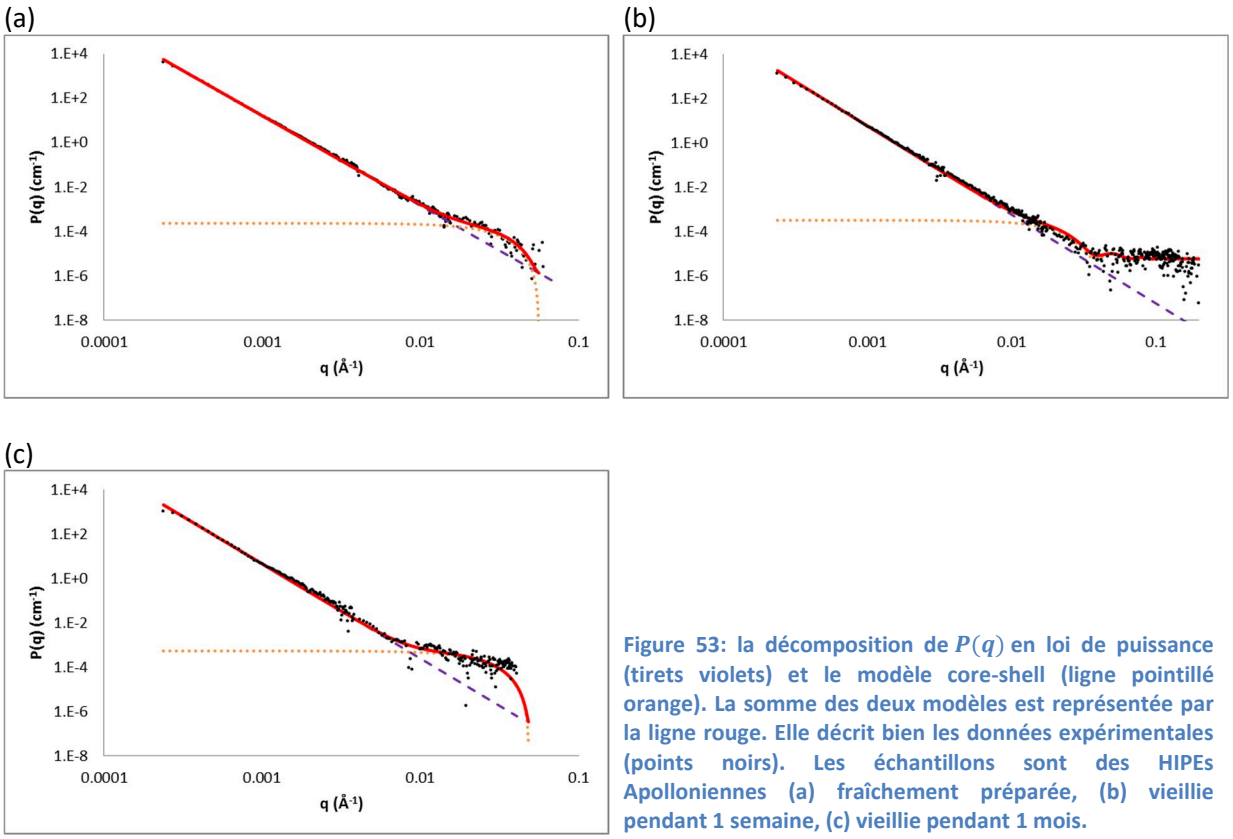

Figure 53: la décomposition de $P(q)$ en loi de puissance (tirets violets) et le modèle core-shell (ligne pointillé orange). La somme des deux modèles est représentée par la ligne rouge. Elle décrit bien les données expérimentales (points noirs). Les échantillons sont des HIPEs Apolloniennes (a) fraîchement préparée, (b) vieillie pendant 1 semaine, (c) vieillie pendant 1 mois.

Tableau 8: modélisation de P(q) des HIPEs Apolloniennes par une loi de puissance et un modèle core-shell. Les objets qui contribuent à l'épaulement ont des diamètres de 17 – 24nm.

Âge of l'HIPE Apollonienne	Exposante de la loi de puissance	Rayon du noyau (Å)	Épaisseur de la couche C12 (Å)	Épaisseur de la couche POE (Å)	Diamètre des objets (nm)	Fraction volumique des objets
Fraîche	4,2609	82,4	7	7	19,3	$4,1 \times 10^{-6}$
1 semaine	3,9935	105,9			24,0	$1,2 \times 10^{-6}$
1 mois	4,0558	70,6			16,9	$2,8 \times 10^{-6}$

Les spectres expérimentaux $P(q)$ sont très bien décrit par la somme de la loi de puissance et le modèle core-shell (les lignes rouges dans la Figure 53). Les exposantes de la loi de puissance sont les mêmes que dans le Tableau 7 et les diamètres des objets engendrant cet excès de signal sont de 19,3nm, 24,0nm et 16,9nm pour une HIPE Apollonienne fraîche, vieillie pendant 1 semaine et 1 mois respectivement (Tableau 8). La modélisation trouve une fraction volumique pour ces petits objets de 1 – 4 x 10^{-6}, mais sachant que $P(q)$ est mesuré à partir d'une HIPE diluée 40x, cela veut dire que dans HIPEs non diluées, ils ne sont présents qu'à une fraction volumique très faibles, soit ϕ = 4,8 x 10^{-5} – 1,6 x 10^{-4}. Cela explique pourquoi leur signal est masqué dans les spectres concentrés.

Des micelles C12E6 dans de l'eau pure existent sous forme sphérique aux températures inférieures à 25°C[124]. Leur spectre de diffusion aux neutrons ou aux rayons-X peuvent être modélisés par des structures core-shell de diamètre entre 5,8 – 6,7nm[125,126]. De même, la diffusion quasi-élastique de la lumière mesure un diamètre hydrodynamique de 7,4nm[81]. Si on compare ces valeurs aux diamètres trouvés dans nos échantillons (Tableau 8), on peut déduire que ces objets sont des micelles de C12E6 gonflées avec un peu d'huile minérale.

8.2.5.1 Deux populations de micelles gonflées

On a répété cette expérience devant le faisceau SWING au synchrotron SOLEIL. De même, on a trouvé une population de micelles gonflées de 17,5 – 26,3nm de diamètre qui ont donné un épaulement à q ≈ 0,005 – 0,03Å^{-1} (Figure 54, lignes pointillées en orange). On a nommé cette population α, puisque l'on a également trouvé une seconde population β de micelles gonflées plus petites, soit 6nm de diamètre, qui diffusent à q ≈ 0,03 – 0,2Å^{-1} (lignes pointillées en bleu dans la Figure 54b et Figure 54c). Les micelles β sont particulièrement visibles dans l'HIPE Apollonienne à 11 mois. Si on réexamine les spectres mesurés à ESRF, l'émulsion Apollonienne à 1 semaine (Figure 53b) semble présenter ce second épaulement β mais son intensité est trop proche du fond pour une interprétation significative.

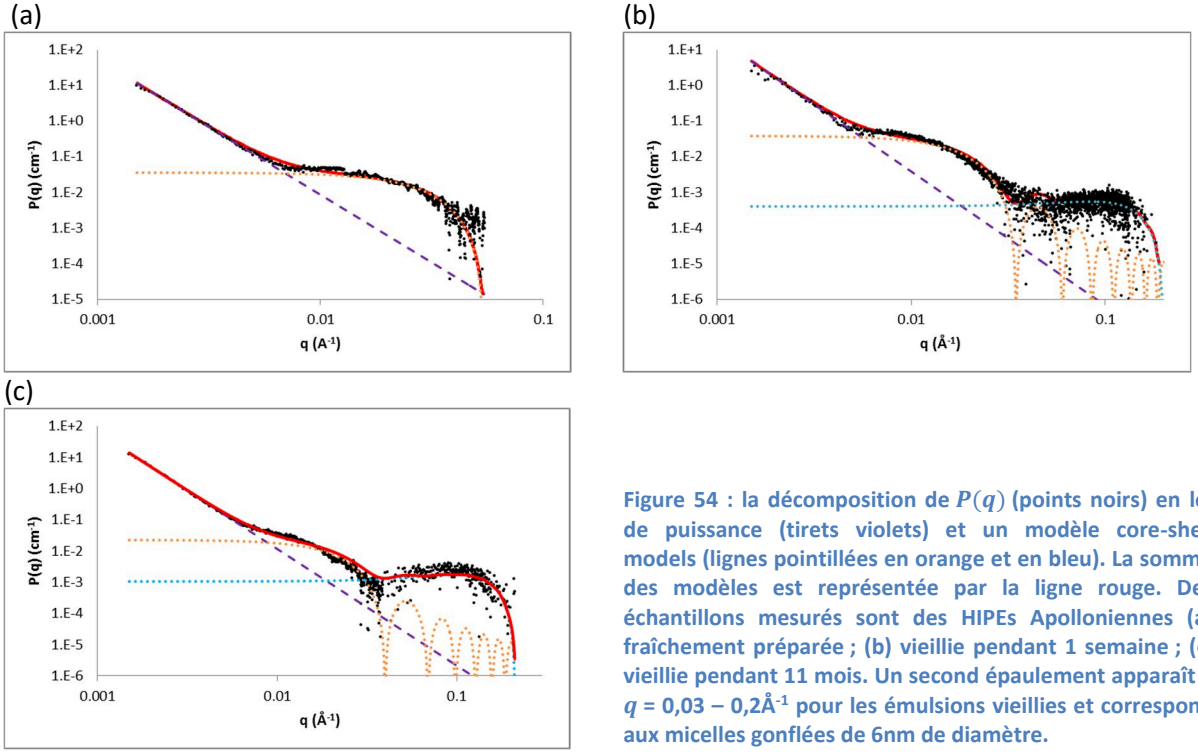

Figure 54 : la décomposition de $P(q)$ (points noirs) en loi de puissance (tirets violets) et un modèle core-shell models (lignes pointillées en orange et en bleu). La somme des modèles est représentée par la ligne rouge. Des échantillons mesurés sont des HIPEs Apolloniennes (a) fraîchement préparée ; (b) vieillie pendant 1 semaine ; (c) vieillie pendant 11 mois. Un second épaulement apparaît à q = 0,03 – 0,2Å^{-1} pour les émulsions vieillies et correspond aux micelles gonflées de 6nm de diamètre.

Tableau 9: la modélisation de $P(q)$ des émulsions Apolloniennes à différents stades d'évolution par une loi de puissance et des modèles core-shell. On en distingue deux populations de micelles gonflées dans les échantillons vieillis : la population α dont le diamètre fait 18 – 26 nm, et la population β dont le diamètre fait 5,7 – 6nm.

Âge of l'HIPE Apollonienne	Exposante de la loi de puissance	Rayon du noyau radius (Å)		Épaisseur de la couche C12 (Å)	Épaisseur de la couche POE (Å)	Diamètre des micelles gonflées (nm)		Fraction volumique des micelles gonflées (10^{-4})	
		α	β			α	β	α	β
Fraîche	3,7956	73,4	Absent	7	7	17,5	-	3,9	-
1 semaine	3,7486	117,7	15,8			26,3	6,0	1,1	1,4
11 mois	3,7372	101,3	14,5			23,1	5,7	0,95	22

En analysant la fraction volumique des micelles gonflées α et β, il semble que **les micelles β soient un produit du vieillissement de l'émulsion** (Tableau 9) : dans l'HIPE vieillie pendant 1 semaine, les deux types de micelles sont présentes à la même proportion. Cependant, dans l'HIPE vieillie pendant 11 mois, la quantité de micelles β devient 20 fois plus importante que la population α qui, quant à elle, n'a à peine varier. L'existence de deux populations implique que des gouttes, qu'elles soient grosses ou petites, n'ont toujours pas atteint l'équilibre même après 11 mois d'évolution.

On s'est pose la question si ces micelles gonflées peuvent être créées par la dilution des HIPEs Apolloniennes par un excès de phase continue lors de la mesure de $P(q)$. Si c'était le cas, alors la fraction volumique trouvée pour chaque population, α et β, aurait été la même pour tous les échantillons dans les Tableaux 8 et 9, car on les a dilués toujours de la même façon (même opératrice, même facteur de dilution, même durée d'attente entre la dilution et le passage devant le faisceau, soit < 30minutes).

On a ensuite vérifié l'identité de ces micelles gonflées β en les comparant à celles fabriquées par la méthode de l'inversion des phases par la température (PIT).

8.2.5.2 Fabrication des micelles gonflées par la PIT

On a fabriqué des microémulsions (des micelles gonflées à l'équilibre thermodynamique) selon la méthode décrite par Roger et al. (2010)[127]. Les détails se trouvent dans le chapitre « 4.2.5.2 Making swollen micelles by the PIT method ». On trouve que le diamètre des microémulsions ainsi faites est entre 7 – 10nm. Pour vérifier si ces gouttelettes sont effectivement des micelles gonflées avec un peu d'huile, on a comparé leur spectre de diffusion par SAXS à celui des micelles vides de C12E6 dans de l'eau pure. Les spectres bruts, sans soustraction ni dilution, se trouve dans la Figure 55.

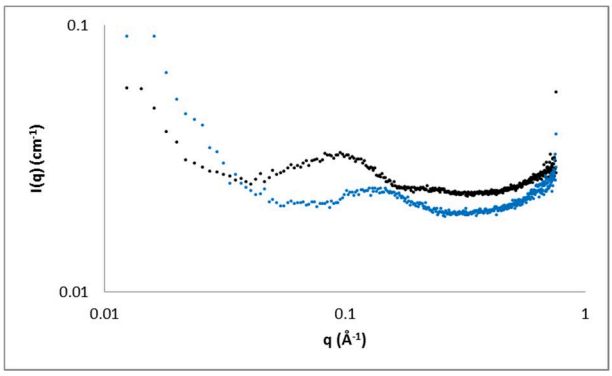

Figure 55 : le spectre brut des micelles gonflées (microémulsions) faites par la méthode PIT (en noir) et le spectre brut d'une solution de C12E6 pur dans l'eau dissout à 0,6% en masse (en bleu).

En effet, la microémulsion faite par la PIT donne un spectre différent d'une solution pure de tensioactif (des micelles vides). On note que **le spectre de la microémulsion est situé à q = 0,03 – 0,18Å^{-1}, la même gamme de q que les micelles gonflées β**, tandis que le spectre des micelles vides est situé aux valeurs de q encore plus grandes, soit 0,07 – 0,22Å^{-1}.

Par la suite, on a pris l'eau comme le fond à soustraire de la Figure 55. Le spectre résultant de la microémulsion (Figure 56, gauche) est modélisé par le même modèle core-shell et le même profil SLD montrés dans la Figure 52. Le rayon du noyau de la microémulsion est donné par la modélisation comme 14,5Å. En ajoutant les épaisseurs des couches C12 et POE, on retrouve **un diamètre des microémulsions qui vaut 5,7nm, la même taille que les micelles gonflées β** calculée dans le Tableau 9.

En revanche, le spectre des micelles vides peut être modélisé par un modèle core-shell où le cœur est simplement des chaînes hydrocarbonées C12, et la coquille est les groupements de POE (Figure 56, droite). On trouve alors un rayon du noyau qui vaut 18Å, la longueur étendue d'une chaîne hydrocarbonée du tensioactif. En fixant la fraction volumique à 0,006 (parce que la concentration de la solution micellaire était à 0,6%), on a pu ajuster le modèle pour déduire l'épaisseur de la coquille POE : on trouve 7,7Å. Ainsi, le diamètre total des micelles vides est de 5,1nm, un peu plus faible que 5,7nm rapporté par Penfold et al. (1997). C'est possible que la différence soit due au fait qu'ils travaillaient à une concentration plus élevée en tensioactif, à 5%C12E6, et ils ont également supposé que des micelles possédait une distribution de taille Schulz pour modéliser leur spectre obtenu par la diffusion aux neutrons.[125] En outre, Wijaya et al. (2016) ont rapporté 6,7nm comme le diamètre des micelles de C12E6, mais ils travaillaient à des températures plus élevées (25°C and 50°C)[126], alors que la température ambiante de nos expériences était 21 – 22°C.

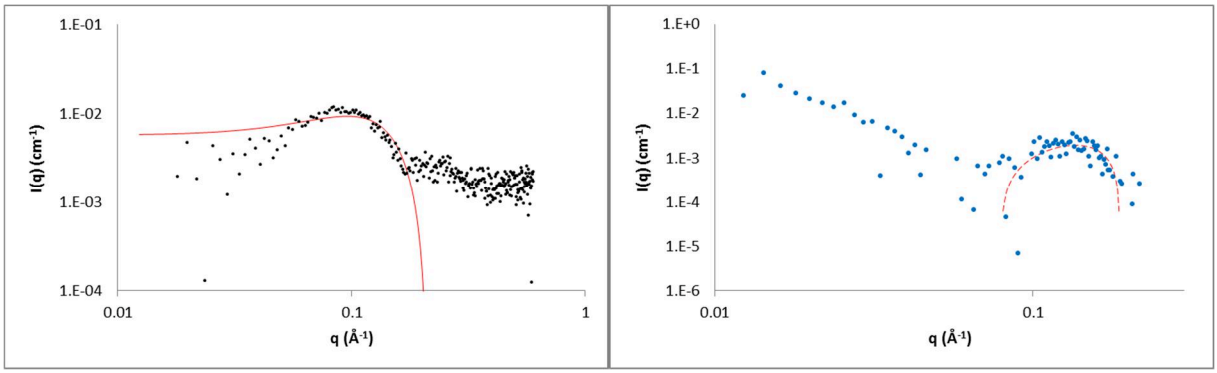

Figure 56 : la modélisation du spectre d'une microémulsion (gauche) et du spectre d'une solution de micelles pures (droite). Un modèle core-shell convient très bien dans les deux cas (lignes en rouge). En ajustant le modèle, on trouve 5,7nm pour le diamètre de la microémulsion et 5,1nm pour celui des micelles vides.

8.3 Discussions sur des HIPEs Apolloniennes

On a vu à travers de nos expériences que les HIPEs liquides peuvent subir la coalescence à cause de la faible disponibilité en tensioactif. On a aussi établi que leurs gouttes sont non déformées au repos et que leur distribution de tailles suit une loi de puissance, probablement en raison de la fragmentation à haute énergie à une fraction volumique très élevée. Ces HIPEs liquides évoluent de manière continue et l'empilement de leurs gouttes devient un empilement Apollonien après une semaine. En même temps, cette évolution s'accompagne de la création des micelles gonflées et des petites gouttelettes d'émulsion, ce qui suscite à une croissance en surface interfaciale totale. Une fois Apollonienne, une émulsion est exceptionnellement métastable : elle reste émulsifiée au cours d'un an et garde sa structure Apollonienne, malgré l'évolution qui se poursuit. Les discussions suivantes cherchent à répondre de manière qualitative aux questions qu'on se pose à partir de nos observations expérimentales. On inclut également quelques résultats expérimentaux supplémentaires s'ils sont disponible pour soutenir nos points d'arguments.

Dans ce chapitre, on va montrer que le mécanisme de coalescence dans une structure aussi bondée qu'une HIPE liquide à ϕ = 0,95 est très différente de la coalescence typique dans les émulsions diluées. Pour celles-ci, la coalescence crée les gouttes de plus en plus grosses pour diminuer la surface totale, ce qui entraîne à l'expulsion de tensioactif en excès. Ces tensioactifs peuvent disparaître dans le volume important de phase continue. Toutefois, dans une HIPE liquide, ces tensioactifs expulsés n'ont pas cette facilité. On pense que la conséquence de cette limitation conduit à un mécanisme d'évolution radicalement différent, où des petites gouttelettes d'émulsion sont créées en même temps que des grosses. On a nommé ce mécanisme la « coalescence-fragmentation ». La conséquence de la coalescence-fragmentation est alors une structure Apollonienne.

Dans le chapitre « 8.3.1.1 Comment sont-elles créées lors de la coalescence? » on examinera un mécanisme géométrique de la coalescence-fragmentation par laquelle ces gouttelettes sont créées, et dans le chapitre « 8.3.1.2 Pourquoi sont-elles créées lors de la coalescence? », on étudiera sa compatibilité avec la thermodynamique, malgré le fait que des idées traditionnelles de la coalesce impose une diminution de surface totale pour réduire l'énergie de surface. Le chapitre « 8.3.2 D'où vient la métastabilité d'une HIPE Apollonienne? » est consacré à la discussion de la métastabilité inattendue des HIPEs Apolloniennes, malgré la coalescence continue en présence de si peu de tensioactif. Puis dans le chapitre « 8.3.2.1 Mesure de la vitesse de coalescence », on mesure et on compare la vitesse de coalescence des émulsions Apolloniennes à d'autres émulsions polydisperses à plus faible fraction volumique ; on montre que la métastabilité ne vient pas d'une vitesse plus lente de la coalescence, mais c'est plutôt grâce à leur mécanisme évolutif particulier (chapitre « 8.3.2.2 La conséquence de la coalescence-fragmentation ». Finalement, on appliquera des arguments thermodynamiques pour interpréter la persistance d'une structure Apollonienne dans une HIPE comme un minimum local en énergie libre.

8.3.1 La création des petites gouttelettes dans une HIPE

8.3.1.1 Comment sont-elles créées lors de la coalescence?

On considère la coalescence de deux gouttes aléatoires, de rayon a_1 et a_2. Le volume total est nécessairement conservé comme la quantité de matière ne change pas dans le système. Alors, on peut avoir les situations suivantes :

- Deux gouttes donnent une seule grosse goutte : la coalescence typique.

Le rayon de la goutte fille, a, sera $({a_1}^3 + {a_2}^3)^{1/3}$. Cela est le cas de coalescence typiquement rencontrée. Si la coalescence est hiérarchique de telle sorte que $a_1 \approx a_2$ à chaque stade, alors l'évolution peut être décrite par le modèle de Smoluchowski (cf. « 3.2.4.3 Smoluchowski coalescence algorithm »). Cependant, la distribution des tailles obtenue à la fin ne sera pas une loi de puissance puisque l'on obtiendra rapidement une goutte énorme macroscopique.

- Deux gouttes donnent deux

Ce processus correspond au réarrangement dans l'espace des gouttes.

- Deux gouttes donnent plusieurs gouttelettes filles : la coalescence-fragmentation.

On a vérifié par la simulation numérique (faite par Robert Botet) que cette situation engendre en effet des distributions de tailles en loi de puissance. Ainsi, pour obtenir une population extrêmement polydisperse, **un événement de coalescence doit se produire en même temps que la fragmentation** (puisque le nombre de gouttes à la fin est plus important que le nombre initial). Or, on a trouvé que l'exposante de la loi de puissance dépend du nombre de gouttelettes filles créées à chaque reprise. Mettons la condition la plus stricte : on suppose que chaque événement de coalescence produit 3 gouttelettes filles sans chevauchement. L'exposante trouvée est toujours inférieur à 2, beaucoup trop faible par rapport au 3,47 pour un empilement Apollonien (car l'exposante = $d_f + 1$). La Figure 57 montre les résultats d'une telle simulation, où on a commencé par deux gouttes de la même taille et elle s'est terminé par 10^8 gouttelettes par des coalescences successives.

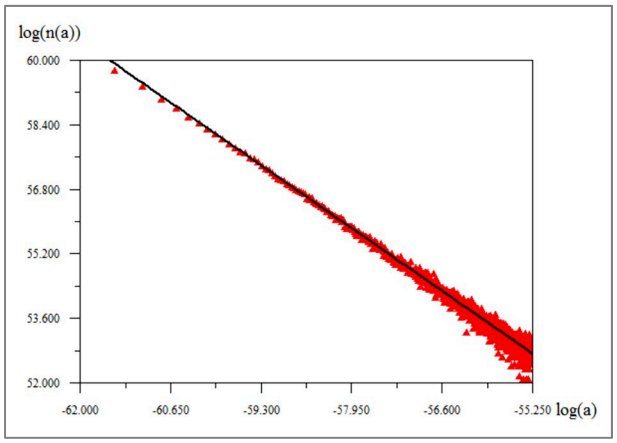

Figure 57 : la simulation numérique de la coalescence entre 2 gouttes pour donner 3 gouttelettes filles à chaque reprise. On retrouve une distribution de tailles en loi de puissance, mais son exposante est beaucoup trop faible, soit environ 1,2.

Si on détend la condition sur le nombre de filles créées, l'exposante devient plus grande et on *peut* obtenir la bonne distribution de tailles. Cependant, ces simulations ne prennent pas en compte l'organisation spatiale de tous les gouttelettes engendrées : on a observé dans le chapitre « 8.1.4 La distribution de tailles dans chaque type de HIPE » (Figure 33, Tableau 2) que l'on peut avoir la bonne exposante si on laisse avoir lieu des déformations entre des gouttelettes (comme dans une HIPE hybride). Donc, les conditions qui mènent à une bonne distribution de tailles ne sont pas suffisante ; on doit considérer également des conditions qui mènent à une géométrie sphérique sans déformation.

Dans une HIPE liquide, des gouttes sphériques n'ont qu'un seul point de contact les unes avec les autres. Par conséquent, on a employé une simulation plus généralisée où deux gouttes qui coalescent peuvent donner un nombre quelconque de filles sans chevauchement, tout en respectant la conservation du volume et des contraintes de tangence. On a nommé ce processus « l'algorithme des Lapins » puisque les lapins sont renommés pour leur prouesse de prolifération. Pratiquement, cela veut dire que des gouttelettes filles sont créées de telle sorte qu'elles occupent le maximum de volume possible dans le vide laissé par les parents, mais qu'elles peuvent également occuper d'autres vides voisins, tant qu'elle ne se chevauchent pas avec d'autres gouttelettes qui délimitent ces vides. Le remplissage au maximum d'un vide est justifié par la nature liquide des gouttes qu'on cherche à simuler. Le remplissage des vides voisins est permis par l'écoulement capillaire. La simulation se fait suivant les étapes ci-dessous (Figure 58):

1. 60 sphères de tailles identiques sont aléatoires places dans un volume unitaire. On autorise des chevauchements à ce stade afin d'identifier des paires de sphères qui subiront la coalescence. (Figure 58a)

2. Une paire de sphères est choisie au hasard. On calcule leur volume total v_{12} et leur centre de masse x_{12}. On enlève cette paire de sphères, ce qui reste un vide principal plus ou moins centré sur x_{12}.

3. On considère des vides autour de x_{12}, y compris le vide principal, de telle sorte que le volume total des vides fasse $2v_{12}$. Cette condition restreint le système pour qu'ils n'examinent que des vides aux alentours de l'événement de coalescence qui aura lieu.

4. Les vides ainsi trouvés sont remplis systématiquement, du plus gros au plus petit. Une sphère fille qui respecte des contraintes de tangence est créée pour occuper chaque vide. Le processus s'arrête lorsque le volume total de sphères filles créées atteigne v_{12} (Figure 58b).

5. On répète les étapes 2 – 4 (Figure 58c–e) jusqu'à ce qu'il ne reste plus de sphères chevauchantes dans le système (Figure 58f).

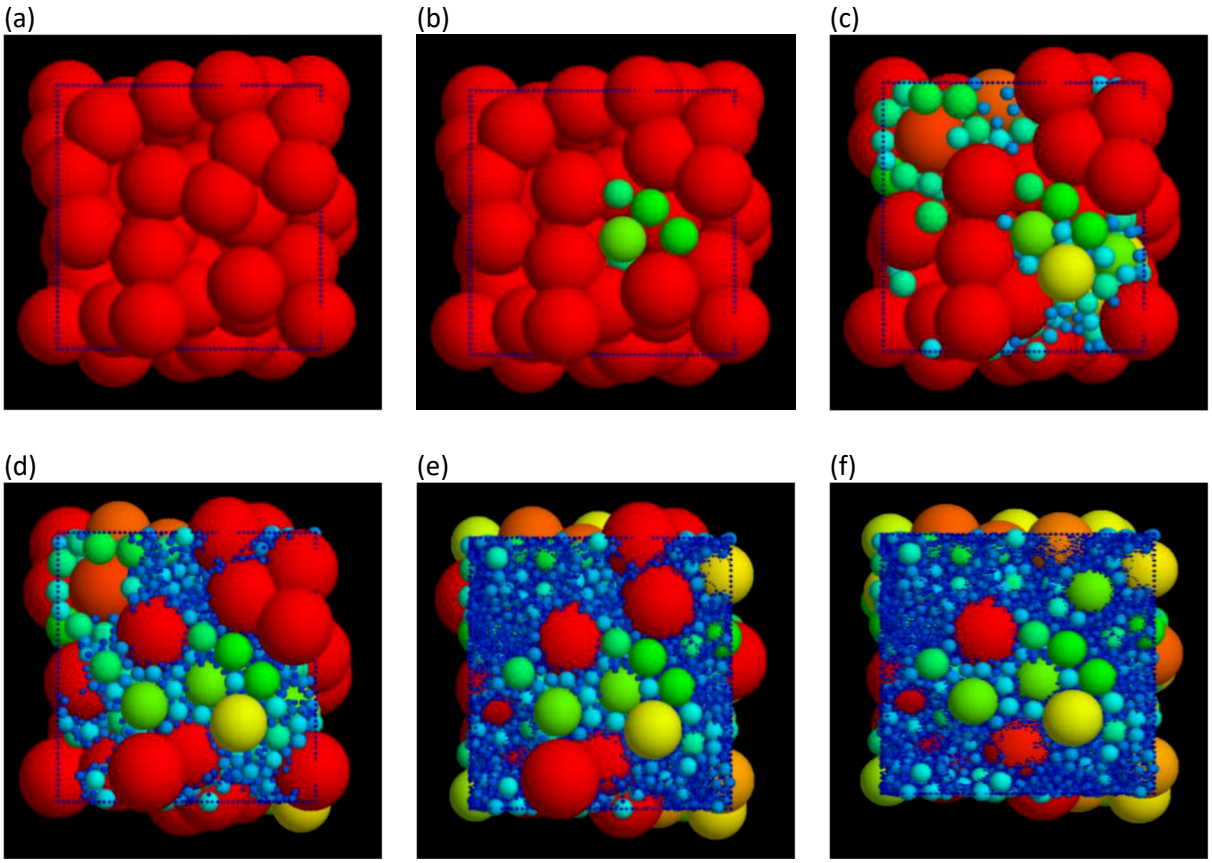

Figure 58 : la simulation numérique par l'algorithme des Lapins. (a) On créé des paires de sphères qui se chevauchent. Puis on les remplace par des sphères « filles » qui occuperont le vide principal et des vides aux alentours. (b) montre la première itération. Toutes les 4èmes itérations sont montrées par la suite (c) – (e). L'état final du système (f) à la fin de l'algorithme des lapins est atteint lorsqu'il n'y a plus de sphères chevauchantes qui restent. Les sphères sont colorées pour montrer leur taille différente, bleu étant les plus petites et rouge étant plus grandes.

La première itération de l'algorithme a produit 13 gouttelettes filles (Figure 58b). Chaque itération par la suite a produit entre 22 et 8210 gouttelettes filles. Il fallait 32 itérations de l'algorithme des Lapins pour éliminer tous les chevauchements dans le système (Figure 58f). On a remarqué que lors d'une itération vers la fin, il y a eu un évènement de coalescence qui n'a engendré que 2 goutte filles non chevauchantes (Figure 59). On a vérifié que cela correspondait effectivement à un réarrangement dans l'espace des parents, où une goutte a légèrement grossi en volume au dépense de l'autre pour mieux occuper les vides selon les contraintes de tangence.

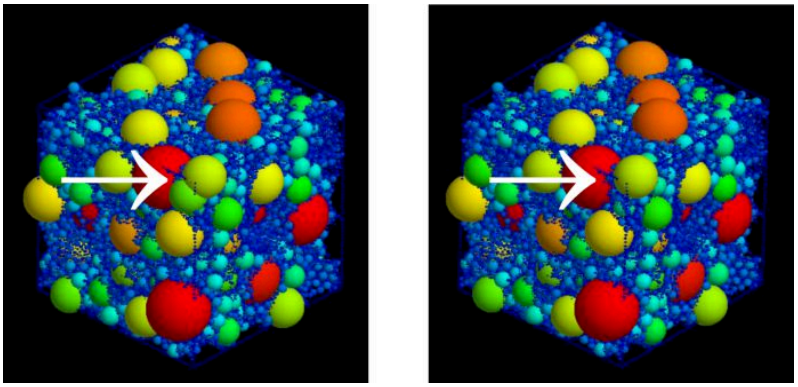

Figure 59 : (gauche) des gouttes chevauchantes identifiées par la flèche blanche. Le résultat de cette itération par l'algorithme des Lapins a donné deux gouttes filles sans chevauchement (droite). C'est effectivement un réarrangement local des parents pour mieux occuper des vides.

Un lecteur attentif remarquera que la maximisation des rayons des sphères dans les vides est bien consistante avec la définition d'une construction Apollonienne locale, selon Mandelbrot (1983)[58]. Ainsi, il paraît que **l'algorithme des Lapins crée des structures Apolloniennes localement, et l'ensemble de ces structures est un empilement Apollonien global.** On a vérifié que c'est bien le cas en examinant la distribution de tailles à l'issu de la simulation des Lapins et on a trouvé qu'il s'agit d'une loi de puissance dont l'exposante est très proche d'un empilement Apollonien (Figure 60). Le $S(q)$ calculé à partir d'une simulation des Lapins à ϕ = 0,85 a également produit le même $S_{cal}(q)$ qu'un empilement Apollonien simulé à ϕ = 0,92 (Figure 61). Les deux facteurs de structure présentent un pic S_{max} très écrasé, ce qui veut dire qu'il n'y a aucun ordre positionnel dans le système. Autrement dit, la probabilité de trouver une gros ou un petit voisin est indépendante de la taille de la goutte considérée.

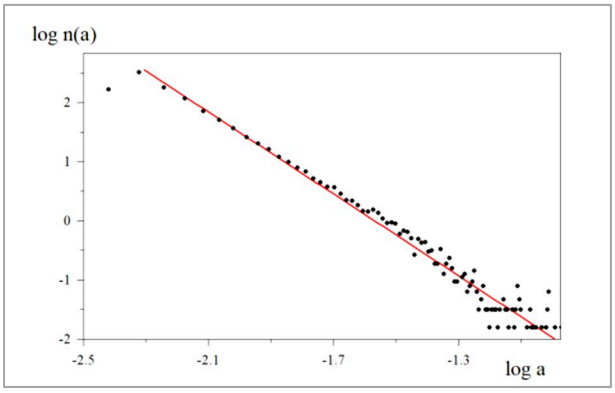

Figure 60 : la distribution de tailles à partir d'une simulation numérique de l'algorithme des Lapins. La ligne rouge représente une loi de puissance dont l'exposante fait -.3,47, ce qui correspond à la d_f = 2.47 d'un empilement Apollonien.

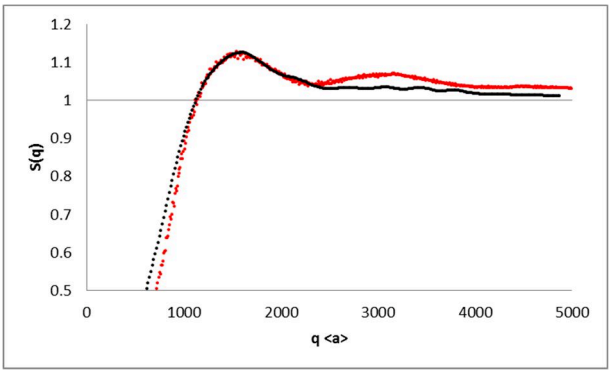

Figure 61 : $S_{cal}(q)$ pour une simulation numérique de l'algorithme des Lapins à ϕ = 0,85 (noir). Il a les mêmes caractéristiques $S_{cal}(q)$ pour une simulation numérique d'un empilement Apollonien à ϕ = 0,92 (rouge).

Puisqu'il semble que l'algorithme des Lapins soit une autre façon d'obtenir un empilement Apollonien, on a comparé son facteur de structure calculé aux facteurs de structures mesurés pour nos HIPEs Apolloniennes. On a trouvé un bon accord entre eux (Figure 62). En examinant la variation de surface spécifique par l'algorithme des Lapins, on a trouvé qu'elle croît avec le temps (Figure 63), ce qui valide nos observations expérimentales par la diffraction du laser et par SAXS. En conséquence, notre déduction que beaucoup de petites gouttelettes sont créées lors de l'évolution des émulsions apolloniennes est aussi validée.

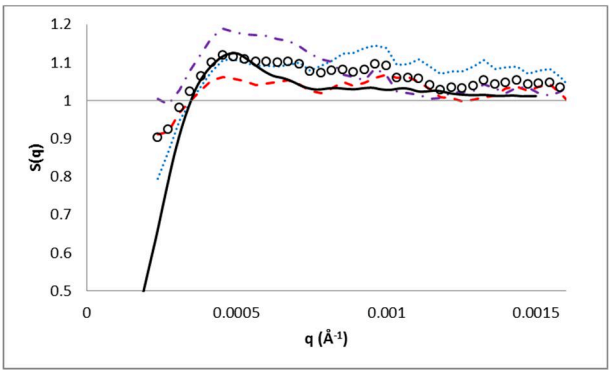

Figure 62 : la comparaison entre $S_{cal}(q)$ de l'algorithme des Lapins (ligne noire) et $S_{exp}(q)$ des HIPEs Apolloniennes à ϕ = 0,95 vieilles pendant 1 mois, fabriquées à 250rpm (points bleus), 500rpm (tirets rouges) et 1000rpm (points-tirets violets). Les cercles sont des valeurs moyennées sur les trois échantillons.

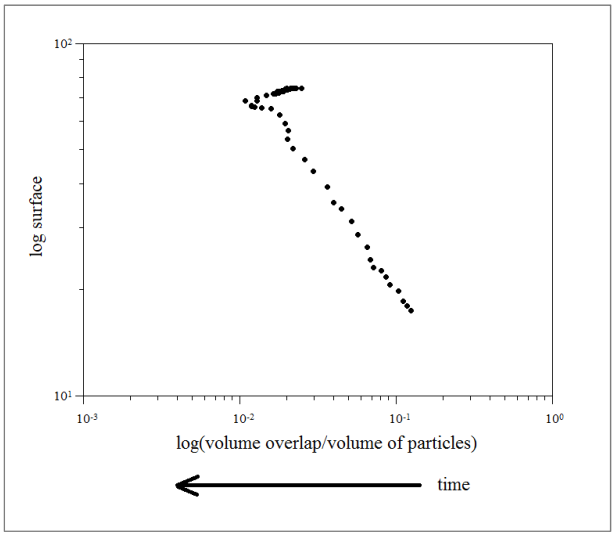

Figure 63 : la variation de surface totale en fonction de la proportion de chevauchement restant dans le système. La quantité de chevauchement diminue lorsque la simulation des Lapins s'avance, donc le temps va de droite à gauche sur cette figure. Il y a donc une augmentation nette de surface totale avec le temps.

On peut donc déduire qu'**une HIPE liquide évolue selon un mécanisme de coalescence-fragmentation comme celui décrit par l'algorithme des Lapins : beaucoup de petites goutteles sont engendrées à chaque évènement de coalescence** entre des gouttes afin de remplir des vides de façon optimale. La somme de toutes ces constructions Apolloniennes locales donne alors un empilement Apollonien global et donc une émulsion Apollonienne.

8.3.1.2 Pourquoi sont-elles créées lors de la coalescence?

L'algorithme des Lapins est un mécanisme purement géométrique qui élimine des chevauchements dans le système et qui crée des petites gouttelettes. Il n'y a donc aucune considération énergétique. Il faut donc qu'on examine si la création des gouttelettes peut avoir lieu, et pourquoi elle aura lieu. Des calculs sont donnés dans le chapitre « 4.3.1.2 Why are smaller droplets created during coalescence in a liquid HIPE? » et on résumera ci-dessous des résultats principaux.

Des tensioactifs expulses ne peuvent pas être accommodés par la phase continue

On considère ce qui se passe tout de suite après une coalescence entre deux gouttes. On suppose que les surfaces des gouttes sont saturées par des molécules de tensioactif. Dans une émulsion typique, si une seule goutte « fille » est créée, alors le rayon de la fille sera plus petit (car volume est conservé), ce qui entraîne une perte de surface interfaciale. Cela suscite l'expulsion des molécules de tensioactifs.

Normalement, dans une émulsion à faible ϕ, il y a beaucoup de phase continue. Ces molécules de tensioactif peuvent disparaitre dans le réservoir de phase continue sans provoquer une variation conséquente de la concentration en tensioactif. Cependant, dans une HIPE liquide à ϕ = 0,95, si on suppose une répartition homogène de phase continue autour de chaque goutte d'huile, la solubilisation de tensioactif expulsé dans ce petit volume de phase continue entraînera une augmentation importante en potentiel chimique au voisinage de la coalescence (Figure 64). Donc, **dans une HIPE à ϕ = 0,95, contrairement aux émulsions typiques, des tensioactifs expulsés lors de la coalescence ne peuvent pas être accommodés par la phase continue.**

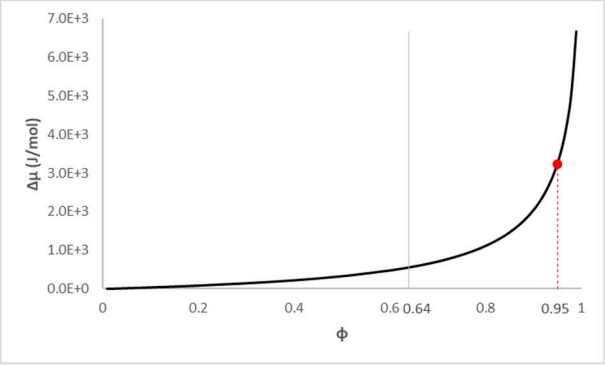

Figure 64 : la variation du potentiel chimique, $\Delta\mu$, en fonction de la fraction volumique de l'émulsion, si toutes les molécules de tensioactif sont solubilisées dans la phase continue aux alentours suite à un événement de coalescence. Cette variation est une fonction exponentielle dans le domaine des HIPEs (ϕ > 0,64). Le point rouge représente une HIPE Apollonienne à ϕ = 0,95.

Les tensioactifs expulsés sont confinés localement

Jusqu'à présent, on a supposé que les tensioactifs expulsés sont confinés à un tout petit volume de phase continue aux alentours des gouttes d'huile en coalescence. Cette considération cinétique est correcte mais que sur une échelle de temps très courte tout de suite après la coalescence. Est-il possible que les tensioactifs diffusent ailleurs sans conséquence ?

Mettons à côté l'augmentation en potentiel chimique, on suppose que les tensioactifs expulsés peuvent former des micelles vides. On a trouvé que le diamètre de ces micelles vaut 5,1nm par SAXS (Figure 56). On peut calculer le coefficient de diffusion par l'équation de Stokes-Einstein : D = 8,5 x 10^{-11} m^2/s.

Par ailleurs, Guinier et Fournet (1955) ont montré que dans la diffusion des rayons-X, au-delà d'une $q_0 = 2\pi/x_0$ où x_0 correspond aux dimensions moyennes dans l'échantillon irradié, l'intensité diffusée deviennent négligeable.[128] À partir de nos mesures de $P(q)$ (Figure 53 et Figure 54), la loi de puissance se termine vers q = 0,005$Å^{-1}$, ce qui correspond à une distance physique de $x = 126nm$. On peut alors faire l'approximation que ceci est une longueur caractéristique dans nos HIPEs.

Comme la longueur caractéristique de la diffusion s'écrit :

$$x = 2\sqrt{Dt}$$

Une micelle vide n'aura que 50µs pour diffuser avant qu'elle rencontrera d'autres gouttes d'huile et leur phase continue associée. Notre considération cinétique est donc valable car des tensioactifs ne peuvent pas former des micelles vides qui peuvent librement circuler dans une structure aussi dense qu'une HIPE Apollonienne sans provoquer une augmentation en potentiel chimique assez conséquente.

Où peuvent-ils aller, ces tensioactifs rejetés? Notre hypothèse, en lien avec nos observations expérimentales, est que **ces molécules de tensioactifs expulsées sont absorbées par la création des petites gouttelettes**, soit aux interfaces des gouttelettes filles au voisinage (comme le démontre l'algorithme des Lapins), soit des micelles gonflées (comme trouvées par SAXS). On montre par la suite que la création de ces petites gouttelettes est énergétique réaliste.

L'énergie libre est réduite en créant des petites gouttelettes qu'en gardant des films minces

Soit G, l'énergie libre de Gibbs pour la monocouche de tensioactif autour d'une petite gouttelette. G est la somme de W, l'énergie de flexion élastique du film de gouttelettes, et de F, l'énergie de surface.

Safran (1991) a montré que W est minimum à la courbure spontanée $H_0 = 1/R_0$. Pour les microémulsions sphériques qui sont des objets à courbure spontanée, $W = 0$.[130] On a trouvé par SAXS que des micelles gonflées β sont effectivement des microémulsions sphériques, donc **la création des micelles gonflées β est très favorable comme elle ne suscite pas une augmentation en énergie libre de Gibbs.**

Voyons ce qui se passe pour des micelles gonflées α et des petites gouttelettes filles de l'HIPE créées par le mécanisme de coalescence-fragmentation. Clairement, ces objets ne sont pas à courbure spontanée.

Si on suppose que ces objets n'existent pas, des gouttes en coalescence devront alors garder des films minces entre elles (des chevauchements dans l'algorithme des Lapins). On calcule l'énergie libre de Gibbs pour un film et pour une petite gouttelette de rayon R (cf. chapitre « 4.3.1.2 – Free energy is reduced by creating small droplets rather than maintaining flat films »). On trouve que pour toutes valeurs de $R > R_0$ (c'est-à-dire toutes les gouttelettes plus larges que des micelles gonflées β), $G_{film} > G_{droplet}$.

On peut donc conclure que **la création des micelles gonflées α et/ou des petites gouttelettes de HIPEs diminuera de manière favorable l'énergie libre de Gibbs,** car les films minces stockent plus d'énergie.

8.3.1.3 Résumé du mécanisme de la coalescence-fragmentation

Lorsque la coalescence se produit dans une émulsion, le système cherche à diminuer son énergie libre en éliminant des films minces liés à la déformation des gouttes et en créant des gouttes sphériques. Dans une émulsion typique à faible fraction volumique, deux gouttes en coalescence engendre une goutte « fille ». La perte de surface interfaciale mène à l'expulsion des molécules de tensioactif dans la phase continue sans conséquences majeures.

Cependant, dans une HIPE où le volume de phase continue est très limitée, les tensioactifs rejetés ne peuvent pas être accommodés par leur environ immédiat sans provoquer une augmentation importante du potentiel chimique ; ils ne peuvent non plus diffuser très loin dans une structure aussi bondée sans rencontrer le même problème. En conséquence, ils sont confinés localement, ce qui entraîne un excès temporaire de tensioactif au voisinage d'un événement de coalescence. Dans ce cas-là, deux gouttes en coalescence peuvent créer de nombreuses gouttelettes « filles » dont l'interface peuvent loger ces tensioactifs en plus. Ce processus est la coalescence-fragmentation. La création des gouttelettes sont gérées par trois conditions :

1. Le nombre et la taille des gouttelettes créées doivent respecter la conservation de volume.
2. Les gouttelettes créées cherchent à occuper le plus de volume possible, en raison de leur nature liquide.
3. Les gouttelettes créées doivent respecter les contraintes de tangence par rapport à leurs voisines puisqu'il est coûteux en terme d'énergie libre à créer des films minces.

Ces trois conditions de la coalescence-fragmentation dans une HIPE garantissent alors la construction locale selon des principes Apolloniens, ce qui donnent globalement une émulsion Apollonienne.

8.3.2 D'où vient la métastabilité d'une HIPE Apollonienne ?

On a observé visuellement que les HIPEs Apolloniennes restent émulsifiées jusqu'à un an malgré la faible quantité de tensioactif qui leur est disponible. Cela contredit des attentes usuelles de la stabilité d'une émulsion qui a autant de gouttes en contact qui sont mal protégées.

8.3.2.1 Mesure de la vitesse de coalescence

On aurait pu croire que la métastabilité exceptionnelle des HIPEs Apolloniennes viennent d'une cinétique de coalescence plus lente liée au confinement local des molécules de tensioactif. Pour tester cette hypothèse, on a mesuré la vitesse de coalescence dans des émulsions à plus faible ϕ préparée de la même manière que les HIPEs Apolloniennes, c'est-à-dire à la même concentration en tensioactif – soit 0,6%C12E6 en masse – dans la phase continue. Or, puisque ces émulsions sont très polydisperses et leur distribution de tailles initiales dépendent des conditions propres à l'émulsification, il fallait comparer leur vitesse de coalescence à un modèle plutôt que les comparer directement l'une à l'autre. Pour ce faire, on a utilisé la simulation numérique (développée par Robert Botet) pour prédire la vitesse de coalescence de ces émulsions polydipserses par le modèle de Smoluchowski. Dans le modèle, on a supposé que des gouttes sont sujettes au mouvement Brownien et chaque simulation prend en compte la distribution de tailles initiale mesurée expérimentalement pour l'échantillon. Les détails de l'algorithme se trouvent dans le chapitre « 3.2.4.3 Smoluchowski coalescence algorithm ».

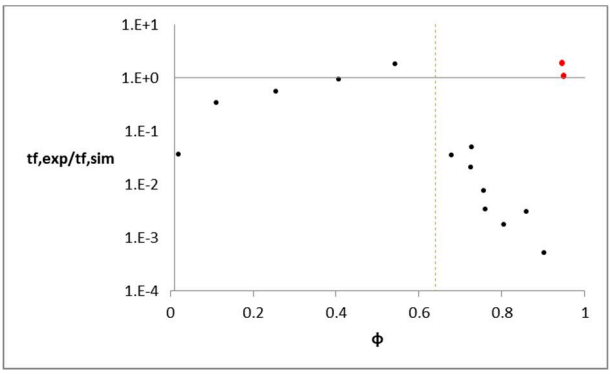

Figure 65 : des vitesses de coalescence mesurées expérimentalement pour des émulsions polydisperses à différentes valeurs de ϕ. On les a comparés à la vitesse prédite par le modèle de Smoluchowski au noyau Brownien. Cette comparaison s'exprime comme $t_{f,exp}/t_{f,sim}$ sur l'axe vertical. Les points rouges représentent des HIPEs Apolloniennes à ϕ = 0,95. Une ligne pointillée a été tracée à ϕ = 0,64 pour démarquer la limite de compacité d'un empilement aléatoire des sphères.

La comparaison des vitesses de coalescence expérimentalement mesurées aux vitesses prédites par le modèle de Smoluchowski s'exprime comme $t_{f,exp}/t_{f,sim}$. Ces valeurs pour des émulsions à ϕ = 0,0208 – 0,9491 se trouvent dans la Figure 65. Puisque ces émulsions sont très polydisperses, leur empilement sera aléatoire : pour cette raison, on a démarqué la limite de compacité maximale à ϕ = 0,64[27] plutôt qu'à 0,74 (l'empilement compact des sphères monodisperses), afin de définir la fraction volumique à partir de laquelle une émulsion sera considérée comme une HIPE. Or, comme on n'a pas pu mesurer leur facteur de structure, on ne peut pas dire de manière définitive si ces HIPEs s'organisent comme un empilement Apollonien ou non. Les seules HIPEs dont on est certain de l'empilement Apollonien sont celles à ϕ = 0,95, représentées par des points rouges sur la figure.

Pour l'émulsion la plus diluée dont ϕ = 0,0208, la vitesse de coalescence expérimentale est trente fois plus lente que la prédiction par le modèle Smoluchowski. Cela est tout à fait attendu : on a mesuré la surface totale des gouttes dans cette émulsion – 3,3 x 10^{-12} m^2 – et on a trouvé que la quantité de tensioactif mise dans la phase continue est suffisante pour couvrir une surface qui vaut 8,4 x 10^{-10} m^2. On peut donc supposer que toutes les gouttes sont saturées à l'interface par des molécules de tensioactif, ce qui donne une excellente protection contre la coalescence. De plus, la faible fraction volumique de l'émulsion assure que les gouttes d'huile se rencontrent peu fréquemment. Dans le domaine des émulsions « diluées », jusqu'à ϕ = 0,5432, on constate une croissance de la vitesse de coalescence expérimentale avec ϕ, même s'il y a toujours suffisamment de tensioactif pour saturer les interfaces des gouttes. On explique cette tendance par le fait qu'une fraction volumique plus élevée veut dire que des gouttes se rencontrent plus fréquemment dans la structure pour pouvoir coalescer.

Une fois dans le domaine des émulsions concentrées (ϕ > 0,64), la tendance croissante s'inverse. On a calculé le taux de couverture à l'interface par les molécules de tensioactif et on a trouvé qu'il y a toujours une quantité suffisante pour saturer les interfaces, même à ϕ = 0,9028. Pourtant, malgré des rencontres des gouttes plus fréquentes lorsque ϕ augmente, le modèle de Smoluchowski commence à surestimer la vitesse de coalescence de 30 – 2000 fois. Finalement, on remarque une hausse importante de **la vitesse de coalescence pour les HIPEs Apolloniennes qui rejoint la vitesse prédite par le modèle de champ moyen de Smoluchowski.** Cette fois-ci, pour ces émulsions Apolloniennes à ϕ = 0,9454 and ϕ = 0,9491, on a trouvé qu'il y a un défaut de tensioactif dans le système, le taux de couverture étant inférieur à 100%.

On a trouvé qu'il est possible d'expliquer ces tendances par les effet de la viscosité effective, $\eta^*(\varphi)$, des émulsions. On peut la comprendre en interprétant que le système paraît d'autant plus visqueuse s'il y a plus de gouttes d'huile lorsque ϕ augmente et donc il y aura moins de volume libre pour la circulation des gouttes. En 1906, Einstein a donné l'expression de η^* pour une dispersion très diluée des sphères monodisperses dans un milieu de viscosité η_0 [132,133]:

$$\eta^* = \eta_0(1 + 2.5\varphi)$$

En général, cette expression n'est valable que pour des valeurs de ϕ < 0.05.[134] À une fraction volumique plus importante, l'expression devient une fonction polynomiale de ϕ puisqu'il faut prendre en compte des interactions entre des sphères. Les valeurs des coefficients dépendent alors des modèles d'interaction considérés[135]. Pour contourner ce problème, il est possible d'utiliser une approche différentielle, c'est-à-dire de considérer qu'on puisse construire une dispersion concentrée à partir d'une autre plus diluée en faisant des petits incréments de $\Delta\varphi$. Roscoe (1952) a ainsi trouvé l'expression :

$$\eta^* = \eta_0(1 - \varphi)^{-2.5}$$

qui reste valable pour tout ϕ < 1 et même pour une dispersion polydisperse.[134]

Revenons à l'interprétation de nos résultats. Notre algorithme de coalescence par le modèle de Smoluchowski n'a pas pris en compte la viscosité effective. Puisque on a laissé les gouttes de circuler selon le mouvement Brownien, on peut interpréter $t_{f,exp}/t_{f,sim}$ comme η_0/η^*.

Dans le régime dilué, 0,0208 ≤ ϕ ≤ 0,5432, l'équation de Roscoe converge vers l'équation d'Einstein par la linéarisation puisque ϕ ≪ 1. Toutefois, il faut qu'on prenne en compte la différente importante entre la viscosité d'huile (1,26 Pa.s) et celle de la phase continue (1 mPa.s). Cela veut dire que η^* dépend essentiellement de la viscosité des gouttes d'huile, et donc $\eta^* \gg \eta_0$. Cette correction, appliquée à l'équation d'Einstein (ou à l'équation de Roscoe linéarisée) mène alors à :

$$\eta^* - \eta_0 \approx \eta^* = 2.5\eta_0\varphi$$

$$\eta^*/\eta_0 = 2.5\varphi$$

On trouve effectivement que cette équation corrigée décrit très bien nos émulsions diluées (Figure 66, ligne violette). Ce qui nous a surpris est que les HIPEs Apolloniennes sont également décrites par cette équation corrigée : en dépit de leur fraction volumique très élevée, des gouttes des émulsions Apolloniennes se déplacent facilement comme si elles étaient dans un milieu dilué homogène, sans ressentir des effets des autres gouttes d'huile. Cette observation rejoint celles que l'on a déjà faites des émulsions Apolloniennes : que des gouttes sont sphériques ce qui implique qu'elles n'exercent pas de forces l'une sur l'autre (Figure 32), et qu'elles s'écoulent comme un fluide visqueux Newtonien (Figure 31) qu'on a postulé est possible puisque les plus petites gouttes se comportent comme un fluide lubrifiant homogène du point de vue des grosses. En effet, prenons la mesure de viscosité effective pour une HIPE Apollonienne (Figure 31) : on a mesuré η^*= 3 Pa.s. Faisons l'application numérique pour l'équation d'Einstein corrigée : on trouve η_0 = 1,26 Pa.s, la viscosité de la phase huileuse. Ainsi, il semble que notre hypothèse soit validée – **dans une HIPE Apollonienne, des gouttes d'huile se comportent comme si elles nageaient dans un milieu homogène constitué par d'autres gouttes d'huile.** Cela expliquera aussi pourquoi la vitesse de coalescence dans une HIPE

Apollonienne à structure autosimilaire suivra le modèle de Smoluchowski qui est un modèle de champ moyen : les gouttes se comportent comme si elles appartenaient à une émulsion diluée.

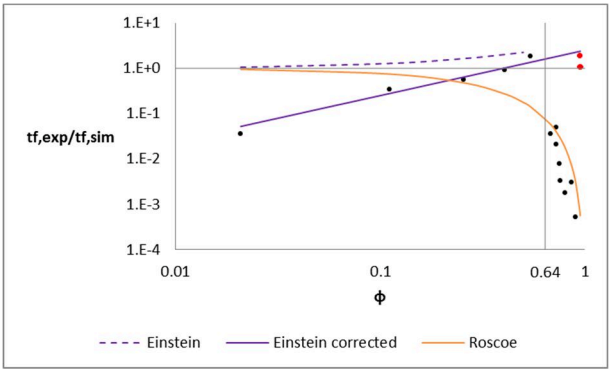

Figure 66 : l'explication des vitesses de coalescence par l'effet de la viscosité effective. Les HIPEs Apolloniennes se comportent comme des émulsions diluées tandis que la viscosité effective des autres HIPEs (qu'on soupçonne ne soient pas encore Apolloniennes) ont un effet significatif pour ralentir le mouvement des gouttes.

Quant aux autres HIPEs à 0,6795 ≤ ϕ ≤ 0,9028, l'équation de Roscoe (Figure 66, ligne orange) les décrit bien. Dans ces HIPEs, la viscosité effective devient plus importante avec ϕ, ralentissant le mouvement Brownien des gouttes d'huile, ce qui expliquera la vitesse de coalescence plus lente par rapport à celle prédite par Smoluchowski.

À ce stade, on n'est pas sûr pourquoi une HIPE à ϕ = 0,9028 se comporte de manière aussi différente que des HIPEs Apolloniennes à ϕ = 0,95. Il est bien possible que l'émulsion à ϕ = 0,9 ne soit pas encore Apollonienne, puisqu'on a trouvé qu'il y a suffisamment de tensioactif, même à 0,6% dans la phase continue, pour saturer les interfaces. Il est aussi possible que dans l'émulsion à ϕ = 0,9, il y a plus de volume libre, ce qui aura peut-être un effet. Afin de répondre à cette question, il sera idéal de varier ϕ de manière systématique à partir de 0,9, de mesurer le facteur de structure des HIPEs, de calculer le taux de couverture des interfaces, et de mesurer $t_{f,exp}/t_{f,sim}$.

8.3.2.2 La conséquence de la coalescence-fragmentation

Ayant déterminé que la cinétique de coalescence n'est pas plus lente pour les HIPEs Apolloniennes et qu'elle soit même très bien décrite par le modèle de Smoluchowski, on pense que **la métastabilité exceptionnelle des HIPEs Apolloniennes vient de la coalescence et la fragmentation simultanées.** Considérons une gamme de tailles intermédiaires dans une émulsion Apollonienne – la coalescence typique provoquera un déplacement vers les grandes tailles en épuisant les petites ; dans une HIPE Apollonienne, le confinement local de tensioactif suite à un événement de coalescence permet la création de nombreuses petites gouttelettes par la fragmentation. De ce fait, les petites tailles sont rapprovisionnées. Ainsi, le flux de gouttelettes qui rentrent dans cette gamme de tailles considérée compensera partiellement le flux sortant, ce qui contribue à l'observation qu'une émulsion Apollonienne reste émulsifiée pendant si longtemps.

On sait que la compensation du flux n'est pas exacte, puisque la distribution de tailles des gouttes dans une HIPE Apollonienne se déplace vers les grandes valeurs avec le temps (Figure 43). En même temps des micelles gonflées sont créées, que l'on a pu détecter par SAXS. Finalement, **l'HIPE Apollonienne cassera à cause de la séparation gravitationnelle**. On a observé cela après plus d'un an. Elle a lieu lorsque des gouttes créées par la coalescence sont tellement grosses que leur différence de masse volumique avec le reste de l'émulsion les fait crémer. On obtient alors une phase huileuse

macroscopique. Bien entendu, l'émulsion restante sous la crème n'est plus à ϕ = 0,95 et elle perd éventuellement sa structure apollonienne. Il est donc possible qu'en absence de la gravité, une émulsion Apollonienne restera Apollonienne indéfiniment parce qu'on raisonne que la structure Apollonienne soit un minimum local en énergie libre. La séparation de phases macroscopique est alors le minimum global.

8.3.2.3 Des réflexions thermodynamiques

Les calculs faits se trouvent dans le chapitre « 4.3.2.3 Thermodynamic considerations ». On donne un résumé qualitatif ci-dessous.

La variation d'énergie libre de Gibbs pour une émulsion s'écrit :

$$\Delta G = \Delta U - T\Delta S$$

où ΔU représente la variation d'énergie interne du système à volume et température constants. T est la température du système, aussi supposée constante, et ΔS est la variation d'entropie du système.

ΔS dans une structure Apollonienne

En 1877, Boltzmann a publié son équation qui lie l'entropie dans un système au nombre de micro-états accessibles au système.[136,137] Aujourd'hui, l'équation s'écrit couramment sous la forme :

$$S = k_B \ln \Omega$$

avec k_B la constant de Boltzmann et Ω le nombre de micro-états. Puisque Ω est la somme de toutes les permutations configurationnelles permises à chaque objet du système, il est clair que l'entropie dépendra du nombre total d'objets, ainsi que le degré de liberté pour chaque objet.

Dans une émulsion Apollonienne, les gouttes étant sphériques ont plus de degrés de liberté que d'autres géométries à facettes – celles-là peuvent se mettre en rotation et en translation, preuve en est l'écoulement Newtonien, tandis que des gouttes polyédriques des HIPEs du type « Lissant » sont coincées et présentent un seuil d'écoulement. Donc, pour le même nombre de gouttes, une émulsion Apollonienne maximisera l'entropie par rapport aux HIPEs solides ou hybrides.

De plus, comme le démontre notre algorithme des Lapins (Figure 58), chaque événement de coalescence entre deux gouttes engendre plus de gouttelettes finales. Si on considère alors l'évolution d'une HIPE liquide, en faisant l'approximation simpliste où Ω est le nombre de gouttelettes dans le système, alors ΔS est clairement une fonction croissante avec le temps.

ΔU dans une structure Apollonienne

L'énergie interne d'une HIPE est principalement composée de l'énergie élastique stockée dans les interfaces et l'énergie de surface de toutes les gouttes :

$$\Delta U = \Delta E_{elastic} + \Delta E_{surface}$$

Énergie élastique

Une HIPE Apollonienne possède une quantité minimale d'énergie élastique en raison de ses gouttes sphériques non déformées. Par contre, les HIPEs solides ou hybrides à facettes stockent beaucoup d'énergie élastique dans les films minces de tensioactif (et elles ont donc des G' plus élevés). Cette

tension subie par les gouttes déformées fait que ces HIPEs solides et hybrides soient facilement diluées. Princen a aussi observé ce comportement pour ses HIPEs (solides) et il l'a expliqué que la dilution soulagera la pression osmotique élevée dans les régions entre les gouttes déformées[14,20]; la pression de Laplace est alors neutralisée et les gouttes déformées peuvent récupérer leur forme sphérique.[24] Cette explication de Princen est soutenue par nos calculs de l'énergie de flexion d'un film mince comparée à celle d'une gouttelette de la même surface dans le chapitre « 4.3.1.2 – Free energy is reduced by creating small droplets rather than maintaining flat films ».

Nos calculs montrent de plus qu'une fois sphérique, il n'est pas favorable thermodynamiquement de déformer la goutte en créant des films plats. Dans nos HIPEs Apolloniennes, dès qu'un chevauchement se produise entre des gouttes, l'évolution a lieu par la coalescence-fragmentation. On crée ensuite des gouttelettes sphériques qui respectent des contraintes de tangence, ce qui garde l'énergie élastique à son minimum donc $\Delta E_{elastic} < 0$.

Énergie de surface

Princen et Levison (1987) ont calculé l'énergie de surface du tétrakaidécaèdre minimal de Kelvin – la géométrie d'une cellule unitaire dans une mousse idéale. Autrement dit, la forme polyédrique d'une goutte de HIPE solide possède une surface 9,7% plus grande qu'une sphère du même volume.[11] Recourant à l'argument géométrique, une émulsion Apollonienne aura une énergie de surface plus petite qu'une HIPE solide ou hybride si elles possèdent toutes le même nombre de gouttes.

Si on examine maintenant l'évolution des émulsions Apollonienne, malgré la création des microémulsions à courbure spontanée, considérées comme sans énergie de surface, nos résultats expérimentaux indiquent une croissance de surface totale avec le temps (Figure 42 et Figure 50) à cause des nombreuses gouttelettes créées par la coalescence-fragmentation. Ainsi, ΔU est une fonction en croissance avec le temps, puisque :

$$\Delta U = \Delta E_{elastic} + \Delta E_{surface} = \sigma \Delta A$$

Par conséquent, l'évolution d'une émulsion Apollonienne permet au système de s'approcher à une structure Apollonienne de plus en plus « parfaite ». Or, le gain en entropie est contrebalancé par l'augmentation de l'énergie de surface :

$$\Delta G = \sigma \Delta A - T \Delta S$$

D'après nos raisonnements, on pense que ce va-et-vient entre ΔA et ΔS fait osciller ΔG dans une structure Apollonienne, donnant effectivement un minimum local qui peut expliquer la métastabilité prolongée des émulsions Apolloniennes. On propose alors la voie d'évolution pour une HIPE liquide à ϕ = 0,95 dans la Figure 67.

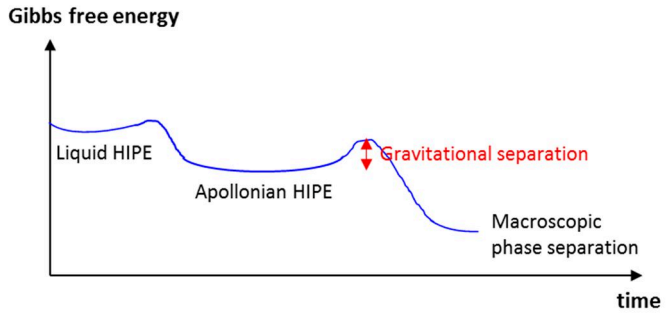

Figure 67 : la voie d'évolution proposée pour une HIPE liquide vers la séparation macroscopique des phases.

9. Conclusion

En réduisant de manière significative la disponibilité des tensioactifs, on a permis aux émulsions à haut rapport de phase interne (HIPEs) de coalescer, ce qui a engendré un nouveau type de HIPE inconnu auparavant. Ce nouveau type d'émulsion possède une structure qui remplit tout l'espace avec un ensemble de sphères très polydisperses, selon les principes prescrits par Apollonius de Perge il y a plus de 2000 ans. En son honneur, on a nommé ces HIPEs à fraction volumique interne proche de l'unité des « émulsions Apolloniennes ». Leur fabrication est à la fois très simple et reproductible : il suffit d'ajouter lentement, sous agitation continue, de la phase interne à une phase externe qui contient du tensioactif stabilisant, tout comme la recette d'une mayonnaise. Contrairement à la fabrication des HIPEs classiques qui ont préoccupé la communauté de la physicochimie jusqu'à présent, ces émulsions Apolloniennes nécessitent très peu de tensioactif et il suffit de les laisser évoluer spontanément après émulsification.

La distribution de tailles des gouttes sphériques dans une émulsion Apollonienne prend la forme d'une loi de puissance à l'exposante $-(d_f + 1)$, où la dimension fractale, d_f, est toujours très proche de celle d'un empilement Apollonien, soit d_f = 2,47. On a ensuite effectué des mesures par la diffusion aux petits angles des rayons-X, et on les a comparées à un empilement Apollonien généré par la simulation numérique. Le bon accord entre les résultats expérimentaux et la simulation nous a permet de conclure que nos émulsions possèdent une structure Apollonienne. On a déduit également que des gouttes sphériques dans nos émulsions Apolloniennes ne sont pas séparées par des films minces. Cela assure la minimisation de l'énergie élastique dans le système et par conséquent, des émulsions Apolloniennes coulent spontanément comme un liquide Newtonien alors que d'autres émulsions concentrées sont typiquement rhéofluidifiantes. L'écoulement Newtonien résulte probablement du comportement sans interactions entre les gouttes d'une émulsion Apollonienne où chaque goutte considère les autres comme étant un fluide homogène : en effet, on a trouvé que la viscosité effective d'une émulsion Apollonienne suit l'équation d'Einstein qui décrit des dispersions diluées si on considère la phase continue soit constituée des autres gouttes d'huile. Il n'y a aussi pas de seuil d'écoulement pour des HIPEs Apolloniennes, au contraire aux autres HIPEs étudiées jusqu'à présent qui se comportent comme des gels.

Nos résultats expérimentaux suggèrent que le mécanisme d'évolution dans ces HIPEs liquides pauvre en tensioactif est très différent du mécanisme de coalescence dans des émulsions diluées typiquement rencontrées. Dans celles-ci, la coalescence typique engendre de moins en moins de gouttes mais de taille de de plus en plus large afin de diminuer la surface totale. Des tensioactifs en excès sont expulsés après chaque événement de coalescence et elles disparaissent dans le réservoir de phase continue. Dans des HIPEs liquides, la surface totale augmente avec le temps, ce qui implique la création de beaucoup de petites gouttelettes. On a utilisé la simulation numérique pour reproduire nos systèmes expérimentaux et on a démontré que chaque coalescence entre deux gouttes donne beaucoup de gouttelettes « filles ». On a donc appelé ce mécanisme particulier la « coalescence-fragmentation » (ou l'algorithme des lapins pour être plus humoristique). Les gouttelettes créées logent des tensioactifs rejetés puisque ces molécules ne peuvent pas être accommodées par le petit volume de phase continue disponible dans une HIPE liquide, à risque de provoquer une augmentation conséquente du potentiel chimique. On a également déterminé les trois conditions de la coalescence-fragmentation à respecter : la conservation du volume, le remplissage optimal des vides en maximisant les rayons des gouttelettes « filles », et la non création

des films minces qui sont coûteux en énergie libre. Si ces trois conditions sont respectées, on obtient des structures construites localement selon les principes Apolloniens, ce qui donne un empilement global Apollonien dans une HIPE liquide. À partir de nos résultats de SAXS, on a trouvé que des gouttelettes créées par la coalescence-fragmentation peuvent prendre la forme des micelles gonflées, qu'elles soient à la courbure spontanée ou un peu plus grandes.

Dès qu'une HIPE atteigne sa structure Apollonienne, elle démontre une métastabilité exceptionnellement stable, au contraire des attentes usuelles pour des émulsions à une fraction volumique aussi élevée stabilisées par aussi peu de tensioactif. Tandis que la coalescence usuelle épuise le nombre de gouttes total en faisant croître les tailles des gouttes, la coalescence-fragmentation permet aux émulsions Apolloniennes de s'alimenter en créant des petites gouttelettes, ce qui donne l'impression d'une HIPE qui reste émulsifiée pendant un temps très long. On a également déterminé que la cinétique de coalescence pour une HIPE Apollonienne peut être prédite par le modèle Smoluchowski au noyau Brownien pour des émulsions polydisperses. Cela peut sembler paradoxal puisqu'une structure Apollonienne est autosimilaire alors que le modèle de Smoluchowski est un modèle de champ moyen.

On a ensuite interprété la métastabilité exceptionnelle d'une émulsion Apollonienne comme un minimum local thermodynamique, où l'augmentation en énergie libre est partiellement compensée par une augmentation entropique grâce à la création de nombreuses gouttelettes. Le système finira par la création des gouttes tellement larges qu'elles se séparent du reste de l'émulsion par la séparation gravitationnelle. Au final, le système perdra sa structure Apollonienne et descend la courbe d'énergie libre, vers le minimum global qui donne la séparation macroscopique entre l'huile et la phase aqueuse.

10. References

1. Weiner, Z. Physics: History. in *Science: Abridged Beyond the Point of Usefulness* 1 (2017).

2. Stewart, J. 450-Year-Old Painting Contains Over 100 Proverbs We Still Use Today. *My Modern Met - Art History* https://mymodernmet.com/dutch-proverbs-pieter-bruegel/ (2017).

3. Pickering, S. U. CXCVI.—Emulsions. *J. Chem. Soc., Trans.* **91**, 2001–2021 (1907).

4. Ostwald, W. Beiträge zur Kenntnis der Emulsionen. *Zeitschrift für Chemie und Ind. der Kolloide* **6**, 103–109 (1910).

5. Evonik Industries. Emulsifiers - The Evonik History Portal - The History of Evonik Industries. http://history.evonik.com/sites/geschichte/en/inventions/emulsifiers/.

6. Viard, A., Fouret & Pierhugue. *Le cuisinier royal: ou l'Art de faire la cuisine, la patisserie et tout ce qui concerne l'office, pour toutes les fortunes*. (J.-N. Barba, 1820).

7. European Food Emulsifiers Manufacturers Association. EFEMA - History. http://www.emulsifiers.org/ViewDocument.asp?ItemId=9.

8. Halliday, H. L. The fascinating story of surfactant. *J. Paediatr. Child Health* **53**, 327–332 (2017).

9. Groves, M. J. & Scarlett, B. Polyhedral Emulsion Particles. *Nature* **207**, 288–289 (1965).

10. Lissant, K. J. The Geometry of High-Internal-Phase-Ratio Emulsions. *J. Colloid Interface Sci.* **22**, 6–2 (1966).

11. Princen, H. M. & Levinson, P. The Surface Area of Kelvin's Minimal Tetrakaidecahedron: The Ideal Foam Cell (?). *J. Colloid Interface Sci.* **120**, 172–175 (1987).

12. Leonard, R. A. & Lemlich, R. A study of interstitial liquid flow in foam. Part I. Theoretical model and application to foam fractionation. *AIChE J.* **11**, 18–25 (1965).

13. Lissant, K. J. Geometry of Emulsions. *J. Soc. Cosmet. Chem.* **21**, 141–154 (1970).

14. Princen, H. . Highly concentrated emulsions. I. Cylindrical systems. *J. Colloid Interface Sci.* **71**, 55–66 (1979).

15. Princen, H. M., Aronson, M. P. & Moser J.C. Highly concentrated emulsions. *J. Colloid Interface Sci.* **75**, 246–270 (1980).

16. Princen, H. M. Osmotic pressure of foams and highly concentrated emulsions. I. Theoretical considerations. *Langmuir* **2**, 519–524 (1986).

17. Princen, H. M. & Kiss, A. D. Osmotic pressure of foams and highly concentrated emulsions. 2. Determination from the variation in volume fraction with height in an equilibrated column. *Langmuir* **3**, 36–41 (1987).

18. Princen, H. M. Pressure/Volume/Surface Area Relationships in Foams and Highly Concentrated Emulsions: Role of Volume Fraction. *Langmuir* **4**, 164–169 (1988).

19. Princen, H. M. Rheology of foams and highly concentrated emulsions. II. experimental study of the yield stress and wall effects for concentrated oil-in-water emulsions. *J. Colloid Interface Sci.* **105**, 150–171 (1985).

20. Princen, H. M. Rheology of foams and highly concentrated emulsions. I. Elastic properties and yield stress of a cylindrical model system. *J. Colloid Interface Sci.* **91**, 160–175 (1983).

21. Schwartz, L. W. & Princen, H. M. A theory of extensional viscosity for flowing foams and concentrated emulsions. *J. Colloid Interface Sci.* **118**, 201–211 (1987).

22. Sonneville-Aubrun, O. Mousses Biliquides. (Université de Paris VI, 1997).

23. Vold, R. D., Mittal, K. L. & Hahn, A. U. Ultracentrifugal Stability of Emulsions. in *Surface and Colloid Science* 45–97 (Springer US, 1978). doi:10.1007/978-1-4615-7966-3_2.

24. Mason, T. G. *et al.* Osmotic pressure and viscoelastic shear moduli of concentrated emulsions. *Phys. Rev. E* **56**, 3150–3166 (1997).

25. Princen, H. M. & Kiss, A. . Rheology of foams and highly concentrated emulsions. *J. Colloid Interface Sci.* **128**, 176–187 (1989).

26. Kabalnov, A. & Wennerstrom, H. Macroemulsion Stability : The Oriented Wedge Theory Revisited. *Langmuir* **12**, 276–292 (1996).

27. Mason, T. G., Bibette, J. & Weitz, D. A. Elasticity of Compressed Emulsions. *Phys. Rev. Lett.* **75**, 2051–2054 (1995).

28. Kim, H. S. & Mason, T. G. Advances and challenges in the rheology of concentrated emulsions and nanoemulsions. *Adv. Colloid Interface Sci.* **247**, 397–412 (2017).

29. Parsegian, V. A., Rand, R. P., Fuller, N. L. & Rau, D. C. [29] Osmotic stress for the direct measurement of intermolecular forces. in *Methods in Enzymology* vol. 127 400–416 (1986).

30. Mason, T. G., Graves, S. M., Wilking, J. N. & Lin, M. Y. Effective structure factor of osmotically deformed nanoemulsions. *J. Phys. Chem. B* **110**, 22097–22102 (2006).

31. Graves, S., Meleson, K., Wilking, J., Lin, M. Y. & Mason, T. G. Structure of concentrated nanoemulsions. *J. Chem. Phys.* **122**, 1–6 (2005).

32. Degiorgio, V., Piazza, R. & Bellini, T. Static and dynamic light scattering study of fluorinated polymer colloids with a crystalline internal structure. *Adv. Colloid Interface Sci.* **48**, 61–91 (1994).

33. Mason, T. G. & Bibette, J. Emulsification in Viscoelastic Media. *Phys. Rev. Lett.* **77**, 3481–3484 (1996).

34. Mason, T. G., Bibette, J. & Weitz, D. A. Yielding and Flow of Monodisperse Emulsions. *J. Colloid Interface Sci.* **179**, 439–448 (1996).

35. Mason, T. G. & Bibette, J. Shear Rupturing of Droplets in Complex Fluids. *Langmuir* **13**, 4600–4613 (1997).

36. Mabille, C. *et al.* Rheological and shearing conditions for the preparation of monodisperse emulsions. *Langmuir* **16**, 422–429 (2000).

37. Welch, C. F., Rose, G. D., Malotky, D. & Eckersley, S. T. Rheology of High Internal Phase Emulsions. *Langmuir* **22**, 1544–1550 (2006).

38. Bibette, J. & Mason, T. Emulsion Manufacturing Process. 48 (1997).

39. Grace, H. P. Dispersion Phenomena in High Viscosity Immiscible Fluid Systems and Application of Static Mixers as Dispersion Devices in Such Systems. *Chem. Eng. Commun.* **14**, 225–277 (1982).

40. Tcholakova, S. *et al.* Efficient Emulsification of Viscous Oils at High Drop Volume Fraction. *Langmuir* **27**, 14783–14796 (2011).

41. Aronson, M. P. & Petko, M. F. Highly Concentrated Water-in-Oil Emulsions: Influence of Electrolyte on Their Properties and Stability. *J. Colloid Interface Sci.* **159**, 134–149 (1993).

42. Shinoda, K. & Arai, H. The effect of phase volume on the phase inversion temperature of emulsions stabilized with nonionic surfactants. *J. Colloid Interface Sci.* **25**, 429–431 (1967).

43. Lu, J. R. *et al.* Neutron reflection from a layer of monododecyl hexaethylene glycol adsorbed at the air-liquid interface: the configuration of the ethylene glycol chain. *J. Phys. Chem.* **97**, 8012–8020 (1993).

44. Lobo, L. & Svereika, A. Coalescence during emulsification: 2. Role of small molecule surfactants. *J. Colloid Interface Sci.* **261**, 498–507 (2003).

45. Shi, L., Tummala, N. R. & Striolo, A. C12E6 and SDS surfactants simulated at the vacuum?water interface. *Langmuir* **26**, 5462–5474 (2010).

46. Roger, K., Botet, R. & Cabane, B. Coalescence of repelling colloidal droplets: A route to monodisperse populations. *Langmuir* **29**, 5689–5700 (2013).

47. Hoffmann, H. Fascinating phenomena in surfactant chemistry. *Adv. Colloid Interface Sci.* **32**, 123–150 (1990).

48. Taisne, L., Walstra, P. & Cabane, B. Transfer of Oil between Emulsion Droplets. *J. Colloid Interface Sci.* **184**, 378–390 (1996).

49. Aronson, M. P. The role of free surfactant in destabilizing oil-in-water emulsions. *Langmuir* **5**, 494–501 (1989).

50. Schott, H. Saturation adsorption at interfaces of surfactant solutions. *J. Pharm. Sci.* **69**, 852–854 (1980).

51. Cameron, N. R. & Sherrington, D. C. High Internal Phase Emulsions (HIPEs) - Structure , Properties and Use in Polymer Preparation. *Adv. Polym. Sci.* **126**, 163–214 (1996).

52. Kiel, O. Method of fracturing subterranean formations using oil-in-water emulsions. 19 (1973).

53. Graham, J. W., Gruesbeck, C. & Salathiel, W. M. Method of fracturing subterranean formations using oil-in-water emulsions. 10 (1976).

54. Cawiezel, K. E. & Hodge, R. High internal phase ratio water-in-oil emulsion fracturing fluid. 16 (1994).

55. Zhang, H. & Cooper, A. I. Synthesis and applications of emulsion-templated porous materials. *Soft Matter* **1**, 107 (2005).

56. Joanicot, M., Wong, K., Richard, J., Maquet, J. & Cabane, B. Ripening of cellular latex films. *Macromolecules* **26**, 3168–3175 (1993).

57. Silverstein, M. S. & Cameron, N. R. PolyHIPEs - Porous Polymers from High Internal Phase Emulsions. in *Encyclopedia of Polymer Science and Technology* (John Wiley & Sons, Inc., 2010). doi:10.1002/0471440264.pst571.

58. Mandelbrot, B. B. *The Fractal Geometry of Nature*. (W.H. Freeman and Company, 1983).

59. Borkovec, M., De Paris, W. & Peikert, R. The Fractal Dimension of the Apollonian Sphere Packing. *Fractals* **2**, 521–526 (1994).

60. Anishchik, S. V. & Medvedev, N. N. Three-dimensional apollonian packing as a model for dense granular systems. *Phys. Rev. Lett.* **75**, 4314–4317 (1995).

61. Sauerbrei, S., Haß, E. C. & Plath, P. J. The Apollonian decay of beer foam bubble size distribution and the lattices of young diagrams and their correlated mixing functions. *Discret. Dyn. Nat. Soc.* **2006**, 1–35 (2006).

62. Kwok, S., Botet, R., Sharpnack, L. & Cabane, B. Apollonian Packing in Polydisperse Emulsions. (2019).

63. Thomas, I. Apollonius of Perga. in *Selections Illustrating the History of Greek Mathematics* (eds. Page, T. ., Capps, E., Rouse, W. H. ., Post, L. . & Warmington, E. .) 276–356 (William Heinemanm Ltd, 1957).

64. Pappus of Alexandria. *Pappus of Alexandria: Book 4 of the Collection*. (Springer London, 2010). doi:10.1007/978-1-84996-005-2.

65. Viète, F. Apollonius Gallus. Seu, Exsuscitata Apolloni Pergæi Περι Επαφων Geometria. in *Francisci Vietae Opera mathematica* (ed. Van Schooten, F.) 325–346 (Lugduni Batavorum, 1646).

66. Wikipedia.org. Problem of Apollonius. https://en.wikipedia.org/wiki/Problem_of_Apollonius#History (2019).

67. Descartes, R. CCCXXV Descartes À Elisabeth. in *Correspondance IV* (eds. Adam, C. & Tannery, P.) 37–42 (Léopold Cerf, 1643).

68. Leibniz, G. W. Leibniz to Des Bosses 11 March 1706. in *The Leibniz-Des Bosses Correspondence* (eds. Look, B. C. & Rutherford, D.) 30–38 (Yale University Press, 2007).

69. Soddy, F. The Bowl of Integers and the Hexlet. *Nature* **139**, 77–79 (1937).

70. Reis, S. D. S., Araújo, N. A. M., Andrade, J. S. & Herrmann, H. J. How dense can one pack spheres of arbitrary size distribution? *Europhys. Lett.* **97**, 18004 (2012).

71. Aste, T. Circle, sphere, and drop packings. *Phys. Rev. E* **53**, 2571–2579 (1996).

72. Amirjanov, A. & Sobolev, K. Fractal properties of Apollonian packing of spherical particles. *Model. Simul. Mater. Sci. Eng.* **14**, 789–798 (2006).

73. Farr, R. S. & Griffiths, E. Estimate for the fractal dimension of the Apollonian gasket in d dimensions. *Phys. Rev. E* **81**, 061403 (2010).

74. Varrato, F. & Foffi, G. Apollonian packings as physical fractals. *Mol. Phys.* **109**, 2663–2669 (2011).

75. Das, A. K. & Ghosh, P. K. Concentrated emulsions. Investigation of polydispersity and droplet distortion and their effect on volume fraction and interfacial area. *Langmuir* **6**, 1668–1675 (1990).

76. Lin, M. Y. *et al.* Universal diffusion-limited colloid aggregation. *J. Phys. Condens. Matter* **2**, 3093–3113 (1990).

77. Weitz, D. A., Huang, J. S., Lin, M. Y. & Sung, J. Limits of Fractal Dimension for Irreversible Kinetic Aggreation of Gold Colloids. *Phys. Rev. Lett.* **54**, 1416–1419 (1985).

78. Rojanski, D., Huppert, D., Bale, H. D., Xie, D. & Schmidt, P. W. Integrated Fractal Analysis of Silica: Adsorption, Electronic Energy Transfer, and Small-Angle X-Ray Scattering. *Phys. Rev. Lett.* **56**, 2505–2508 (1986).

79. Burns, J. L., Yan, Y., Jameson, G. J. & Biggs, S. A Light Scattering Study of the Fractal Aggregation Behavior of a Model Colloidal System. *Langmuir* **13**, 6413–6420 (1997).

80. Ibaseta, N. & Biscans, B. Fractal dimension of fumed silica: Comparison of light scattering and electron microscope methods. *Powder Technol.* **203**, 206–210 (2010).

81. Brown, W., Johnsen, R., Stilbs, P. & Lindman, B. Size and shape of nonionic amphiphile (C12E6) micelles in dilute aqueous solutions as derived from quasielastic and intensity light scattering, sedimentation, and pulsed-field-gradient nuclear magnetic resonance self-diffusion data. *J. Phys. Chem.* **87**, 4548–4553 (1983).

82. Berthod, A., Tomer, S. & Dorsey, J. G. Polyoxyethylene alkyl ether nonionic surfactants: Physicochemical properties and use for cholesterol determination in food. *Talanta* **55**, 69–83 (2001).

83. Royal Society of Chemistry. C12E6. *ChemSpider: Search and share chemistry* http://www.chemspider.com/Chemical-Structure.17269.html (2019).

84. Mitchell, D. J., Tiddy, G. J. T., Waring, L., Bostock, T. & McDonald, M. P. Phase Behaviour of Polyoxyethylene Surfactants with Water. *J. Chem. Soc., Faraday Trans. I* **79**, 975–1000 (1983).

85. Merck. Silicone oil - viscosity 10000 cSt (25C). *Sigma-Aldrich Catalog* https://www.sigmaaldrich.com/catalog/product/aldrich/378402?lang=fr&region=FR (2019).

86. Persello, J., Magnin, A., Chang, J., Piau, J. M. & Cabane, B. Flow of colloidal aqueous silica dispersions. *J. Rheol. (N. Y. N. Y).* **38**, 1845–1870 (1994).

87. Malvern Instruments Limited. Mastersizer S, Mastersizer 2000 and Mastersizer 3000: method transfer - how to get the same results on all three systems. 13–16 (2015).

88. Guinier, A., Fournet, G. & Yudowitch, K. L. Origin and Characteristics of Small-Angle X-Ray Scattering. in *Small-Angle Scattering of X-Rays* (ed. Goeppert Mayer, M.) 1–4 (John Wiley & Sons, Inc., 1955).

89. Narayanan, T. *et al.* A multipurpose instrument for time-resolved ultra-small-angle and coherent X-ray scattering. *J. Appl. Crystallogr.* **51**, 1511–1524 (2018).

90. Perez, J., Gabriel, D., Menneglier, C., Meneau, F. & Lyon, O. SAXS for biology optimized on the beamline SWING. https://www.synchrotron-soleil.fr/fr/file/6964/download?token=6lgu_7R-.

91. Sztucki, M. SAXSUtilities. (2016).

92. Doucet, M. *et al.* SasView. (2018) doi:10.5281/zenodo.1412041.

93. Boyd, D. W. Osculatory packings by spheres. *Can. Math. Bull.* **13**, 59–64 (1970).

94. Teixeira, J. Experimental methods for studying fractal aggregates. in *On Growth and Form* (eds. Stanley, H. E. & Ostrowsky, N.) 145–162 (Springer Netherlands, 1986). doi:10.1007/978-94-009-5165-5.

95. Gudowska-Nowak, E., Lindenberg, K. & Metzler, R. Preface: Marian Smoluchowski's 1916 paper—a century of inspiration. *J. Phys. A Math. Theor.* **50**, 380301 (2017).

96. Evans, D. F. & Wennerstrom, H. Colloidal Stability. in *The Colloidal Domain: Where Physics, Chemistry, Biology, and Technology Meet* 417–420 (Wiley-VCH, 1999).

97. Winter, H. H. & Chambon, F. Analysis of Linear Viscoelasticity of a Crosslinking Polymer at the Gel Point. *J. Rheol. (N. Y. N. Y).* **30**, 367–382 (1986).

98. Winter, H. H. & Mours, M. Rheology of Polymers Near Liquid-Solid Transitions. in *Neutron Spin Echo Spectroscopy Viscoelasticity Rheology* 165–234 (Springer Berlin Heidelberg, 1999). doi:10.1007/3-540-68449-2_3.

99. Das, A. K., Mukesh, D., Swayambunathan, V., Kotkar, D. D. & Ghosh, P. K. Concentrated emulsions. 3. Studies on the influence of continuous-phase viscosity, volume fraction, droplet size, and temperature on emulsion viscosity. *Langmuir* **8**, 2427–2436 (1992).

100. Otsubo, Y. & Prud'homme, R. K. Effect of drop size distribution on the flow behavior of oil-in-water emulsions. *Rheol. Acta* **33**, 303–306 (1994).

101. Hayakawa, K., Kawaguchi, M. & Kato, T. Protective Colloidal Effects of Hydroxypropyl Methyl Cellulose on the Stability of Silicone Oil Emulsions. *Langmuir* **13**, 6069–6073 (1997).

102. Pal, R. Shear Viscosity Behavior of Emulsions of Two Immiscible Liquids. *J. Colloid Interface Sci.* **225**, 359–366 (2000).

103. Rutgers, I. R. Relative viscosity of suspensions of rigid spheres in Newtonian liquids. *Rheol. Acta* **2**, 202–210 (1962).

104. Seto, R., Mari, R., Morris, J. F. & Denn, M. M. Discontinuous Shear Thickening of Frictional Hard-Sphere Suspensions. *Phys. Rev. Lett.* **111**, 218301 (2013).

105. Åström, J. A. & Herrmann, H. J. Fragmentation of grains in a two-dimensional packing. *Eur. Phys. J. B* **5**, 551–554 (1998).

106. Iliev, P. S., Wittel, F. K. & Herrmann, H. J. Evolution of fragment size distributions from the crushing of granular materials. *Phys. Rev. E* **99**, 012904 (2019).

107. Steacy, S. J. & Sammis, C. G. An automaton for fractal patterns of fragmentation. *Nature* **353**, 250–252 (1991).

108. Valentas, K. J., Bilous, O. & Amundson, N. R. Analysis of Breakage in Dispersed Phase Systems. *Ind. Eng. Chem. Fundam.* **5**, 271–279 (1966).

109. Babinet, J. Mémoires d'optique météorologique. in *Comptes rendus hebdomadaires des séances de l'Académie des Sciences* 638–648 (Gauthier-Villars, 1837).

110. Guinier, A., Fournet, G. & Yudowitch, K. L. Remarks on the Babinet Principle of Reciprocity. in *Small-Angle Scattering of X-Rays* (ed. Goeppert Mayer, M.) 38–40 (John Wiley & Sons, Inc., 1955).

111. Martin, J. E. Scattering exponents for polydisperse surface and mass fractals. *J. Appl. Crystallogr.* **19**, 25–27 (1986).

112. Martin, J. E. & Hurd, A. J. Scattering from fractals. *J. Appl. Crystallogr.* **20**, 61–78 (1987).

113. Farris, R. J. Prediction of the Viscosity of Multimodal Suspensions from Unimodal Viscosity Data. *Trans. Soc. Rheol.* **12**, 281–301 (1968).

114. Baram, R. M., Herrmann, H. J. & Rivier, N. Space-Filling Bearings in Three Dimensions. *Phys. Rev. Lett.* **92**, 4 (2004).

115. Fidleris, V. & Whitmore, R. L. The physical interaction of spherical particles in suspensions. *Rheol. Acta* **1**, 573–580 (1961).

116. Godet, M. The third-body approach: A mechanical view of wear. *Wear* **100**, 437–452 (1984).

117. Feigin, L. A. & Svergun, D. I. *Structure Analysis by Small-Angle X-Ray and Neutron Scattering*. (Springer US, 1987). doi:10.1007/978-1-4757-6624-0.

118. Cabane, B. *et al.* Hiding in Plain View: Colloidal Self-Assembly from Polydisperse Populations. *Phys. Rev. Lett.* **116**, 1–5 (2016).

119. van Beurten, P. & Vrij, A. Polydispersity effects in the small-angle scattering of concentrated solutions of colloidal spheres. *J. Chem. Phys.* **74**, 2744–2748 (1981).

120. Kruif, C. G. D., Briels, W. J., Vrij, A. & May, R. P. Hard-sphere colloidal silica dispersions. the structure factor determined with SANS. *Langmuir* **4**, 668–676 (1988).

121. Porod, G. Particle Scattering, General Treatment. in *Small Angle X-ray Scattering* (eds. Glatter, O. & Kratky, O.) 29–32 (Academic Press, 1982).

122. Porod, G. Die Röntgenkleinwinkelstreuung von dichtgepackten kolloiden Systemen. *Kolloid-Zeitschrift* **124**, 83–114 (1951).

123. Debye, P., Anderson, H. R. & Brumberger, H. Scattering by an Inhomogeneous Solid. II. The Correlation Function and Its Application. *J. Appl. Phys.* **28**, 679–683 (1957).

124. Balmbra, R. R., Clunie, J. S., Corkill, J. M. & Goodman, J. F. Effect of temperature on the micelle size of a homogeneous non-ionic detergent. *Trans. Faraday Soc.* **58**, 1661 (1962).

125. Penfold, J., Staples, E., Tucker, I. & Cummins, P. The Structure of Nonionic Micelles in Less Polar Solvents. *J. Colloid Interface Sci.* **185**, 424–431 (1997).

126. Wijaya, E. C., Separovic, F., Drummond, C. J. & Greaves, T. L. Micelle formation of a non-ionic surfactant in non-aqueous molecular solvents and protic ionic liquids (PILs). *Phys. Chem. Chem. Phys.* **18**, 24377–24386 (2016).

127. Roger, K., Cabane, B. & Olsson, U. Formation of 10−100 nm Size-Controlled Emulsions through a Sub-PIT Cycle. *Langmuir* **26**, 3860–3867 (2010).

128. Guinier, A., Fournet, G. & Yudowitch, K. L. General Expression for the Scattered Intensity. in *Small-Angle Scattering of X-Rays* (ed. Goeppert Mayer, M.) 33–37 (John Wiley & Sons, Inc., 1955).

129. Helfrich, W. Elastic Properties of Lipid Bilayers: Theory and Possible Experiments. *Zeitschrift für Naturforsch. C* **28**, 693–703 (1973).

130. Safran, S. A. Saddle-splay modulus and the stability of spherical microemulsions. *Phys. Rev. A* **43**, 2903–2904 (1991).

131. Bibette, J., Morse, D. C., Witten, T. A. & Weitz, D. A. Stability criteria for emulsions. *Phys. Rev. Lett.* **69**, 2439–2442 (1992).

132. Einstein, A. Eine neue Bestimmung der Moleküldimensionen. *Ann. Phys.* **324**, 289–306 (1906).

133. Einstein, A. Berichtigung zu meiner Arbeit: „Eine neue Bestimmung der Moleküldimensionen". *Ann. Phys.* **339**, 591–592 (1911).

134. Roscoe, R. The viscosity of suspensions of rigid spheres. *Br. J. Appl. Phys.* **3**, 267–269 (1952).

135. Hsueh, C. H. & Wei, W. C. J. Analyses of effective viscosity of suspensions with deformable polydispersed spheres. *J. Phys. D. Appl. Phys.* **42**, 075503 (2009).

136. Boltzmann, L. On the Relationship between the Second Fundamental Theorem of the Mechanical Theory of Heat and Probability Calculations Regarding the Conditions for Thermal Equilibrium. *Sitzungberichte der Kais. Akad. der Wissenschaften. Math. Classe. Abt. II* **76**, 373–435 (1877).

137. Sharp, K. & Matschinsky, F. Translation of Ludwig Boltzmann's Paper "On the Relationship between the Second Fundamental Theorem of the Mechanical Theory of Heat and Probability Calculations Regarding the Conditions for Thermal Equilibrium" Sitzungberichte der Kaiserlichen Akademie d. *Entropy* **17**, 1971–2009 (2015).

138. Rice, R. W. *Porosity of Ceramics*. (CRC Press, 2017). doi:10.1201/9781315274539.

139. Zhang, S., Campagne, C. & Salaün, F. Influence of Solvent Selection in the Electrospraying
 Process of Polycaprolactone. *Appl. Sci.* **9**, 402 (2019).

140. Mircioiu, C. *et al.* Mathematical Modeling of Release Kinetics from Supramolecular Drug Delivery Systems. *Pharmaceutics* **11**, 140 (2019).

141. Busatto, C., Pesoa, J., Helbling, I., Luna, J. & Estenoz, D. Effect of particle size, polydispersity and polymer degradation on progesterone release from PLGA microparticles: Experimental and mathematical modeling. *Int. J. Pharm.* **536**, 360–369 (2018).

142. D'Aurizio, E. *et al.* Biodegradable Microspheres Loaded with an Anti-Parkinson Prodrug: An in Vivo Pharmacokinetic Study. *Mol. Pharm.* **8**, 2408–2415 (2011).

143. Cooney, D. O. Effect of geometry on the dissolution of pharmaceutical tablets and other solids: Surface detachment kinetics controlling. *AIChE J.* **18**, 446–449 (1972).

144. Patel, A. Ocular drug delivery systems: An overview. *World J. Pharmacol.* **2**, 47 (2013).

11. Supplementary Information

The following mathematical calculations were performed by Robert Botet of Laboratoire de Physique des Solides, University of Paris-Sud.

11.1 Deducing d_f from the double-log plot of Light Scattering measurements

If the Light Scattering instrument uses a geometrical progression to bin the measured diameters of the particles, a, then:

$$a_k = a_0 \rho^k$$

where a_0 is the smallest detected diameter, $\rho > 1$ is the common ratio of the geometrical progression, and k is the k-th sampling class.

Assuming that $n(a)$ is the actual continuous distribution of sizes in the sample, $n(a)\, da$ is then the number of particles of diameters between $a - da/2$ and $a + da/2$. This means that the distribution in the sampling class k (i.e. sampling class with the nominal diameter a_k) given by the instrument is

$$n_{DLS}(a_k) \propto \int_{a_k}^{a_{k+1}} n(a)\, da$$

If the size distribution in our sample follows a power law, then $n(a) \propto 1/a^{(d_f+1)}$ where d_f is the fractal dimension. Substituting this relation in the expression of $n_{DLS}(a_k)$, we find:

$$n_{DLS}(a_k) \propto \int_{a_k}^{a_{k+1}} \frac{1}{a^{(d_f+1)}}\, da$$

$$n_{DLS}(a_k) \propto \frac{1}{d_f}\left[\frac{1}{{a_k}^{d_f}} - \frac{1}{{a_{k+1}}^{d_f}}\right]$$

$$n_{DLS}(a_k) \propto \frac{1}{d_f}\left[\frac{1}{(a_0\rho^k)^{d_f}} - \frac{1}{(a_0\rho^{k+1})^{d_f}}\right]$$

$$n_{DLS}(a_k) \propto \frac{1}{(a_0\rho^k)^{d_f}}$$

Therefore, when the measured size distribution given by the instrument is expressed as a double-logarithmic:

$$\log n_{DLS}(a) = -\, d_f \log a$$

we find that the slope of the plot corresponds to the fractal dimension of the sample.

11.2 Polydispersity as a function of fractal dimension

Let a be the diameter of a particle. If the collection of particles follows a power-law distribution, then the particle-size distribution, $n(a)$, is of the form:

$$n(a) \sim a^{-(d_f+1)}$$

For $a_0 < a < a_1$, and $n(a) = 0$ outside the interval, the moment of the order k is defined as:

$$\langle a^k \rangle \equiv \int_{a_0}^{a_1} a^k n(a) da$$

Substituting the expression of $n(a)$, we find, for any $k \neq d_f$:

$$\langle a^k \rangle = \frac{1}{d_f - k}\left({a_0}^{k-d_f} - {a_1}^{k-d_f}\right)$$

At the same time, the definition of polydispersity, f, is given by the expression:

$$f^2 = \frac{\langle a^2 \rangle \langle a^0 \rangle}{\langle a^1 \rangle^2} - 1$$

Therefore,

$$f^2 = \frac{\left({a_0}^{2-d_f} - {a_1}^{2-d_f}\right)}{\left(d_f - 2\right)} \frac{\left({a_0}^{-d_f} - {a_1}^{-d_f}\right)}{d_f} \left(\frac{d_f - 1}{{a_0}^{1-d_f} - {a_1}^{1-d_f}}\right)^2 - 1$$

For massive particles, $d_f > 2$ necessarily. All the powers of a_1 may also be neglected with respect to the powers of a_0 because $a_1 \gg a_0$. Then, the expression of f^2 becomes greatly simplified:

$$f^2 \approx \frac{\left({a_0}^{2-d_f}\right)}{\left(d_f - 2\right)} \frac{\left({a_0}^{-d_f}\right)}{\left(-d_f\right)} \left(\frac{d_f - 1}{{a_0}^{1-d_f}}\right)^2 - 1$$

$$f^2 = \frac{\left(d_f - 1\right)^2}{d_f\left(d_f - 2\right)} - 1$$

Thus,

$$f = \left[d_f\left(d_f - 2\right)\right]^{-1/2}$$

and we find that polydispersity is a decreasing function of fractal dimension.

11.3 Rate of drug release by Apollonian distributions of spheres

11.3.1 By diffusion from within a spherical carrier

Based on an experimentally validated model of drug release derived from the analytical solution to Fick's second law of diffusion (D'Aurizio et al., 2011)[142]:

$$\frac{M_t}{M_\infty} = 1 - \frac{6}{\pi^2}\sum_{n=1}^{\infty}\left(\frac{1}{n}\right)^2 exp\left(-\frac{Dn^2\pi^2}{R^2}t\right)$$

where M_t and M_∞ are the cumulative number of drug molecules released by a spherical particle or droplet of radius R at time t and at infinite time respectively. D is the drug molecule's coefficient diffusion inside the sphere.

If c_0 is the initial concentration (in molecules/m^3) of drugs in the sphere, then $M_\infty = (4/3)\pi R^3 c_0$. Let $m = M_t/M_\infty$ be the proportion of drug molecules already released from the sphere at time t. We define $\tau = Dt/R^2$, a reduced unit of time. The above equation can then be rewritten in a simpler form:

$$\frac{dm}{d\tau} = 6\sum_{n=1}^{\infty} exp(-n^2\pi^2\tau)$$

For an Apollonian distribution of spheres, where $n(a) \sim a^{-(d_f+1)}$ with d_f = 2.47, we define the width of the distribution as $\rho = a_1/a_0$. To facilitate comparison with the monodisperse case, we consider an Apollonian distribution where the average volume of the spheres is the same as in the monodisperse collection. Then $\langle a^3 \rangle = R^3$ and

$$a_0 = R\left(\frac{3-d_f}{d_f}\frac{1-1/(\rho^{d_f})}{\rho^{3-d_f}-1}\right)^{1/3}$$

$$a_1 = \rho a_0$$

We then find the equation for the rate of drug release:

$$\frac{dm}{d\tau}(\rho,t) = \frac{3d_f}{1-1/(\rho^{d_f})}\left(\frac{a_0}{\pi R}\right)\sum_{n=1}^{\infty}\left[\rho^{1-d_f}\, E_{\frac{3-d_f}{2}}\left(\frac{n^2\tau}{\rho^2}\left(\frac{\pi R}{a_0}\right)^2\right) - E_{\frac{3-d_f}{2}}\left(n^2\tau\left(\frac{\pi R}{a_0}\right)^2\right)\right]$$

in which $E_v(z)$ represents the generalized exponential integral function. The auxiliary quantity $\pi R/a_0$ depends only on ρ and d_f according to the above-given expression of a_0. In the limit of $\rho \to 1$, independent of the value of d_f, we recover the same expression of $dm/d\tau$ previously found for the monodisperse case. For an Apollonian distribution, $\rho \gg 1$, the above equation can be greatly simplified into the following approximation, which turns out to be a power-law function of τ:

$$\frac{dm}{d\tau}(\rho,t) \approx \frac{\omega}{\tau^{(d_f-1)/2}}$$

with $\omega = \frac{3d_f}{\pi^{d_f}}\left(\frac{3-d_f}{d_f\cdot\rho^{3-d_f}}\right)^{d_f/3}\Gamma\left(\frac{d_f-1}{2}\right)\zeta(d_f-1)$.

11.3.2 By dissolution of a solid spherical substrate

This mode of delivery confers the advantage of zero-order kinetics, with equilibrium rate constant k_0, as described by Hopfenberg's model for controlled release from erodible spheres[140]:

$$m = \frac{M_t}{M_\infty} = 1 - \left(1 - \frac{k_0 t}{c_0 R}\right)^3$$

For an Apollonian distribution of homogeneous solid spheres dissolving in a liquid, replacing M_∞ by the value $(4/3)\pi R^3 c_0$ (because $\langle a^3 \rangle = R^3$ since we intend to compare with a monodisperse collection of solid spheres), we find:

$$\frac{dm}{dt} = 3\frac{k_0}{c_0}\frac{\langle (a - k_0 t/c_0)^2 \rangle}{R^3}$$

Its average value may be calculated by considering the temporal condition $a > k_0 t/c_0$. If we averaged over the Apollonian distribution of width ρ, we obtain the explicit expressions:

$$\frac{dm}{d\tau} = \begin{cases} 3\,\dfrac{3-d_f}{1-\rho^{d_f-3}}\left(\dfrac{\rho^{d_f}-1}{d_f}\tau^2 - 2\dfrac{\rho^{d_f}-1}{d_f-1}\tau + \dfrac{\rho^{d_f-2}-1}{d_f-2}\right) & \text{if } \tau < \frac{1}{\rho} \\ 3\,\dfrac{3-d_f}{1-\rho^{d_f-3}}\left(\dfrac{2}{d_f(d_f-1)(d_f-2)}\tau^{2-d_f} - \dfrac{1}{d_f-2} + \dfrac{2}{d_f-1}\tau - \dfrac{\tau^2}{d_f}\right) & \text{if } \frac{1}{\rho} < \tau < 1 \\ 0 & \text{if } \tau > 1 \end{cases}$$

with the auxiliary time variable $\tau = \alpha t \rho^{-(d_f/3)}$ and α a constant coefficient that is proportional to $k_0/(Rc_0)$.

The definition of time, τ, now includes the factor $\rho^{-(d_f/3)}$ which is significant.

List of figures

List of tables

RÉSUMÉ

On a étudié des émulsions à haut rapport de phase interne (HIPEs), dont la fraction volumique d'huile dispersée faisait ϕ = 0.95, et la phase continue était une solution aqueuse de tensioactif non-ionique, le monododecyl éther d'hexaéthylène glycol (C12E6). Suivant la concentration du C12E6, on a obtenu 2 types de HIPEs, qualifiés de « solide » ou de « liquide ». Dans les HIPEs formulées à fort taux de C12E6 (> 8% dans la phase continue), les gouttes se déforment en polyèdres séparés par des films minces de la phase continue. Grâce à ces films, ces HIPEs se comportent comme un « solide élastique » sous cisaillement et elles sont rhéofluidifiantes au-delà du seuil d'écoulement. En réduisant le taux de tensioactif à moins de 3%, on a permis à l'HIPE de coalescer, ce qui a engendré une structure non observée auparavant : les gouttes restent sphériques sans déformation et remplissent tout l'espace grâce à une population extrêmement polydisperse dont la distribution des diamètres, $n(a)$, s'exprime comme une loi de puissance: $n(a) \sim a^{-(d_f+1)}$. d_f est la dimension fractale de l'ensemble des gouttes et vaut toujours 2.48-2.50 après une semaine d'évolution dans ces HIPEs « liquides ». Cette valeur est très proche de celle d'un empilement Apollonien des sphères (RAP). En effet, on a confirmé par la diffusion des rayons-X que les gouttes de ces HIPEs pauvres en tensioactif s'empilent comme un RAP. Il s'agit de la première fois depuis 2200 ans qu'on a réussi à fabriquer un empilement Apollonien dans un système réel. Ces émulsions Apolloniennes sans films minces s'écoulent spontanément comme un liquide visqueux Newtonien ; un comportement auparavant inconnu dans des émulsions à ϕ > 0.6. Les HIPEs Apolloniennes sont exceptionnellement métastables et persistent au-delà d'un an, malgré la croissance des gouttes par la coalescence. L'aire totale des émulsions Apolloniennes augmente avec le temps, ce qui indique un mécanisme évolutif différent de la coalescence des émulsions diluées. Par la simulation numérique, on a trouvé que deux gouttes qui coalescent dans une émulsion Apollonienne engendrent de nombreuses gouttelettes sphériques par la fragmentation, afin de remplir de façon optimale des vides aux alentours, tout en minimisant l'énergie élastique dans le système. On a nommé ce mécanisme « la coalescence-fragmentation ». Elle a lieu parce que les tensioactifs rejetés lors de la coalescence ne peuvent pas être accommodés par le peu de phase continue dans une HIPE, à risque de provoquer une augmentation conséquente du potentiel chimique. Ces tensioactifs en excès peuvent alors se loger sur des interfaces qui viennent d'être créées. La création des gouttelettes sphériques est favorisée par rapport à la déformation mutuelle entre les grosses puisque celle-là est moins couteuse en énergie libre. On a ainsi postulé qu'un empilement Apollonien soit un minimum local thermodynamique.

MOTS CLÉS

émulsion ; polydisperse ; coalescence ; Apollonien ; Newtonian ; écoulement

ABSTRACT

We studied oil-in-water high internal-phase-ratio emulsions (HIPEs) at internal volume fraction ϕ = 0.95, stabilized by non-ionic surfactant, hexaethylene glycol monododecyl ether (C12E6). By varying C12E6 concentration, we obtained two distinct types of HIPEs that we qualified as "solid" or "liquid". Surfactant-rich HIPEs formulated with > 8%C12E6 in the continuous phase are of the "solid" variety: their droplets are distorted into polyhedrons separated by thin films of continuous phase. These films confer an "elastic solid" property on the HIPEs, which display shear-thinning flow beyond their yield stress at high strain rates. By reducing surfactant concentration to below 3%C12E6, we allowed coalescence and obtained a new HIPE structure: oil droplets retaining their spherical shapes, filling space with an extremely polydisperse population. Their diameter distribution, $n(a)$, obeyed a power law: $n(a) \sim a^{-(d_f+1)}$. d_f is the fractal dimension of the set of droplets and was consistently 2.48-2.50 after a week of emulsion evolution, a similar value to that of a Random Apollonian Packing (RAP) of spheres. We confirmed by X-ray Scattering that oil droplets in these surfactant-poor HIPEs are indeed a RAP. This is the first recorded instance of an Apollonian packing fabricated in real physical systems in 2200 years. Apollonian emulsions flow spontaneously like a viscous Newtonian liquid, a behaviour previously unknown in emulsions beyond ϕ = 0.6. They also have exceptional metastability, remaining emulsified up to a year, even though droplet sizes grow through on-going coalescence. We found that overall surface area increased with time in Apollonian HIPEs, indicating a different evolutionary mechanism from coalescence in dilute emulsions. Through numerical simulation, we determined that two coalescing droplets in an Apollonian emulsion fragment into multiple smaller spherical droplets to optimally fill voids in the vicinity while maintaining minimal elastic energy in the system by avoiding droplet deformation. We named this mechanism "coalescence-fragmentation", made possible because surfactant molecules evicted during coalescence cannot be evacuated into the very limited amount of continuous phase without causing a steep rise in chemical potential. We found that it is lower in free energy costs to create small spherical droplets than to allow larger droplets to deform one another. Thus, we postulated that an Apollonian packing may be a local thermodynamic minimum.

KEYWORDS

emulsion ; polydisperse ; coalescence ; Apollonian ; Newtonian ; flow